ASPECTS OF FOULING IN DAIRY PROCESSING

A thesis presented in partial fulfilment of the requirements for the degree of

Doctor of Philosophy
in
Food Engineering

at Massey University, Palmerston North, New Zealand.

HAYDEN ALBERT EDWARD BENNETT

2007

ABSTRACT

Fouling of heat treatment equipment in the dairy processing industry is an expensive and persistent problem. The objective of this work was to develop a better understanding of the mechanisms of dairy fouling in heat exchangers and identify methods to control this build-up. This was part of a larger project investigating the interaction between spore-forming thermophilic bacilli (thermophiles) contamination and fouling deposits on internal surfaces of equipment.

Two systems were developed to monitor the onset and build-up of fouling on the internal surfaces of two research heat exchangers. The first used a commercial sensor to measure the local heat flux and the temperature on the hot side of a plate type heat exchanger. The heat transfer coefficient was calculated and normalised with its value at the start of the run to reflect the contribution of fouling deposits to the thermal resistance, thus giving a real-time estimate of the rate of fouling. The second system used an energy balance over a tubular type heat exchanger and measured inlet and outlet temperatures to estimate the overall heat transfer coefficient thus giving a global measurement of fouling over the tubular heat exchanger.

In both systems the plot of normalised heat transfer coefficient over time often stayed constant over an induction period, which was followed by a falling period indicative of growth in the fouling layer thickness and/or mass. Each system was validated by comparing the final value of the normalised heat transfer coefficient with direct measurements of fouling made at the end of a run namely: fouling deposit height for the local measurement and fouling deposit mass for the global measurement. The normalised heat transfer coefficient reported by each system correlated well with the corresponding direct measurement of the fouling layer.

An important factor identified in this study was the effect of air bubble nucleation on fouling deposits. It was shown that bubbles that formed on the heated surface greatly reduced the length of the induction period to a matter of seconds rather than

hours, as found in previous studies of fouling in the absence of surface bubbles. The rate of fouling was also enhanced while the bubbles remained at the surface. The structure of bubble type fouling layers was linked to the behaviour of the bubbles at the heated surface. Visual observations of these bubbles showed evidence of growth, vibration and coalescence during their period of attachment to the heated surface.

Deposits from bubble type fouling consisted of all solid components found in the original milk solution, except lactose, in approximately the same ratio. By contrast fouling deposits reported in the literature with systems operating under the traditional protein denaturation mechanism were reported to consist mainly of whey proteins.

Bubble induced fouling can be limited in a number of ways, the most effective being to maintain a high operating pressure in the equipment to ensure nucleation does not occur. Experiments conducted in this study showed that a pressure of 130 kPa.g was sufficient to suppress all bubble nucleation at the heated surface at a temperature of 90°C.

Another method identified was the use of high linear fluid velocities to entrain any surface bubbles into the processing stream immediately upon nucleation. Linear velocities above 1.0 m/s were shown to achieve this goal in the miniature plate heat exchanger tested. However, this method is only partially successful because the local linear velocity varies with position in heat exchange equipment of complex geometries and can drop below the mainstream average velocity causing surface bubbles to form, especially in recirculation regions behind flow obstacles.

A more reliable method, in situations where high operating pressures could not be used, involved conditioning the heated surface with a thin protein layer during the first few minutes of a run. Conditioning the surface resulted in bubble suppression even at high temperatures and low pressures, thus greatly extending the length of the induction period.

Trials performed in this study showed that the addition of a proteolytic enzyme produced by psychrotrophic microbes greatly increased fouling. The enzyme destabilised the caseins which could attach directly to the heat exchange surface

independently from the bubble fouling mechanism. Thus the quality of the milk is another important factor to consider. However, the addition of enzymes produced by thermophilic bacilli isolated from milk powder plants did not increase fouling.

A theory describing the air bubble induced fouling mechanism is presented along with recommendations on how to reduce this fouling contamination in processing equipment.

ACKNOWLEDGEMENTS

Firstly, I would like to thank my chief supervisor, Dr. K. Tuoc Trinh for his guidance throughout my study. I appreciate the hard work Tuoc put into providing an excellent study environment with impeccable resources. The knowledge and experience I gained from this exercise was invaluable for which I am indebted to him. Thanks also to my second supervisor, Dr. Graham Manderson, who provided a kind and gentle approach to my supervision. I will not forget the support, humour and kindness both of you brought to my study.

I would like to thank my sponsor the former New Zealand Dairy Board, now part of Fonterra Co-operative Limited. Without their financial support, this study would not have been possible. Also Dr. David Woodhams, the manager of the Milk Powder Plant Availability Project, for his helpful comments throughout the project including critiques of reports submitted during the course of this study.

Special thanks must be given to technicians Mr. Byron McKillop and Mr. Mark Dorsey who worked closely with me during the design and construction of the pilot plant. Their technical knowledge and experience made the construction of the pilot plant a success.

Technical support from Mr. Garry Radford, Mr. Don McClean, Dr. Binh Trinh, Mr Bryden Zaloum, Dr. Yacine Helmar, Dr. Palatasa Havea and Mr. Steve Glasgow was also appreciated. Thanks to Dr. Hugh Morgan and staff at Thermophile Research Unit at the University of Waikato for thermophile species identification.

Fellow students Mr. Richard Croy, Dr. Andrew Hinton, Miss Carol Ma, and Dr. Mark Downey provided a happy and supportive group environment. I wish success to you all for your future.

Finally, I would like to thank family and friends who helped and encouraged me on this journey.

TABLE OF CONTENTS

LIST OF FIGURES

LIST OF TABLES

NOMENCLATURE

Roman

a	gradient constant
A	surface area (m^2) or heat exchange surface area (m^2)
A_p	proteinase activity
b	y-axis intercept constant
c	constant
c_p	heat capacity of fluid (J/kg.K)
$c_{p,p}$	heat capacity of the process fluid (J/kg.K)
C_k	concentration of para-κ-casein
d_e	equal diameter of process fluid cross section (m)
d_i	inner diameter of inside tube (m)
d_o	outer diameter of inside tube (m)
D	hydraulic diameter (m)
D_0	hydraulic diameter at t=0 (m)
D_i	inner diameter of outside tube (m)
D_o	outer diameter of outside tube (m)
E	activation energy (J/mol)
f	friction coefficient
F	heat flux calibration factor (Wm^{-2}/binary unit)
k_a	rate constant
k_d	deposition rate constant (s^{-1})
L	length of pipe (m) or length of inner tube fouling region (m)
m	rate coefficient
$\dot{m}$	mass flow rate of fluid (kg/s)
N_f	normalised overall heat transfer coefficient
ΔP	differential pressure (Pa)
q	heat transfer flux (W/m^2)
Q	flow rate of process fluid (l/h) or (m^3/h)
R	total heat transfer resistance (m^2.K/W)
R_a	aluminium tape thermal resistance (m^2.K/W)

R_f	fouling thermal resistance (m^2.K/W)
R_g	universal gas constant (J/mol.K)
R_{hf}	heat flux sensor thermal resistance (m^2.K/W)
R_{hm}	heat medium thermal resistance (m^2.K/W)
R_p	process fluid thermal resistance (m^2.K/W)
R_{ss}	stainless steel wall thermal resistance (m^2.K/W)
R_w	wall and its attachment thermal resistance (m^2.K/W)
Ra	relative surface roughness (μm)
Re	Reynolds number = $dv\rho/\mu$ (dimensionless)
S	cross sectional area of process fluid (m^2)
T	solid-liquid interface temperature (°C)
U	heat transfer coefficient (W/m^2.K)
U_0	heat transfer coefficient at t=0 (W/m^2.K)
U_i	internal overall heat transfer coefficient (W/m^2.K)
U_{i0}	initial internal heat transfer coefficient (W/m^2.K)
v	flow velocity (m/s)
V	milk velocity (m/s)

Greek

α	fouling parameter
Φ	fouling rate (s^{-1})
$\Delta\theta$	temperature difference (^oC)
$\Delta\theta_1$	temperature difference of side 1 (°C)
$\Delta\theta_2$	temperature difference of side 2 (°C)
$\Delta\theta_{LMTD}$	log mean temperature difference (^oC)
$\Delta\theta_m$	mean temperature difference (^oC)
θ_c	correct temperature (^oC)
θ_{hf}	outer temperature of heat flux sensor (°C)
θ_{hm}	temperature of heating medium (^oC)
θ_i	inlet temperature of test fluid (^oC)
θ_o	outlet temperature of test fluid (^oC)
θ_p	temperature of process fluid (^oC)
θ_r	recorded temperature (^oC)
Θ_{hm}	outlet temperature of the heating medium (^oC)
Θ_p	outlet temperature of the process fluid (^oC)

μ	dynamic fluid viscosity (kg/m.s)
μ_p	viscosity of process fluid (Pa.s)
ρ	density of fluid (kg/m^3)
ρ_p	density of process fluid (kg/m^3)
ϕ	heat transfer rate (W)
ϕ_{hm}	rate of heat lost by the heating medium (W)
ϕ_p	rate of heat gained by the process fluid (W)

INTRODUCTION

Heat treatments are very common in dairy processes because they render milk safe for human consumption and change both the physical and chemical properties of the milk to yield desirable properties in the finished products. A by-product of heating is the deposition of milk components on the equipment surfaces. The formation of this deposit, often referred to as fouling, leads to reduced heat transfer and increased pressure drop in process equipment. The presence of fouling in dairy processing plants not only leads to increased production costs due to reduced run times but also increases in capital, energy and maintenance costs including costs associated with product losses.

Fouling deposits may also provide sites for thermoduric (heat resistant) bacteria to attach, become embedded and ultimately be protected during cleaning regimes. Spore-forming thermophilic bacilli (thermophiles) are an important group of thermoduric bacteria that are characterised by the ability of their spores to survive pasteurisation and thermalisation heat treatments and grow at 45°C and above. Increasingly strict requirements have been placed on thermophilic bacteria and spore counts in milk powders which have culminated in reduced run times between cleaning of processing equipment in general and of heat exchangers in particular (Refstrup, 2000)

In New Zealand, the majority of milk produced is converted into powder, hence, there is a vested economic interest in reducing costs associated with its production. Any increases in production time, even if only of a few hours, will result in saved expenditure. Therefore, it is very important to control fouling to ensure run lengths are increased and product specifications met.

This work was carried out as part of a larger investigation into extending milk powder plant run times. The investigation, named Plant Availability Project, was organised by the former New Zealand Dairy Board and involved a number of research providers and dairy co-operatives. At Massey University, the research group

led by Dr. Trinh was asked to investigate the interaction between fouling and thermophile contamination in milk powder plants.

Two Doctoral projects were set up. The first approached the investigation from the point of view of thermophile attachment to surfaces both clean and fouled and their movement from these surface colonies to the bulk fluid. It also studied the potential for protection of thermophiles from cleaning agents by the fouling deposits (Hinton, 2003). Hinton (2003) focussed his attention mainly on the preheating section of milk powder plants. The second (current) project studied thermophile contamination from the evaporators to complement data obtained by Hinton. At the same time it tackled the problem of reduced run times in preheating systems by investigating the factors that affect fouling kinetics and patterns. The idea was for the two projects to eventually meet in an overlap area that would give a reasonably comprehensive picture of thermophilic contamination and fouling in thermal systems.

It was found early in the experimental programme that thermophile contamination of the product was inconsequential in the pilot scale evaporator used. Only two formal runs were completed before the thermophile work was discontinued. Due to the lack of results, firm conclusions were not made and a report of the findings can be found elsewhere (Bennett *et al.*, 2002).

1.1 OBJECTIVES

The specific objectives of this project were to:

- Design and build two research heat exchangers that mimic geometry conditions found in industrial tubular and plate type heat exchangers. Each heat exchanger must incorporate multiple test surfaces that can be isolated at any point in a run. This candidate concentrated on building a rig of six miniature plate heat exchangers while Andrew Hinton concentrated on building a rig of six tubular heat exchangers.
- Develop methods to monitor fouling *in situ* within each heat exchanger and compare the results of these methods to direct measurements of fouling deposits.

- Investigate factors that affect the formation and build up of fouling in heating equipment by dairy fluids. These factors include process variables (e.g. pressure) and product variables (e.g. enzyme content).
- Identify methods to reduce and control the formation of fouling deposits in heat treatment equipment.

LITERATURE REVIEW

2.1 INTRODUCTION

This literature review examines the process of fouling and the factors that affect the formation of these deposits on the surfaces of dairy heat treatment equipment. The review also describes the experimental setups used to obtain the data on which the above findings are based. This includes descriptions of the test fluids, typical experimental equipment and the methods of fouling measurement.

2.2 FOULING DURING DAIRY PROCESSING

Fouling in the dairy industry has been a problem since the first heat exchanger was introduced as part of the pasteurisation process (Bott, 1990). Initial research into the problem (Johnson & Roland, 1940a; Johnson & Roland, 1940b) concentrated on plant cleaning as a practical solution as pointed out by Fryer *et al.* (1995). It was not until the mid 1940s that researchers started to investigate the mechanism of fouling. For example, Bell & Sanders (1944) found that the amount of fouling could be reduced in a tubular heat exchanger by pre-holding the raw milk in jacketed vessels at 75°C for 10 min. From these and other results Bell & Sanders (1944) go on to suggest that fouling was due to the denaturation of proteins and the decrease in solubility of milk salts with increasing temperature which is now widely confirmed. The literature on fouling of dairy processing systems has grown substantially only in the last three decades; most probably because the financial costs of fouling became important as the dairy industry grew in size. Detailed research into fouling started with Harold Burton and his co-workers at the National Institute for Research in Dairying (NIRD), Shinfield (UK). Their investigations provided a platform for many subsequent studies by groups such as: the University of Wisconsin and the North Carolina State University in the United States (e.g. Bixby, 1974; Lund & Sandu, 1981; Swartzel, 1983); the Technical University of Munich (e.g. Kessler & Beyer, 1991; Petermeier *et al.*, 2002); INRA in France (e.g. Tissier & Lalande, 1986; Delplace *et al.*, 1997); the Netherlands Institute for Dairy Research (e.g. De Jong, 1997; Visser & Jeurnink, 1997); and the universities of Reading, Cambridge and Birmingham in the United Kingdom (e.g. Foster *et al.*, 1989; Fryer & Belmar-Beiny, 1991; Gotham *et al.*,

1992; Fryer & Slater, 1994; Grandison, 1996). The literature on milk fouling is now extensive and much progress has been made in the understanding of the underlying chemistry of the process. The composition and structure of fouling have been investigated extensively and several theories concerning the mechanisms of fouling have been published. These findings will be reviewed in the remainder of this chapter.

2.2.1 Milk

Milk is a complex fluid containing many components in several states of dispersion. The major components of raw milk are water, fat, lactose, proteins (caseins and serum proteins) and minerals (mainly inorganic salts). Milk also contains numerous other elements in trace quantities (trace elements, organic acids, gases, vitamins, non-protein nitrogenous compounds, endogenous enzymes and bacteria). The typical composition of raw milk is given in Table 2.1.

Table 2.1 Typical composition of raw milk (Walstra *et al.*, 1999)

Component	Composition (% w/w)		
	Typical content (liquid basis)	Range (liquid basis)	Typical content (dry basis)
Water	87.3	85.5 – 88.7	
Lactose	4.6	3.8 – 5.3	36
Fat	4.0	2.5 – 5.5	31
Protein	3.3	2.3 – 4.4	25
Minerals	0.7	0.57 – 0.83	5.4
Organic acids	0.17	0.12 – 0.21	1.3
Miscellaneous	0.15		1.2

Lactose is the distinctive carbohydrate of milk. It is a reducing disaccharide composed of glucose and galactose and exists in two closely related interchangeable anomeric forms known as α- and β-lactose which differ in solubility and other properties. Lactose is the principal carbon source for most microorganisms that grow in milk.

Milk fat is a complex and variable mixture of lipids largely made up of triglycerides (98%). Other lipids that are present include cholesterols, diglycerides, free fatty

acids, phospholipids, and cerebrosides. In raw milk, the fat occurs mostly in the form of globules (spherical particles of about 1 – 10 µm diameter). The globules are covered with a native fat globule membrane made up mainly of phospholipids and glycoproteins which helps to maintain colloidal stability and protects the fat from oxidation and enzyme attack.

The milk proteins fall into one of two classes: caseins and whey or serum proteins. Caseins account for approximately 80% of the total milk proteins and consist of four major proteins: α_{S1}- (38%), α_{S2}- (10%), β- (36%) and κ- (13%) casein. They occur in milk (together with some of the calcium and inorganic phosphate) in the form of colloidal particles known as micelles. The κ-casein plays an important role in stabilising these micelles by preventing their aggregation or precipitation.

In milk caseins are precipitated by acid at pH 4.6. What remains in the milk are the whey or serum proteins that account for about 20% of the total protein content. The major whey proteins are: β-lactoglobulin (β-Lg), α-lactalbumin (α-La), bovine serum albumin (BSA) and various immunoglobulins (Ig). β-Lg and α-La constitute the majority of the whey proteins making up 10 and 4 % w/w of the total protein content.

The cations of sodium, potassium, calcium, and magnesium, and the anions of chloride and inorganic orthophosphate make up the majority of the mineral substances found in milk. Along with citrate (an organic acid) these substances are commonly referred to as the “milk salts”.

2.2.2 Heat treatment

The manufacture of virtually all milk and dairy products involves heat treatment. Such treatment is mainly aimed at the killing of microorganisms, inactivating enzymes and promoting beneficial chemical changes. The results greatly depend on the intensity of the treatment, i.e. the combination of temperature and duration of heating (Walstra *et al.*, 1999).

There are two types of heat transfer methods employed in the dairy industry: direct and indirect. Direct heating is where the heating medium is mixed with the product e.g. to sterilise milk by steam injection and is favoured for fast heating. Indirect

heating utilises a partition to separate the product and heating or cooling medium. Heat is transferred from or to the medium through the partition to or from the product. This method is preferred when there are concerns with contamination of the product by impurities in the heating medium or dilution effects. Common heat treatments used in the dairy processing industry are listed in Table 2.2.

Table 2.2 Typical heating processes utilised in the dairy industry

Heat treatment	Temp range (°C)	Holding time (s)	Method
Thermisation	63 - 65	15 – 20	Indirect
Pasteurisation	72 or 85	15 or 1	Indirect
Ultra pasteurisation	125 - 138	2 – 4	Indirect & Direct
Preheat treatment	70 - 110	15 – 120	Indirect & Direct
Ultra-high-temperature treatment (UHT)	130 - 145	1 – 30	Indirect & Direct

If evaporation is conducted the milk enters the evaporator at approximately 68-75°C and exits at approximately 45-50°C with a residence time between 10 and 15 minutes.

More specific reasons for heat treatment of milk are:

- *To ensure that products are safe for human consumption*. This is concerned specifically with killing pathogens that occur naturally in the milk as well as those bacteria that may have been unintentionally introduced.
- *To increase their keeping quality*. This is concerned primarily with killing spoilage organisms and/or their spores. It includes the inactivation of enzymes (native milk enzymes and/or those excreted by microorganisms).
- *To establish specific product properties*. For example: to obtain a satisfactory consistency of yoghurt.

Heat treatment can make numerous changes to the properties of milk and milk-derived products. Many in depth accounts have been published focussing on the effects of thermal processing on the major milk components (Burton, 1988; Fox, 1995; Walstra *et al.*, 1999). Some examples of the chemical and physical changes caused by heat treatments include:

- Removal of gases including CO_2.

- Denaturation of serum proteins making them more reactive.
- Formation of free sulfhydryl groups.
- Inactivation of enzymes.
- Reactions between protein and lactose (Maillard reactions in particular).
- Aggregation of casein micelles which may eventually lead to coagulation.
- Increase in the amount of colloidal phosphate and decrease in the concentration of the calcium ion.

2.2.3 Phases of fouling

Fouling is a transient process; the heat exchanger is clean at first, and then becomes fouled. The build up of a fouling layer with time can take place in two distinct periods: induction and fouling periods (Paterson & Fryer, 1988; Fryer *et al.*, 1995). To illustrate this concept researchers often plot the fouling resistance (R_f) over time. R_f refers to the resistance to heat transfer contributed by the fouling layer which is different from the thermal resistance of the liquid. Figure 2.1 summarises the possible changes in fouling resistance over time.

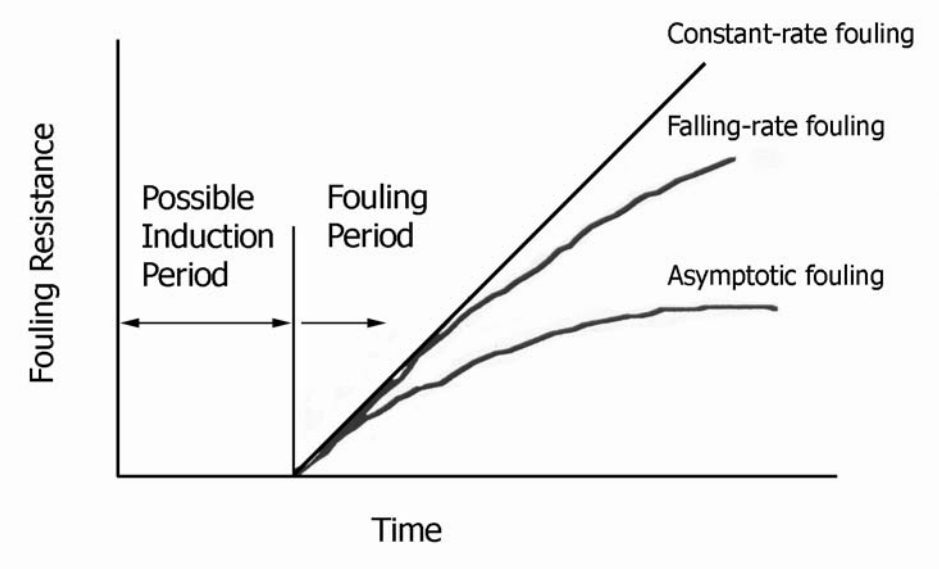

Figure 2.1 Idealised fouling curves (Fryer *et al.*, 1995).

The induction period represents a conditioning or initiation period during which the heat transfer surface is modified so that eventually fouling can take place. The fouling deposit at the end of the induction period is very thin and there is negligible resistance to heat transfer. In some instances, this thin fouling induction deposit may enhance surface roughness which increases the heat transfer coefficient slightly

(De Jong, 1997). Induction periods may be less obvious (or not observed at all) with equipment with complex geometries such as plate heat exchangers (Visser & Jeurnink, 1997).

The fouling period which follows starts when the layer is sufficiently thick to create a resistance to heat transfer. This period represents a steady growth of deposition on the surface during which the rate of fouling is controlled primarily by surface bond formation which is governed by protein-protein interactions (Fryer, 1989; Fryer & Pritchard, 1989; Belmar-Beiny & Fryer, 1993). During the fouling period, the curve may exhibit a constant, falling or an asymptotic character. A constant rate curve is achieved if the fouling rate increases linearly with time. If the deposition rate decreases with time a falling rate curve is observed and if this reaches a constant value then the behaviour is described as asymptotic (Fryer *et al.*, 1995; Changani *et al.*, 1997).

2.2.4 Composition

The composition of fouling deposits can vary widely depending on processing (e.g. temperature, flow velocity, heat treatment methods) and product factors (e.g. composition, age and pH of milk). It is generally accepted among researchers that fouling deposits fall into one of two categories, as first proposed by Burton (1968):

- The first, called Type A, starts to form when the temperature exceeds about 75°C. It reaches a maximum in the temperature range 95-110°C and then reduces in amount at higher temperatures (Burton, 1968; Lalande *et al.*, 1984). This deposit generally has a high protein content (50-70%) and a lower mineral content (30-40%). At the lower end of the temperature range most of the protein in the deposit is denatured β-Lg (60%) but there is a shift to predominantly casein (40%) at the top end of the range.
- The second type, named Type B, forms at higher temperatures and increases in quantity up to the highest temperature reached in the heat exchanger (140°C). It is predominantly mineral (70-80%) with only small amounts of protein (10-20%) (Lyster, 1965; Lalande *et al.*, 1984).

Figure 2.2 shows a graphical representation of the fouling types described above that may be found in an indirect heat exchanger operating on raw milk.

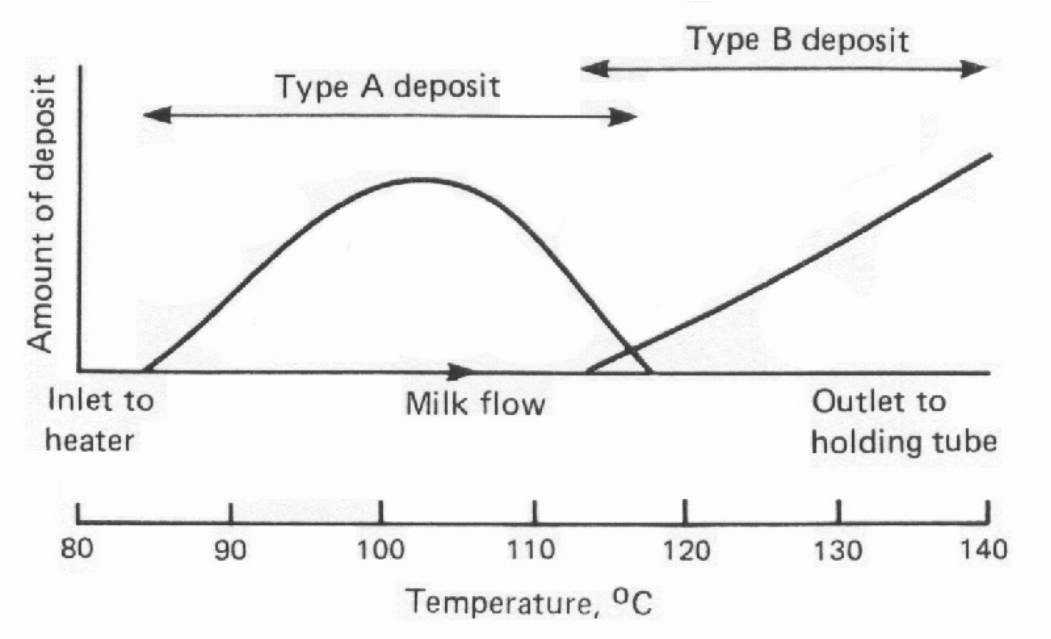

Figure 2.2 Diagrammatic representation of fouling distribution in an indirect heat exchanger operating on raw milk (Burton, 1988).

Lactose is scarcely found in milk deposits because it is water-soluble. Only at high temperatures (>100°C) when caramelisation or intense Maillard reactions may take place will lactose contribute to a deposit (Jeurnink *et al.*, 1996c; Visser *et al.*, 1997). Kessler & Schraml (1996) found that upon heating whey protein concentrates containing 25% dry matter, spongy layers of protein aggregates were formed, entrapping some of the heated fluid. As a result these deposits contained up to 50% (dry matter basis) lactose.

Some authors (e.g. Burton, 1968; Lalande *et al.*, 1984; Visser *et al.*, 1997) state that fat plays a minor role in the process of milk fouling. Although there is evidence of fat being located within the fouling deposit, these authors maintain that milk fat has little effect on deposition process. Furthermore, Maas *et al.* (1985) found that in spite of the high fat content of whipping cream (85% of the total solids) the fouling behaviour of this cream resembled that of whole milk. However, high amounts of fat have been found in fouling deposits (e.g. Johnson & Roland, 1940a; Skudder *et al.*, 1986; Jeurnink & Brinkman, 1994; Jeurnink *et al.*, 1996c; Fung, 1998). Jeurnink *et al.* (1996c) quoted Newstead (1994) who found that recombined milk made of skim milk powder and anhydrous milk fat, homogenised at 130 bar, fouled rapidly and the deposit contained up to 60 % (w/w dry matter basis) fat, present as fat globules.

The authors concluded that this observation suggests active deposition of emulsion particles possibly due to an enhanced activity of the proteinaceous membrane.

The extreme variability of the composition of fouling layers published in the literature is highlighted by the selection in Table 2.3.

Table 2.3 Composition of fouling layers from a selection of studies.

Reference	Milk type	Milk temp (°C)	Equipment	Composition (% dry basis)
Lyster (1965)	Whole	85	Plate heat exchanger (regenerative section)	Protein: 60 Mineral: 25 Fat: 12
Lalande *et al*. (1984)	Whole	65-70	Plate heat exchanger (regenerative section)	Protein: 50 Mineral: 40 Fat: 1
	Whole	120-138	Plate heat exchanger (heating section)	Protein: 15 Mineral: 75 Fat: 3
Fung (1998)	Whole	4-90	Tubular heat exchanger	Protein: 32 Mineral: 5 Fat: 50
	Whole (damaged)	4-90	Tubular heat exchanger	Protein: 32 Mineral: 4 Fat: 49
Tissier *et al*. (1984)	Whole	72	Pasteuriser	Protein: 50 Mineral: 15 Fat: 25
	Whole	90	Steriliser	Protein: 50 Mineral: 40 Fat: 1
	Whole	138	Steriliser	Protein: 12 Mineral: 75 Fat: 3
Yoon & Lund (1989)	Whole	88	Plate heat exchanger (preheat)	Protein: 43 Mineral: 45 Fat: ND
	Whole	120	Plate heat exchanger (steriliser)	Protein: 45 Mineral: 40 Fat: ND
Calvo & Rafael (1995)	Whole	80	Plate heat exchanger (heating)	Protein: 52 Mineral: 9 Fat: 23
Grandison (1988)	Whole	110-140	Plate heat exchanger (regenerative and heating)	Protein: 19-44 Mineral: 57-20 Fat: 1-28

Table 2.3 (continued)

Jeurnink *et al*. (1989)	Whole	85	Tubular heat exchanger	Protein: Mineral: Fat:	64 18 15
	Whole	120	Tubular heat exchanger	Protein: Mineral: Fat:	43 49 3
Delsing & Hiddink (1983)	Skim	76	Tubular heat exchanger	Protein: Mineral: Fat:	78 17 -
Jeurnink & Kruif (1995)	Skim	85	Plate heat exchanger	Protein: Mineral: Fat:	44 45 -
Skudder *et al*. (1986)	Whole	80-110	Plate heat exchanger (regenerative)	Protein: Mineral: Fat:	51 20 6
	Whole	110-140	Plate heat exchanger (heating)	Protein: Mineral: Fat:	22 53 5
Ma *et al*. (1998)	Whole	85	Tubular heat exchanger	Protein: Mineral: Fat:	20 4 45
	Skim	85	Tubular heat exchanger	Protein: Mineral: Fat:	64 13 -
Johnson & Roland (1940a)	Whole	82	Tubular heat exchanger	Protein: Mineral: Fat:	35 5 52
Truong (2001)	Whole	110	Downstream from direct steam injector (rig)	Protein: Mineral: Fat:	39 8 39
	Whole	105	Downstream from direct steam injector (plant)	Protein: Mineral: Fat:	63 20 3

Tissier *et al*. (1984) detailed those milk proteins which constitute the protein phase of the deposit over pasteurisation and UHT temperature ranges (Table 2.4). The detailed break down of protein contributions in fouling layers is relatively rare and do not agree with one another exactly. However, there appears to be a consensus that the contribution of β-Lg dominates in Type A fouling (Fryer *et al*., 1995; Visser *et al*., 1997).

Table 2.4 Detailed protein composition of fouling deposits (Tissier *et al.*, 1984)

Composition (%)	Pasteuriser (72°C)	Steriliser (138°C)
β-lactoglobulin	50	-
α_{s1}-casein	18	27
β-casein	-	50
Immunoglobulins	23	-
Other	9	23

2.2.5 Microstructure

Many detailed investigations of the microstructure of milk and whey fouling on stainless steel surfaces have been reported (e.g. Tissier & Lalande, 1986; Britten *et al.*, 1988; Foster *et al.*, 1989; Foster & Green, 1990; Belmar Beiny & Fryer, 1992; Belmar-Beiny & Fryer, 1993; Fryer & Bird, 1994; Jeurnink & Brinkman, 1994; Schraml & Kessler, 1996; Truong *et al.*, 1996; Visser & Jeurnink, 1997; Robbins *et al.*, 1999; Andritsos *et al.*, 2002; Morison & Tie, 2002; Truong *et al.*, 2002). It was found that Type A is curd like, creamy and voluminous and consists of a compact thin sub-layer adjacent to the wall (rich in calcium and phosphorus) and a spongy and porous top-layer (predominantly protein). The top layer consists of small particles that are randomly linked by bridges and anchored to the sub-layer (Figure 2.3). Minerals, fat globules, casein micelles and microorganisms can be embedded within this structure. Due to its voluminous nature this type of deposit is responsible for restricting flow passages and causes increases in operating pressures.

In contrast, Type B fouling is grey in colour, brittle and gritty and does not have two distinct layers but one thin sublayer where protein is concentrated near the outside of the deposit with calcium, phosphorus and magnesium located near the heat exchange surface. This deposit tends to interfere more with heat transfer than with flow owing to its physical structure (Foster & Green, 1990; Changani *et al.*, 1997).

There has been much disagreement amongst researchers as to which component deposits first (protein or mineral). This is discussed further in section 2.2.6.1.

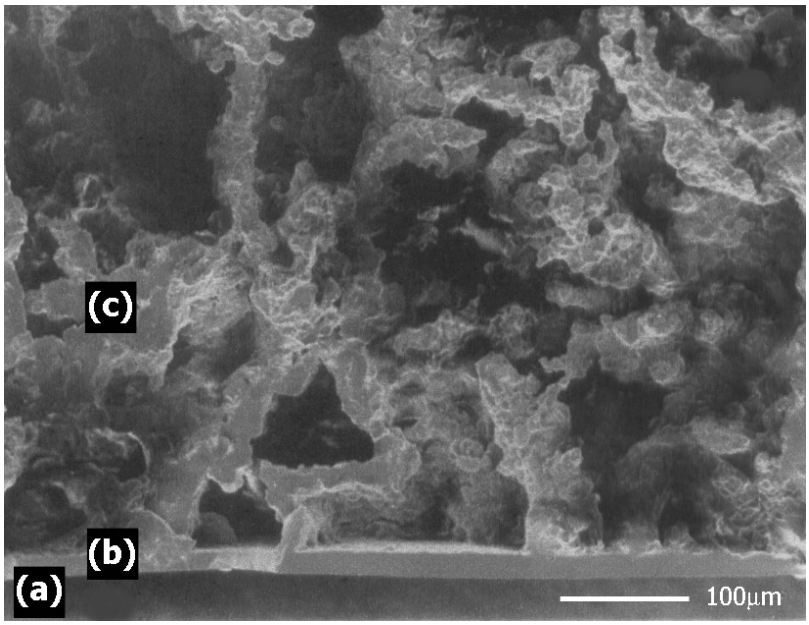

Figure 2.3 Scanning electron micrograph of Type A deposit structure (a) stainless steel surface (b) sub-layer (c) top-layer (Truong, 2001).

2.2.6 Fouling mechanisms

Many studies have been carried out in an attempt to identify the mechanisms of fouling using a variety of different dairy fluids, processing equipment and analytical techniques. The mechanisms are complicated and involve chemical reactions, momentum, heat and mass transfer processes (Changani *et al.*, 1997).

Burton (1988) lists the following possible processes involved in the formation of fouling deposits:

1. Reactions in the product (e.g. heat denaturation) which convert one or more of its constituents into a form capable of being deposited on the surface.
2. Transportation of the product constituents (foulant or foulant precursor) to the surface.
3. Adsorption of a layer of some fouling material to the surface to form an initial layer.
4. Deposition of other fouling material or more of the same on the initial layer.
5. Build-up of the fouling layer by deposition of further material, compensated by the mechanical removal of material through shearing forces caused by the flow of product across the deposit-liquid interface.

2.2.6.1 Induction layer

Fouling of equipment surfaces may begin with a thin induction layer. A number of studies have attempted to determine which milk components deposit onto the heated surface first (Hegg & Larsson, 1981; Delsing & Hiddink, 1983; Foster *et al.*, 1989; Fryer, 1989; Foster & Green, 1990; Belmar-Beiny & Fryer, 1993; Kim & Lund, 1998). However, there has been no agreement between researchers. Delsing & Hiddink (1983) concluded that a conditioning film of proteinaceous material was most likely to be the first fouling layer to form. They also found that further growth of the fouling layer only appeared possible if calcium was present.

Fryer (1989) suggested that the presence of a layer of mineral salts adjacent to the heated surface shows that this layer was the first to be deposited. However, Foster & Green (1990) argued that the proteinaceous layer was diffuse and irregular and that it seems very probable that salts could pass through it thus allowing the salts and protein layers to be built up simultaneously.

Belmar-Beiny & Fryer (1993) concluded from their surface analysis results that proteins were most likely to be the first species to adhere to the stainless steel surface. “Proteins are very surface active and a clean metal surface has a large free surface energy gradient. Proteins will therefore be adsorbed to the surface reducing this free surface energy” (Belmar-Beiny & Fryer, 1993).

2.2.6.2 Rate determining step

If deposit formation results only from a combination of mass transfer and chemical reactions then the slowest of these processes will be the rate-controlling step. Belmar-Beiny *et al.* (1993) considered the following two cases:

1. If fouling is mass transfer controlled then the slowest process will be the transfer of reacted protein to the wall. In this case, the rate of deposit formation will not be a strong function of temperature.
2. If the fouling process is reaction controlled, deposit formation will be a function of temperature where the controlling reaction takes place. Reactions in a number of different places could control the process:
    a. *Surface reaction*. If only surface processes control fouling, deposition will occur wherever the wall temperature is hot enough for protein denaturation and aggregation to occur, regardless of the bulk milk

temperature. The process will be a function of the wall temperature, not the bulk milk temperature.

b. *Bulk reaction*. If the controlling reaction for fouling takes place in the bulk, then two conditions can be envisaged:
    i. If the wall temperature is such that protein denaturation and aggregation will occur and the bulk temperature is such that native protein is thermally stable then fouling will result from deposition of protein which has been denatured and aggregated in the thermal boundary layer adjacent to the wall.
    ii. If both the boundary layer and the turbulent core are hot enough for protein denaturation and aggregation then protein denatured and aggregated in both regions will contribute to deposit formation.

If a surface reaction is responsible for fouling, the amount of fouling should depend only on the wall temperature. If the bulk processes contribute to fouling, then the amount of fouling should increase when the fluid bulk becomes hot enough to produce denatured and aggregated protein and thus be a function of both bulk temperature and fluid velocity.

Belmar-Beiny *et al*. (1993) used a tubular heat exchanger fouled with whey protein concentrate to study the bulk and surface effects. They found that a simple model in which fouling was correlated with the volume of fluid hot enough to produce denatured and aggregated protein produced reasonable agreement between theory and experiment, indicating the possible importance of bulk reactions.

2.2.6.3 Activation and transport of depositing species

Jeurnink *et al*. (1996c) proposed a schematic representation of the fouling mechanisms during the heating of whey and milk in heat exchangers as shown in Figure 2.4. The process can be described as follows: “When a solution containing whey proteins comes into contact with a stainless steel surface, even at room temperature, a monolayer of protein immediately adsorbs. If whey proteins undergo heat denaturation further deposition of protein onto the monolayer may occur. These heat denatured proteins, or ‘fouling intermediates’ form in the bulk solution and are

transported to the surface. Their deposition is through reactions with other deposited molecules most likely through the formation of a disulfide bond. The deposition of the fouling intermediate may be enhanced in the presence of calcium. Calcium phosphate may precipitate directly onto the stainless steel wall, which is thought to be partly driven by a large temperature difference between the bulk and the surface. In whey solutions calcium phosphate may associate with β-Lg aggregates or when casein micelles are present, in the case of milk, calcium phosphate may also associate with casein micelles. In milk, the active β-Lg molecules may associate with the κ-casein at the surface of the casein micelle and may entrap the micelles in the deposit" (Jeurnink *et al.*, 1996c).

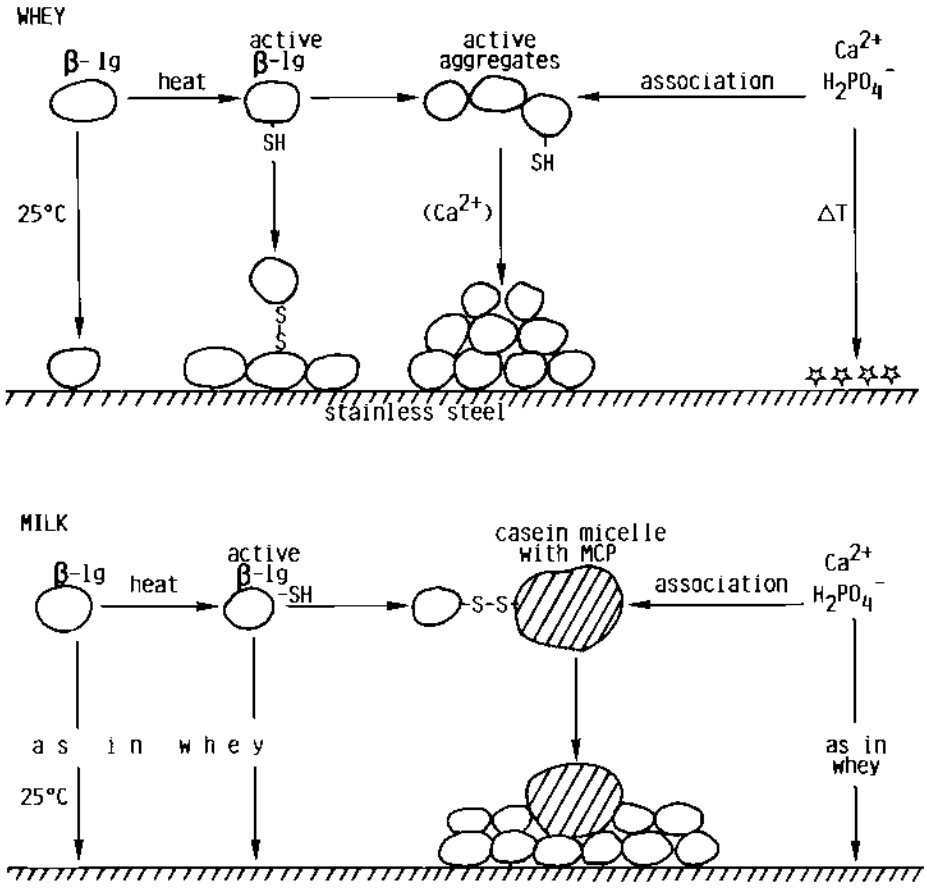

Figure 2.4 Schematic representation of the fouling mechanisms during the heating of whey and milk (Jeurnink *et al.*, 1996c).

The fouling intermediate species described by Jeurnink *et al.* (1996c) refers to a component of a model constructed by Roefs & Kruif (1994). The partly unfolded and therefore activated β-Lg molecules are defined as the fouling intermediates. This

model describes the aggregation of β-Lg in analogy to a radical chain reaction; upon raising the temperature a thiol group of β-Lg is exposed and becomes accessible to disulfide-thiol exchange reactions. This activated molecule acts like a radical. The rate of deposition is proportional to the concentration of these activated β-Lg molecules, as calculated on the basis of the model.

Skudder *et al.* (1981) and Skudder (1981) found that the addition of potassium iodate, a sulphydryl oxidising agent, reduced the amount of deposit formed during milk processing thus demonstrating that disulphide exchange reactions and protein aggregation are important in fouling. Jeurnink (1995b) found that if serum proteins were almost totally absent in milk, there was a large decrease in fouling compared to normal milk.

Transport to or from the surface is determined by the flow rate, the geometry of the apparatus and the difference in concentration of activated species between the surface and the bulk. During this transport an activated molecule of β-Lg can be inactivated through reactions with other β-Lg molecules or with other components in the milk including:

- other denatured whey proteins (e.g. α-lactalbumin) (e.g. Burton, 1984; Mulvihill & Donovan, 1987; Corredig & Dalgleish, 1996a; Oldfield *et al.*, 1998b; Anema, 2001)
- κ-casein and α_{S2}-casein of casein micelles (Creamer *et al.*, 1978; Singh & Fox, 1985; Singh & Fox, 1986; Mulvihill & Donovan, 1987; Parnellclunies *et al.*, 1988; Jeurnink, 1991; Singh & Creamer, 1991; Jeurnink, 1992; Corredig & Dalgleish, 1996a; Oldfield *et al.*, 1998a; Anema, 2001)
- proteins of the milk fat globule membranes (Houlihan *et al.*, 1992; Corredig & Dalgleish, 1996b)

For protein deposition to occur it is necessary that the free exposed SH-group is oriented towards the surface thus enabling it to react with a disulphide bond of an already adsorbed protein molecule in such a way that a new disulphide bond can be formed (Hegg *et al.*, 1985; Roscoe & Fuller, 1994; Itoh *et al.*, 1995; Jeurnink *et al.*, 1996b; Murray & Deshaires, 2000). Not every collision with the surface will lead to deposition because the reaction depends on the orientations of both the approaching molecule and the already deposited molecules (Visser *et al.*, 1997).

The presence of positively charged calcium ions leads to a reduction in the electrostatic repulsion between β-Lg molecules thus enabling the formation of larger aggregates upon the heating of serum protein. In the presence of calcium ions the deposition of proteins may also occur through formation of non-covalent bonds, in which the specific orientation of the approaching protein molecule is no longer needed and therefore the sticking probability of serum proteins to the stainless steel surface will increase (Jeurnink *et al.*, 1996c). This general argument about the significant role of β-Lg in dairy fluid fouling is supported by others (e.g. Lalande *et al.*, 1984; Lalande *et al.*, 1985; Fryer, 1989; De Jong *et al.*, 1992; Gotham *et al.*, 1992; Jeurnink, 1995b; Jeurnink *et al.*, 1996b).

Although α-lactalbumin also denatures and associates with other proteins upon heating, its contribution to the fouling process has been considered less important than β-Lg (Visser *et al.*, 1997). This is probably because α-lactalbumin does not have a free –SH group (therefore less reactive) and its concentration in milk is about half that of β-Lg.

According to Jeurnink *et al.* (1996c) casein micelles can be attached to fouling deposits not only through surface bound β-Lg (as stated before) but through aggregation by two mechanisms: when the colloidal stability is low or when the milk is heated to a high temperature. At room temperature almost all the casein molecules in milk are associated into casein micelles. Upon heating to 80-90°C both the size and the mutual interactions of these micelles increase through association with β-Lg. Since β-Lg is reactive towards casein micelles and to stainless steel, this molecule may act as a sticking agent between the micelles and the stainless steel surface (Jeurnink, 1991; Visser *et al.*, 1997).

If the colloidal stability of casein micelles in milk is decreased, the deposition process may no longer be controlled by denaturation of the serum proteins but directly by coagulation of casein micelles at the stainless steel wall (highest temperature). Furthermore, under these conditions (decreased colloidal stability) a decrease in the heat stability of the milk may also be observed. This parallel in behaviour suggests a link between these two processes. Hence the mechanism for deposition of casein micelles upon heating milk may be similar to that of the heat coagulation of milk (Jeurnink *et al.*, 1996c).

High pressure treatment can also disrupt the structure of casein micelles and denature the whey proteins β-Lg & α-La (Huppertz *et al.*, 2002). However, the pressures required to achieve this are much higher than those typically experienced in dairy processing e.g. >100 MPa for β-Lg, >500 MPa for α-La and >250 MPa for casein micelles (Huppertz *et al.*, 2004).

The second major contribution to fouling is mineral components of milk. There is an inverse relationship between calcium phosphate solubility and temperature. In milk, the main calcium salts are present in several forms of calcium phosphate and calcium citrate. The first precipitating form of calcium phosphate is usually dicalcium phosphate dihydrate which may be converted into the more stable calcium phosphate afterwards (Jeurnink *et al.*, 1996c). Calcium phosphate may precipitate from the solution and deposit directly on the stainless steel surface or it may deposit onto the casein micellar surface and/or onto β-Lg molecules in the serum phase (Visser *et al.*, 1997).

2.2.7 Factors affecting fouling

2.2.7.1 Milk pH

Burton (1968) states that it has long been recognised that milk of high acidity (pH values approaching 6) is likely to coagulate in a heat exchanger, so a reduction in the pH of milk would give a larger amount of deposit within a normal range of temperature where coagulation does not occur.

If the natural pH of milk (6.7 ± 0.1 at 20°C) was reduced (e.g. to 6.59 or 6.47) the rate of fouling was increased by a factor of 2.5 – 8.5 (Yoon & Lund, 1989). Similar trends have been shown by others (e.g. Burton, 1961; Burton, 1965; Gordon *et al.*, 1968; Skudder *et al.*, 1986; Foster *et al.*, 1989; Calvo & Rafael, 1995). The relationship between deposit formation and pH is non-linear and the effect of pH becomes greater as the pH falls (Burton, 1961; Burton, 1965; Gordon *et al.*, 1968; Foster *et al.*, 1989;). At the other end of the pH spectrum Skudder *et al.* (1986) showed that deposit formation was reduced as the value of pH increased.

The composition of the deposit altered with falling pH of milk (Skudder *et al.*, 1986; Foster *et al.*, 1989). The proportion of minerals decreased and the protein content

increased. Skudder *et al*. (1986) and Yoon & Lund (1989) also noted that the major group of proteins being deposited changed from serum proteins (at natural pH level) to casein micelles at low pH. Increased levels of fat were also reported by Skudder *et al*. (1986).

The increase in deposit formation may be explained by increased calcium activity and by casein micelles becoming unstable during heating as milk acidity is increased (low pH). Acidification causes the casein micelles to destabilise or aggregate by decreasing their electric charge towards that of the isoelectric point where casein becomes insoluble (Walstra *et al*., 1999). In addition, casein micelle reaction rates with β-Lg increase at low pH (e.g. Corredig & Dalgleish, 1996b). Casein micelles were also shown to form aggregates with fat in the low pH milk which may explain the elevated levels of fat found in the deposit at higher acidity.

2.2.7.2 Milk age

Storage of milk at room or refrigerated temperatures for 12-24 hours prior to processing, without change in pH, significantly reduces deposit formation (Burton, 1966; Burton, 1968; Al-Roubaie & Burton, 1979). Storage for extended periods however leads to an increase in fouling (Burton, 1968; Jeurnink, 1991).

Al-Roubaie & Burton (1979) proposed that the initial fall in deposit was due to the lipolysis of milk fat to fatty acids by the natural lipases found in the milk. One fatty acid (liberated during lipolysis) in particular, capric acid, had a marked effect in reducing deposit on the heated surface even at low concentrations (~ 1 mg/l). Capric acid was found to adsorb to the casein micelles and hence interfere with the casein aggregation during the build-up of deposits. Alternatively, Burton (1968) suggested the reduction may be caused by a redistribution of some of the mineral components following a drop in temperature when the milk leaves the udder or by the disappearance of some minor protein component on ageing.

The rise in deposition after extended storage may be due to the action of proteolytic enzymes, produced from psychrotrophic bacteria (organisms that grow readily in the temperature range 4-15°C) found in the milk. Proteolytic enzymes hydrolyse κ-casein, resulting in a decreased heat stability of the casein micelle, which will coagulate when heated forming an additional protein deposit (Jeurnink, 1991).

Jeurnink (1991) based this conclusion on results of experiments carried out with skim milk and similar results were reported by Ma *et al.*, 2001 for whole milk. Ma *et al.* (2001) suggest that the product of the hydrolysed κ-casein, para-κ-casein, may be a new active fouling species and modified the traditional fouling model to include it:

$$\Phi = \frac{k_d}{Re}\left[\exp\left(\frac{-E}{R_g T}\right) + (C_k)\right] \qquad (2.1)$$

where Φ = rate of fouling
k_d = deposition rate constant
Re = Reynolds number
E = activation energy
R_g = universal gas constant
T = temperature of solid-liquid interface
C_k = concentration of para-κ-casein

The concentration of the active species C_k was expressed in terms of the enzymatic activity:

$$C_k = k_a A_p \qquad (2.2)$$

where k_a = rate constant
A_p = proteinase activity

2.2.7.3 Seasonal variation

Milk, being a complex biological fluid, varies considerably in composition. This may be the result of natural variation or changes occurring after the milk has been drawn (Walstra & Jenness, 1984). Natural variation is caused by differences between breeds, stage of lactation, age of cow, gestation and environment factors such as feed, climate and stress. The variability in composition is reflected in the fouling formed during heat treatment.

Burton (1967) showed that there was a direct link between the stage of lactation (also Burton, 1972) feeding regime and breed of cow with deposit formation. More recently, Grandison (1988) found that deposits formed in the steam-heated section

(110-140°C) of a UHT pilot plant were more susceptible to variation over the year compared with deposits from the pasteurisation section (80-110°C). They were unable to correlate herd diet with fouling deposit however.

2.2.7.4 Milk preheating

The preheating of milk (often called forewarming) causes whey proteins to denature and to aggregate, which results in a reduction in fouling in later downstream processes (Bell & Sanders, 1944; Kessler & Beyer, 1991). Bell & Sanders (1944) first demonstrated this method in a UHT pilot plant where milk was held for 5-600 s at temperatures between 75-95°C. They found the higher the temperature the more significant the reduction in fouling rate in subsequent unit operations. However, the length of the holding time proved not as important. The effects of milk preheating on proteinaceous deposits have been investigated extensively using various combinations of preheating temperatures and holding times (Bell & Sanders, 1944; Lyster, 1965; Burton, 1966; Burton, 1968; Lalande *et al.*, 1984; Mottar & Moermans, 1988; Foster *et al.*, 1989; Jeurnink *et al.*, 1989; Yoon & Lund, 1989; Kessler & Beyer, 1991; De Jong *et al.*, 1992). Several theories have been proposed but most agree the principal reason for the benefits of preheating is due to the denaturation of the whey proteins, particularly β-Lg. Further reductions in fouling can be achieved by providing a holding section with a high volume to surface ratio which allows the conversion of native β-Lg to the aggregated form (De Jong *et al.*, 1992; Jeurnink *et al.*, 1996a).

2.2.7.5 Dissolved gases

The solubility of air in milk decreases upon heating (Walstra *et al.*, 1999) and if the local pressure is too low (below the saturation pressure), air bubbles can develop (Jeurnink, 1995a). Some researchers (Burton, 1968; Thom, 1975; Jeurnink, 1995a; Walstra *et al.*, 1999) have suggested that if these bubbles form at the heated surface they may act as nuclei for the formation of deposits and therefore greatly enhance the fouling rate.

It has been suggested that air in milk encourages fouling only if it forms bubbles on the heating surface (Burton, 1968; Jeurnink, 1995a). This point was illustrated by Gordon *et al.* (1968) who purposely entrained air into the milk flow to investigate the effect on fouling deposits. They found that fouling did not increase with increasing

air content. They concluded that the manner in which the air was incorporated did not duplicate conditions in commercial heating equipment. This was not expected because it is known that air leaks in commercial equipment lead to increased deposits (Wennerberg, 1981).

Theories have been provided to explain the role of dissolved air in fouling (Thom, 1975; Walstra & Jenness, 1984; Jeurnink, 1995a; Walstra *et al.*, 1999). At the start of the fouling process air bubbles generated by heating have been held responsible for inducing turbulence. This results in an increased heat transfer rate (Delsing & Hiddink, 1983). In their study, Delsing & Hiddink (1983) argued "In our case, it was particularly air bubble formation at the heat transfer surface in the early stages of the process which was held responsible for inducing turbulence and an increased heat transfer rate. The formation and attachment of air bubbles were seen to be greatest with protein-containing liquids, the protein stabilising the air bubbles. With UF permeate, air bubble formation was almost absent, as was the increase in heat transfer rate." However, the authors did not mention anywhere facilities for observing air bubbles on the heated surface during the runs except to say that the unheated outer surface of the annuli were made of glass. It is hard to see how one could have observed bubbles on the heated surface of the inner tube through the opaque fouling solutions.

Walstra *et al.* (1999) state that "At a hot surface in contact with a liquid, air bubbles of about 1 mm may readily form if the liquid contains sufficient air for it to become supersaturated at the high temperature. The air in the bubbles is, of course, saturated with water vapour. If a bubble remains at the surface, it can considerably enhance fouling. This is illustrated in Figure [2.5] for casein micelles, but it applies equally well to other substances depositing, say, serum protein. Protein adsorbs onto the bubble (1). The bubble acts as an insulator, whereby the temperature at (2) is higher than at (3), say 90°C and 80°C, respectively. This causes water to evaporate near (2) into the bubble, and to condense near (3), whereby water and heat are transferred...the relative water vapour pressures would be 0.72 and 0.48, respectively, and a substantial driving force for water transport thus exists. The liquid near (2) now becomes concentrated, leading to (greatly) enhanced deposition of protein. To overcome this problem, the milk should be evacuated before or during

heat treatment, or the milk should be kept at a sufficiently high pressure during heating."

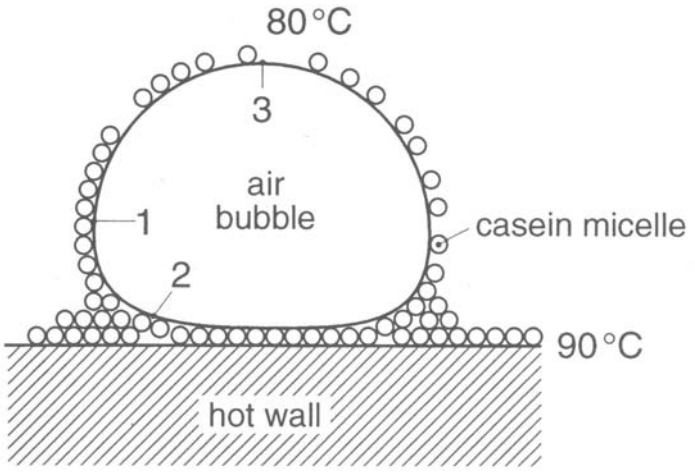

Figure 2.5 Air bubble formed at a heated surface and processes occurring near it. See text for explanation. Highly schematic and not to scale (Walstra *et al.*, 1999).

Jeurnink (1995a), a student from the same University as Professor Walstra and using the same equipment as Delsing & Hiddink (1983), provided a slightly different argument. "Air bubbles can contribute to the deposit if the surface to which they may attach becomes dry. As a consequence, there is an increase in the temperature difference between the hot stainless steel surface and the bulk of the liquid resulting in evaporation of water at the vapour-liquid interface. Due to this evaporation milk is transported from the bulk to the surface where the air/vapour bubble is attached. Here milk protein accumulates and because of the local increase in concentration and the high temperature the protein may coagulate and deposit on the surface. Eventually the air/vapour bubble bursts [*sic*] and part of the membrane is carried away with the liquid. The contribution of air/vapour bubbles to the deposit is determined by the amount of air present in the milk, the temperature difference between the surface and the bulk, the operational pressure in the heat exchanger and the wall shear stress." Figure 2.6 shows the schematic provided by Jeurnink (1995a) to illustrate the above argument.

It is also suggested that a similar phenomenon may occur in film evaporators processing dairy products as a result of nucleate boiling or insufficient product distribution over the heated surface (Jeurnink *et al.*, 1996c).

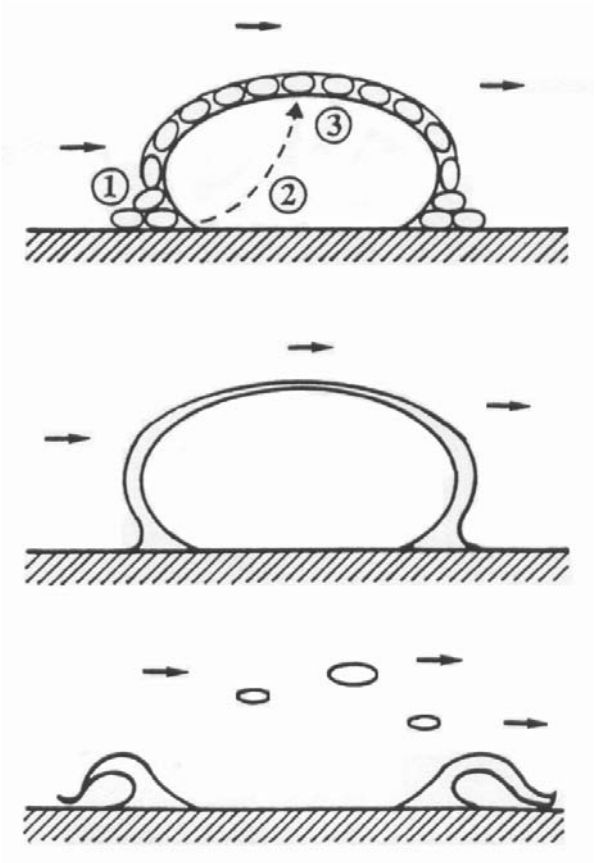

Figure 2.6 Schematic representation of the participation of an air bubble in the fouling process of milk (1) adsorption/deposition at the vapour/liquid interface (2) evaporation (3) condensation (Jeurnink, 1995a).

2.2.7.6 Surface condition

It is conceivable that since fouling occurs at the solid/liquid interface, the roughness of the surface may play an important role. Researchers agree that after the first deposit layer is established the surface roughness no longer plays a role in the fouling growth (Britten *et al.*, 1988; Yoon & Lund, 1989; Visser & Jeurnink, 1997). This is due to a shift from surface-deposit interactions to deposit-deposit interactions (Fryer *et al.*, 1995). It is generally accepted that rough surfaces favour deposit growth whereas smooth surfaces do not, but evidence on this issue is conflicting (e.g. Burton, 1988; Bott, 1989; Yoon & Lund, 1989; Bott, 1990). Yoon & Lund (1989) showed electropolished stainless steel did exhibit a slight decrease in fouling rate. But the savings in fouling reduction did not justify the cost of polishing the surface.

The first material deposited is important because it is responsible for the strength of the deposit-surface bond which may affect the cleaning rate (Fryer *et al.*, 1995).

Modifications of the surface properties may, in theory, prevent or limit the onset of fouling (Bott, 1989). Several studies have attempted to change the surface charge by bombarding the surface with highly accelerated ions (Muller-Steinhagen & Zhao, 1997; Beuf *et al.*, 2004; Santos *et al.*, 2004). The procedure does reduce fouling significantly and even reduces the tendency for the attachment of micro-organisms (Flint *et al.*, 2000). Other people have attempted coating the surfaces with a film of polymer or glass layer. But the results were mixed (e.g. Baier, 1981; Britten *et al.*, 1988; Yoon & Lund, 1989; Yoon & Lund, 1994b; Rosmaninho *et al.*, 2002; Santos *et al.*, 2004). Britten *et al.* (1988) found that different coatings on the heating surface did not affect the amount of deposit, but did affect the strength of adhesion. They concluded that the polar binding potential of the coated surfaces was the main factor influencing the strength of adhesion. Yoon & Lund (1989) showed there was little advantage gained when surfaces were coated with Teflon or sulphonated polyurethane since neither resulted in a decreased fouling rate.

2.2.7.7 Flow velocity

Generally, the higher the absolute fluid velocity in a heat exchanger the less fouling deposition takes place (Lund & Bixby, 1975; Bott, 1989; Bott, 1990; Belmar-Beiny *et al.*, 1993). Burton (1988) suggests a possible explanation for this general observation: at lower velocities the thickness of the laminar sub-layer adjacent to the heating surface is greater, so that the volume of material subject to higher temperatures, and the volume which remains for relatively long periods near to the surface, are greater.

Gordon *et al.* (1968) demonstrated that both the amount and extent of fouling decreased with increasing flow rates in a tubular heat exchanger. However, it is more difficult to relate fouling to flow rate in plate heat exchangers because of the complex flow geometries involved (Fryer *et al.*, 1995). It has been reported, upon heating simulated milk ultra filtrate in a rotating disk device, that deposition was eliminated if the wall shear stress exceeded 15 Pa (Jeurnink *et al.*, 1996c). The benefits of increasing fluid velocity to reduce fouling must be balanced against the additional pressure drop and associated pumping costs (Bott, 1989).

Most people studying the effect of Reynolds number on fouling operate in the transition region, which complicates the conclusions reached from the experimental

work (e.g. whether reductions in fouling occur due to changes in wall shear stress or changes in the flow regime from laminar to turbulent) (Visser *et al.*, 1997). In transport phenomena it is well known that the wall shear stress determines the friction factor which is a function of the Reynolds number, hence, flow velocity (Thomson, 2000). Therefore the limit of 15 Pa is not an absolute criterion but one that will change with the dimensions of the apparatus and the flow rate (and therefore Reynolds number). In conclusion, more work is required in order to understand the mechanisms which give rise to a decrease in fouling when the fluid velocity is increased (Visser *et al.*, 1997).

2.2.7.8 Equipment geometry

Low shear regions (dead spaces or stagnation areas called recirculation regions in fluid mechanics) located at complex valve assemblies, branches in pipeline systems and connections to measurement devices or sample ports are often prone to fouling (Bradley & Fryer, 1992; Truong, 2001). Bott (1989) states that stagnant areas can distort the temperature distribution and give rise to accelerated fouling reactions.

Plate heat exchangers with herringbone plates foul less than straight corrugated plates (up to 50% less). Herringbone plates have high mixing intensities that promote aggregation in the bulk rather than on the surface (Delplace & Leuliet, 1995).

Some novel heat exchangers (e.g. pulsatile flow, fluidised bed) have been shown to reduce fouling by inducing turbulence at the surface (Bradley & Fryer, 1992). This turbulence causes high surface shear stresses and eddy mixing and therefore the fluid spends less time at the surface (Bradley & Fryer, 1992).

2.3 EXPERIMENTAL SETUPS FOR FOULING INVESTIGATIONS

The majority of fouling studies discussed in the previous sections were based on laboratory and pilot scale investigations. Research equipment employed in these studies varied from simple stainless steel particles (e.g. Itoh *et al.*, 1995) to fully instrumented pilot scale heat exchangers (e.g. Jeurnink *et al.*, 1989). Most of this equipment was operated under low flow conditions and high temperature differences in order to achieve a reasonable amount of fouling in a short time and at the minimum cost of raw material. For example, the Netherlands Institute for Dairy

Research typically operated at 30 l/h for little over an hour in each run (e.g. Delsing & Hiddink, 1983; Jeurnink, 1991). Sometimes, flow rates as low as 5 l/h were used (e.g. Jeurnink, 1995a; Jeurnink, 1995b). However, important data such as characteristics of the fouling layer (physical, mechanical and chemical properties), fouling kinetics and extent of fouling resulting from different heat treatment regimes were obtained from these investigations. A limited number of studies were conducted by researchers able to obtain sponsorship from manufacturers of processing equipment and operated under actual industrial situations (e.g. Schreier & Fryer, 1995). It is interesting to note that the data of these industrial scale experiments do not contradict the data from the smaller scale pilot plant studies provided the authors have been careful enough to clearly define and control the parameters that affect the development of fouling.

The following sections outline the different test fluids used, the major designs of equipment and devices in pilot plant and laboratory studies and finally the techniques for the measurement of fouling.

2.3.1 Test fluid

Fresh whole or skim milk are obvious choices for the test fluid used during dairy fouling experiments, but researchers have used other fluids to study the phenomenon of dairy fouling for a variety of reasons. Many authors (Belmar Beiny & Fryer, 1992; Gotham *et al.*, 1992; Belmar-Beiny & Fryer, 1993; Belmar-Beiny *et al.*, 1993; Delplace *et al.*, 1994; Fryer & Bird, 1994; Delplace & Leuliet, 1995; Fryer *et al.*, 1996) argue for the use of model solutions made from reconstituted powders to avoid seasonal effects associated with fresh milk. The most common model solution used was made by reconstituting whey protein concentrate powders because the thermal stability of β-Lg is strongly linked with the formation of fouling deposits (Gotham *et al.*, 1992). However, it has also been noted that extension of the results to milk fouling is not straightforward owing to the influence of other milk constituents (Davies *et al.*, 1997).

Jeurnink (1995a) investigated the use of reconstituted skim milk as a model fluid. He found that reconstituted milk gave much less fouling than fresh milk and argued that “the already denatured serum proteins are less active in the fouling reaction”. He also stated that “The process of powder making and reconstitution presumably

caused other changes affecting the fouling behaviour. For example, the calcium concentration and the calcium ion activity in reconstituted milk had decreased by 9 and 11% respectively." These statements are perplexing. For example, it is difficult to visualise how the calcium concentration in milk could have been changed by the spray drying process. This would surely not be supported by a classical mass balance over the spray dryer. The best explanation that one can propose for the experimental results comparing calcium concentration and calcium ion activity between fresh and reconstituted milk presented by Jeurnink (1995a) is that even though the total calcium content is the same, the equilibrium between colloidal and soluble calcium has shifted after spray drying. However, the descriptions of experimental methods in that paper are so incomplete and the resulting arguments so vague that any retrospective conclusions by the reader about the significance of the work has to be a best guess at extrapolating what is said. For example, Jeurnink (1995a) reports that "calcium was determined after digestion according to NEN 6465 and by atomic absorption spectroscopy (NEN 6446)". But the paper only mentions sampling the clean-in-place fluid for analysis of calcium and nitrogen content which would refer to the composition of the deposits. There is no mention anywhere of sampling the fresh and reconstituted milk used in the runs.

Thus, one needs to be aware that the ability to reproduce fouling by fresh dairy products through the use of "model" fluids recombined from powders is limited even though it has advantages. More importantly, there is no strong experimental evidence that can yet explain the reasons for the difference in behaviour between fresh and reconstituted products.

2.3.2 Equipment

Burton (1961) used a U shaped tube made of stainless steel fitted with a threaded brass union at each end. The 'U-tube' was connected by the unions to lagged pipes through which oil was pumped at a constant flow rate from a thermostatically controlled oil bath. The tube was immersed in a stainless steel vessel of elliptical cross-section. The vessel was thermally insulated with felt and filled with milk. A small stirrer was fitted to the vessel through a Perspex lid to agitate the milk.

The amount of protein in the fouling deposits was correlated by dissolving it in an alkaline solution and forming a purple complex between copper salts in the solution

and substances in the fouling layer containing two or more peptide bonds. Burton (1961) showed that the optical density of the solution was repeatable with a better than 10% error in two series of triplicate runs. However, the relationship between the so-called 'Biuret' measurements and the actual weight of deposit were not as good and involved errors up to 200%. Burton (1961) suggested that this large scatter was caused by variations in the amount of dissolved minerals between the different experiments. The apparatus had the advantage of using small volumes of milk during trials that could be repeated from a common bulk.

Burton (1965) improved his original design by immersing a platinum wire heated by an electrical current in a pressurised vessel containing milk at rest. The purpose of controlling the pressure above the milk with a stream of compressed air was to "prevent boiling of the milk at the heating wire surface". The weight of fouling after 90 minutes was very small, an average of 0.63 mg dried deposit for 68 runs. Burton (1965) used the difference in temperature between the wire and the milk as an indication of the rate of fouling. This apparatus was used to study differences in deposit formation resulting from changes in milk pH, composition or preheat treatment.

Britten *et al*. (1988) described a laboratory apparatus in which deposits were formed on preheated or coated stainless steel discs under controlled conditions. The apparatus consisted of a chamber in which hot oil was circulated at 100°C. The surface of the chamber was covered with a disc, the test piece, which was held down by a nut pressing onto an O-ring. This chamber was inserted in the milk container, a jacketed vessel placed on a magnetic stirrer, so that the fouling surface was completely immersed in the milk. The temperature of the jacket was kept constant at 60°C while the stirring rate was set at 200 rev/min to ensure renewal of milk material close to the surface without inducing severe shear stress at the surface.

This system was used to determine the adhesion strength of deposits formed on various polymer-coated surfaces and surfaces of different degrees of roughness. The amount of fouling material deposited and its strength of adhesion were related to the surface properties of the disc. "An adhesion parameter was defined as the proportion of deposited material remaining on the surface after a stress had been applied to remove it. The stress was obtained in an ultrasonic bath (35 kHz)". The authors do

not describe how the stress was calculated from the parameters monitored in the ultrasonic bath.

Fryer & Pritchard (1989) used a heated radial flow cell (RFC) "originally developed by Fowler" and successfully used by Duddridge *et al*. (1982), to study the influence of surface shear stress on the adhesion and removal of bacteria in flowing liquid. Fryer *et al*. (1985) used the RFC to study the fouling of reconstituted skim milk. The device consisted of a pair of flat parallel discs. The fluid entered through the centre of one disc and flowed radially outwards. Its velocity and therefore the surface shear stress on the discs decreased from the centre outwards. The fouling deposits obtained varied across the surface of the plate and corresponded to different temperature differences monitored by thermocouples situated at difference positions. This provided "several data points simultaneously, and this is the information that would be of most value when using the device as a monitor". Due to the gap being narrow (usually less than 2 mm) the device was not useful to study heavy fouling.

Fryer & Pritchard (1989) compared the RFC to another device called the tapered tube. This device consisted of a tapered tube, 400 mm in length, varying in internal diameter from 19.0 mm at the inlet to 12.7 mm at the outlet. Like the RFC, a range of shear stresses and surface velocities was produced simultaneously for a given flow rate, but the converging flow was more stable than the diverging flow of the RFC. The authors note, however, that both the tapered tube and the radial flow cell would need to be installed in side streams of heat treatment equipment. Therefore it would be difficult to simulate the same type of treatment in the side stream as found in the rest of the equipment.

Many researchers used plate heat exchangers to study fouling (e.g. Burdett, 1974; Lalande & Corrieu, 1981; Skudder *et al*., 1981; Lalande *et al*., 1984; Sandu *et al*., 1984; Yoon & Lund, 1989; Delplace *et al*., 1994; Yoon & Lund, 1994a; Calvo & Rafael, 1995; Delplace & Leuliet, 1995; Jeurnink, 1995a; Jeurnink & Kruif, 1995; Fryer *et al*., 1996; Schreier *et al*., 1996; Christian *et al*., 2002). Unlike the fouling devices described previously, pilot scale plate heat exchangers simulate more effectively designs found in commercial plants. However, plate heaters are hydrodynamically complex equipment where fluid flows between a series of corrugated plates induce a range of shear rates and temperatures, both of which

affect the rate of fouling. Furthermore, the designs of the plates vary greatly among manufacturers, thus it is extremely difficult to develop models for understanding either kinetics or mechanisms of deposition. However, plate heat exchangers allow deposit distribution and composition to be determined by disassembling the heat exchanger at the end of a run.

Another common apparatus used by researchers to study fouling is the tubular heat exchanger (e.g. Burton, 1968; Lund & Bixby, 1975; Swartzel, 1983; Jeurnink *et al.*, 1989; Belmar-Beiny *et al.*, 1993; Fryer & Bird, 1994; Jeurnink, 1995a; Davies *et al.*, 1997; Fung, 1998; Benning *et al.*, 2003). Usually the tubes are held in a bundle making fouling deposits inaccessible. Therefore, the deposit's distribution and composition cannot be determined directly. Generally, the fouling material is removed by rinsing solutions which can be chemically analysed. Some authors (Belmar-Beiny *et al.*, 1993; Fung, 1998) have used model tubular heat exchangers in which tubes can be removed thus eliminating this disadvantage. The advantage of using a tubular heat exchanger for fouling studies is that the equations for predicting heat transfer and friction factors are well known.

2.3.3 Measurements of fouling

2.3.3.1 Direct

Researchers often measure the amount of fouling simply by physical methods such as mass or thickness of the deposit. Obviously these methods are intrusive and require the system to be shutdown and therefore are only suitable for laboratory or pilot plant studies.

The methodology for weighing fouling deposits varies slightly among researchers (Skudder *et al.*, 1981; Skudder *et al.*, 1986; Yoon & Lund, 1994a; Delplace & Leuliet, 1995; Fryer *et al.*, 1996). The generic procedure is as follows:

- Fouled plates from the heat exchanger are flushed with a minimum amount of water.
- Plates are dried in ambient air or oven.
- Drying duration varies from 6 hours to overnight.
- Plates are weighed directly.

Fouling deposit weight measurements cannot take place with conventional shell and tube heat exchangers. Therefore this method is generally only applicable to plate heat exchangers and model tubular heat exchangers with removable tubes. The weighing technique only gives an overall measurement of fouling over the entire surface at the end of a run.

Local measurements of fouling are based on thickness measurements usually made with conventional measuring devices such as micrometers or verniers (Jeurnink *et al.*, 1989; Truong *et al.*, 1998). Again, they can only be made at the end of the run but allow a better understanding of the distribution of fouling across the surface. Deposit thickness measurements are difficult to obtain on plate heat exchanger plates that are corrugated. Similarly, thickness measurements can usually only be obtained at the ends of the tubes of a tubular heat exchanger.

Direct techniques also allow other important fouling data to be obtained including physical and chemical properties of the deposit. Microscopic methods such as light microscopy and scanning electron microscopy have been used to characterise the topography and structure of the deposits. Transmission electron microscopy has been used to define internal structures and to locate protein, fat and mineral components within the deposits.

2.3.3.2 Indirect

Measurements of fouling during a run have to be obtained from inline sensors that measure some parameter that is affected by the formation of fouling deposits.

- *Heat transfer coefficient*

This method involves the calculation of the decrease in heat transfer coefficient (local or overall) as a result of fouling deposit build up. The basic heat transfer equation relating the heat flux across a surface, q, to the temperature driving force, $\Delta\theta$, between a hot and cold fluid can be given by:

$$q = U\Delta\theta \tag{2.3}$$

The actual parameter that one needs to monitor fouling is the thermal resistance of the fouling deposit, R_f. This is obtained by subtracting the resistances to heat

transfer contributed by the wall, the hot fluid and the test fluid from the overall resistance, which is the inverse of the overall heat transfer coefficient. Assuming that the system is completely steady during a run, the sum of these resistances will remain constant and equal to the inverse of the overall heat transfer coefficient at the beginning of the run before fouling has developed. Thus:

$$\frac{1}{U} = \frac{1}{U_0} + R_f \tag{2.4}$$

where U_0 = heat transfer coefficient at t = 0

In practice, the heat transfer rate $\phi = qA$ is calculated from the increase in temperature of the test fluid across the heat exchanger:

$$\phi = c_p m(\theta_o - \theta_i) \tag{2.5}$$

where c_p = heat capacity of test fluid
m = mass flow rate of the test fluid
θ_o = outlet temperature of test fluid
θ_i = inlet temperature of test fluid

The temperature driving force in equation (2.3) must be a log mean temperature difference, $\Delta\theta_{LMTD}$, across the entire heat exchanger. This method only gives a global measure of fouling over the entire apparatus. As fouling proceeds the overall heat transfer coefficient decreases and a rate of fouling can be derived by taking its derivative with respect to time. This derivative is sometimes called the Biot number (e.g. Fryer, 1989).

There are a number of uncertainties in the assumptions underlying this method. For example, the conductivity of the wall will be affected by the temperature. Similarly, as the fouling layer builds up the flow channels will reduce in size affecting both the velocity and the heat transfer coefficient (e.g. Visser *et al.*, 1997). However, under normal conditions the reduction in channel diameter is small and the changes in Reynolds number are relatively minor.

- *Pressure drop*

As fouling proceeds the reduction in size of the flow channels result in an increase in pressure drop over the heat exchanger. In severe fouling systems, typically UHT heat exchangers, this process can easily be monitored with reasonable accuracy by using differential pressure sensors (Visser *et al.*, 1997).

For a given flow rate, the relationship between the differential pressure, ΔP, and the hydraulic diameter, D, of a flow channel is given by the following equation (McCabe *et al.*, 2001):

$$\Delta P = \frac{2fL\rho v^2}{D} \tag{2.6}$$

where f = friction coefficient
L = length of pipe
ρ = density of the fluid
v = flow velocity

Corrieu *et al.* (1986) used the change in hydraulic diameter to define a fouling parameter, α:

$$\alpha = \frac{D_0 - D}{D_0} \tag{2.7}$$

where D_0 = hydraulic diameter at t = 0

Corrieu *et al.* (1986) then stated that the friction factor is a function of the Reynolds number:

$$f \approx Re^{k_2} \tag{2.8}$$

Where the Reynolds number is defined as:

$$Re = \frac{Dv\rho}{\mu} \tag{2.9}$$

where μ = dynamic fluid viscosity

The f and v terms can be eliminated from equation (2.6) by using equations (2.8) and (2.9). Corrieu *et al*. (1986) argue that the final expression for the fouling parameter is:

$$\alpha = 1 - \left(\frac{\Delta P_0}{\Delta P} \right)^{\frac{1}{3}} \tag{2.10}$$

where ΔP_0 = differential pressure at t = 0

The assumptions used by Corrieu *et al*. (1986) in their derivation are not clearly stated and the definition of the hydraulic diameter in particularly does not follow standard definitions in fluid mechanics (e.g. McCabe *et al*., 2001). The reader is well advised to read the paper carefully before using the equations proposed by Corrieu *et al*. (1986).

The pressure drop rises towards the breaking stress of the equipment when any location in a flowing stream of the PHE is blocked by fouling. This can happen in UHT operations (e.g. Fryer *et al*., 1996), however, for systems that have a low level of fouling, equation (2.10) shows that the change in pressure drop is not large which prompted Burton (1966) to state “Pressure drop measurements should never be used as a means to determine deposit quantities…”.

2.3.3.3 Local fouling measurements

It is well known that the velocity and temperature distributions of real heat exchangers are very complex. Therefore, the rate of fouling is not the same in different parts of the equipment. The design of heat exchanger geometries that would minimise fouling requires the measurement of local fouling.

The problem with local measurements of fouling is that the rate of heat transfer can no longer be measured by a change in temperature of the fluid expressed in equation (2.5). This has been replaced by the use of heat flux sensors (e.g. Jones *et al*., 1994; Truong *et al*., 1996; Davies *et al*., 1997; Truong *et al*., 1998; Croy *et al*., 2002). These sensors consist of a thermopile across the two faces of a thin wafer of known thermal conductivity that generates a voltage which can be measured. Jones *et al*. (1995) used such a device to successfully monitor milk fouling in a small heated cell. Truong *et al*. (1998) successfully used heat flux sensors to measure

locally the rate of fouling on unheated surfaces in two commercial plants. However, they found that ambient conditions near the sensor made the trace difficult to interpret. To solve this problem, the temperature of the external pipe wall was also monitored which allowed calculation of the internal overall heat transfer coefficient. This coefficient was normalised with its initial value which collapsed data from disturbed and undisturbed ambient conditions into a more reproducible pattern. Pilot plant trials carried out by the same authors showed the probe could detect fouling deposit thickness up to 3 mm.

Withers (1994) developed and tested an ultrasonic device mounted on a pipe to detect and monitor fouling during UHT processing in a pilot scale plant. The device operated on the following principle: an ultrasonic pulse from a transmitter takes a finite time to travel through the pipe wall, the product and the opposite pipe wall, determined by the velocities of the sound in those materials. This time will remain constant (providing all other factors are constant) until a fouling film forms. Assuming that the velocity of sound in the fouling film is different from that of the product then the time taken for the sound to travel through the system, known as the time of flight, will change as the film replaces some of the product. If the change in time of flight is measured and the sound velocity in the fouling film is known, then the thickness of the film can be determined. The prototype sensor was able to detect the presence of deposits with a minimum thickness of 0.1 mm and measure the thickness of films over the range 0.5 to 6.0 mm. Compensation for temperature effects was applied to the technique for both milk and water products over the temperature range 20-130°C. Flow rates up to 10 l/min and processing pressures up to 3×10^5 Pa did not affect the sensor, however, further testing at different process conditions is still required.

Withers (1996) described the use of an optical sensor for the detection of fouling. The technique relies on the ability to install ‘sight glasses’ in experimental equipment, or in the case of commercial application, pipes of processing plants. Obviously, any sight glass used will need to exhibit fouling characteristics similar to that of the stainless steel pipe. The principle of operation relies on the light-reflectance characteristics of the boundary between the transparent sight glass and the product changing in the presence of a fouling film. In practice, a preliminary sensor, developed by the Danish Biotechnological Institute, was affected by process

conditions including flow rate and temperature. Development and refinement of the sensor has led to a complex design in which the product was forced to flow along a specially designed channel within the sensor so that fouling produced there matches that produced in other parts of the plant, such as in heat exchangers. The lower limit of sensitivity in terms of film thickness was in the order of 0.01 mm.

The Danish Technological Institute also developed another sensor based on the principles of acoustic emission (Withers, 1996). The sensor was especially designed for use in plate heat exchangers in which a small vibrating transducer was bonded to the surface of a plate on the process fluid side of the plate pack. The presence of a fouling film on the sensor has two effects: first, it damps down the amplitude of the vibrations; second; it shifts the natural frequency slightly. Both of these effects can be measured and related to the degree of fouling. The sensor was found to be sensitive to temperature (but this could be reliably compensated for at the signal processing stage) and could operate under realistic processing conditions, these being 100-200 kPa, 5-140°C and 0-30 l/min.

Measurement methods developed after 2003 are not included in this literature review.

2.4 CONCLUSION

The phenomenon of fouling with particular regard to the dairy industry has been investigated extensively over the years. Important information regarding the composition, chemistry, mechanisms and factors that affect fouling has been provided. However, there are still important aspects that have not been resolved including issues regarding experiment reproducibility, investigation of the all important induction period, and detailed investigation into the effect of low flow rates and pressures on fouling experimental results. In particular, much speculation has been offered on the role of air in fouling without any formal investigation or factual proof provided. Other factors that affect fouling including milk quality and enzymatic damage, have been poorly investigated in the literature.

MATERIALS AND METHODS

3.1 INTRODUCTION

This chapter describes the methods, materials and equipment used to investigate fouling on heated surfaces. The preheating equipment developed specifically for this work was embedded into a milk powder pilot plant designed and built jointly by a team of five postgraduate students with help from the Institute of Food, Nutrition and Human Health (IFNHH) technicians. The pilot plant is described in section 3.2 with each subsection covering a specific part of the plant or its operation. Section 3.3 describes the methods of measurements and analysis. Specific details (descriptions and sources) of all equipment and materials used in this research are summarised in Tables A.1, A.2 & A.3 of Appendix A. A brief overview of the experimental program is given in section 3.4.

3.2 PILOT PLANT

The pilot plant consisted of a storage vat, a preheating section, an evaporator, a spray dryer and a clean-in-place (CIP) system. The plant was built in several stages the first of which concentrated on the preheating section. Bennett (2000) and Croy (2000) provide detailed descriptions of this section. A small three-effect falling film evaporator was added next followed by a spray dryer.

A simplified schematic of the pilot plant including the preheating and evaporator sections is given here for the reader's convenience in Figure 3.1. Detailed schematics of the major research equipment including piping and instrumentation diagrams of the entire plant (excluding spray dryer) are given in Figures A.1 – A.6 of Appendix A. A photograph of the plant up to and including the evaporator is shown in Figure 3.2. A list of components used in the construction of the pilot plant is provided in Table A.1 of Appendix A and the major plant items relevant to this research are described in detail below.

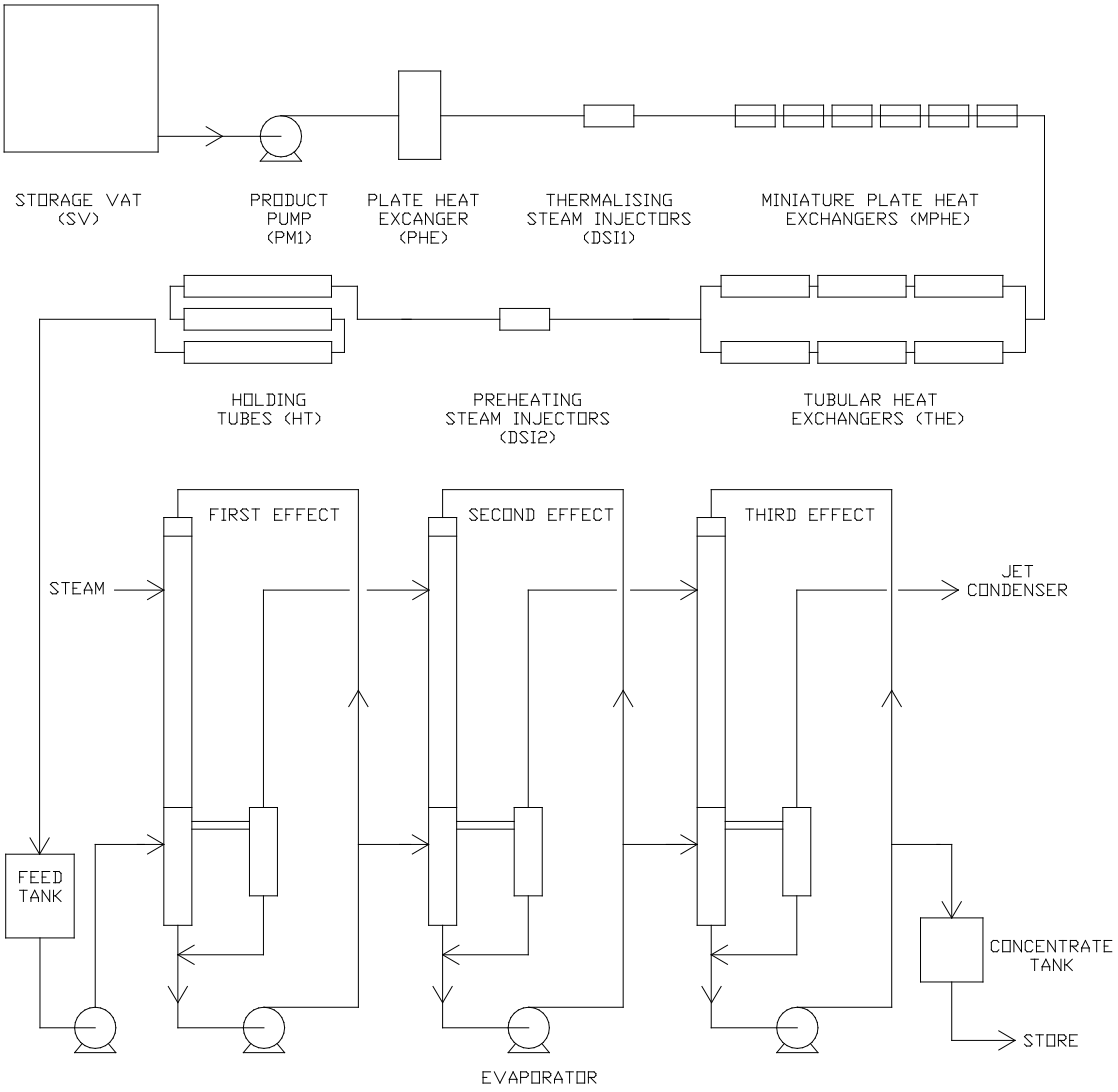

Figure 3.1 Schematic diagram of pilot plant depicting standard set up of process fluid flow.

The plant was built mainly of 12.7 mm industry grade stainless steel (316 or 304) tubing with a number 4 finish (approximate relative surface roughness Ra = 1.0 μm). Hygienic dairy unions were used to connect piping between unit operations but in some instances (e.g. heating fluid side) regular unions were employed to reduce costs. Flow was normally routed with stainless steel ball and butterfly valves but needle valves were used when fine flow control was required (e.g. outlet of the tubular heat exchanger).

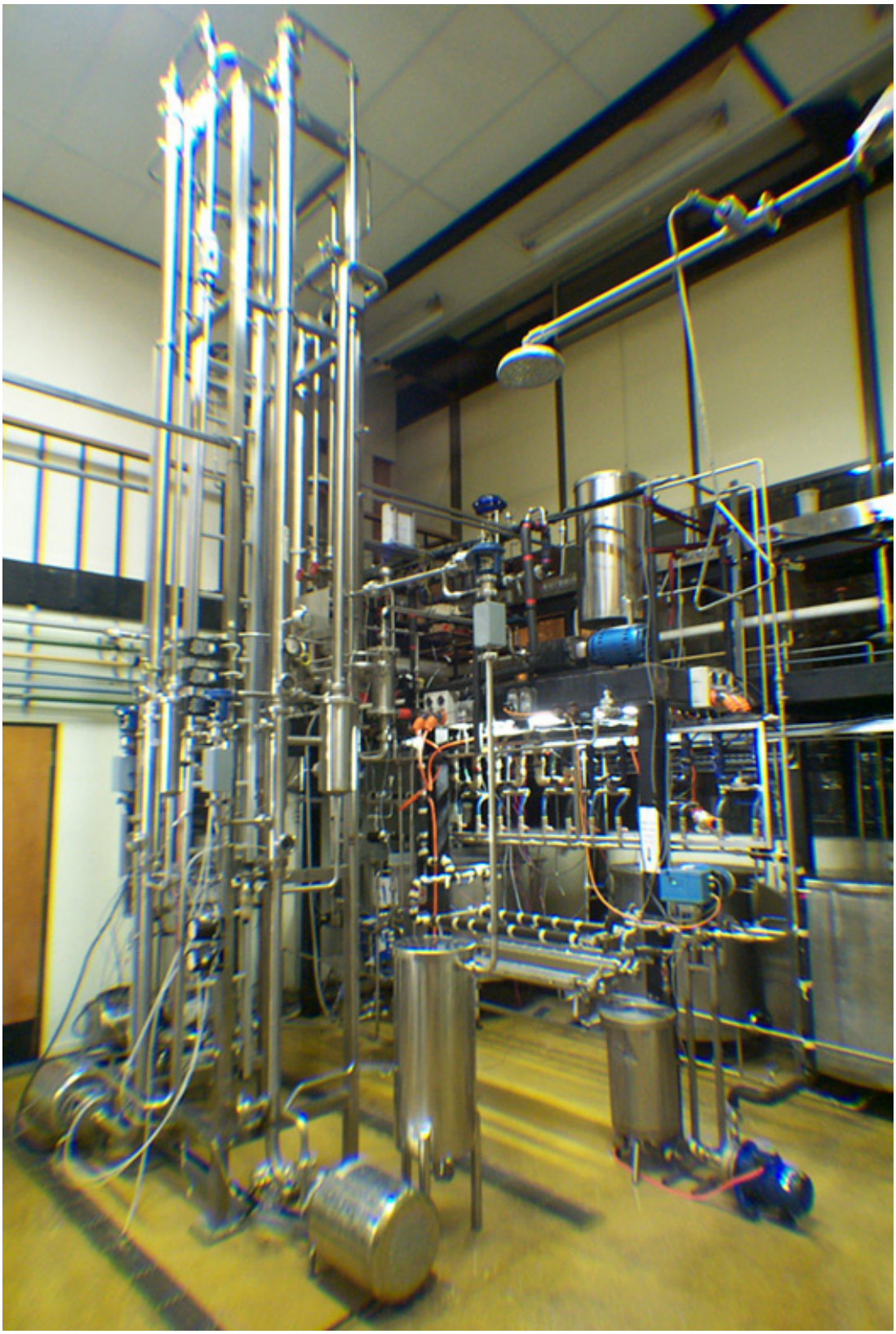

Figure 3.2 Photograph of the pilot plant showing preheating (right) and evaporator (left) sections.

3.2.1 Preheating

The preheating section consisted of components that can be assembled in a variety of configurations depending on the nature of the experiment. The standard assembly is shown in Figure 3.1. The process fluid (milk supplied from a local dairy factory (properties reported in Appendix F.3), reconstituted whey (Appendix F.2) or water) was stored in an 850 litre refrigerated tank (SV) with agitator (SVA). The fluid could be pumped at flow rates in the range 30-2 000 l/h from the vat using a centrifugal pump (PM1) controlled by a variable speed drive (VSD1). A commercially manufactured plate heat exchanger (PHE) brought the temperature of the process fluid from the refrigerated temperature (e.g. 4°C) to the target experimental temperature usually in the range 30-70°C. Direct steam injection (DSI) units (DSI1) could be used in conjunction with the PHE to provide instant temperature elevations of 5-20°C depending on the experimental flow rate. DSI was used predominantly in microbial type experiments particularly when the growth of thermophiles was targeted into specific items of equipment and growth in connecting pipes was discouraged. DSI was generally not used in fouling experiments because the injected steam introduced flow rate spikes detrimental to the successful monitoring of fouling rates. Two research heat exchangers (THE and MPHE) followed and the process fluid could be routed through either one first depending on the nature of the experiment. Before entering the evaporator feed tank (FT) the process fluid was heated (via a second DSI unit: DSI2) and could be held at constant temperature (in a holding tube bank: HT) if required.

3.2.1.1 Miniature plate heat exchanger (MPHE) rig

Custom built fouling modules were designed for the pilot plant to provide a suitable surface for the study of fouling and bacterial contamination during processing. Six modules were built into an array so that a number of heat exchange surfaces could be studied in any one run. The array was known as the miniature plate heat exchanger (MPHE) rig. The design of the rig was based on the following objectives:

- To provide an easily accessible fouling surface which could be inspected at any stage during the operation of the plant. The surface also had to be removable so that the fouling could be photographed and examined under such equipment as a microscope before being disturbed from the surface.

- To allow the independent isolation of each module from the plant flow at any time during processing so that the heat exchange surface could be inspected without stopping the product flow.
- To ensure each module did not significantly increase the temperature of the fluid moving through the process side. The aim was to have the temperature profile across the rig as uniform as possible so that the modules would be comparable in terms of process fluid temperature.
- To allow the heat exchange surface to be subject to relatively high and stable heat fluxes. This meant that a liquid to liquid heat transfer scenario with the two fluids separated by a wall similar to that found in a plate heat exchanger was preferred to liquid to air heat transfer.
- To allow the installation of sensors to monitor heat flux and temperature.

Figure 3.3 shows a three-dimensional model of the module developed. Each module consisted of two stainless steel chambers separated by a thin (0.6 mm) removable stainless steel plate. The process fluid flowed through one side and hot water (heating medium) passed through the other. To create a tight seal between the three components two silicone rubber gaskets were inserted, one on either side of the removable plate. When the module was packed the gaskets lined up with the chambers' flanges. The packed module was held together by 4 wing-nuts and bolts, one located at each corner of the flanges. One module provides approximately 10 cm^2 of heat exchange surface.

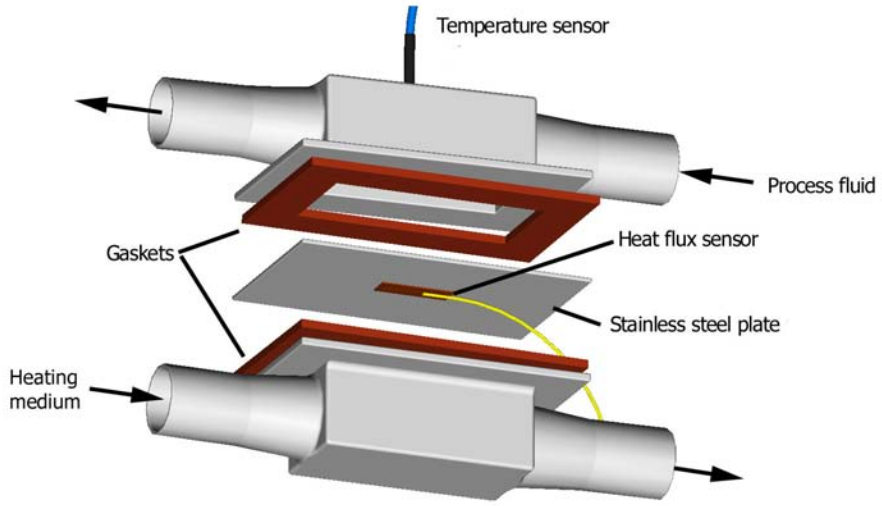

Figure 3.3 A three-dimensional representation of a module developed for the study of fouling and bacterial contamination.

The MPHE rig was constructed from six modules connected together in series. A photograph of the array is shown in Figure 3.4. A detailed piping and instrumentation diagram of the MPHE rig is provided in Figure A.2 of Appendix A. The rig can be described as two headers (one each for the processing and heating sides) with twenty-four branches (four for each module). During start up, the process and heating fluids initially flowed through the headers while the branches are isolated by a series of valves (i.e. no fluid entering the module). To activate a module the corresponding valves on the header lines are shut while the valves on the branches are opened. In this state the entire volumes of the processing and heating fluids passed through the module.

Figure 3.4 Photograph of the miniature plate heat exchanger rig.

Through the same system of valves a single module could be isolated (essentially reversing the activation process) at any point during operation allowing the run to continue uninterrupted. After isolation, the MPHE could be disassembled allowing the test plate to be inspected and physical measurements such as deposit weight to be made. To allow isolation, the utility side of the module was deliberately connected to the rig using a flexible plastic hose fitting. This gave the heating medium chambers some movement when the wing-nuts were removed.

The heating medium used in the current research was hot water generated by an electric element (HE2) installed in a 50 litre stainless steel tank (HM). The water was recirculated through a circuit that provided heating to both the MPHE rig and the tubular heat exchanger by a centrifugal pump (PM2) as shown in Figure A.1 of Appendix A.

A heat flux sensor (e.g. H1) could be attached to the test plate within the heat exchange surface area. The installation and description of the heat flux sensor is discussed in detail in section 3.3.2.2.

A temperature sensor was installed within the process fluid chamber. Initially, a resistance temperature device (RTD) was installed in the MPHE using a tube socket weld union but this was later replaced by a type-T thermocouple (e.g. T9) due to lag and error in the RTD-well measurement as discussed further in section 3.2.2.2.

3.2.1.2 Tubular heat exchanger (THE) rig

The tubular heat exchanger (THE) rig was designed to study fouling on heat exchange surfaces in a similar manner to the MPHE. The THE rig had a much larger heat exchange surface area than the MPHE so sufficient amounts of fouling could be produced to be chemically analysed. As well as meeting the objectives of the MPHE the THE had to provide a surface area at a controlled temperature for the colonisation of thermophiles. This allowed the release of thermophiles into the bulk milk flow to be studied at the optimum range of thermophile growth.

Figure 3.5 shows the tubular heat exchanger rig installed in the pilot plant. A detailed piping and instrumentation diagram of the THE rig is provided in Figure A.3 of Appendix A. The THE was arranged into two parallel banks of three tubes in series. The tubes were designed concentrically with three tubes inside one another. The process fluid flowed through the central chamber while the heating medium could flow on either or both sides of the product, providing heating on both the inner and outer surfaces if necessary. A schematic drawing of a single tubular heat exchanger is given in Figure 3.6, which shows this configuration. For this project heating was provided only by the inner tube to avoid complexities in the monitoring of fouling. In this case, fouling would only develop on the outer surface of the inner tube which will be referred to as the test tube for the remainder of this thesis.

Figure 3.5 Photograph of the tubular heat exchanger rig.

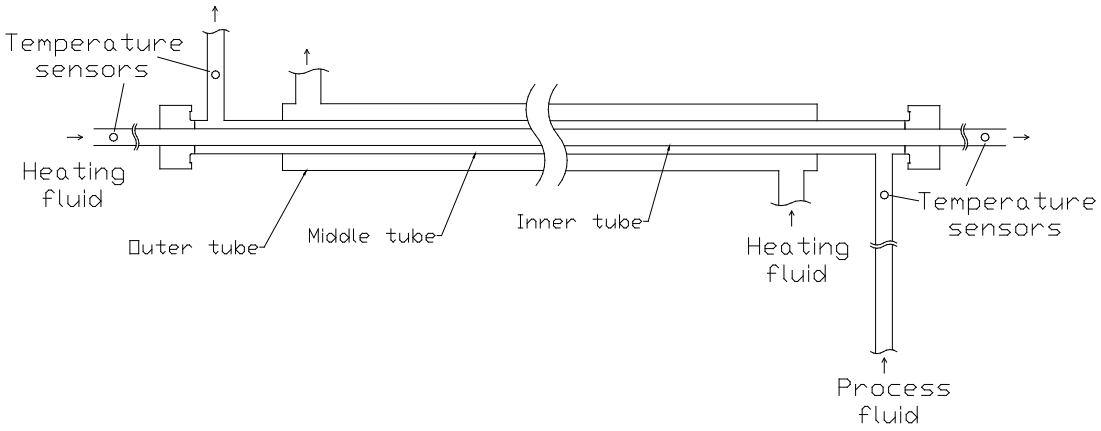

Figure 3.6 The assembly of an individual tubular heat exchanger.

Temperature sensors (RTDs or thermocouples) were installed at the inlets and outlets of each tube on both the heating and process fluid sides. Combined with a flow meter (F1) installed at the heat exchanger inlet, these sensors were used to monitor the onset and build up of fouling in each individual tube. Section 3.3.2 provides further detail on these sensors and the monitoring of fouling.

The THE rig was especially designed for easy disassembly for examination of the test tube surfaces after a run. This enabled visual and analytical study of the fouling

produced. This design also allowed individual test tubes to be isolated through a system of piping bypasses, without stopping the process flow. Any test tube could therefore be removed and studied at any time during a run. This is shown in the piping and instrumental diagram of the THE in Figure A.3 of Appendix A. This design feature was used during Hinton's study but not in the current project.

3.2.2 Instrumentation and data acquisition

3.2.2.1 Control room and data acquisition

All on-line sensors in the pilot plant were wired back to a Programmable Logic Controller (PLC) housed in a control cabinet located in the control room. The PLC was connected to a computer which provided a user interface and along with the PLC was used to control various process variables in the plant. A photograph of the control room and cabinet is shown in Figure 3.7.

Figure 3.7 Pilot plant control room and cabinet showing PLC (right).

The PLC consisted of an Allen Bradley SLC 5/03 processor and two racks each with 12 module bays. The modules installed in the bays included: 2 analog current (32

channels), 2 counter (8 channels), 5 analog (20 channels), 2 relay output (16 channels), 5 thermocouple (20 channels) and 4 RTD input (16 channels) modules. A total of 112 channels were available to the plant for sensor input and delivery of control outputs. On occasion, a standalone Supervisory Control and Data Acquisition (SCADA) station was coupled to the PLC to provide additional sensor channels (e.g. used when experiments required the operation of all six MPHE modules and all six THE tubes at the same time).

The control computer was used to display and log data from the PLC and also provide PID feed back control to the pilot plant via the PLC. This was achieved using FIX DMACS Version 7.0 software installed on a Microsoft Windows NT 4.0 platform. Although the PLC was capable of PID control calculations, these were carried out by writing control loops in FIX DMACS to allow quick reprogramming of the control loops.

All sensor measurements were available to the plant operator via the control screens used to interface with the plant. Real-time trending of variables could be viewed using the historical display software which also ran while the plant was in operation.

All data managed by the computer were logged to disk automatically. A sample of each sensor measurement was logged to disk every second. Control variables such as pump speeds were logged every 30 seconds. Data required for further analysis would be exported from the FIX DMACS software into comma-delimited text files so that they could be manipulated as a spreadsheet in Microsoft Excel.

The FIX DMACS software was also used to perform simple calculations in real-time. These included all sensor calibration calculations and important analytical data calculations like overall heat transfer coefficients. The calculated values were automatically logged to disk and could be displayed in real-time on the control screens and/or historical data display.

3.2.2.2 Temperature measurement

A combination of T-type thermocouples and resistance temperature devices (RTDs) were used to measure temperature across the preheating section of the pilot plant (T1-31). The majority of temperature measurements were made by thermocouples,

with RTDs only being used in less crucial areas (e.g. feed vat) where measurement accuracy was less important. Originally, RTDs were used for all temperature measurements but during the commissioning stage it was found they had a slow response time and could not accurately measure rapid changes in temperature. This function was important to the successful monitoring of fouling particularly when coupled with heat flux sensors. Bennett (2000) discusses in detail the issue of temperature measurement and gives a full account of the change from RTD to thermocouple sensors.

All temperature sensors were calibrated by recording the temperature of distilled ice/water slurry (0°C) and boiling distilled water (100°C), designated as θ_0 and θ_{100} respectively. Measurements were recorded at each temperature every second for five minutes and averaged to obtain the recorded temperature (θ_r). The calibration constants were obtained by assuming a linear relationship between the recorded and correct (θ_c) values:

$$\theta_c = a\,\theta_r + b \tag{3.1}$$

where θ_c = correct temperature
θ_r = recorded temperature
a = gradient constant
b = y-axis intercept constant

For the freezing and boiling points of water these constants are:

$$a = \frac{100}{\theta_{100} - \theta_0} \tag{3.2}$$

$$b = -\theta_0 a \tag{3.3}$$

These equation constants were entered into the computer interface to display the calibrated values on-screen, not the raw recorded values. A sample calculation is provided in Appendix D.1.

3.2.2.3 Flow rate measurement

Several flow meters where used to monitor process fluid and cleaning flow rates throughout the plant. Two electromagnetic flow meters were used in the preheating

section, one for low flow rates (30 – 300 l/h: F1) and one for higher flows (300 – 10 000 l/h: F2). They were installed in parallel and the flow could be diverted through either one depending on how the pilot plant was being used at the time. The larger flow meter was generally only used to monitor CIP fluid flow through the plant but was sometimes used during visualisation experiments when large flow rates were required. The smaller flow meter was used the rest of the time.

Each flow meter was calibrated by operating at a range of flows, in which the flow meter was needed, and recording the actual flow rate with a measuring cylinder and stopwatch. Collected data were recorded in a spreadsheet and linear equations fitted to create calibration equations relating recorded flow to actual flow rate. As with the temperature calibration, the constants from these equations were entered into the computer interface so that the calibrated measurement was displayed on-line and in real time.

3.2.2.4 Pressure measurement

Pressure sensors were installed throughout the plant to monitor pressures in the process and steam lines. Locations of the pressure transmitters are given in the pilot plant's piping and instrumentation diagrams of Appendix A. Depending on the pressure at each location either a 0 – 50 PSI.g or a 0 – 15 PSI.a sensor was used.

On-line measurement of pressure was critical to the successful operation of the plant. In the preheating section the sensors were used to ensure good performance from the DSI units because when the process line pressure approached the steam pressure, the performance of the DSI units dropped. Also, the operating pressure of the heat exchangers was found to be very important during fouling experiments. Accurate measurements of the pressure in the process line were therefore required before and after the throttling valves leading to the research heat exchangers.

All pressure sensors were calibrated against a calibrated manual pressure gauge over a range of different pressures.

3.2.3 Operating procedures

Operating procedures and experimental protocols used for the pilot plant were developed over 12 months of commissioning. Control of small details in the operating

procedures was essential for the successful replication of fouling experiments. This was clearly realised through the long and expensive months of commissioning because even small innocuous changes in the operation protocol created significant differences in the fouling patterns. Therefore, the operating procedures in this work are reported in detail. A generic operating procedure is described in the following section and details of individual experiments noting variations from this generic procedure are given in the data disk outlined in Appendix H. A worksheet listing the steps that were followed and information recorded for a standard fouling run is also given in Appendix B.

3.2.3.1 Plant preparation

All heat exchange test surfaces (THE tubes and MPHE plates) were prepared according to the following protocol:

- Submerge in a 1 % v/v caustic solution at 60°C for 1 hour.
- Remove from the solution, manually wipe with a cloth and rinse in water at 60°C.
- Submerge in a 1 % v/v nitric acid solution at 60°C for 1 hour.
- Remove from the solution, manually wipe with a cloth and rinse in water again at 60°C.
- Dry in ambient air.
- Assemble the research heat exchangers.

If heat flux sensors were used they were attached to the MPHE plates before installation into the rig as described in section 3.3.2.2.

3.2.3.2 Start up protocol

- Switch on the main power supply and control computer.
- Inspect the control cabinet and computer for errors. Troubleshoot if errors are present.
- Ensure all the on-line sensors are displayed correctly on the computer.
- Open the steam, water, vacuum and compressed air isolating valves.
- Fill the heating medium tank to the research heat exchangers with water.
- Switch on the heating medium recycle pump and set the temperature controller to the desired value (e.g. 90°C).
- Manually adjust the water flow rate to the DSI supplying the plate heat exchanger to reach the desired temperature (e.g. 70°C).
- Fill the 350 l CIP tank with water.

- Manipulate the valve system to connect the feed pump to the CIP tank.
- Switch on the feed pump and set its speed to pump water at the flow rate used in the experiment.
- Adjust the back pressure valves after the PHE and the research heat exchangers to the required level (e.g. 90 and 50 kPa.g).
- Switch on the temperature controllers of the DSI units and manually adjust the set points.
- When temperature readings are steady switch the controllers to automatic mode.
- The plant is now running in steady state conditions with regards to flow, pressure and temperature.

3.2.3.3 Run protocol

- Prepare the process fluid and transfer to the main holding vat.
- Switch the feed supply from water in the 350 l CIP tank to the process fluid in the main holding vat.
- Make minor adjustments to temperature, pressure and flow rate if required and allow the system to stabilise.
- During the run remove air released by the heating process from high locations in the plant using sterile syringes via the rubber septa used for taking process fluid samples.
- In areas of the plant where high air build up is observed insert a syringe permanently to removed air continuously.
- At the end of a run switch the fluid supply back from the holding vat to the 350 l CIP tank flush with warm water for 15 minutes.
- Stop all pumps, release back pressure valves and open all drain valves.
- Remove all the fouling test surfaces used and replace with blank surfaces.

3.2.3.4 Clean In Place (CIP) protocol

A standard CIP procedure similar to that used in the New Zealand dairy industry was used for cleaning the plant before and after each experiment. This consisted of five steps including a caustic and nitric acid cycle with hot water rinses before and after each cycle.

- Fill the 350 l CIP tank with water heated by direct steam injection to 60°C.

- Prepare the CIP chemicals by adding the appropriate amounts of caustic soda and nitric acid to heated water (60°C) in order to create 1% v/v solutions of each. Each CIP fluid has a dedicated tank that can be manipulated to supply the CIP pumps through a series of manual butterfly valves.
- Pump the CIP fluids at 2 000 l/h through the plant in the following order:
    - Water, once-through for 15 minutes
    - Caustic, once-through for 5 minutes then recirculate for 25 minutes
    - Water, once-through for 10 minutes
    - Nitric acid, once-through for 5 minutes then recirculate for 25 minutes
    - Water, once-through for 15 minutes

During all cycles the CIP pump was used in conjunction with the process fluid pump to produce turbulent flow conditions (Re = 24 000) in the preheating section of the plant. The cleaning procedure was repeated in the evaporator section using the evaporator feed pump and the three calandria recycle pumps. At the completion of the cleaning, the plant was ready for another experiment or for shut-down. More detail on the CIP equipment and CIP optimisation can be found in Croy (2000).

3.2.3.5 Shut-down protocol

- Set all DSI control valves to zero.
- Turn off all pumps and set all temperature controllers to zero.
- Close all utility valves and open all drain valves.
- Backup all the experimental data.
- Turn off main electrical supply including control computers.

3.3 METHODS OF MEASUREMENT AND ANALYSIS

3.3.1 Direct fouling measurement

Direct measurements of fouling, some of which were used to validate the indirect measurements, are described in this section. These include mass and height measurements as well as the recording of fouling structures through photography during and after a run.

3.3.1.1 Mass

Cleaned and dried heat exchange surfaces were measured before and after a run with sensitive balances. THE tubes were weighed on a three decimal place flat base

balance with a precision of ± 0.01 g. MPHE plates were weighed on a four decimal place balance with a precision of ± 0.001 g. The total mass of foulant was obtained by subtracting the weight of the original clean surface from the fouled surface. The foulant was then removed from the surface by scraping and weighed. The masses recorded from the measurements of the scraped foulant and the undisturbed foulant were within 3% of each other.

3.3.1.2 Thickness

The fouling correlated with the heat flux sensors (section 3.3.2.2) on the MPHE plate could not be weighed because the sensors occupied only a small section of the plate. A special device was developed to measure the thickness of a fouling layer at the completion of an experiment. The instrument consisted of a plate support, a metal needle mounted on a dial depth gauge and a multimeter. The precision of the depth gauge was ± 0.01 mm. Figure 3.8 shows a photograph of the instrument.

Figure 3.8 Photograph of the deposit thickness measuring device (a) plate support (b) dial depth gauge (c) multimeter.

The multimeter was connected to the support plate on one end and to the needle on the other end. A fouled MPHE plate was mounted on the support plate, the needle lowered to the deposit surface until a connection was made. This was indicated by a non-overload value of resistance on the multimeter. The depth gauge reading was recorded and the needle was further lowered through the fouling until it was stopped

by the MPHE surface. The difference in the two depth gauge readings gave the local deposit thickness.

To validate the output of the heat flux probe (described in section 3.3.2.2) it was important to take thickness measurements directly above the location of the probe on the plate. A template built into the plate support ensured that thickness measurements were only made above the area of the plate where the probe had been attached. Five random measurements were made within the area indicated by the template, which gave an average thickness measurement.

3.3.1.3 Photography

- *Still camera*

The structure of the fouling on the heat exchange surfaces was captured using digital cameras. The THE tubes were secured in a brace that could move along a track in front of a camera. This ensured the tube was always the same distance away from the camera and therefore, always in focus. Approximately 22 photos were taken on each side (upper and lower) of the tubes. The topography of a MPHE plate could be captured in one frame so they were placed flat on a bench with a camera fixed directly above the plate. All photos were taken in a darkened room with light being provided by two adjustable lamps. All cameras were connected to a television monitor so an enlarged image could be previewed before the photo was taken.

Some magnified images were also taken with a digital camera connected to a light microscope. Different magnifications could be obtained from this set up depending on the final use of the image.

- *Video camera*

A digital video camera was used during the whey and water trials to capture the topography of a heat exchange surface during a run. The camera was installed directly above a modified MPHE module shown in Figure 3.9. The MPHE module had the top removed and replaced with a flange similar to the bottom side. A Perspex section was fixed to the top flange through a series of nuts, bolts and a gasket.

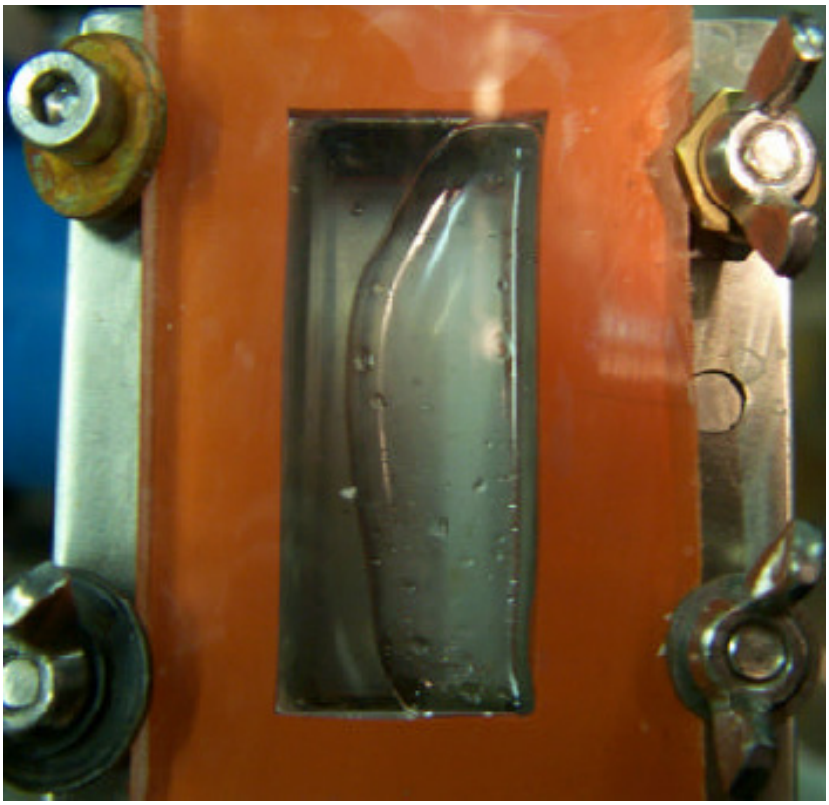

Figure 3.9 Photograph of the modified MPHE showing transparent Perspex section.

To ensure that the video camera could record events on the MPHE heated surface a dilute solution was required. Simple laboratory experiments showed that a 0.1% whey solution could provide adequate foulant material while still remaining translucent.

- *Image analysis*

Photographs of fouling structures including stills captured from videos taken during the runs were analysed using Sigmascan Pro Image Analysis software Version 5.0. Although the software was powerful and many different types of measurements could be made, several months were spent configuring the program to complete the required tasks. For example, to determine the percentage of the heat exchange surface covered by fouling the following procedure was developed:

1. Import the image (digital photo or frame capture) into Sigmascan and crop areas not required for analysis (usually areas outside of the heat exchange surface).
2. Increase the contrast between the fouled and non-fouled regions using the historical stretch function.

3. Apply a measure overlay to the fouled area (usually achieved by assigning a pixel intensity threshold).
4. Apply a measure overlay to the area outside of the heat exchange surface.
5. Configure Sigmascan to measure desired characteristics of the image (in this case, number of pixels).
6. Activate the count.
7. Calculate the percentage of heat exchange area covered by fouling from the resulting data.

Figure 3.10 shows screen shots of the Sigmascan software using the above technique. In this example, the area of heat exchange surface covered by fouling was approximately 23%. Determining the area of the heat exchange surface covered by fouling allowed the foulant loading to be calculated. In this thesis, the foulant loading was expressed as the total mass of fouling per unit area of the heat exchange surface covered by fouling.

Sigmascan was also used to determine feret diameters of fouling protuberances during and after a run. In Sigmascan, the feret diameter gives the diameter of a pseudo circular object that has the same area as the current object. Scans of sodium dodecyl sulphate polyacrylamide gel electrophoresis (SDS-PAGE) gels were also analysed and compared against densitometry outputs.

Due to the large number of images produced in any single run, macros were written in Visual Basic to automate the complex image analysis tasks that would otherwise be carried out manually.

Further details of methodologies used with the Sigmascan software are provided in Appendix E.

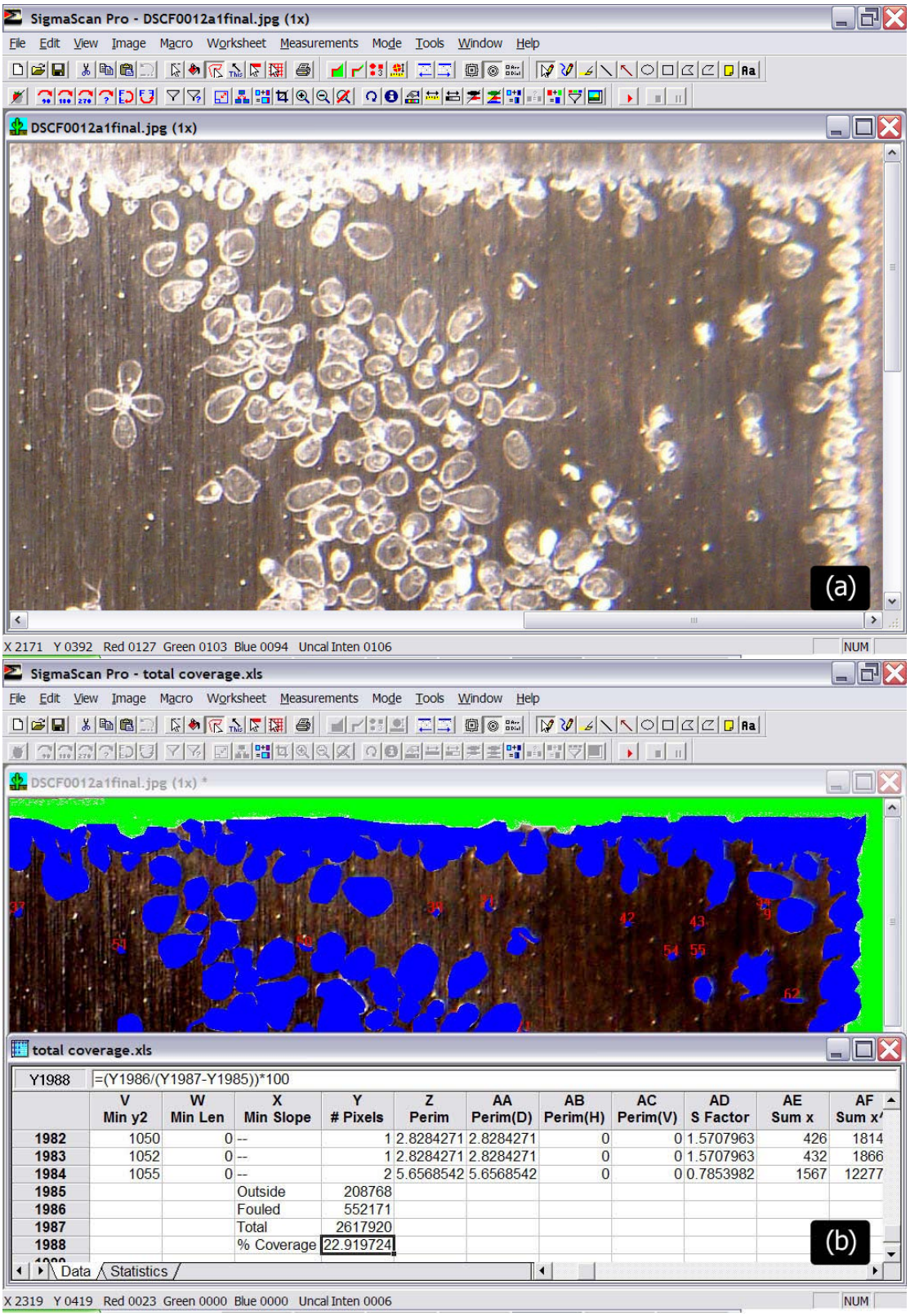

Figure 3.10 Sigmascan Pro Image Analysis software showing the original image (a) and the analysed image including the measurement output (b). Note: the blue overlay indicates the areas of fouling and the green overlay indicates the area outside the heat exchange surface (not measured).

3.3.2 Indirect fouling monitoring

Two methods of monitoring fouling *in situ* are described in this section. They both rely on using the heat transfer coefficient to estimate the heat transfer resistance which is linked to the mass of fouling deposit. The first method measures the global amount of fouling in the equipment. The second measures local fouling development over a small surface area of the heated surface.

3.3.2.1 Theory

The heat transfer flux, q, is given by:

$$q = \frac{\phi}{A} = U\,(\theta_{hm} - \theta_p) \tag{3.4}$$

where ϕ = rate of heat transfer

A = surface area

U = overall heat transfer coefficient

θ_{hm} = temperature of the heating medium

θ_p = temperature of the process fluid

The overall heat transfer coefficient is defined as the inverse of the total heat transfer resistance, R. In our case, heat is transferred from the heating medium through the heat exchanger wall to the process fluid as shown in Figure 3.11. The total heat transfer resistance is made up of several components: the resistance contributed by the process fluid, R_p; the resistance contributed by the fouling layer, R_f; the resistance contributed by the stainless steel wall and its attachment, R_w; and the resistance contributed by the heating medium, R_{hm}. The overall heat transfer coefficient at a given time is therefore represented by:

$$U = \frac{1}{R} = \frac{1}{R_p + R_f + R_w + R_{hm}} \tag{3.5}$$

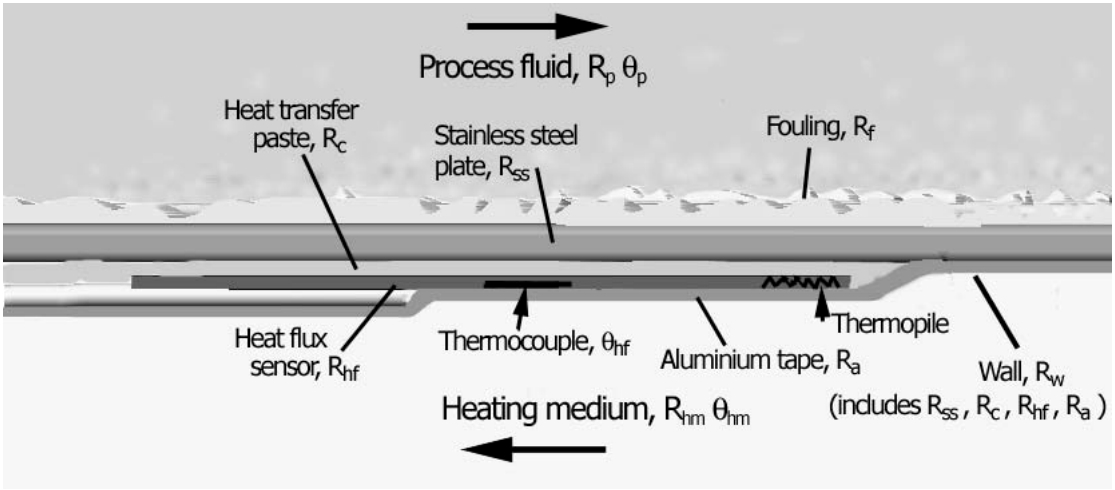

Figure 3.11 Schematic drawing of the sectional view of a fouled surface showing the thermal resistances across the heat exchanger.

With a constant flow of heating medium and product, the sum of resistances, R_p, R_w and R_{hm} may be approximated by the inverse of the initial overall heat transfer coefficient, U_0, measured at the beginning of the run when the surface is clean. Therefore the resistance of the fouling layer can be estimated from calculations of the overall heat transfer coefficient:

$$R_f = \frac{1}{U} - \frac{1}{U_0} \tag{3.6}$$

Rearranging equation (3.6) gives a normalised overall heat transfer coefficient, N_f:

$$N_f = \frac{U}{U_0} = \frac{1}{1 + R_f\ U_0} \tag{3.7}$$

In theory, N_f values range from 0 to 1. At the start of a run R_f equals 0 and therefore N_f equals 1. During a run where fouling builds to a sufficient level to affect the heat transfer, N_f begins to decrease below 1. The difference between the local and the global measurement of fouling lies in the calculation of the heat flux. A sample calculation is provided in Appendix D.3.

3.3.2.2 Local measurement of fouling

In the local monitoring system, the heat flux was measured directly by thin-foil heat flux sensors (Appendix A.1). The heat flux sensors consisted of thermocouples in

series (thermopile) bonded to two sides of a thin 6 x 18 x 0.2 mm wafer of thermal insulating material, polyimide. When heat flows through the sensor, thermal energy generates a small voltage differential between the junctions on the upper and lower surfaces. Since the temperature differential is proportional to the voltage differential and the thermal conductivity of polyimide is known, the heat transfer rate can calibrated directly against the voltage.

The sensors have a sensitivity of 0.317 $\mu V/Wm^{-2}$, a thermal resistance of 0.002 $°C/Wm^{-2}$, a maximum heat flux of 114 kW/m^2 and a response time of 0.4 s. A photograph of the sensor is shown in Figure 3.12.

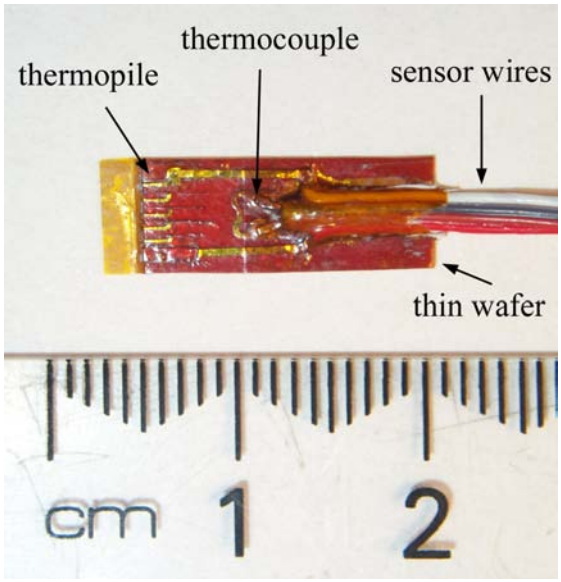

Figure 3.12 Photograph of a thin-foil heat flux sensor.

A Type T thermocouple was incorporated on-board the thin wafer that measured the surface temperature of the heat flux sensor. The thermocouple was located near the centre of the thin wafer on the non-contact surface of the probe.

Each heat flux sensor was supplied with a certificate containing an individual calibration factor and a temperature correction graph that related the sensor temperature to a temperature multiplication factor. The calibration factor of the heat flux sensors was not checked independently by the candidate due to the difficulty in building calibration equipment for heat flux. The method to calculate the heat flux from the raw signal of a sensor is described in detail elsewhere (Bennett, 2000) and is reproduced in the Appendix D.2 for the reader's convenience.

All calculations were performed by the FIX DMACS software in real-time so that calibrated values could be displayed to the operator via the computer interface. All values, including intermediate calculation data, were logged to disk each second.

The sensors were attached to the MPHE removable plates using aluminium tape and heat transfer paste compound. At the end of a run, the sensors could be removed from the plates and be reused. This allowed the plate to be washed easily and the height of the fouling above the sensor location to be measured. A photograph of an attached sensor is shown in Figure 3.13.

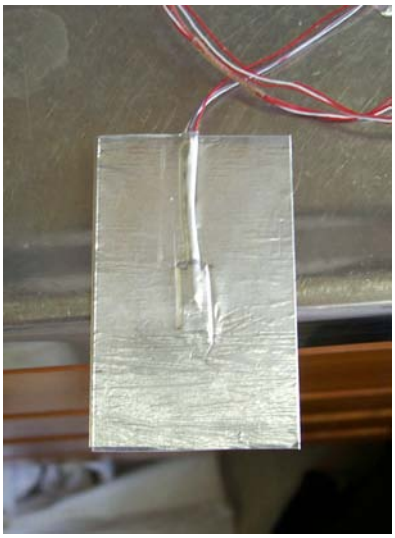

Figure 3.13 Heat flux sensor attached to a MPHE plate.

The method of attaching the sensor has a strong influence on both the overall heat transfer coefficient and the development of fouling on the plate surface immediately above the sensor location (Bennett, 2000). A basic method was developed during the preliminary commissioning runs of the pilot plant. This method was improved upon several times during the experimentation period to provide more consistent and stable contact between the sensor and the MPHE plate. The final method is as follows:

- Aluminium tape was cut into a rectangle larger than the test plate.
- The desired attachment position of probe was marked on the adhesive side of the tape with a scribe using one corner of the tape as a reference point. This desired attachment position was generally at the centre of the test plate.

- The probe was placed on the adhesive side of the tape as indicated by the scribed lines.
- A uniform layer of heat transfer paste was applied to the exposed surface of the probe.
- The tape with attached probe was placed on the plate so that the reference corner of the tape was set flush with one corner of the plate. This would result in the probe being located in the centre of the plate.
- The aluminium tape was pressed down ensuring no air bubbles were caught between tape and plate. It is important to use a paste of high conductivity to minimise added resistances to the system and interference with the fouling development of the product (Bennett, 2000) and air bubbles in the paste should be eliminated.
- The excess tape was trimmed from the plate.

Care was always taken and the same method was always used when applying the sensor to the plate surface to achieve uniformity and consistency between formal experimental runs.

The aluminium tape, the heating medium and the heat flux sensor itself add further thermal resistances (R_a, R_{hm}, R_{hf}) to the stainless wall (R_{ss}). The four of them make up the resistance R_w in local fouling measurements and they should not change over the duration of the run. Because the heat flux sensor comes with an in-built thermocouple the temperature of the wall surface on the hot side is measured and the accuracy of the calculations were improved by using only the internal overall heat transfer coefficient, U_i, by cutting out the resistance in the heating medium and aluminum tape. Therefore, equation (3.6) becomes:

$$R_f = \frac{1}{U_i} - \frac{1}{U_{i0}} = \frac{1}{R_p + R_{ss} + R_c + R_{hf} + R_f} - \frac{1}{R_p + R_{ss} + R_c + R_{hf}} \qquad (3.8)$$

where U_{i0} = initial internal heat transfer coefficient

With the use of this internal heat transfer coefficient defined by equation (3.8) the resistances of the aluminium tape, R_a, and the heating medium, R_m, are no longer relevant. However, the resistances of the heat flux sensor and the conductive paste still affect this coefficient. The successful use of equation (3.8) hinges on the fact

that the resistances of the paste and the heat flux sensor remain stable during a run. The greatest concern is the possible expansion of an air bubble between the sensor and the stainless steel plate because of prolonged heating of the paste during a run. Therefore, care was always taken to ensure the minimal amount of paste was used during attachment of the sensors. The specified resistances of the paste and the heat flux sensor are relatively insensitive to temperature changes.

The temperature on the product side was measured with a T-type thermocouple located directly above the heat flux sensor. Originally RTDs located in temperature wells were installed for this function however, there were many problems. One of the most important problems was the greater thermal inertia of the thermal well. This meant that the readings from the heat flux sensor thermocouples and the RTD were not synchronised and the lag time between the two sensors varied, depending on the conditions of the experimental runs, introducing errors in the value of the calculated heat transfer coefficient. This problem was avoided when using a thermocouple because the thermocouple was placed directly into the product stream without the use of a thermal well. Figure 3.14 shows a schematic diagram of the local monitoring system including the locations of all sensors.

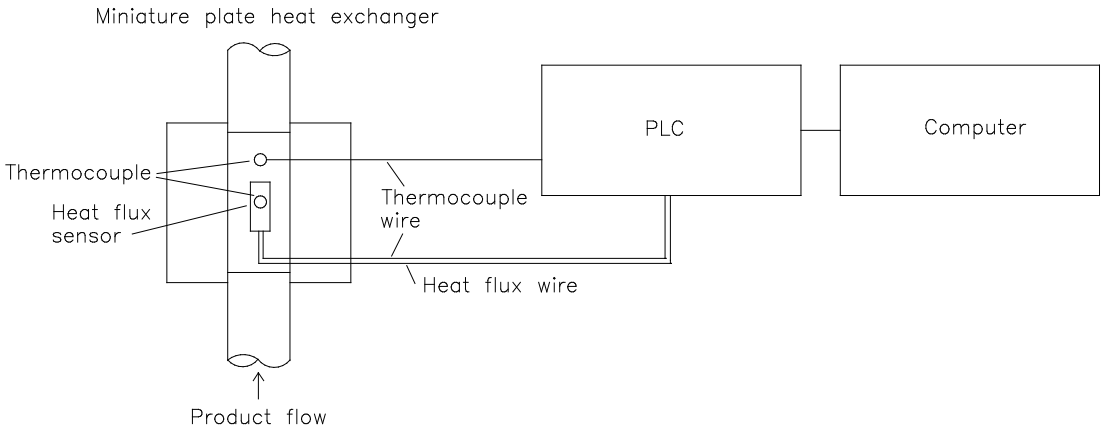

Figure 3.14 Schematic diagram of the local fouling monitoring equipment implemented in the MPHE rig.

3.3.2.3 Global measurement of fouling

In the tubular heat exchanger the overall heat transfer coefficient was calculated from an energy balance between the heating medium and the product streams using the equation:

$$\phi = U\ A\ \Delta\theta_m \tag{3.9}$$

where $\Delta\theta_m$ = mean temperature difference between heating and product streams

Under the assumption that pure counter current conditions exist in the tubular heat exchanger, the mean temperature difference is defined as a logarithmic mean temperature difference, $\Delta\theta_{LMTD}$ given by:

$$\Delta\theta_{LMTD} = \frac{(\theta_{hm} - \Theta_p) - (\Theta_{hm} - \theta_p)}{\ln\left(\frac{\theta_{hm} - \Theta_p}{\Theta_{hm} - \theta_p}\right)} \tag{3.10}$$

where θ_{hm} = inlet temperature of the heating medium

Θ_{hm} = outlet temperature of the heating medium

θ_p = inlet temperature of the process fluid

Θ_p = outlet temperature of the process fluid

Assuming heat loss to the environment is negligible (the system is insulated), the rate of heat transfer was estimated from the measurement of process fluid flow rate as follows:

$$\phi_{hm} = \phi_p = c_{p,p}\ m\ (\Theta_p - \theta_p) \tag{3.11}$$

where ϕ_{hm} = rate of heat lost by the heating medium

ϕ_p = rate of heat gained by the process fluid

$c_{p,p}$ = heat capacity of the process fluid

m = mass flow rate of the process fluid

Figure 3.15 shows a schematic diagram of the global monitoring system including the locations of all sensors.

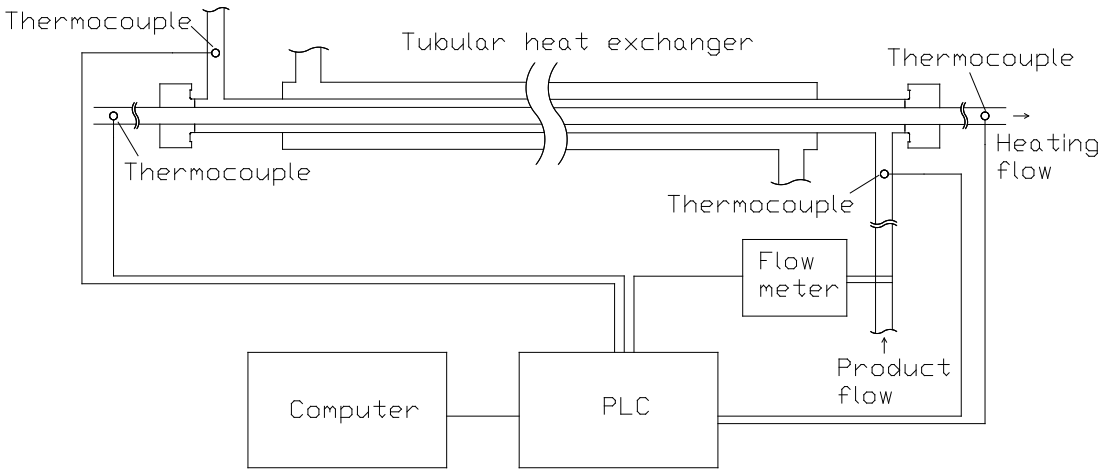

Figure 3.15 Schematic diagram of the global fouling monitoring equipment implemented in the THE rig.

Note that the THE system uses the overall heat transfer coefficient not the internal heat transfer coefficient used in the MPHE system. Therefore, for a successful estimate of the resistance of the fouling layer it was important to keep the heating side stable. Hence, the flow rate and the temperature of the hot side were controlled automatically. In addition, the use of the $\Delta\theta_{LMTD}$ makes this measurement suitable only for an estimate of global fouling over the entire equipment.

3.3.2.4 Calculations from fouling curves

- *Fouling rate*

The fouling rate was estimated from plots of N_f versus time (often named fouling curves). As mentioned in section 2.2.3, fouling curves can exhibit three distinct periods (induction, fouling and post-fouling periods). For estimations of fouling rates, only the linear portion of the fouling period was considered. The limits of the linear portion were selected and the slope of the line between these two points was calculated. It was assumed that the fouling curve was completely linear between these two points and the fitted line was represented by the equation:

$$y = m\,x + c \tag{3.12}$$

where m = rate coefficient

c = constant

The fouling rate was expressed as the rate of change of N_f per second:

$$\frac{dN_f}{dt} = \frac{|m|}{3600} \tag{3.13}$$

To illustrate this methodology an example fouling curve from a THE run is shown in Figure 3.16.

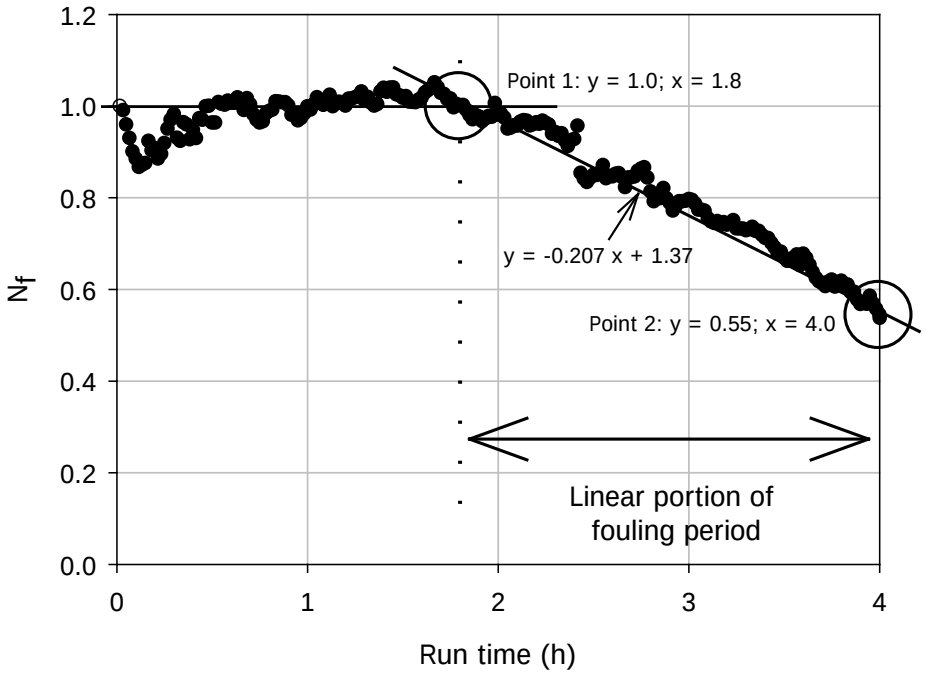

Figure 3.16 Plot of N_f versus run time showing the method used to calculate the fouling rate (R1.4).

In the above case the fouling rate is:

$$\frac{dN_f}{dt} = \frac{0.207}{3600} = 5.76 \text{ x } 10^{-5} \text{ s}^{-1} \tag{3.14}$$

The slope of the line could have been calculated by performing a linear regression over all of the points in the linear portion of the plots. This was carried out for the above example and the calculated fouling rates differed between the two methods by 1.0 %. A decision was made to use the simpler method in this study.

In some runs part of the fouling curve may exhibit a reduced fouling rate which may be indicative of the post-fouling period mentioned in the literature (section 2.2.3). In these cases the fouling rate would be based on the first linear portion of the curve and this value was used as the fouling rate for the whole run. This phenomenon and other characteristics of fouling curves are discussed further in section 4.2.1.

- *Final N_f value*

The final N_f value was determined for fouling curves produced by the local and global systems by averaging the last 2 - 5 minutes of N_f data prior to test surface isolation. These final N_f values were compared to direct measurements of fouling which is discussed further in section 4.2.3. Sample calculations of the above two methods are provided in Appendix D.4.

3.3.3 Chemical procedures

3.3.3.1 Enzyme

- *Whey extraction*

Whey produced from the growth of thermophilic bacteria in milk was crudely extracted based on the method outlined by Jeurnink (1991). Whole milk (3.3% fat) was inoculated with *Bacillus stearothermophilus* (B12 Cm) and incubated at 55°C for 48 hours. During the incubation period the number of thermophiles typically reached a maximum of 10^5 cfu/ml. The supernatant was collected after the milk was centrifuged at 16 400 g for 20 minutes and vacuum filtered. The filtered solution, which contained secreted bacterial enzymes, was stored in sterile containers at -18°C. This method of collecting secreted bacterial enzymes from a thermophile strain represents the worse case scenario. It is highly unlikely that these conditions would be experienced in industry but if these enzymes do not have an effect on fouling it would be safe to assume that there would be no effect in the industrial environment.

- *Preparation and incubation of Neutrase*

Neutrase '0.8L' is a bacterial protease produced by a selected strain of *Bacillus amyloliquefaciens*. Further technical detail of this protease is given in Appendix F.1. Neutrase was microfiltered and diluted 1/100 with deionised water. For the Neutrase trials a fixed quantity of Neutrase solution was added to the milk but the plant operating parameters were modified in different runs.

- *Trichloroacetic acid (TCA) assay for enzyme activity*

Standardised, homogenised whole milk was incubated with whey extract or Neutrase for 1 hour at 4°C. The enzyme reactions were stopped by the addition of 10% trichloroacetic acid (TCA). The mixture was filtered and the filtrate was collected and diluted (1:10) with deionised water. The absorbance of the diluted filtrate was determined in duplicate at 280 nm using a spectrometer.

Activities measured by the TCA assay were converted to standard enzyme units using a tyrosine standard curve. One unit of enzyme activity was defined as "1 millimole of tyrosine produced in whole milk per hour of refrigerated incubation at 4°C". Before each major enzyme trial the enzyme activity was determined using the TCA assay. A single enzyme concentration was used in this work and the enzyme activity, estimated from this assay, remained constant over the duration of the experimental programme.

3.3.3.2 Composition

- *Ash*

Dry ash of the fouling deposit was determined by incineration at 400°C for 20 minutes. Details of this procedure are given in Appendix G.2.

- *Moisture*

Moisture content was determined by drying 3 g of fouling deposit at 108°C for 3 hours. Details of this procedure are given in Appendix G.1.

- *Protein*

The Kjeldahl method was used to determine the protein content of both the milk and the fouling samples. A 1 g sample of each was used for each test. Details of this procedure are given in Appendix G.3.

- *Fat content*

The Mojonnier method was used to determine the fat content of both the milk and the fouling samples. Five gram samples were used for each of the tests. Details of the procedure used are given in Appendix G.4.

- *Reducing SDS-PAGE*

Milk and fouling samples taken after a run were diluted in a sample buffer and heated for 5 minutes at 100°C. Reducing electrophoresis was performed according to Laemmli (1970) and Cho (1994) at pH 8.8 in a 15% polyacrylamide gel. After electrophoresis, the gel was stained in Coomassie Blue. Details of the procedure used are given in Appendix G.5.

3.4 OVERVIEW OF EXPERIMENTAL PROGRAM

Table 3.1 gives an overview of the experimental program undertaken in this study. Details of individual experiments are given in Tables C.1 – C.4 of Appendix C and on the data disk described in Appendix H. The experiment nomenclature is explained in section 4.1.

Table 3.1 Overview of experimental program

Type	Description	Experimental set
Protocol	Developing and testing protocols for: • heat exchange surface preparation • fouling runs • visualisation runs	C1.1-1.14, C2.5-2.7.
Replicate	Determining the level of variation in results of experiments run under identical conditions.	R1.1-1.5.
Compare	Comparing results of direct and indirect measurements of fouling.	R1.1, R1.4, R1.6-1.9, R2.3.
Enzyme	Determining the effect of enzyme addition to milk on results of experiments.	C1.21-1.26, R1.5, R1.10-1.22.
Pressure	Determining the effect of pressure on results of experiments.	C1.15-1.20, C2.8, C2.12, R1.1, R1.4, R1.6-1.9, R2.4-2.5, R2.1, R2.9-2.12
Flow	Determining the effect of flow rate/linear velocity on results of experiments.	C2.9-2.10, C2.13-2.15, R2.4, R2.6, R2.8-2.10, R2.13-2.15.
Geometry	Determining the effect of geometry on results of experiments.	C2.15-2.17, R2.15-2.17.
SCOP	Determining the effect of start up procedure and surface coatings on results of experiments.	C2.1-2.4, C2.11, R2.19-2.24.
Misc.	Fouling curve characteristics examples and singular experiments.	R1.4, R1.18, R1.22-1.23, R2.1-2.2.

RESULTS

4.1 INTRODUCTION

This chapter is organised into two sections reflecting the major areas of work in this study:

1. Fouling of heated surfaces by milk.
2. Influence of bubble nucleation on fouling of heated surfaces.

A summary of the formal experiments that generated the results presented in this chapter is given in Tables C.1 – C.2 of Appendix C. This summary lists the run number, product type and pilot plant processing variables of each experiment. The run nomenclature is based on the equipment in which the experiment was performed e.g. R1.x and R2.x refer to experiments performed in the THE rig and the MPHE rig respectively. A summary of the commissioning and prerun trials is given in Tables C.3 – C.4 of Appendix C. The nomenclature of these runs is the same as that of the results runs except the 'R' is replaced by a 'C' in the run title e.g. C1.x. To aid the reader with this chapter, relevant information from these summaries will sometimes be reproduced in their relevant sections to avoid continued reference to the Appendix.

All photographs of fouling test plates and tubes presented in this chapter are orientated with the flow of the process fluid moving right to left. Stills of video footage from runs using water and whey (visualisation runs) conducted with the windowed module are also orientated this way. All photos (including stills of video footage) are reproduced in the data disk as outlined in Appendix H.

4.2 FOULING OF HEATED SURFACES BY MILK

4.2.1 Characteristics of fouling curves

Figure 4.1 shows an example of the intermediate data collected from a fouling run (R2.1) using the local system in the MPHE rig. As fouling increased on the test plate the heat flux decreased as observed in the output of the heat flux sensor. These data were converted to internal heat transfer coefficients using equation (3.4) and the resulting trace is shown in Figure 4.2.

The trace of U_i provides a more comprehensible representation of the onset and build up of fouling on the heat exchange surface than the heat flux profile alone. In this example, U_i reduced by approximately 36% in a linear fashion as the surface fouled.

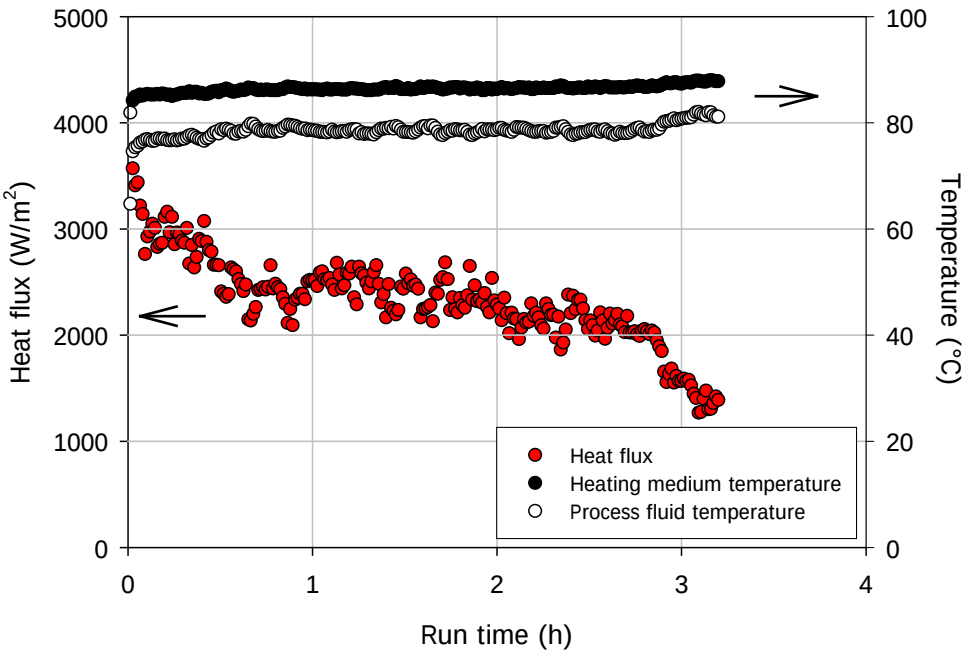

Figure 4.1 Intermediate process data for R2.1.

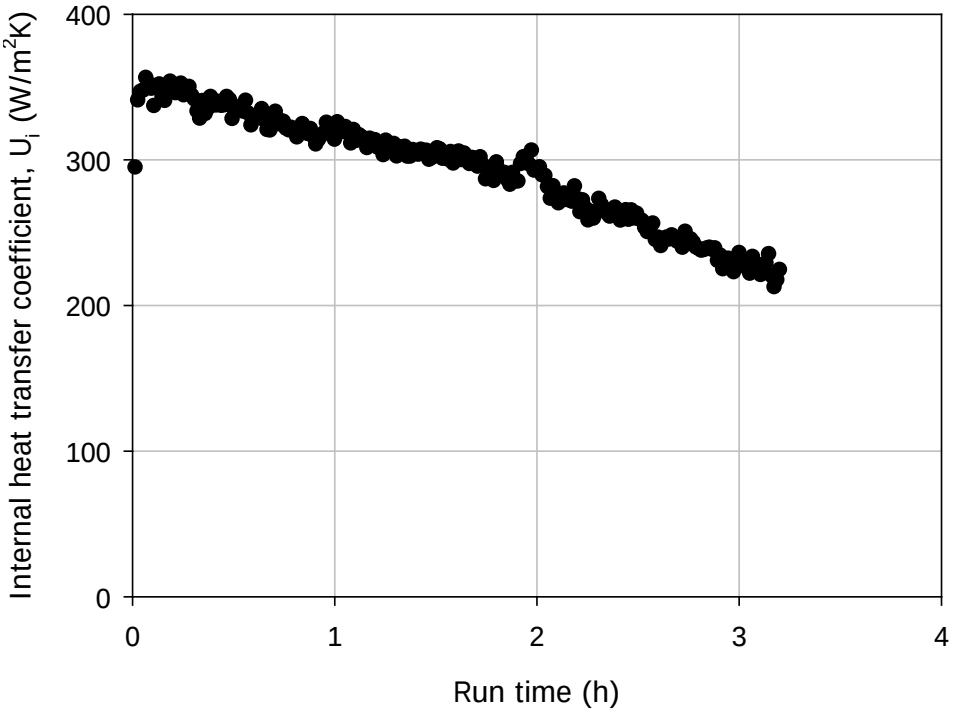

Figure 4.2 Calculated internal heat transfer coefficient versus run time for R2.1.

The global system monitored changes in process fluid flow rate and temperatures of all streams entering and exiting the heat exchanger. An example of these data for a fouling run conducted with the tubular heat exchanger is shown in Figure 4.3. In this run (R1.18) the temperature and flow rate of the process fluid entering the heat exchanger was kept constant. As fouling built up on the surface the outlet temperature of the process fluid decreased while the heating medium outlet increased. Due to the substantial difference in heating and process fluid flow rates the increase in heating medium outlet was much less apparent that the reduction in process fluid outlet temperature.

As with the local system, overall heat transfer coefficients were calculated from these intermediate data using equation (3.4) which is shown in Figure 4.4. In this run, U reduced by approximately 65% at a constant rate.

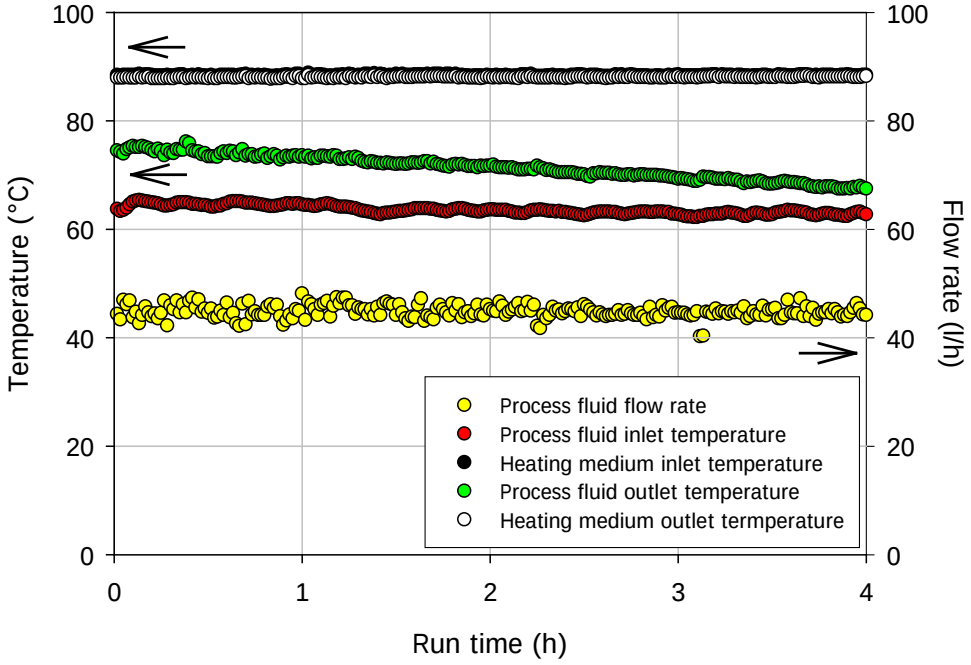

Figure 4.3 Intermediate process data for R1.18.

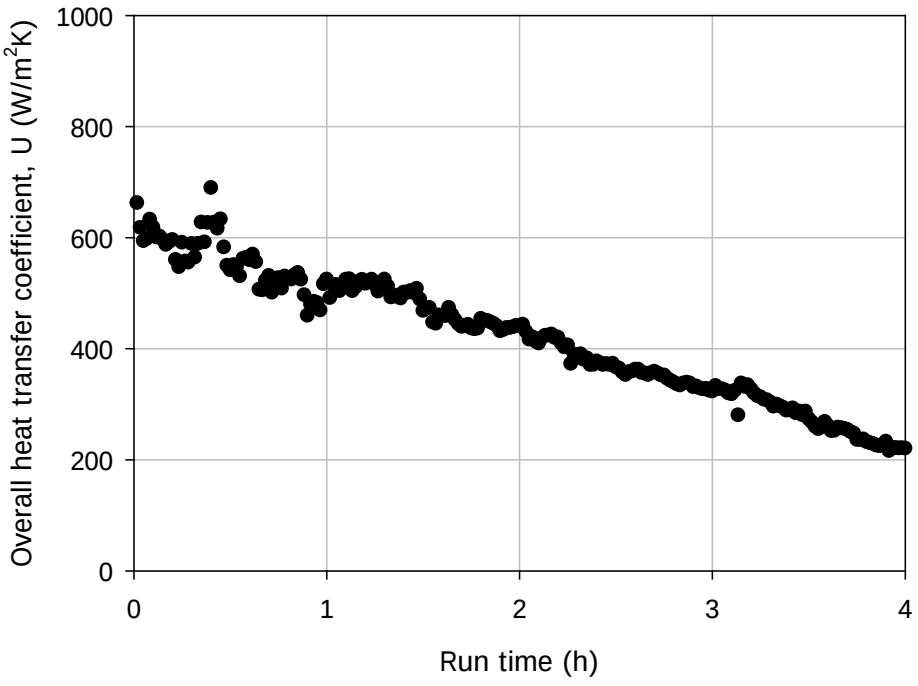

Figure 4.4 Calculated overall heat transfer coefficient versus run time for R1.18.

U_0 used for normalisation in equation (3.7) was typically calculated from the average of U over the first 30 minutes of a run. During this period, any initial fluctuations in U had passed allowing a reliable calculation of U_0 to be made. During some runs

fouling started almost immediately after the process fluid was allowed to enter the heat exchanger. In these cases, U_0 was estimated from a reduced period of U readings. The normalised fouling curves of the two example runs used in this section are shown in Figure 4.5.

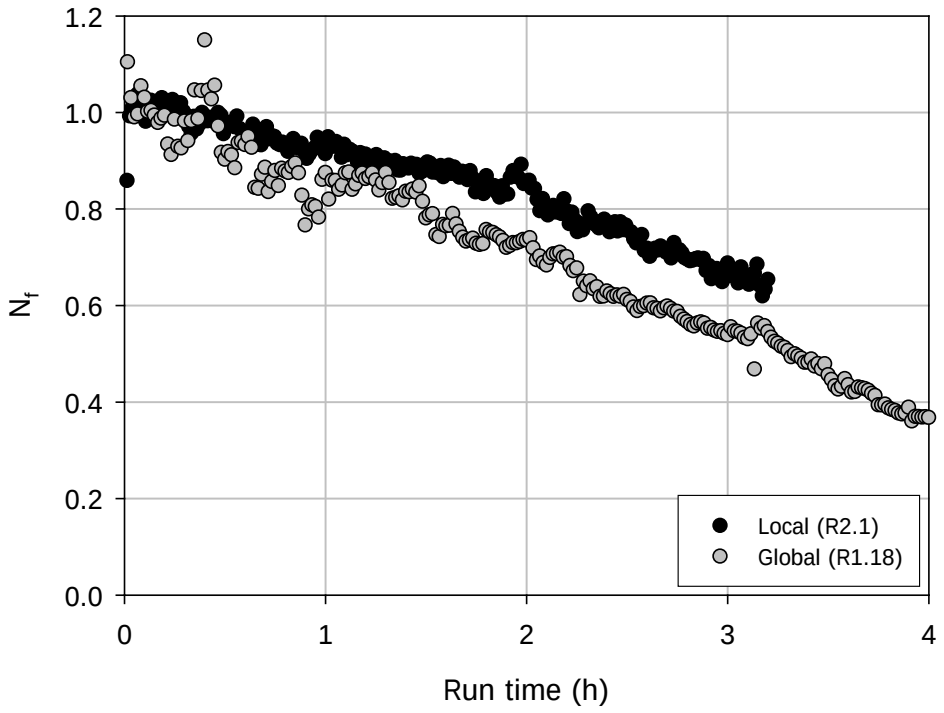

Figure 4.5 Comparisons of N_f calculated from the local and global systems.

It is interesting to note that the two fouling curves compared reasonably well even though they were obtained from two separate pieces of research equipment and were based on different estimates of fouling (local and global). Although, the conditions in both heat exchangers were the same, the local fouling recorded above the heat flux probe appears to be representative of fouling over the entire heat exchange surface as it compared very well to the global measurement of the much larger THE (which would dampen out localised effects of fouling).

Another point to note is that there appears to be little to no induction period associated with either of the above experimental fouling curves. This was not always the case where often the N_f versus time graph would exhibit an induction period as shown in Figure 4.6. Here, after a small period of unsteady state N_f remained relatively constant for the first 1.8 hours which defines the induction period.

Thereafter, N_f significantly decreased with run time signalling the fouling period. The induction period can last for the entire run if there is no fouling as shown in Figure 4.7 for R2.2.

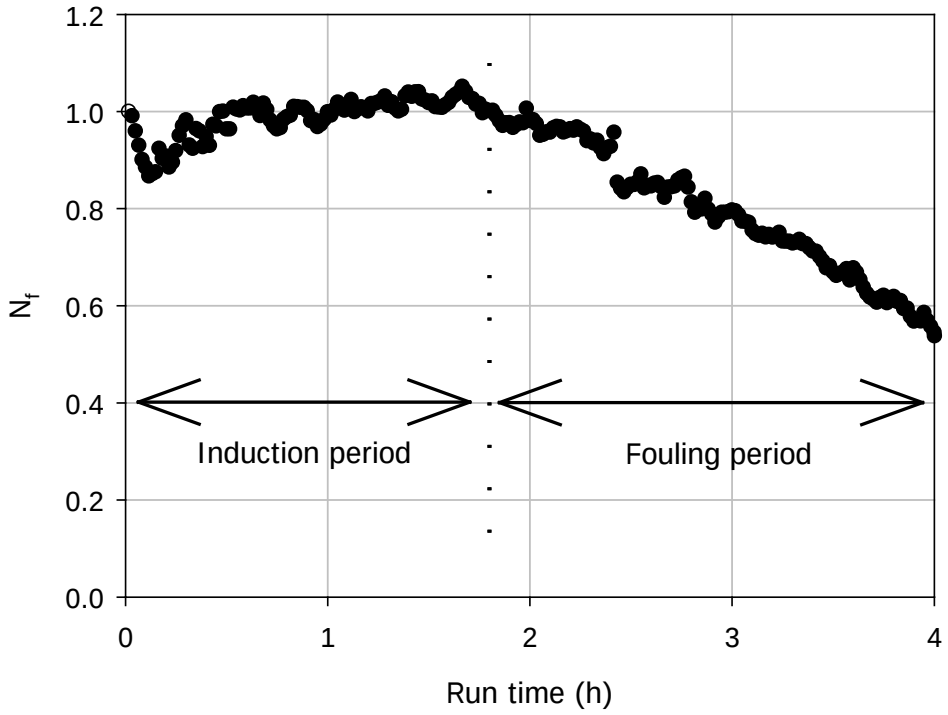

Figure 4.6 N_f versus run time for R1.4 showing induction and fouling periods.

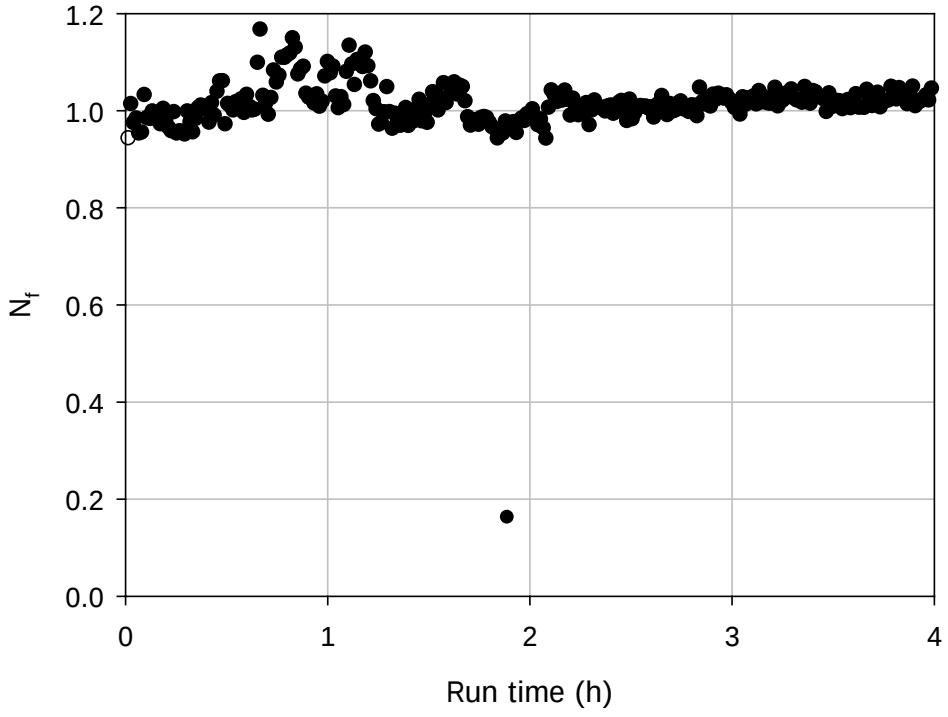

Figure 4.7 N_f versus run time for R2.2 showing no fouling period.

In Figure 4.6 the fouling period was represented by a linear reduction in N_f from which the fouling rate was calculated as outlined in section 3.3.2.4. In some cases the fouling rate reduced over the run time which may represent movement to the post-fouling period mentioned in the literature as shown in Figure 4.8. As mentioned in section 3.3.2.4 in these cases only the initial linear reduction was considered during the calculation of the fouling rate. Although not technically correct, this fouling rate was taken as the representation of fouling rate for the entire run. This method was considered appropriate for the current research and has been used by other researchers (e.g. Truong, 2001).

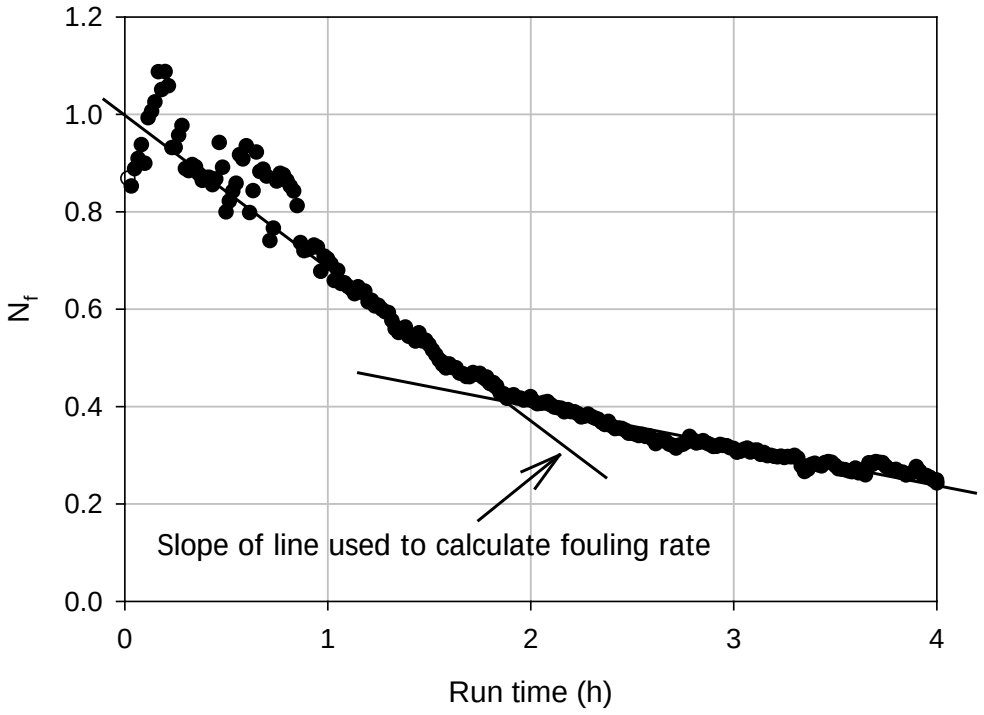

Figure 4.8 N_f versus run time for R1.22 showing two distinct fouling rates.

4.2.2 Reproducibility

The results of fouling experiments reported in the literature often vary significantly even when the composition and quality of milk are kept constant by the use of reconstituted milk. For example, the variation in protein composition and fat content of fouling layers between authors has been discussed in section 2.2.4. The coefficient of variance of fouling weights in replicate runs in well regarded work (e.g. Lalande *et al.*, 1984) are on average 100% and can be up to a maximum of 300% in others (e.g. Newstead *et al.*, 1998). A series of runs was carried out using the standard operating protocol (section 3.2.3) to ascertain the reproducibility in this

work. Homogenised, standardised and pasteurised whole milk (3.3% fat) obtained from the local milk treatment factory (Fonterra Co-op Group Ltd, Longburn, NZ) was heated by the plate heat exchanger before entering the tubular heat exchanger (at 65°C) operating at 83°C on the heating side. For all experiments the flow of milk through the plant was set at 45 l/h (Re = 300) while the process line pressure was adjusted to obtain two sets of replicate data (30 and 50 kPa.g). Each experiment ran for 4 hours after which the tubes were removed, photographed and weighed. Table 4.1 shows the results of the replicate runs.

Table 4.1 Mass of dry foulant obtained from surfaces installed in the THE rig after processing whole milk (replicate runs).

Run	Pressure (kPa.g)	Mass of dry foulant (kg/m^2)	Mean	CV (%)
R1.1	30	2.19×10^{-1}	0.237	6.32
R1.2	30	2.47×10^{-1}		
R1.3	30	2.43×10^{-1}		
R1.4	50	1.61×10^{-1}	0.171	7.88
R1.5	50	1.80×10^{-1}		

The weight of fouling measured at the end of each run showed a high level of reproducibility. The protocol developed for this pilot plant controls most of the important operating parameters crucial to obtaining reproducible fouling results. However, it must be emphasised that this protocol is specific to the present pilot plant and may not apply to other systems with different plant configurations and flow geometries or milk qualities.

The development of fouling was monitored in these runs using the global system described in section 3.3.2.3. Figure 4.9 shows the evolution of N_f over time for the 30 kPa.g replicate runs. Although the plots exhibited the same general trend there were differences in some aspects (e.g. induction periods and final N_f values). For runs R1.2 and R1.3 the duration of the induction period was approximately 30 minutes, while in run R1.1 N_f did not appear to decrease until 60 minutes after the start. Consequently, the fouling period in R1.2 and R1.3 was longer than R1.1 resulting in a lower N_f value recorded at the end of the last two runs. This observation was reflected in the measured mass of fouling recorded at the end of each run (Table 4.1). It is not known why these differences occur, even when

operating under the same conditions, but it is possible that inconsistencies in heat exchanger assembly between runs may be responsible. These inconsistencies could introduce subtle changes in the flow geometry; for example, small eddy disturbances if the connecting pipes are not perfectly aligned.

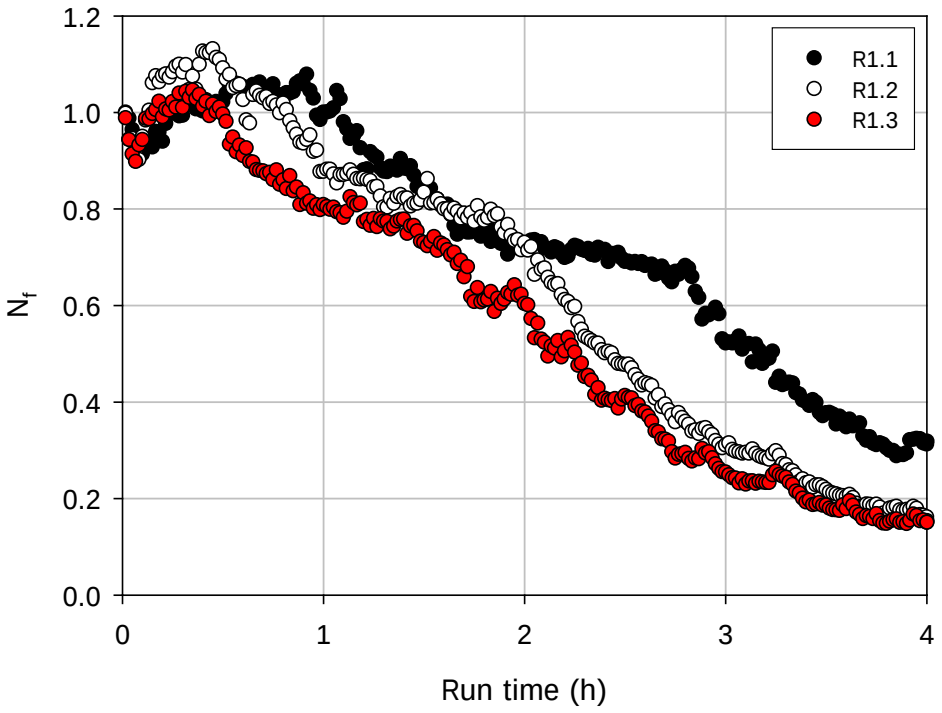

Figure 4.9 N_f versus run time for the 30 kPa.g replicate runs (R1.1-1.3).

4.2.3 Relation between direct and indirect methods of fouling measurement

To relate the direct methods of fouling measurement (mass and height of fouling layers at the end of runs) to the two *in situ* systems (global and local) described in section 3.3.2, two sets of experiments were conducted. The first set involved determining the final N_f value of the local system and comparing it to the average thickness of the fouling layer directly above the probe. In this experiment, six heat flux sensors were installed in the modular heat exchanger rig (MPHE) and the plant was run with whole milk according to the basic operating procedure outlined in section 3.2.3. At various times during the run (R2.3), fouling modules were isolated from the process line, the plates removed and the average thickness of the fouling layer determined with the apparatus described in section 3.3.1.2. The final N_f value

of each module was determined from the average of N_f over approximately 10 minutes prior to module isolation. As with the procedure to determine the U_0 value, this method dampened any fluctuations (see section 4.2.1) thus reducing error in the final N_f value.

Figure 4.10 shows the change in N_f values over time for whole milk heated in the MPHE rig. The value of N_f continued to decrease, in all modules, until approximately 1.3 hours where the value thereafter remained stable indicating an asymptotic fouling rate had been reached. To obtain a selection of N_f values, three modules (4, 5 & 6) were isolated before the asymptotic level was reached. The remaining three (1, 2 & 3) were stopped at different intervals during the lowered fouling rate period.

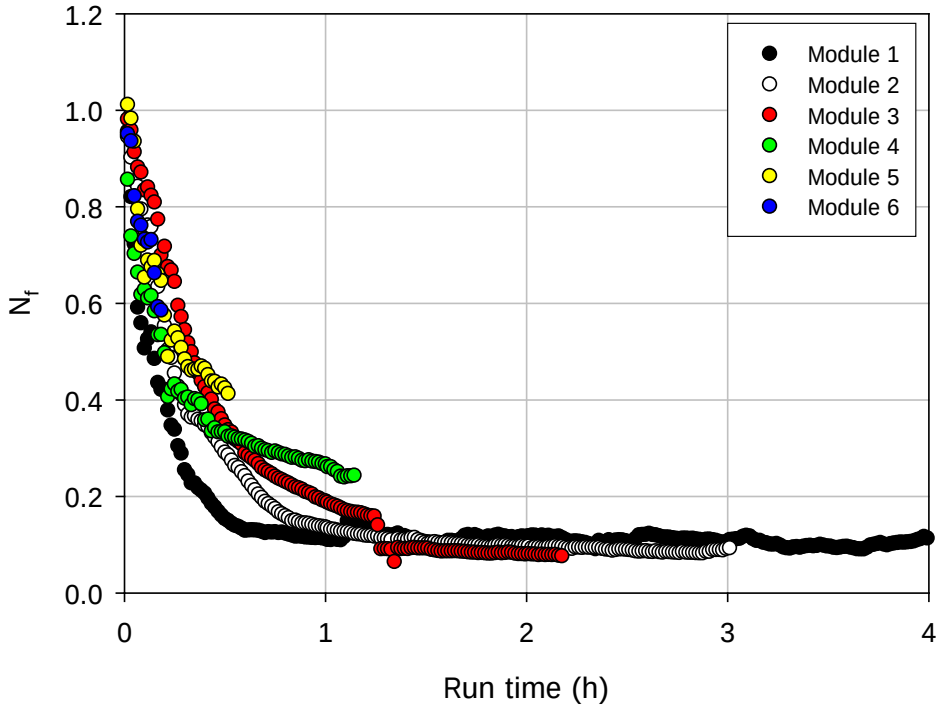

Figure 4.10 N_f versus run time for the local system's validation experiment (R2.3).

Figure 4.11 shows the relation between N_f and the average thickness of the fouling layer obtained from this set of experiments. The wall heat flux strongly correlated with the level of fouling (i.e. deposit thickness) inside the modules. The final three points in Figure 4.11 at a thickness of 0.8 mm involved very small values of heat transfer flux which are at the limit of the sensitivity of the wall heat flux probe used (Appendix A.1). If a straight line is put through the first three points of the curve in

Figure 4.11 all values above a thickness of approx 0.6 mm should be the same as this is the limit of sensitivity of the probe.

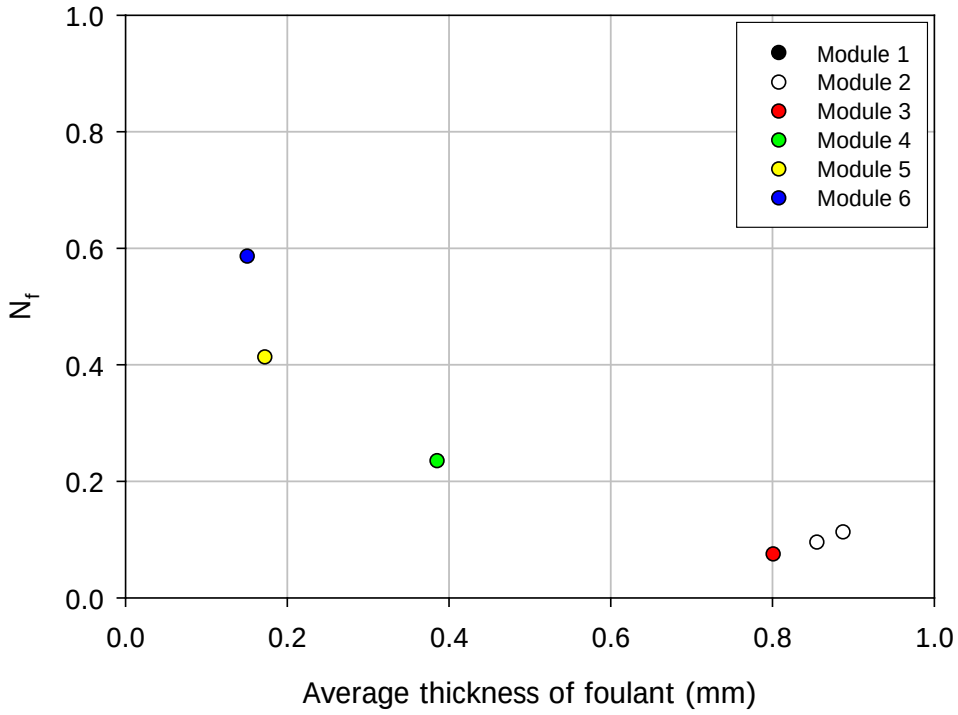

Figure 4.11 Relationship between the N_f and the average deposit thickness of fouling both measured at module isolation (R2.3).

A similar set of experiments was conducted for the global THE fouling monitoring system. Essentially, process conditions were manipulated so that different quantities of fouling developed on the THE tubes. Although the THE was designed to allow tube isolation mid-run, this feature was not used during fouling runs in the current project. During commissioning it was found that instabilities (e.g. air slugs) were introduced into the system when all tubes were activated making the monitoring of fouling in real time difficult. It was decided to use one tube per run so instabilities were minimised and thus several individual experiments (with adjusted process variables) were conducted on separate days (R1.1, R1.4 & R1.6-1.9). At the end of each run the tube was removed and weighed according to the procedure described in section 3.3.1.1.

Figure 4.12 shows the relationship between the mass of dry foulant (per m^2) and the final N_f value calculated for each run. This relationship appeared to be linear. Thus the direct and indirect methods of monitoring fouling are in agreement.

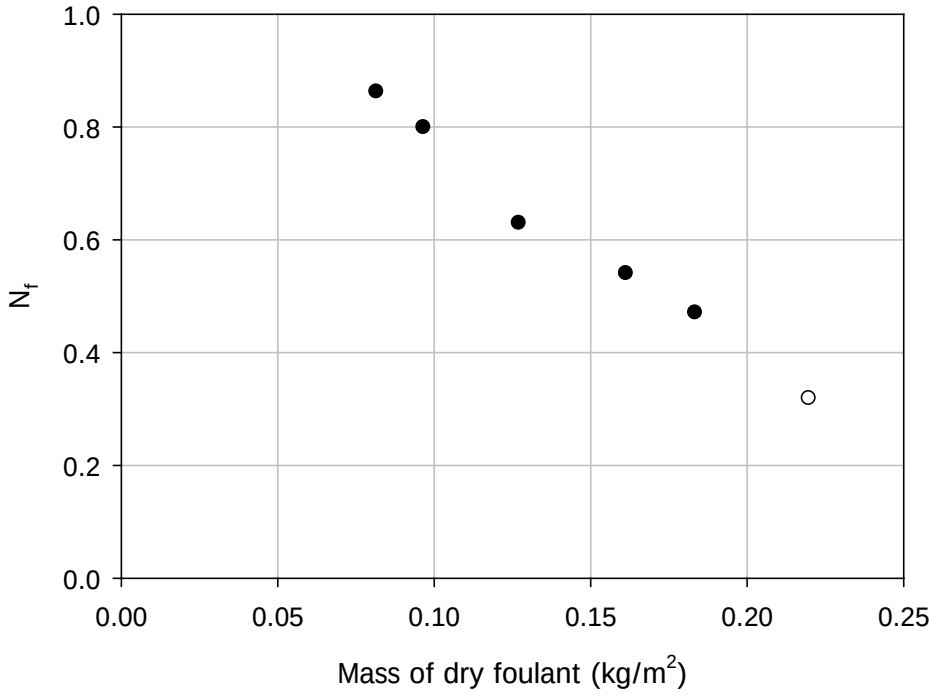

Figure 4.12 Relationship between N_f and the mass of dry foulant both measured at the end of each run.

4.2.4 Enzymatic damage

In R1.10, the influence of extracellular enzymes produced from the growth of thermophilic bacteria on fouling of heat exchangers was studied and compared to the known effect of enzymes produced by psychrotrophs (R1.11).

Whey containing extracellular enzymes from the growth of *Bacillus stearothermophilus* (B12 Cm) (section 3.3.3.1), henceforth called thermophilic enzymes, was added to whole milk before processing in the THE at 88°C and 50 kPa.g (R1.10). Similarly, in a separate trial, a commercial enzyme (Neutrase) obtained from the growth of *Bacillus amyloliquefaciens* was added to whole milk and processed under identical conditions to the thermophilic run (R1.11). After four hours of operation the plant was shut down and tubes were removed, photographed and weighed. For every run a corresponding control experiment was conducted, on the same day using untreated whole milk processed under identical conditions (R1.17 & R1.18). In all these runs the milk entered the THE at a flow rate of 45 l/h and a temperature of approximately 64°C (± 1°C).

The mass of dry foulant (kg/m^2) for each trial is shown in Figure 4.13. The data show clearly that the addition of thermophilic enzymes to whole milk did not increase fouling within the limits of experimental repeatability (R1.10 & R1.17). In contrast, there was a clear difference between fouling of the control and Neutrase damaged milk (~40% increase, R1.11 & R1.18) which is consistent with results from Jeurnink (1991) with skim milk and Ma *et al*. (2001) with whole milk.

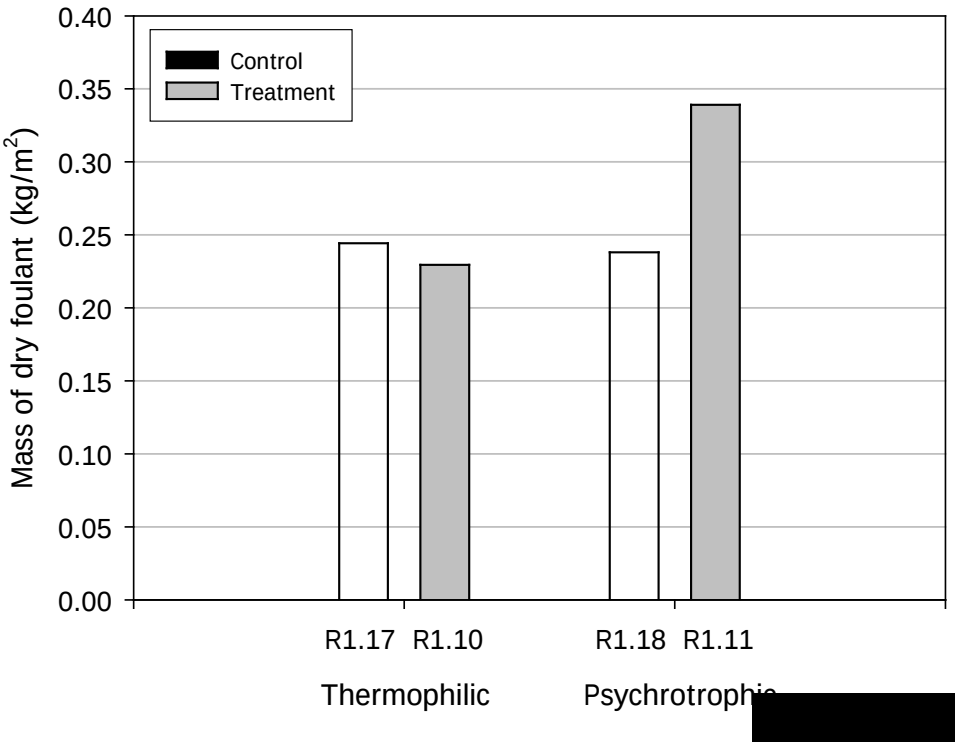

Figure 4.13 The mass of dry foulant measured at the end of each run using the THE processing whole milk with (R1.10, R1.11) and without (R1.17, R1.18) the addition of bacterial enzymes.

To the author's knowledge no previous studies have investigated the influence of thermophilic enzymes on fouling. Since thermophilic bacteria [redacted] heating sections of milk powder plants (e.g. Refstrup, 1998; Hinton, 2003) there were concerns that they may worsen fouling problems by the production of enzymes. The results obtained here were surprising and contrast clearly the effect of thermophilic and psychrotrophic enzymes.

In an effort to understand why thermophilic enzymes act differently to psychrotrophic enzymes, samples of liquid milk were removed every two hours from the refrigerated vat during the fouling runs. The protein composition was determined by reducing gel electrophoresis (section 3.3.3.2). The reducing SDS-PAGE patterns of

the standard whole milk and the enzyme treated milk sampled during the runs are presented in Figures 4.14 (thermophilic enzymes) & 4.15 (Neutrase) for 1, 3 and 5 hours. Figure 4.14 shows that the addition of thermophilic enzymes from the growth of *Bacillus stearothermophilus* (B12 Cm) did not change protein proportions of the milk throughout the run. However, upon the addition of Neutrase to the standard milk, hydrolysis of κ-casein to para-κ-casein was observed and the extent of hydrolysis increased with holding time in the vat and therefore, milk samples as they entered the heat exchanger throughout the run (Figure 4.15). These observations are corroborated by the quantification of the bands shown in Table 4.2.

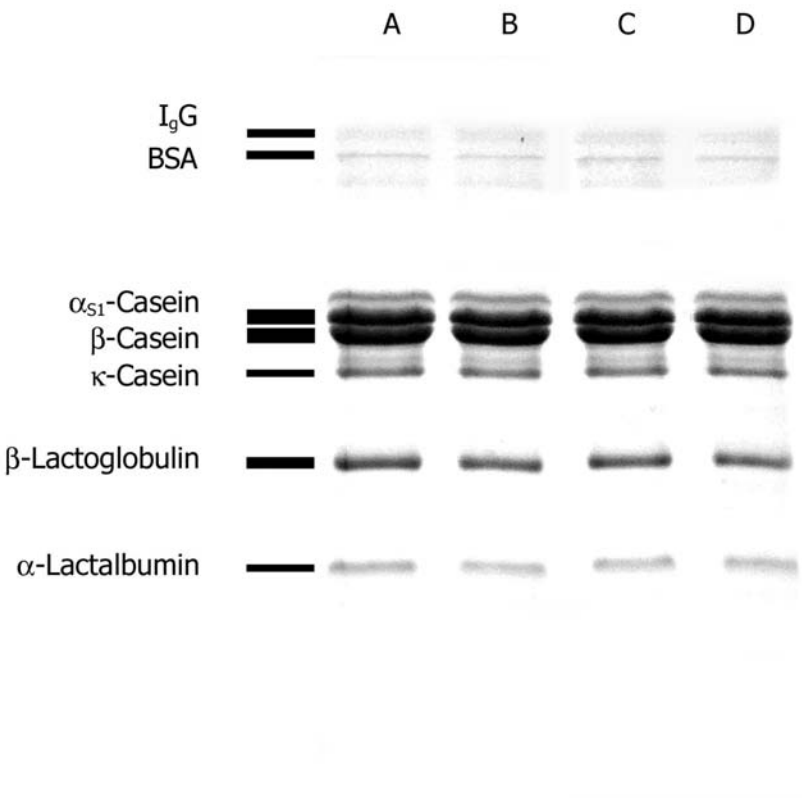

Figure 4.14 Reducing SDS-PAGE of liquid whole milk (A) with addition of extracellular enzymes of *B. stearothermophilus* (B12 Cm) after 1 (B), 3 (C) and 5 (D) hour incubation periods at 4°C.

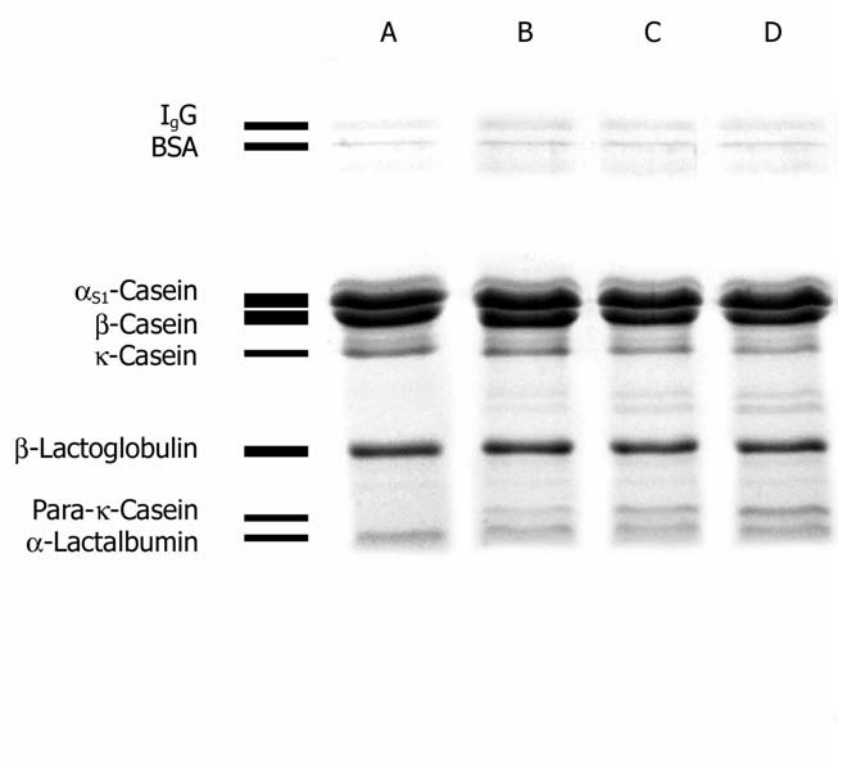

Figure 4.15 Reducing SDS-PAGE of liquid whole milk (A) with the addition of protease enzymes of *B. amyloliquefaciens* (Neutrase) after 1 (B), 3 (C) and 5 (D) hour incubation periods at 4°C.

Table 4.2 Protein composition (percentage intensity) of liquid whole milk incubated with extracellular enzymes of *B. stearothermophilus* and protease enzymes of *B. amyloliquefaciens*.

Run	Protein	Whole milk	Incubation duration (h)		
			1	3	5
R1.17, R1.10	I_gG	2 (2)	2 (2)	2 (2)	1 (2)
	BSA	3 (1)	3 (1)	2 (1)	2 (1)
	α_{S1}-casein	39 (2)	37 (2)	41 (2)	40 (2)
	β-casein	31 (3)	29 (3)	30 (2)	31 (3)
	κ-casein	9 (2)	10 (2)	8 (2)	8 (2)
	β-lactoglobulin	13 (1)	16 (1)	15 (1)	15 (1)
	Para-κ-casein	-	-	-	-
	α-lactalbumin	3 (1)	4 (1)	3 (1)	3 (1)
R1.18, R1.11	I_gG	2 (2)	2 (2)	2 (2)	2 (2)
	BSA	1 (1)	3 (1)	2 (1)	2 (1)
	α_{S1}-casein	37 (2)	37 (2)	38 (2)	39 (2)
	β-casein	29 (2)	27 (2)	27 (2)	25 (2)
	κ-casein	11 (2)	9 (2)	8 (2)	8 (2)
	β-lactoglobulin	15 (1)	15 (1)	14 (1)	14 (1)
	Para-κ-casein	-	3 (1)	4 (1)	6 (1)
	α-lactalbumin	5 (1)	5 (1)	5 (1)	4 (1)

NB: Coefficient of variance (%) shown in parenthesis.

Fouling deposits obtained at the end of each run (R1.10-1.11 & R1.17-1.18) were sampled, dissolved and analysed for protein composition using the same method used for the liquid samples. Figure 4.16 shows the reducing SDS-PAGE patterns of the fouling formed during the heating of untreated and enzyme treated whole milk in the tubular heat exchanger. The protein compositions of fouling from the untreated and treated whole milk resemble that of liquid whole milk except that the bands have shifted slightly upwards. The bands are also not as sharp as that of liquid milk suggesting other forms (dimers and trimers) of the proteins may have developed. This effect may be the result of the extensive heating that the proteins have undergone in the process of fouling. Due to the poor resolution of the fouling SDS-PAGE patterns it was difficult to quantify each protein individually; therefore, groups

of proteins were determined from the densitometer output with the aid of Sigmascan as outline in Appendix E. These groups are shown in Table 4.3.

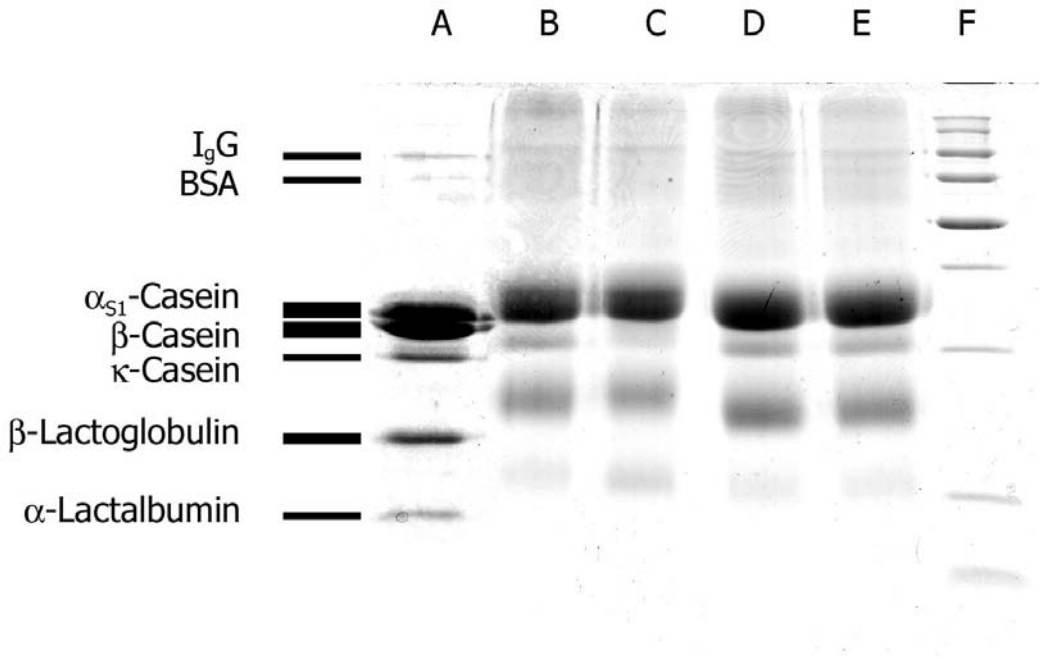

Figure 4.16 Reducing SDS-PAGE of deposit formed by heating milk: (A) liquid whole milk (B) deposit of whole milk (*B. amyloliquefaciens* control – R1.18) (C) deposit of whole milk after incubation with protease enzymes of *B. amyloliquefaciens* (Neutrase – R1.11) (D) deposit of whole milk (*B. stearothermophilus* control – R1.17) (E) deposit of whole milk after incubation with extracellular enzymes of *B. stearothermophilus* (B12 Cm) – R1.10 (F) protein broad band standard.

Table 4.3 Selected protein composition (percentage intensity) of liquid whole milk and deposit formed during control and enzyme addition runs.

Protein group	Whole milk	Whole milk deposit			
		R1.17	R1.10	R1.18	R1.11
α, β-casein	70 (1)	55 (0)	56 (5)	59 (6)	61 (1)
κ-casein	11 (5)	10 (12)	10 (6)	9 (5)	5 (4)
β-lactoglobulin	14 (2)	27 (8)	27 (8)	25 (9)	24 (0)
Para-κ-casein, α-lactalbumin	5 (6)	8 (10)	8 (1)	7 (11)	10 (9)

NB: Coefficient of variance (%) shown in parenthesis.

The protein composition of the deposits showed a similar trend to that of liquid milk shown in Table 4.2. In Table 4.3 there was a shift in κ-casein in the fouling from a

value of 9 in the control sample (R1.18) to a value of 5 with the addition of Neutrase (R1.11). In contrast, the value was 10 for both the control and runs spiked with thermophilic enzymes (R1.17 & R1.10 respectively). Similarly, there was an increase in the value of para-κ-casein Neutrase series from 7 (R1.18) to 10 (R1.11) whereas the value of 8 (R1.17 & R1.10) was unchanged in the thermophilic series.

The results reported here agree with Jeurnink (1991) and others with respect to the effect the addition of psychrotrophic enzymes to milk has on subsequent fouling. However, the same effect was not observed when thermophilic enzymes were added to milk. It is clear from these results that to reduce the amount of fouling it is important to control the growth of psychrotrophic bacteria in the milk. The presence of extracellular enzymes from thermophilic species in the milk appears to be less important.

4.2.4.1 Combined effect of temperature and Neutrase addition on fouling

It is normally agreed that temperature has an effect on the activity of enzymes and it is reasonable to propose that the term related to enzyme activity in the model of Ma *et al*. (2001) should include a temperature effect. A series of trials was carried out to investigate the influence of heating side temperature on fouling of normal and proteolytic-damaged whole milk. Six temperature (set point) levels were investigated from 68 to 93°C in 5°C intervals (R1.5; R1.11-1.16; R1.18-1.22). In each experiment 400 litres of whole milk (3.3% fat) was divided into two batches. To one batch, Neutrase was added at a concentration of 0.1 activity units 1 hour before the start of the heating run in the THE at an operating pressure of 50 kPa.g. In this set of experiments the milk entered the THE at 64.5 ± 1°C. The control (untreated) batch was processed under identical conditions on the same day to negate the influence of variations in the supply milk.

Figure 4.17 shows the effect of surface temperature on the formation of fouling in the tubular heat exchanger for treated and untreated whole milk. For both cases, as the surface temperature increased there was a corresponding increase in fouling. For all temperatures the amount of fouling was more severe with the Neutrase treated milk.

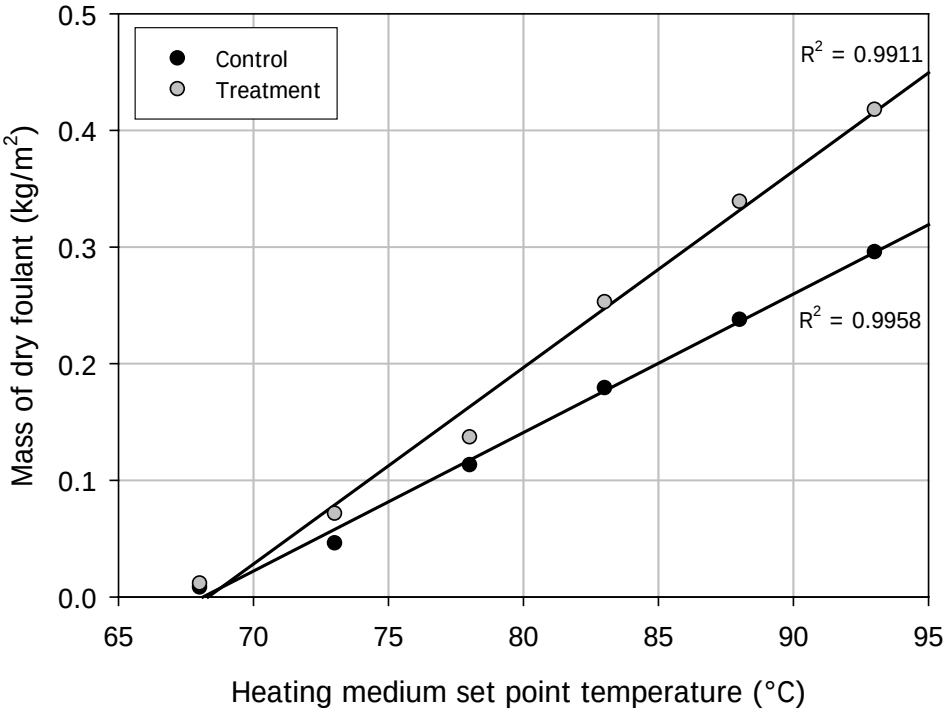

Figure 4.17 The effect of heating surface temperature on the mass of dry foulant obtained at the end of each run using the THE processing whole milk with and without the addition of protease enzymes of *B. amyloliquefaciens* (Neutrase).

The percentage increase in fouling mass collected at the end of the run with the addition of Neutrase remained relatively constant as shown in Table 4.4. The surface temperature of the heater has no effect on this increase. This observation has a simple explanation. The enzyme activity is only a function of the incubation temperature which was 4°C in all these runs (and the runs of Ma *et al.*, 2001). The residence time of the milk in the tubular heat exchanger was not long enough for the milk temperature in that equipment to have any bearing on the action of the enzyme. Therefore, the initial hypothesis that the model of Ma *et al.* (2001) needed a fouling temperature effect in the enzyme coefficient was incorrect. Only the incubation temperature was relevant.

Table 4.4 The effect of heating surface temperature on the mass of dry foulant obtained at the end of each run using the THE processing whole milk with and without the addition of protease enzymes of *B. amyloliquefaciens* (Neutrase).

	Mass of dry foulant (kg/m^2)					
Surface temp (°C)	**68**	**73**	**78**	**83**	**88**	**93**
Control	0.008	0.046	0.113	0.179	0.238	0.296
Treatment	0.012	0.072	0.137	0.253	0.339	0.418
Difference	0.003	0.025	0.024	0.074	0.101	0.122
Percentage increase (%)	41	54	21	41	42	41

Besides the final weight of foulant at the end of the runs, the rate of fouling of both the control and Neutrase damaged milk increase with temperature as shown in Figure 4.18. In all cases the fouling rate calculated from the monitored overall heat transfer coefficient was higher for the protease-damaged milk. The increase in rate of fouling upon addition of Neutrase remained relatively constant for all temperatures tested.

One possible explanation for this observation is the presence of two different effects on fouling in this work. There is a “base” rate of fouling by non-manipulated milk which is temperature dependent, and on top of that there is an increase in the rate of fouling when the caseins in the milk are destabilised by the addition of Neutrase. For the standard one hour incubation the latter is only a function of the amount of Neutrase added which is constant in this set of experiments. Ma *et al*. (2001) showed that the increase in the rate of fouling was a function of the amount of Neutrase added for a fixed temperature.

To investigate further the hypothesis that the fouling mechanism is affected by the addition of Neutrase the composition of the deposit was determined. Table 4.5 gives the composition and detailed protein component breakdown (via SDS-PAGE) of the 78 and 88°C runs.

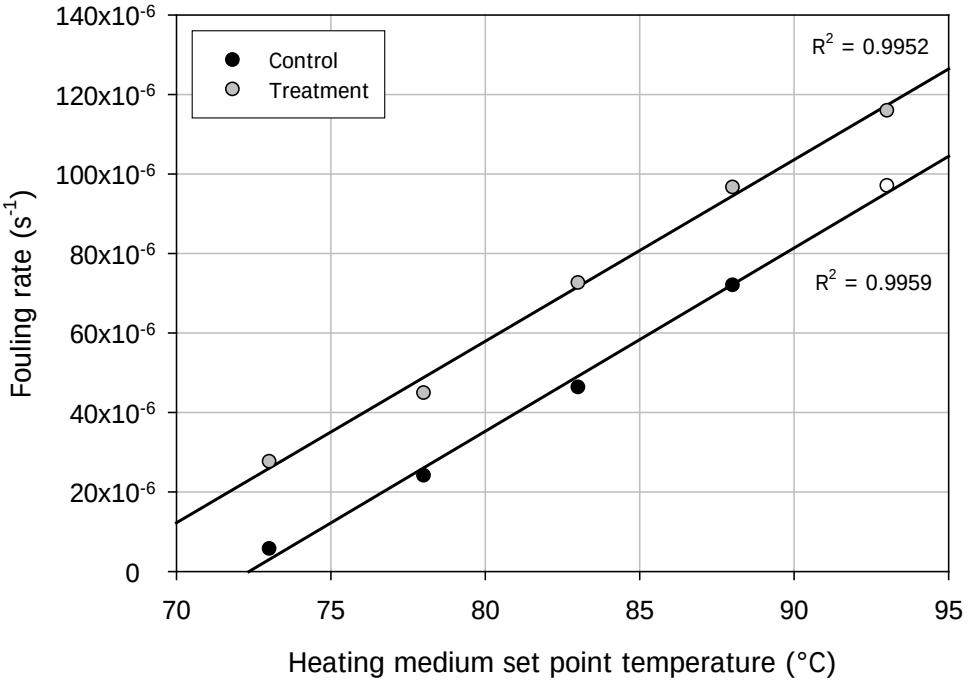

Figure 4.18 The effect of THE surface temperature on the rate of fouling of whole milk with and without the addition of protease enzymes of *B. amyloliquefaciens* (Neutrase).

Table 4.5 The composition of fouling deposit sampled from the THE after processing whole milk with and without the addition of protease enzymes of *B. amyloliquefaciens* (Neutrase). Ash, fat and protein expressed as percentage w/w. Protein components expressed as normalised percent.

	Whole milk	**Whole milk deposit**			
Surface temp (°C)	**-**	**78 (C)**	**78 (T)**	**88 (C)**	**88 (T)**
Run		R1.21	R1.14	R1.18	R1.11
Ash	5.4 (5)	5.3 (5)	5.3 (5)	5.5 (5)	5.2 (5)
Fat	31 (1)	44.5 (1)	38.6 (1)	42.7 (1)	39.2 (1)
Protein	25 (1)	33.6 (1)	35.3 (1)	34.0 (1)	35.2 (1)
α, β-casein	70 (1)	59 (3)	60 (2)	59 (6)	61 (1)
κ-casein	11 (5)	10 (4)	5 (2)	9 (5)	5 (4)
β-lactoglobulin	14 (2)	24 (6)	23 (6)	25 (9)	24 (0)
Para-κ-casein / α-lactalbumin	5 (6)	7 (11)	12 (3)	7 (11)	10 (9)

NB: (C) and (T) denote control and treatment experiments respectively. Coefficient of variance (%) shown in parenthesis.

The supply milk obtained from Fonterra shows no evidence of para-κ-casein. But the Neutrase modified milk shows a value of 6 normalised percent after 5 hours of incubation (Table 4.2). Thus, one would not expect to find any para-κ-casein in the fouling layer of the non-manipulated milk therefore, the value of 7% in R1.21 and R1.18 of Table 4.5 refers entirely to the proportion of α-lactalbumin. The para-κ-casein created by addition of Neutrase (R1.14 & R1.11) finds its way into the fouling layer as evidenced by the combined percentage of para-κ-casein/α-lactalbumin. Simultaneously, there appears to be a reduction in κ-casein that seems to be significant (10 to 5% and 9 to 5% for the 78 and 88°C sets respectively).

The break-down of κ-casein to para-κ-casein is normally accepted as evidence of the destabilisation of the casein micelles that can then aggregate among themselves or attach to the fouling layer or the wall. The fouling research group at Massey agrees with Jeurnink (1991) and Ma *et al*. (2001) that the destabilised casein micelles are responsible for the increase in fouling. But the presence of the para-κ-casein in the fouling layer does not actually prove that this component is the agent that increases the rate of fouling. These previous workers have not described a convincing mechanism of greater initiation of fouling by para-κ-casein. The ratio of α to β casein in the fouling layer from the control and treated milk is essentially the same which suggests that the casein micelles did not break up but attached to the fouling layer as a whole. This brought either the κ-casein or para-κ-casein to the fouling layer depending on their presence in the milk.

Another interesting difference observed between the two types of deposits was the differences in their fat and protein contents. The ratio of fat to protein decreases with the addition of Neutrase to the milk (e.g. 1.32 to 1.09 in the 78°C set). The most plausible explanation is that the base mechanism is unchanged but casein micelles destabilised by the addition of Neutrase may not be attached to fat globules and therefore, the increase in mass of fouling by destabilised casein would be due to an addition of proteins mainly.

One possible candidate for the base mechanism is the formation of deposits around air/vapour bubbles. The majority of fouling formed in this pilot plant has a porous type structure which may be attributed to the presence of air/vapour bubbles on the heated surface. A typical example of the structure of fouling found in this pilot plant

is shown in Figure 4.19 (R1.18). When destabilised caseins are present these porous structures may be filled in (Figure 4.20) and direct deposition of solids onto the heated surface may be observed (Figure 4.21).

Figure 4.19 Example structure of fouling formed in the THE processing whole milk at 88°C (R1.18).

Figure 4.20 Example structure of fouling formed in the THE processing of Neutrase modified whole milk at 88°C (R1.11). Note how the craters have been filled to leave a relatively smooth outer surface.

Figure 4.21 Example structure of fouling formed in the THE processing of Neutrase modified whole milk at 88°C (R1.11). Note milk solids appear to deposit directly onto the stainless steel surface as well as the porous structure.

In published literature this bubble type mechanism has received relatively little attention. The remainder of this work focuses on the role of bubble nucleation on the onset and development of fouling.

4.3 INFLUENCE OF BUBBLE NUCLEATION ON FOULING

As mentioned in the literature review (section 2.2.7.5) fouling is greatly increased at low pressures and flow rates, where one would expect air dissolved in the milk to form bubbles on the heated surfaces (Thom, 1975). The reason for speculating that bubbles increase the amount of fouling is the presence of ring-shaped deposits that can be photographed by either normal photography (e.g. Thom, 1975) or electromicroscopy (e.g. Tissier & Lalande, 1986). However, there are no published direct observations of bubbles formed on surfaces during fouling. Thus, existing theories of the fouling mechanism in the presence of bubbles (e.g. Jeurnink *et al.*, 1996c; Walstra *et al.*, 1999) have not been corroborated by real-time observations.

A series of visual experiments was conducted (R2.4-2.20, R2.24) in the MPHE rig to elucidate the role of air bubbles in fouling of dairy products, first with distilled water flowing at different pressures and flow rates (R2.10-2.16, R2.18-2.19), and second with dilute translucent 0.1% w/w whey protein concentrate (WPC) solutions (R2.4-2.9, R2.17, R2.20, R2.24). The WPC runs are apparently unique to this work because real-time observations of fouling during the formation and evolution of bubbles are made.

4.3.1 Fouling and bubble nucleation

Figure 4.22 shows that there is a clear link between the number of bubbles on the heated surface and the amount of fouling obtained at the end of a 50 minute run. The conditions of each run are summarised in Table 4.6.

Table 4.6 Processing conditions of bubble-fouling linkage trial

Run	Product flow rate (l/h)	Heating medium temp (°C)	Product temp (°C)	Rig operating pressure (kPa.g)	Run duration (min)
R2.4	45	90	66	30	50
R2.5	45	90	67	130	50
R2.6	502	90	66	30	50

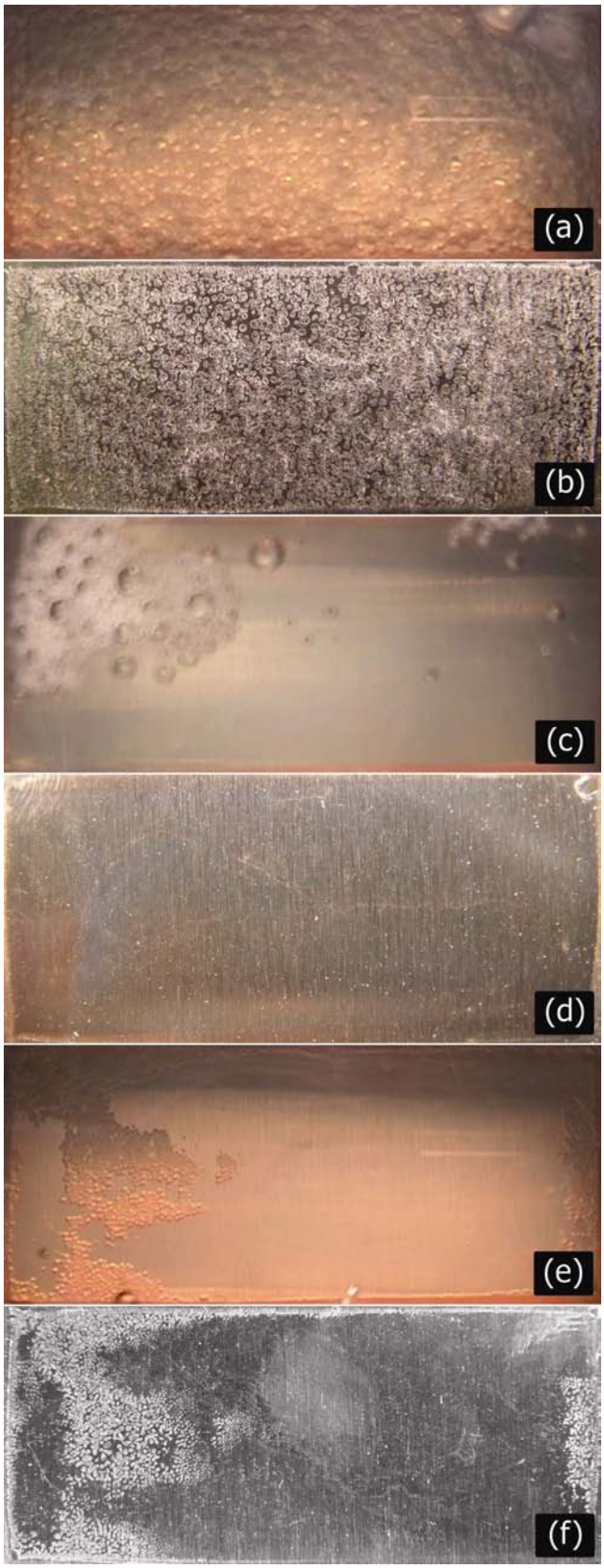

Figure 4.22 Results of the bubble-fouling linkage trial: (a, b) R2.4; (c, d) R2.5; (e, f) R2.6. (a, c, e) Video stills showing the bubble formation on the heated surfaces. (b, d, f) Photographs of the test plates taken after each run showing the fouling pattern.

In Figure 4.22 (a) the surface of MPHE plate was fully covered with air bubbles during the run at 30 kPa.g and 45 l/h. The fouling layer recovered at the end of the 50 minute run shown in Figure 4.22 (b) also covers the entire plate with typical ring like formations that previous workers (e.g. Tissier & Lalande, 1986) have attributed to proteins depositing around the rim of air bubbles. In Figure 4.22 (c) no bubbles were observed on the surface of the MPHE plate because of the high operating pressure (130 kPa.g) even though the flow rate remained at 45 l/h. Note that the large bubbles at the top left hand corner of Figure 4.22 (c) are not located on the heated surface but directly under the viewing window where they had gathered. No fouling was detected by the naked eye in that run (R2.5) as shown in Figure 4.22 (d). When the flow rate was increased to 500 l/h while keeping the pressure at 30 kPa.g only a small number of air bubbles were observed for a short time on the MPHE plate (Figure 4.22 (e)). The pattern of fouling obtained at the end of the run matched the pattern of air bubbles observed during the run almost perfectly (Figure 4.22 (f)). Thus the real-time analysis performed here shows a very strong and clear link between air bubble formation on heated surfaces and fouling.

Table 4.7 shows the mass of dry foulant at the end of the 50 minute runs, the percentage plate area covered by fouling and the foulant loading for the three runs in Figure 4.22. As one would expect, the total mass of fouling increased with the area covered by fouling. However, the foulant loading also varied with the product flow rate. The foulant loading, as defined in the thesis, is the mass of fouling per unit area of coverage and therefore, represents basically the average height of fouling assuming that the density remains constant between the runs. It is important to differentiate between the area covered by the fouling and the area available for heat transfer. The coverage area is often smaller than the heat transfer area.

Table 4.7 Mass of dry foulant and foulant loading on plates installed in the MPHE rig after processing WPC solutions at different flow rates and pressures.

Run No.	Mass of dry foulant (kg/m^2)	Area covered in fouling (%)	Foulant loading (kg/m^2)
R2.4	3.12×10^{-3}	74	4.19×10^{-3}
R2.5	nd	nd	-
R2.6	0.25×10^{-3}	21	1.17×10^{-3}

NB: nd = not detected.

The heated surface area covered by the bubbles during the run does not tell the full story; the residence time of the bubbles on the surface also has an impact. For a given pressure the flow rate affects both the surface area covered by the bubbles and their residence time. For R2.4, the bubbles stayed at the surface for almost the entire run (50 min, 30 kPa.g, 45 l/h) while during R2.6 (50 min, 30 kPa.g, 500 l/h) most bubbles had left the surface by t = 20 min. In fact, it is the linear velocity calculated from the cross-sectional area of the duct and the flow rate that defines the bubble behaviour not the flow rate alone. Thus, the flow rate of 500 l/h in the MPHE module corresponds roughly to a linear velocity of 0.27 m/s which would be about the same as the linear velocity in an industrial heat exchanger (Alfa-Laval, model no. CLIP10-RM) running at 50 000 l/h. The estimate of linear velocity for the industrial heat exchanger is given in Appendix D.5.

Figure 4.23 shows the pattern of the air nucleation on the heated surface over time for R2.6. Originally, approximately 80% of the MPHE surface was covered with tiny bubbles. A number of these left the surface very quickly and the area covered by the bubbles after 15 seconds was approximately 40%. The bubbles that remained grew and it appears, from the database of flow visualisations collected in this work, that the longer the bubble stays on the surface, the larger it becomes. This is more easily seen in visualisation experiments conducted with distilled water reported in section 4.3.2. The area covered by the bubbles decreased steadily over the next few minutes and disappeared almost completely after 20 minutes.

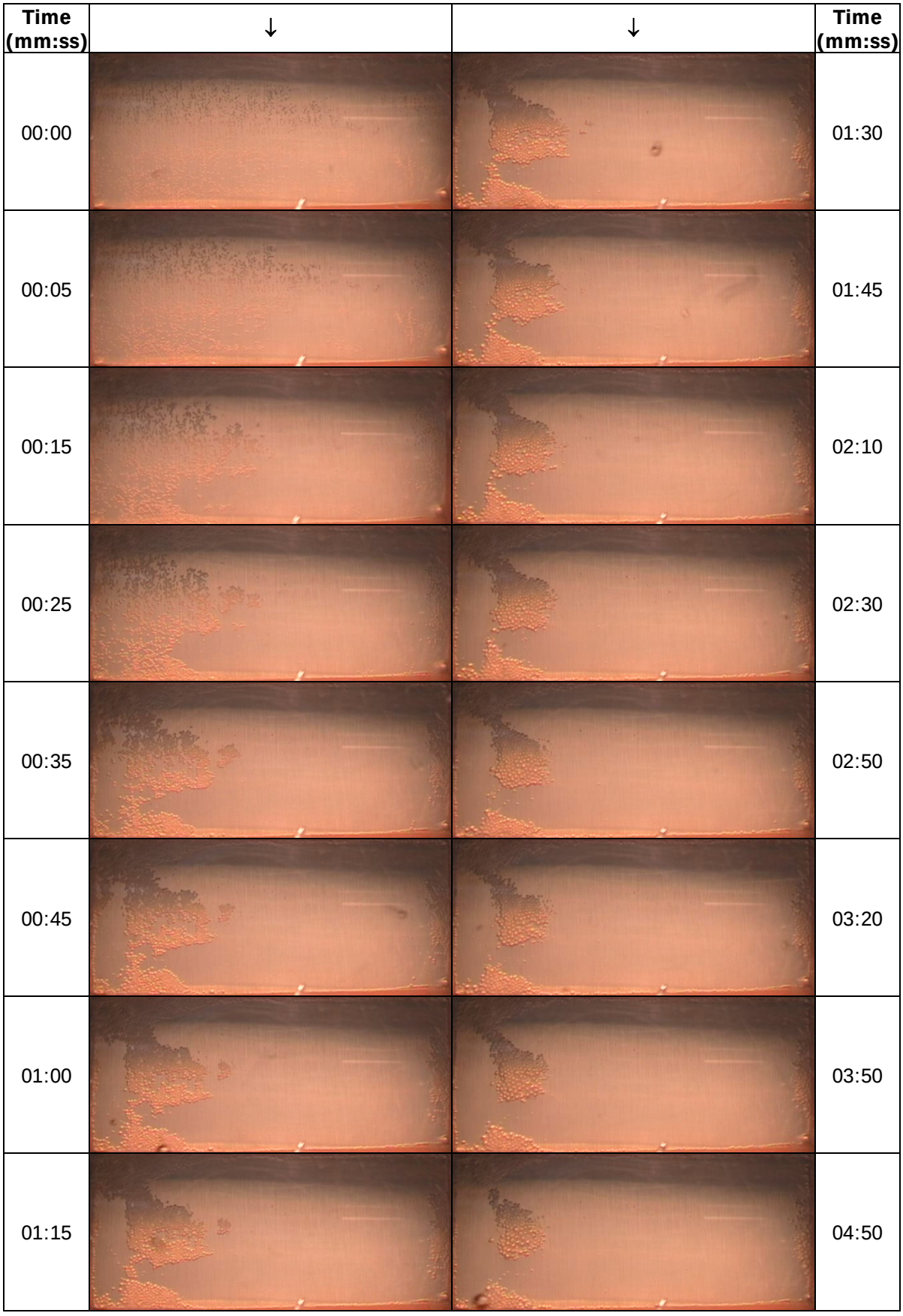

Figure 4.23 Video stills showing the bubble pattern on the MPHE heated surface processing a WPC solution at 502 l/h over the first five minutes of the run (R2.6).

Time (mm:ss)	↓	↓	Time (mm:ss)
05:50	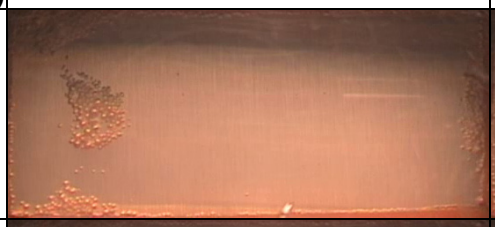	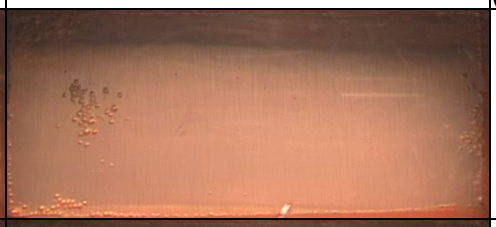	12:00
06:50			15:00
07:50			20:00
08:50			30:00
10:00			50:00

Figure 4.23 (continued) showing bubble pattern for the remainder of the run.

The fouling pattern observed at the end of the 50 minute run appears to be very close to the bubble pattern at t = 1 minute. In this example, no fouling was detected on the surface areas covered by tiny bubbles that left the surface within the first 15 seconds of the run. However, the complexity in the final fouling pattern is such that it was not possible to link individual bubbles that remained on the surface after the first 15 seconds to their corresponding deposits.

It is possible to make further interesting observations by focussing in on an area of the heat exchange surface (square section in Figure 4.24) where bubbles resided for a limited period of time.

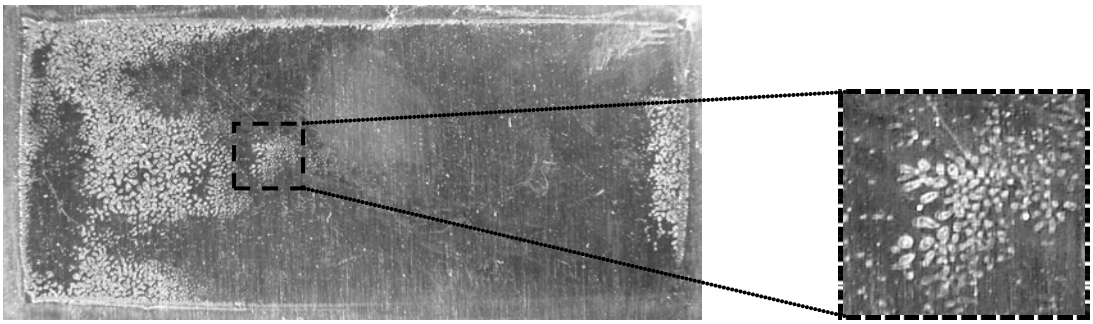

Figure 4.24 The section of the test plate from R2.6 used to make additional observations of bubble-type fouling structures.

The video stills in Figure 4.25 indicate that the bubbles in the area selected in Figure 4.24 have completely left the surface by approximately 3 minutes. Clearly, the bubbles do not have to stay on the surface a long time to induce fouling. In addition, some of the fouling islands appear to be oblong in shape instead of circular as one would expect from formation around bubbles suggested by previous workers (e.g. Tissier & Lalande, 1986).

Time (mm:ss)	00:00	00:05	00:15	00:25	00:35
					
Time (mm:ss)	00:45	01:00	01:15	01:30	01:45
				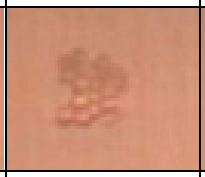	
Time (mm:ss)	02:10	02:30	02:50	03:20	Plate 50:00
		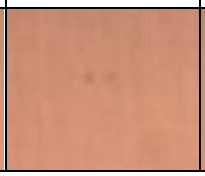	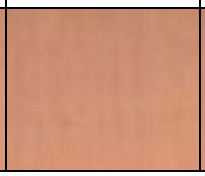	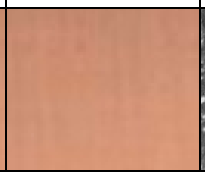	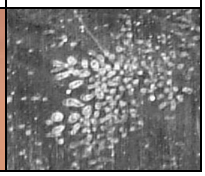

Figure 4.25 Video stills showing bubble nucleation over time in the area selected to make additional observations of the surface during and after the 50 minute run (R2.6).

The oblong fouling islands in the square section of Figure 4.24 were magnified and photographed according to section 3.3.1.3. The new magnified image in Figure 4.26

suggests that a fouling ring indeed forms around the periphery of the bubble but that this bubble, far from remaining static on the surface, actually moves with the local current and creates a series of footprints which give a general oblong shape to the fouling pattern in unmagnified photographs. It also appears from the footprints that the bubble grew with residence time on the surface. Considering that the longest residence time of the bubbles in that selected square area was approximately 3 minutes, each of the 15 or so footprints created by the bubble at the centre of Figure 4.26 would have taken (in a crude estimation) 12 seconds to form.

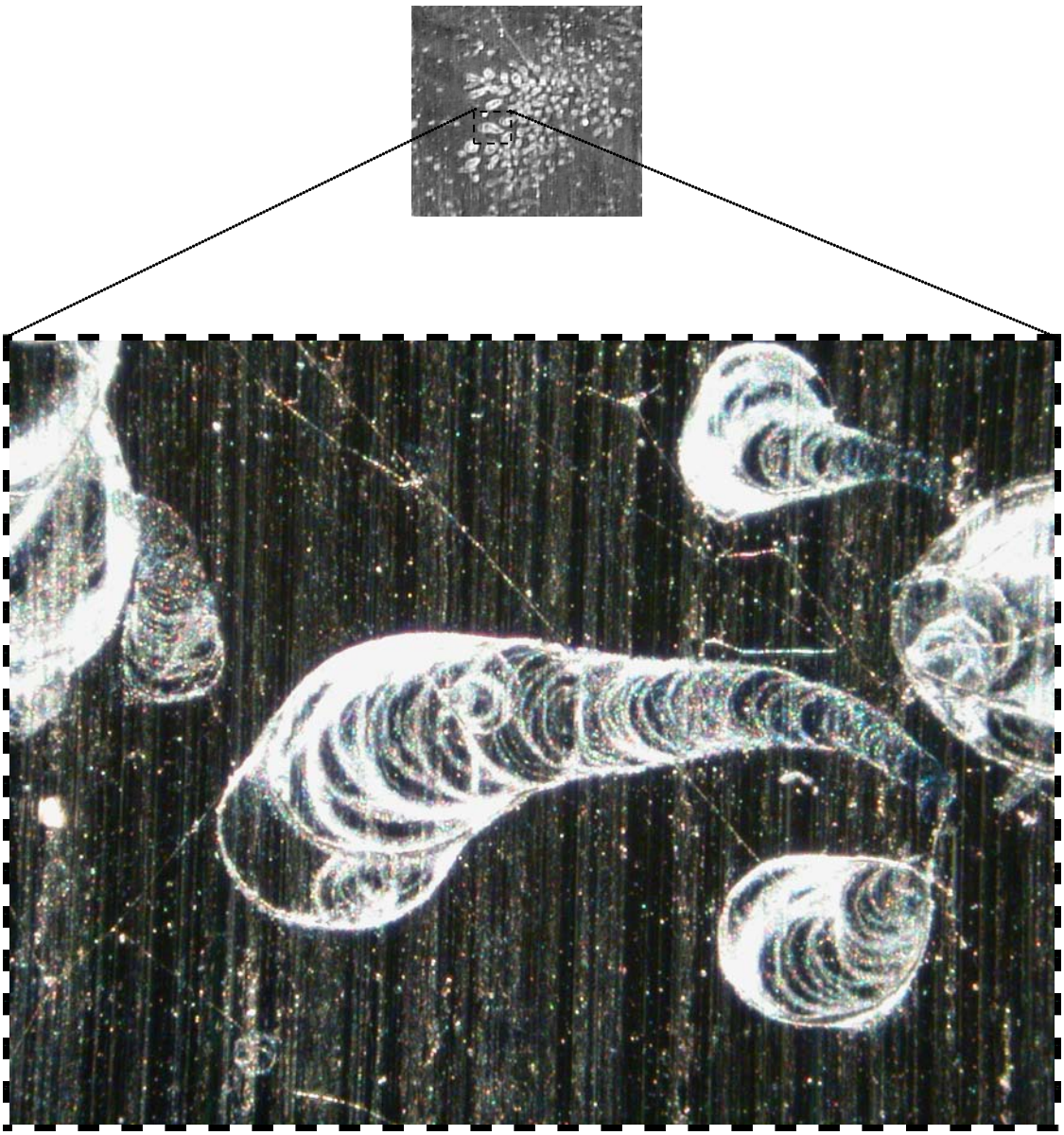

Figure 4.26 Magnified image (20 X) of the test plate fouled with a WPC solution showing evidence of bubble movement over the surface (R2.6).

The previous exercise must be considered only as a crude estimation. A cautious approach was taken here to give a conservative estimate of the induction time of fouling footprints. Others analysing these images might argue that the number of footprints shown are larger, resulting in a smaller estimation of time for the footprints to form.

At the lower flow rate of 45 l/h, the weaker local current has less effect on the bubble surface movement and this is clearly shown in Figure 4.27. The resulting patterns of fouling are varied because of the complexities of the local currents. However, it can be clearly seen that the bubbles still increase in size over time, as evidenced by the larger footprints at the end of the bubble path. Also there is evidence of possible coalescence between adjacent bubbles as shown in Figure 4.27 (d).

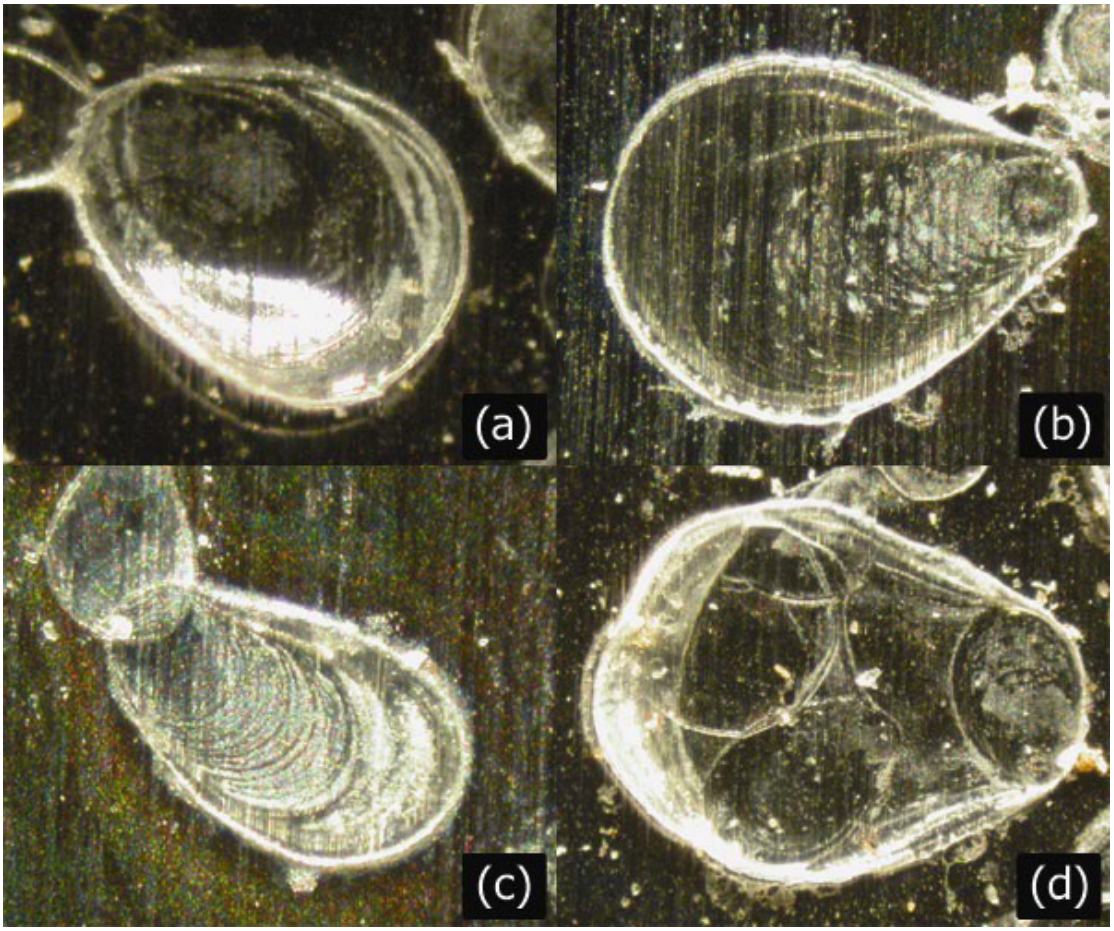

Figure 4.27 WPC fouling showing different types of structures: (a) stationary R2.9 (b) anchor R2.20 (c) shell-like R2.7 (d) coalescence R2.9. All runs processed at 45 l/h.

The higher foulant loading (Table 4.7) at the lower flow rate (R2.4) may now be explained by the creation of more footprints with longer residence times of the bubbles. One would expect that the presence of air bubbles also affects the rate of fouling not just the area of fouling. This point is discussed further in section 4.3.2.1 using data from the tubular heat exchanger.

4.3.2 Process variables and geometry

A number of the parameters that affect fouling, particularly their effect on air bubble nucleation on heated surfaces, are examined in this section: back-pressure, flow velocity and flow geometry. The experiments performed involved measurements of the fouling rate and the final mass of deposits, video footage of fluid and bubble behaviour and digital image analysis using three different fluids; water; WPC solutions and whole milk.

4.3.2.1 Pressure

The effect of pressure on fouling by whole milk in a tubular heat exchanger was investigated in a series of experiments (R1.1, R1.4, R1.6-1.9). Six levels of pressure were applied ranging from 30 to 80 kPa.g, in 10 kPa.g increments. Whole milk (standardised and homogenised 3.3% fat) was heated in the tubular heat exchanger for 4 hours. At the conclusion of each run the test tube was removed, photographed and weighed.

Figure 4.28 shows the effect of operating pressure on the amount of fouling present on the heated surface after four hours of operation. These results show that the operating pressure has a strong influence on the total mass of fouling in this pilot plant and are consistent with the observation in the previous section that there is a strong relationship between air nucleation and fouling. It is well known that the solubility of air in aqueous media depends on the total pressure applied to the system. Hence, the air nucleation at the heated stainless steel surface decreased as the pressure was increased. The rate of fouling also decreased as the pressure increased (Figure 4.29). Thus, the two complementary measurements of the severity of fouling in Figures 4.28 & 4.29 corroborate one another. These data agree qualitatively with the observations by Grasshoff (1988) on the effect of pressure on fouling.

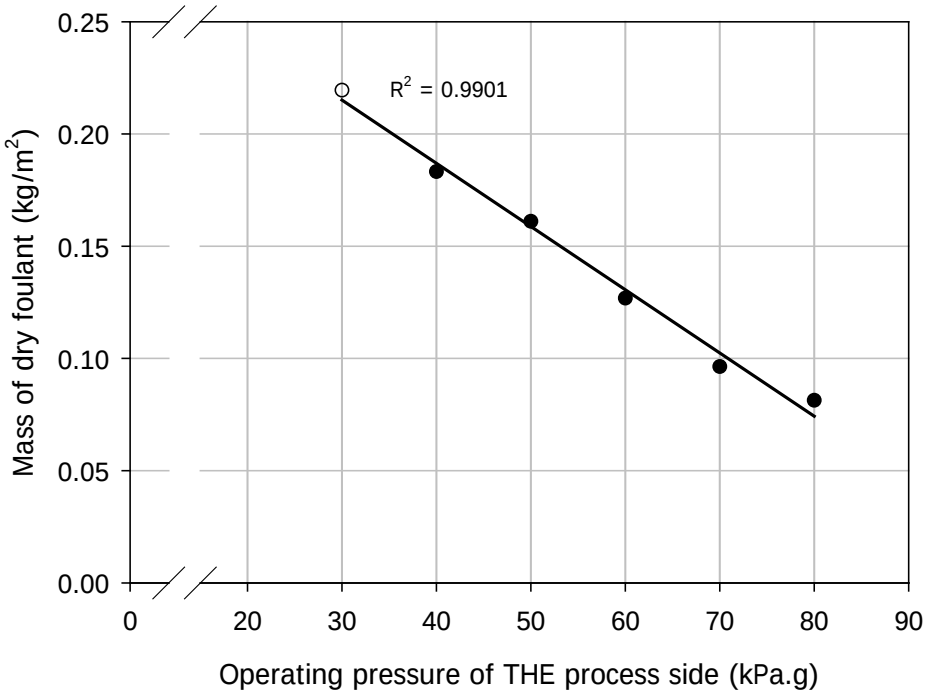

Figure 4.28 The effect of the process side operating pressure on the mass of dry foulant obtained at the end of each run using the THE processing whole milk.

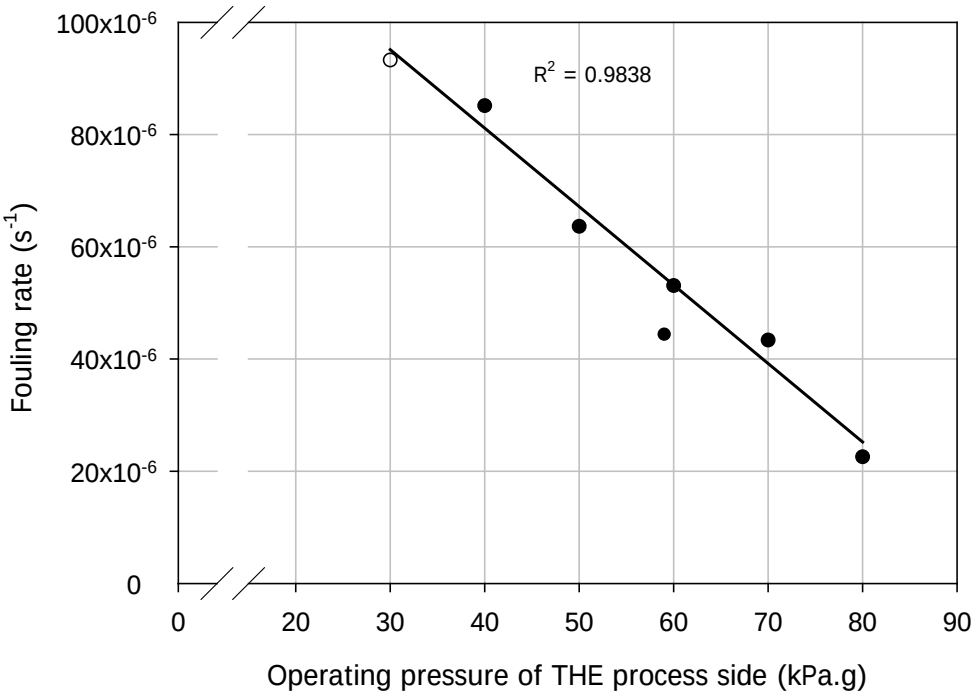

Figure 4.29 The effect of THE process side operating pressure on the rate of fouling of whole milk.

An interesting aspect of the effect of pressure on fouling by whole milk can be observed by analysis of the structure of the fouling deposits. Figures 4.30 & 4.31 show photographs of fouling on the THE test tubes at the end of the two runs (R1.1 & R1.9) operating at different pressures (30 and 80 kPa.g). It must be noted that the two photographs were taken at the same magnification, perspective and show the full diameter of the tube. The two runs were operated under identical conditions of flow rate, temperature and start up procedure. It is obvious that there are major differences in the size and number of fouling subunits (fouling deposited around air bubbles as discussed in section 4.3.1) at the two pressures. There were fewer subunits at 80 kPa.g than at 30 kPa.g but they were considerably larger.

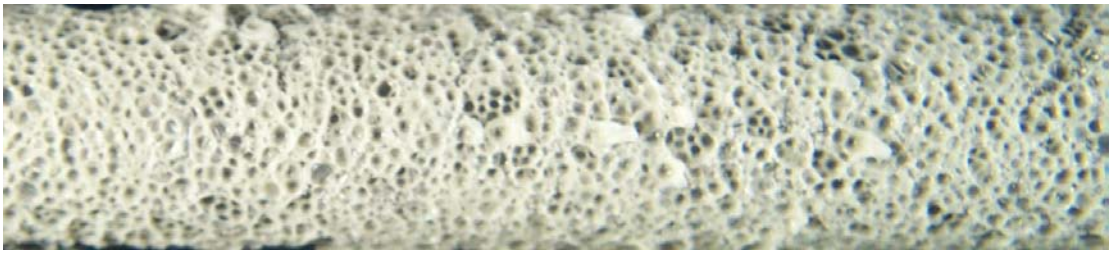

Figure 4.30 An example structure of the fouling obtained after processing whole milk in the THE at an operating pressure of 30 kPa.g (R1.1).

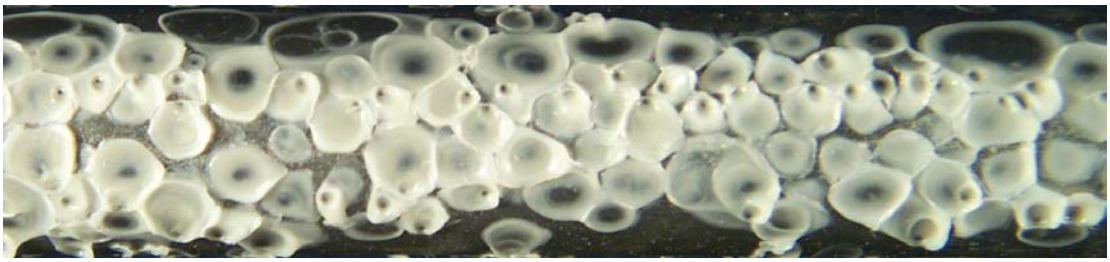

Figure 4.31 An example structure of the fouling obtained after processing whole milk in the THE at an operating pressure of 80 kPa.g (R1.9).

A useful technique for quantifying structural information was developed by digital analysis of these photographs using Sigmascan as described in section 3.3.1.3. Essentially, each pixel was examined for the intensity of the brightness and a threshold was set to distinguish between the whiter fouled areas and the darker clean stainless surface. The pixels below this threshold value were coloured red and overlaid on the original photograph (Figures 4.32 & 4.33). The area of clean stainless steel was determined by the number of coloured pixels in the overlay. The fouled area was determined by subtracting the clean stainless steel area from the total area

of the photographs. For each THE run 44 photos were taken to capture the fouling on a single tube and these were analysed with Sigmascan. The total percentage of fouling coverage was 84 and 57% for 30 kPa.g and 80 kPa.g respectively.

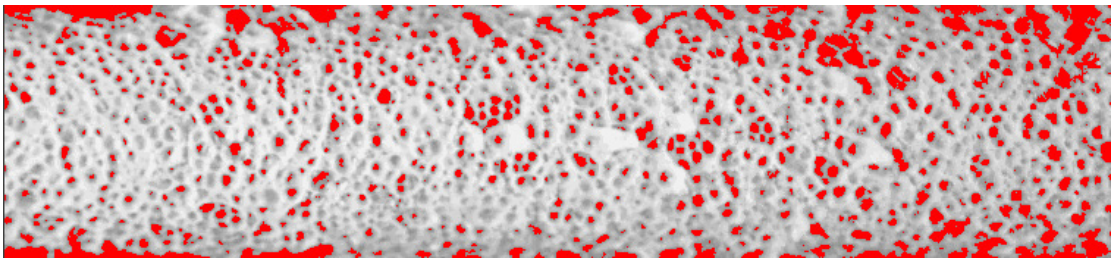

Figure 4.32 Analysed image of Figure 4.30. Red regions indicate the areas of the tube not covered in fouling.

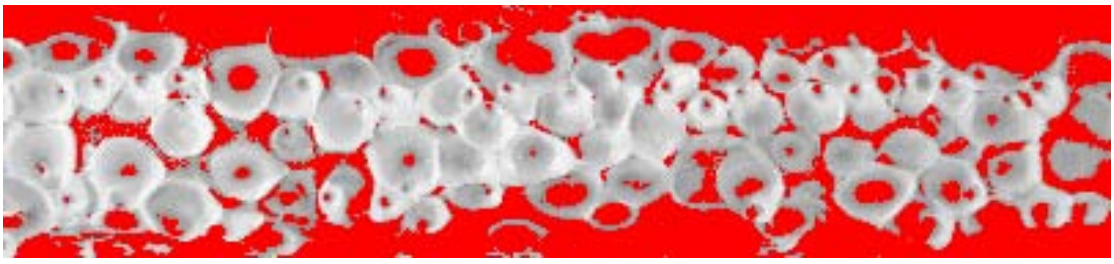

Figure 4.33 Analysed image of Figure 4.31. Red regions indicate the areas of the tube not covered in fouling.

Figure 4.34 shows the effect of operating pressure on the area of the heated surface covered in fouling. There is almost a linear relationship between the fouling area and the operating pressure. However, the noise in the data is relatively high. This type of analysis is not perfect because it relies on a pixel intensity threshold to distinguish between the fouled and non-fouled areas. The success of this method is therefore heavily reliant on the quality of the raw image. Any areas over or under exposed will introduce errors into the analysis. Also, it can be argued that regions on the limbs of the image may be misrepresented due to perspective errors. This error was reduced by cropping the photographs to represent only the size of the outer diameter of the clean stainless steel tube. In Figure 4.33 there are large areas of clean surface in the limb regions. This was a true representation of the surface and not an artefact of perspective. Note that this technique identifies stainless steel locations inside the sub-units as non-fouled areas. There is also a strong correlation between the coverage area of fouling and the mass of fouling at the end of the run (Figure 4.35).

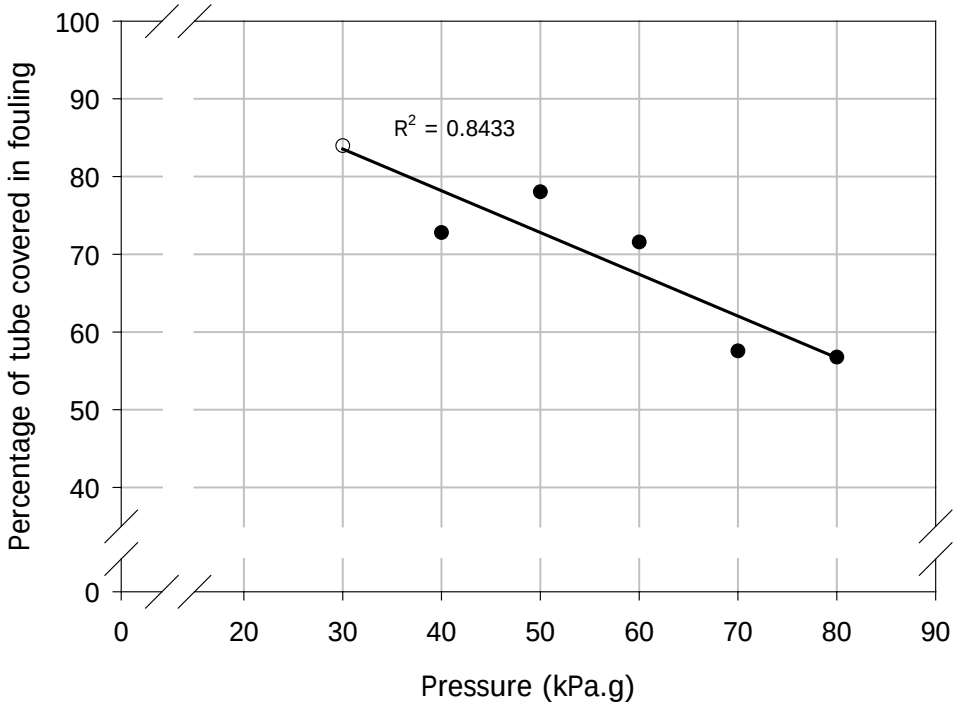

Figure 4.34 The effect of THE process side operating pressure on the area of the heated surface covered in whole milk fouling.

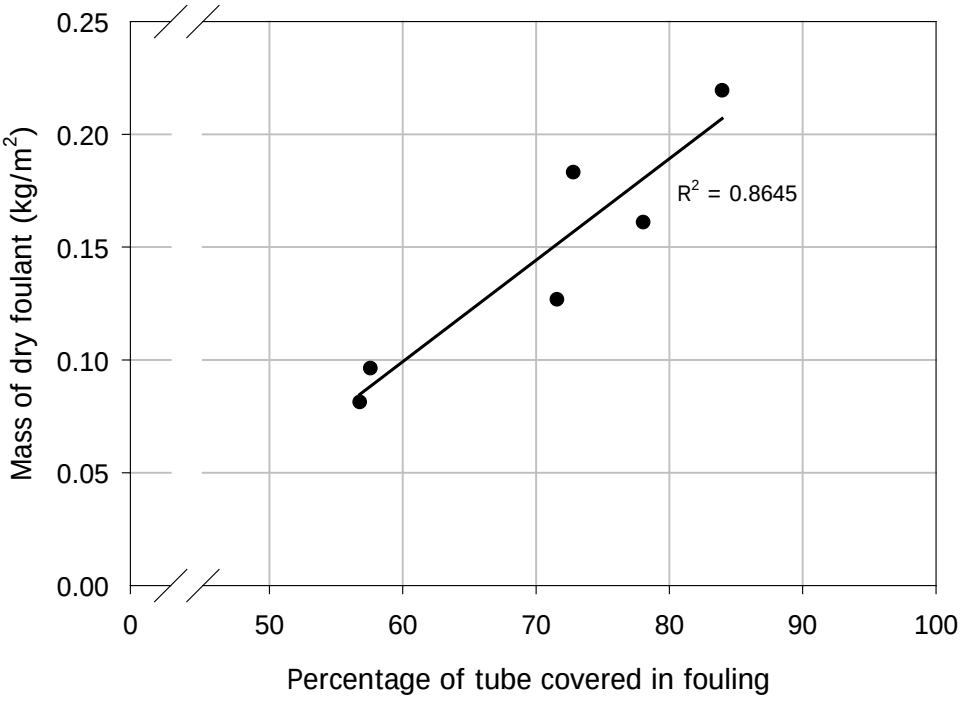

Figure 4.35 Mass of dry foulant obtained at the end of each run versus the area of the heated surface covered in whole milk fouling.

Table 4.8 Mass of dry foulant and foulant loading on tubes installed in the THE rig after processing whole milk at different operating pressures.

Run No.	Rig operating pressure (kPa.g)	Mass of dry foulant (kg/m^2)	Area covered in fouling (%)	Foulant loading (kg/m^2)
R1.1	30	2.19×10^{-1}	84	2.61×10^{-1}
R1.6	40	1.83×10^{-1}	73	2.52×10^{-1}
R1.4	50	1.61×10^{-1}	78	2.06×10^{-1}
R1.7	60	1.27×10^{-1}	72	1.77×10^{-1}
R1.8	70	0.96×10^{-1}	58	1.67×10^{-1}
R1.9	80	0.81×10^{-1}	57	1.43×10^{-1}

NB: nd = not detected.

However, there are other effects that influence the mass of fouling; for example, the operating pressure changes the foulant loading as shown in Table 4.8 & Figure 4.38. A change in foulant loading indicates that the height of the fouling layers is affected by the pressure. This is clearly shown in the expanded photographs of fouled tubes obtained at 30 kPa.g (Figure 4.36) and 80 kPa.g (Figure 4.37) where the area of each tube has been darkened to highlight the side view of the fouling layer over the horizon.

An initial reaction of a casual observer may be to link the difference in height with a decrease in rate of protein deposition on existing fouling layers with increasing pressures. However, the literature of protein chemistry does not suggest any apparent reason for a change in tendency of proteins to deposit on existing fouling layers as the pressure changes. Work in pressure denaturation of proteins (e.g. Huppertz *et al.*, 2004) indicates that the minimum operating pressure required to affect the proteins is much higher than those used in the present experiments.

A more reasonable explanation for the change in foulant loading and height is related to the packing density of the bubbles at different pressures. At the lower pressure (30 kPa.g) there are far more bubbles than at 80 kPa.g and they are more densely packed, which constrains their lateral growth and therefore forces up their vertical height as evidenced in the fouling footprints shown in Figure 4.36.

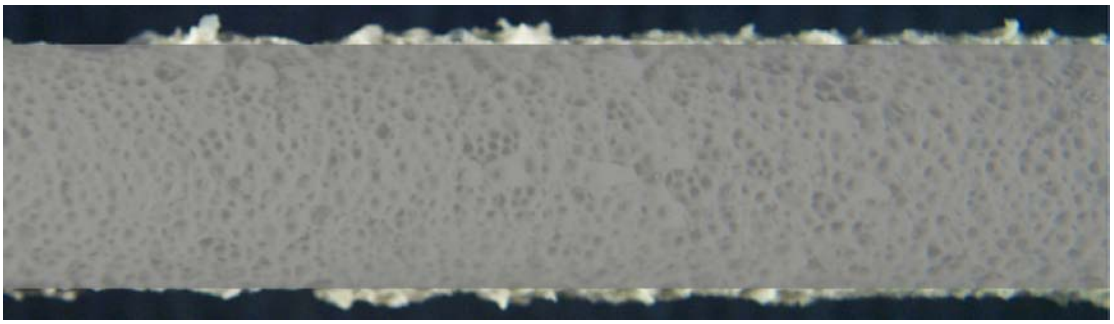

Figure 4.36 Expanded photograph of Figure 4.30 indicating the height of fouling above the horizon. Darkened section indicates the area of the THE tube (R1.1).

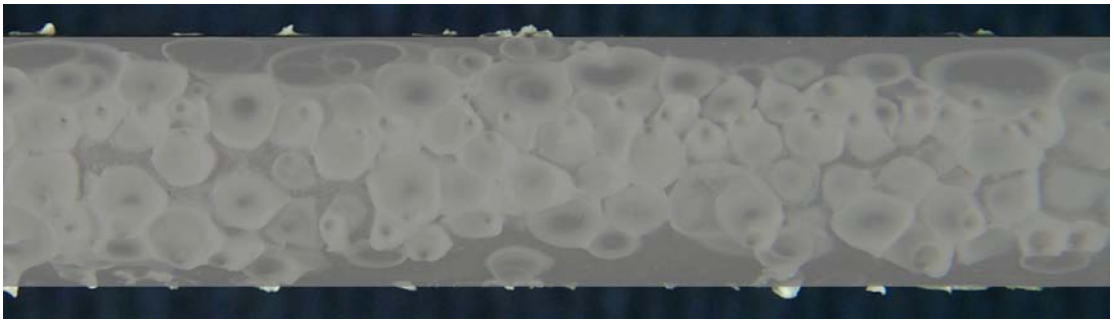

Figure 4.37 Expanded photograph of Figure 4.31 indicating the height of fouling above the horizon. Darkened section indicates the area of the THE tube (R1.9).

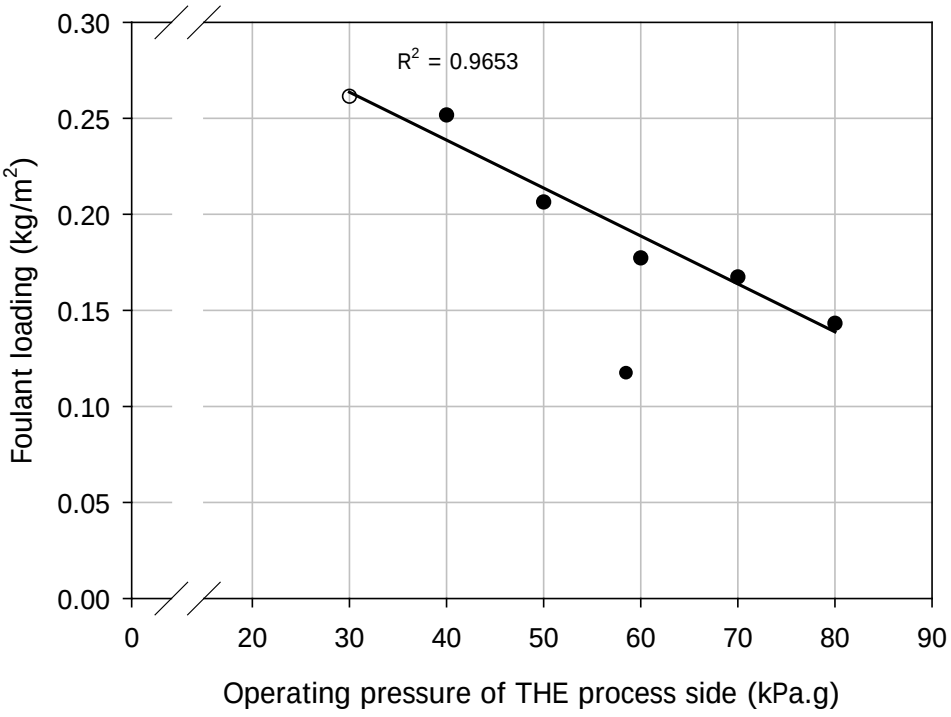

Figure 4.38 The effect of THE process side operating pressure on the foulant loading of whole milk on the heated surface.

The structure of fouling deposits and the linkage between bubble development and fouling shown in section 4.3.1 suggested the need for more information about bubble behaviour on heated surfaces at different pressures. Visualisation runs were performed with water in the MPHE (R2.10-2.12). The quality of video footage obtained was much higher with water as the test fluid than with whey solutions and allowed quantitative analysis of the bubble behaviour.

Figure 4.39 shows the effect of pressure on the development of surface bubbles in water flowing at 45 l/h through the MPHE with the heating fluid at 85°C. Tiny bubbles developed immediately during the 30 and 80 kPa.g runs but not the 130 kPa.g run. The rate at which they grew was affected by the pressure. For example, after 7 minutes the size of bubbles at 30 kPa.g can be seen to be much larger than those seen at 80 kPa.g. At 30 kPa.g large bubbles started to leave the heated surface at 15 minutes and by the end of the run (50 minutes) only a number of smaller bubbles were left. It is interesting to note that water was not recirculated thus fresh water, with the same amount of dissolved air, entered the MPHE continuously throughout the run. Yet no new bubbles were formed to replace the bubbles that had left the surface. At 80 kPa.g the bubbles were still growing on the surface at 15 minutes and there is only a hint of them leaving at 50 minutes. Bubbles never developed at 130 kPa.g over the duration of this experiment.

The size of bubbles in a number of still shots taken from the videos were analysed with the help of Sigmascan. It was clearly not possible to measure the size of all bubbles, even in one photograph. Each photograph was divided into 40 squares where one square represented 25 mm^2 of heat exchange surface. One square representative of the entire surface was selected at random and was analysed in each still taken from the videos. A shape trace of the outline of all bubbles in this square was overlaid on the photographs and the area within the trace calculated with Sigmascan. An average of all bubble diameters in the square was calculated to allow tracking of this nominal diameter with time. The average size and number of bubbles at 30 kPa.g and 80 kPa.g are plotted against the time at which the stills were taken (Figures 4.40 & 4.41).

Time (mm:ss)	30 kPa.g (R2.10)	80 kPa.g (R2.11)	130 kPa.g (R2.12)
00:00			
00:30			
01:00			
02:00			
04:00			
07:00			
10:00			
15:00			
20:00	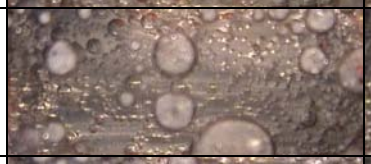		
30:00			
50:00	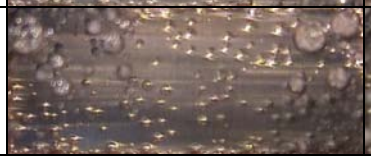	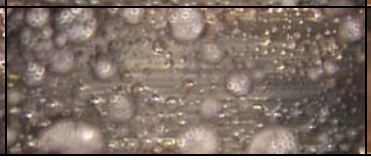	

Figure 4.39 Video stills showing the effect of operating pressure on bubble behaviour on the MPHE heated surface processing water.

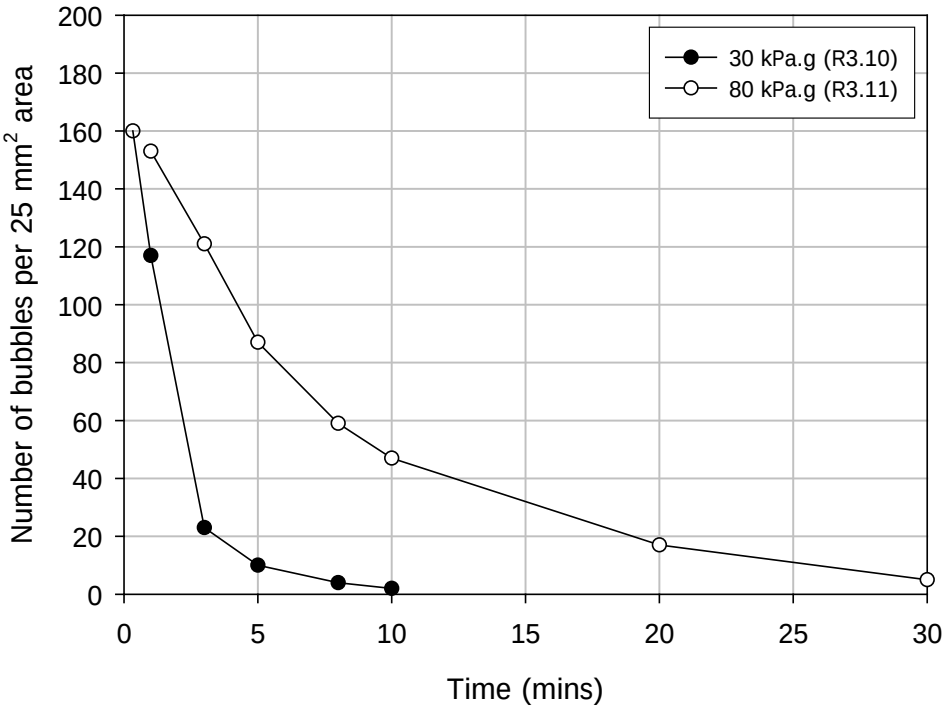

Figure 4.40 The number of bubbles in a 25 mm² section of the heat exchange surface installed in the MPHE processing water at different pressures.

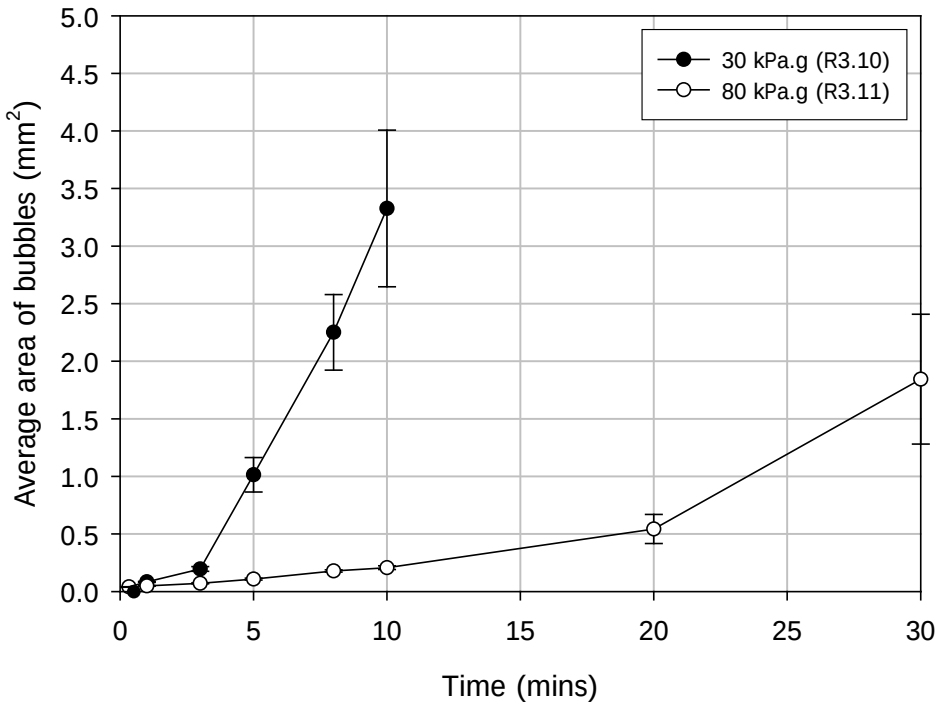

Figure 4.41 The average area of bubbles in a 25 mm² section of the heat exchange surface installed in the MPHE processing water at different pressures.

The size of the bubbles increased with residence time but this increase was much greater at 30 kPa.g than at 80 kPa.g. At the same time the number of bubbles decreased faster at 30 kPa.g than at 80 kPa.g. At t = 20 seconds the number of bubbles in the 25 mm^2 area for the 30 kPa.g run was 160 but had fallen to 2 at t = 10 minutes whereas, this number was 47 for the 80 kPa.g run. Thus, the digitisation method used fully reflects the visual observations of the photographs but allows a much more quantitative analysis. The bubble visualisation explains some of the fouling patterns observed in Figure 4.19 where one sees the presence of small circular footprints of fouling inside larger ones. In the first minute or less there are large numbers of smaller bubbles that created fouling footprints within 30 seconds according to the WPC visualisations (section 4.3.1). Then these bubbles coalesced into much larger bubbles which created their own footprint surrounding the original smaller footprints (e.g. Figure 4.27 (d)).

However, surface bubbles behaved slightly differently in WPC solutions than in water. This is shown in the ten WPC visualisations listed in Appendix C. Stills of video footage showing bubbles in runs at pressures 30 (R2.4), 80 (R2.7) and 130 kPa.g (R2.5) and a flow rate of 45 l/h are shown in Figure 4.42. The field of vision of the surface bubbles is often masked by coalesced bubbles that have risen through the WPC solution and stuck under the viewing window. It appeared that the whey proteins had a stabilising effect on the bubbles which were more difficult to sweep away from the viewing surface than those formed in water. This is compatible with known surfactant properties of dairy proteins (e.g. Pelan *et al.*, 1997). Nevertheless, one can make out from the stills that the residence time of bubbles at the heated surface is much longer in WPC than in water solutions. In fact, after 50 minutes most of the bubbles in the 30 kPa.g run are still on the surface. At 80 kPa.g the bubble coverage in the WPC solution at 50 minutes is still substantial (Figure 4.42) but could not be calculated exactly because of the masking qualities of the bubbles directly under the viewing window. The number of bubbles remaining in the water at 80 kPa.g had dropped from 153 at t = 1 min to approximating 5 per 25 mm^2 after 30 minutes (Figure 4.40). At the high pressure of 130 kPa.g no bubbles were observed and there is no fouling after 50 minutes (Figure 4.43 (c), Table 4.9). This was to be expected from the results of the milk and water runs reported earlier in this section (e.g. Figures 4.28 & 4.39).

Time (mm:ss)	30 kPa.g (R2.4)	80 kPa.g (R2.7)	130 kPa.g (R2.5)
00:00			
00:30	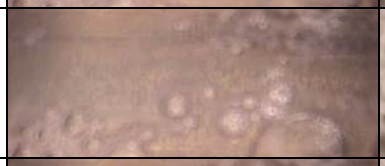		
01:00			
02:00	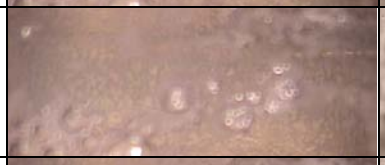		
04:00	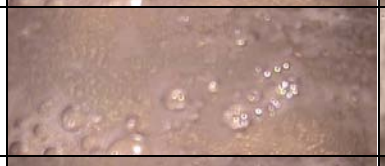		
07:00			
10:00			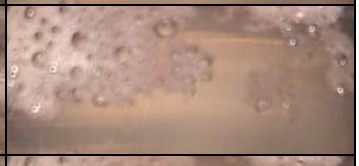
15:00			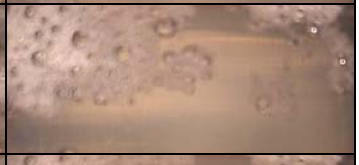
20:00			
30:00	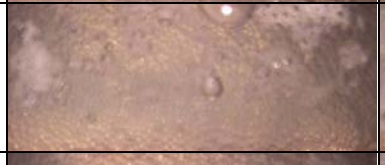		
50:00			

Figure 4.42 Video stills showing the effect of operating pressure on the bubble behaviour on the MPHE heated surface processing WPC solutions.

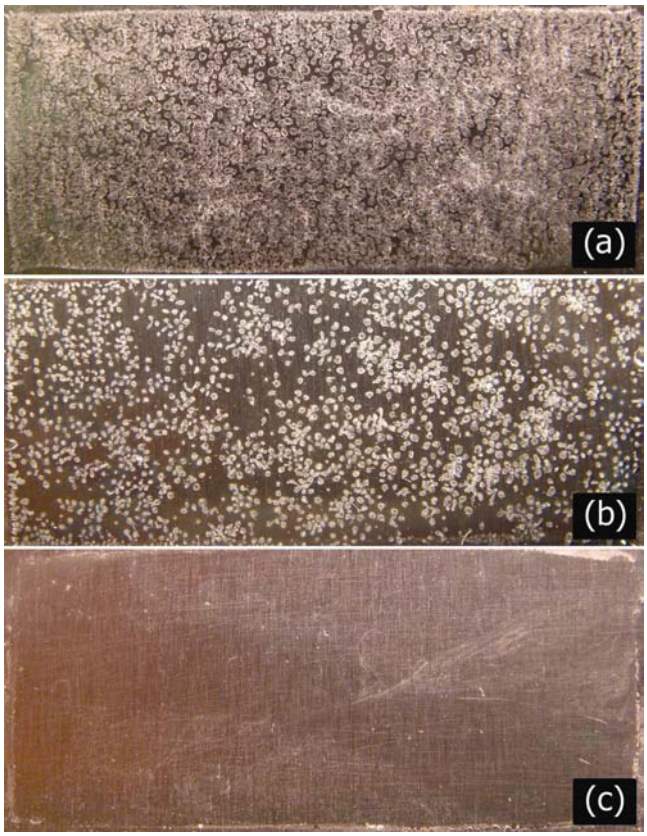

Figure 4.43 Topography of MPHE test plates after processing WPC solutions at different operating pressures (a) R2.4 (b) R2.7 (c) R2.5.

The fouling patterns of the WPC solution were different to that shown in milk. At 80 kPa.g large subunits of milk fouling that touched one another can be seen (Figure 4.31). In Figure 4.43 (b), the fouling islands do not touch one another even though they appear to be slightly bigger than the fouling islands at 30 kPa.g (Figure 4.43 (a)). The low fouling coverage in runs R2.4, R2.7 and R2.5 is probably attributable to the shorter runs in WPC fouling (50 minutes compared with 4 hours) and the much lower solids concentration (0.1 compared with 12% total solids). This indicates that Figure 4.43 reflects the fouling pattern early in the fouling period and with a slower fouling rate than the ones observed with milk (e.g. Figures 4.30 & 4.31).

Table 4.9 Mass of dry foulant and foulant loading on plates installed in the MPHE rig after processing WPC solutions at different pressures.

Run No.	Mass of dry foulant (kg/m^2)	Area covered in fouling (%)	Foulant loading (kg/m^2)
R2.4	3.12×10^{-3}	74	4.32×10^{-3}
R2.7	0.82×10^{-3}	30	2.73×10^{-3}
R2.5	nd	nd	-

NB: nd = not detected.

The effect of pressure on WPC fouling (Table 4.9) is similar to its effect on milk fouling (Table 4.8) in the sense that the mass of dry foulant at the end of the run, the area covered by the fouling and the foulant loading all decrease as the pressure increases.

4.3.2.2 Flow rate

The effect of flow rate on bubble behaviour and fouling by WPC solutions was investigated with water and WPC solutions. The flow rates tested for water and WPC are listed in Tables 4.10 & 4.11 respectively along with other key process variables.

Table 4.10 Process variables of the runs conducted with the MPHE processing water at different flow rates.

Run	Product flow rate (l/h)	Heating medium temp (°C)	Product temp (°C)	Rig operating pressure (kPa.g)	Run duration (min)
R2.10	45	91	65	30	50
R2.13	251	90	67	30	50
R2.14	1940	91	69	59	50

Table 4.11 Process variables of the runs conducted with the MPHE processing WPC solutions at different flow rates.

Run	Product flow rate (l/h)	Heating medium temp (°C)	Product temp (°C)	Rig operating pressure (kPa.g)	Run duration (min)
R2.4	45	90	66	30	50
R2.6	502	90	66	30	50
R2.8	1940	90	69	59	50

Figure 4.44 shows the bubble behaviour at three representative water flow rates. Figure 4.45 shows the bubble behaviour in WPC solutions for the same range of flow rates. The back pressure in all runs was kept at 30 kPa.g except for the runs at 1940 l/h which had to be conducted at 59 kPa.g because of the large pressure drop in the plant downstream from the modules.

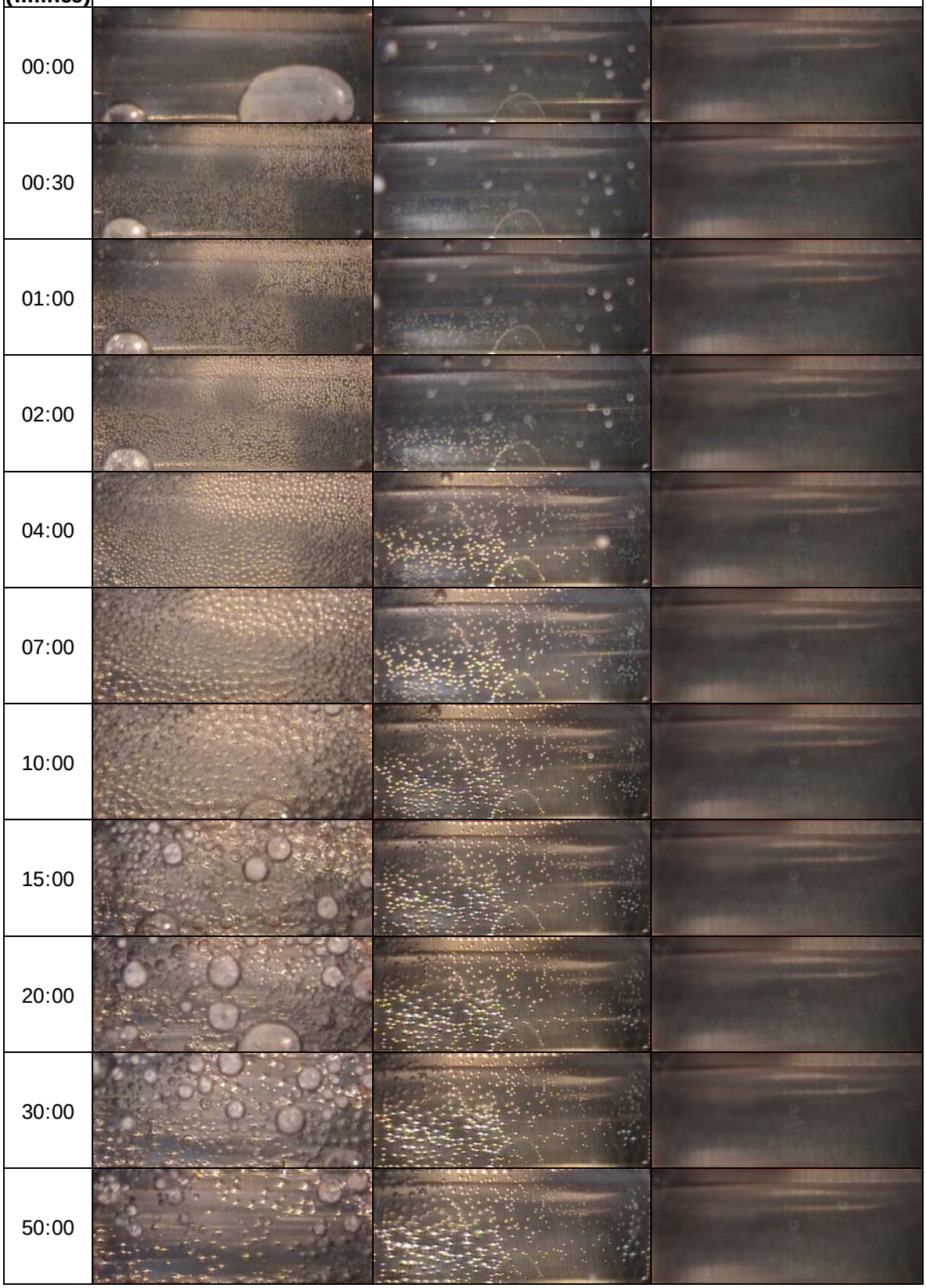

Figure 4.44 Video stills showing the effect of flow rate on bubble behaviour on the MPHE heated surface processing water.

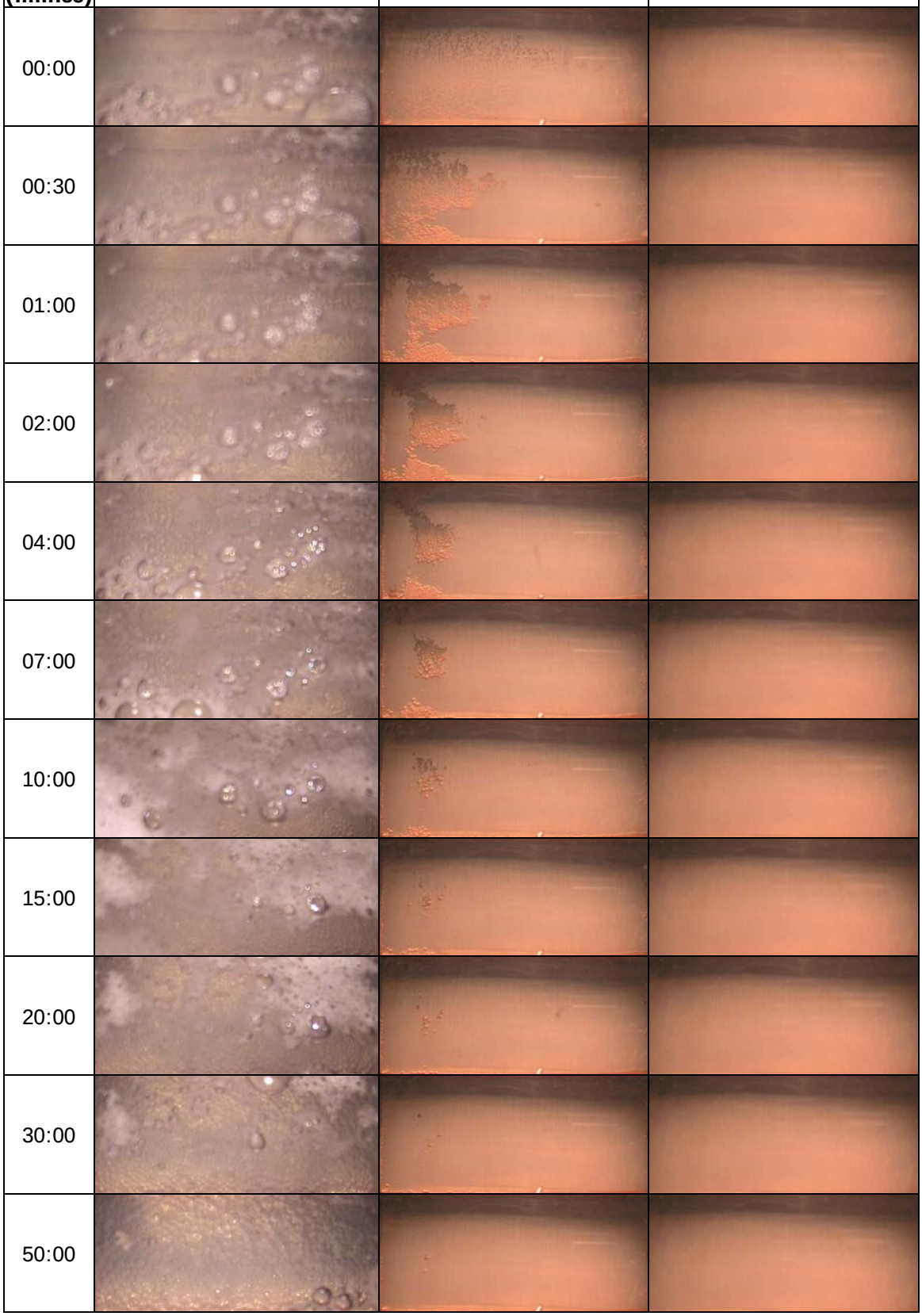

Figure 4.45 Video stills showing the effect of flow rate on bubble behaviour on the MPHE heated surface processing WPC solutions.

No bubbles were observed at 1 940 l/h for either the WPC or water runs. At 45 l/h the plate surface was completely covered with air bubbles after 1 minute of operation and they persisted in the WPC solution whereas most of them had left the surface by 50 minutes in the water solution. Thus, the present visualisation confirms the argument suggested by previous authors (e.g. Jeurnink, 1995a) that the hydrodynamic forces tend to sweep the air bubbles away from the surface at high velocities.

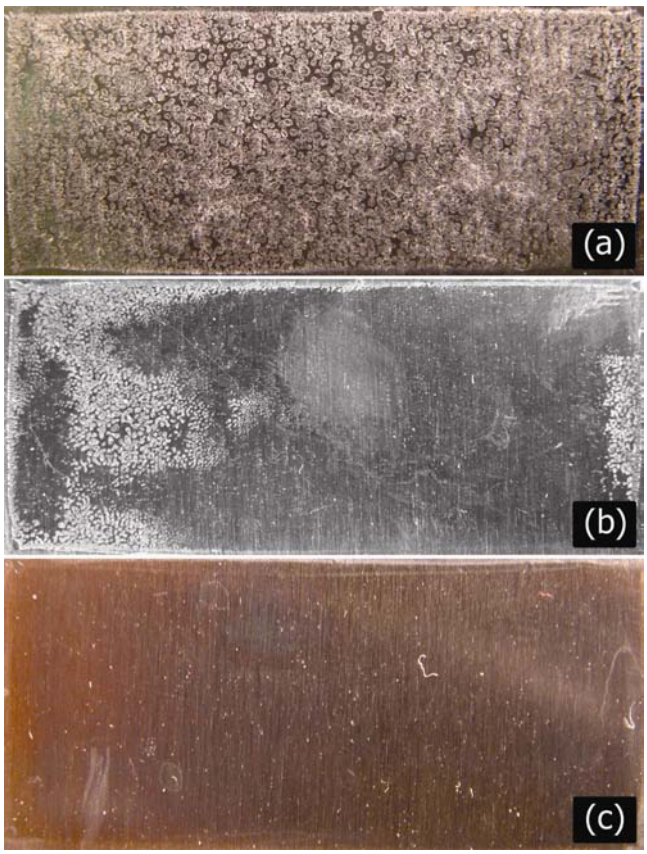

Figure 4.46 Topography of MPHE test plates after processing WPC solutions at different process fluid flow rates (a) 45 l/h - R2.4 (b) 502 l/h - R2.6 (c) 1 940 l/h - R2.8.

As discussed in section 4.3.1, the fouling mirrors the bubble coverage of the heated plate and therefore decreases as the velocity increases as shown in Figure 4.46. As with the pressure case, the fouling loading was severely reduced as the flow rate was increased (Table 4.12). In R2.6 (502 l/h) most of the bubbles were seen to leave the surface by t =15 min although there was partial surface coverage up until t =10 min. Since, fouling starts developing around bubbles shortly after nucleation on the surface (usually within the first minute), the bubbles that stayed for 10 minutes

would have contributed to the fouling coverage but would have had little time to grow because of the relatively short residence time of the bubble at the surface.

Table 4.12 Mass of dry foulant and foulant loading on plates installed in the MPHE rig after processing WPC solutions at different flow rates.

Run No.	Flow rate (l/h)	Mass of dry foulant (kg/m^2)	Area covered in fouling (%)	Foulant loading (kg/m^2)
R2.4	45	3.12×10^{-3}	74	4.32×10^{-3}
R2.6	502	0.25×10^{-3}	21	1.14×10^{-3}
R2.8	1940	nd	nd	-

NB: nd = not detected.

4.3.2.3 Geometry

The argument that bubble residence on heated surfaces is a function of the flow rate is not entirely correct. The variable of importance is likely to be the shearing forces, which depend on the local fluid velocity. The pattern of velocity and shear in a heat exchanger is defined substantially by its geometry. A number of experiments were attempted to prove this point and only two of the more successful ones are reported here.

In R2.15 and R2.16, the effect of an obstruction in the form of a metal strip attached perpendicularly to the heated surface was investigated. R2.15 shows that at a water flow rate of approximately 1 000 l/h and a pressure of 35 kPa.g no bubbles formed on the surface (Figure 4.47). When the obstruction was installed (R2.16), bubbles developed downstream of the obstruction for the same flow rate and pressure. It is easily demonstrated in modern computer fluid dynamic (CFD) packages (e.g. Norton & Sun, 2006) that a wake region occurs behind an obstruction normal to the flow. The velocity in that wake, often called a recirculation region, is much lower than the velocity of the bulk stream which is why air bubbles can be formed locally even at this high flow rate. One would expect, therefore, that fouling would occur in those recirculation regions in the plant, but there was no time left to carry out the fouling validating experiments in this thesis.

Time (mm:ss)	999 l/h (R2.15)	1 002 l/h (R2.16)
00:00		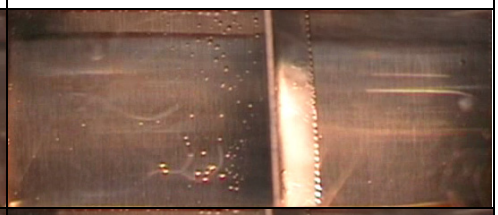
00:30		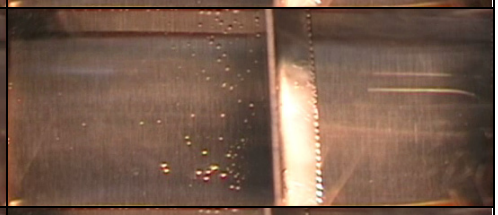
01:00		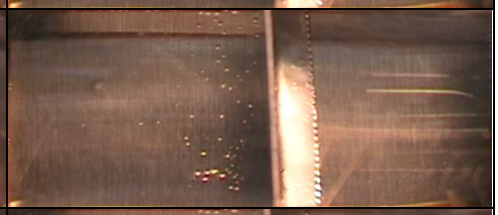
02:00		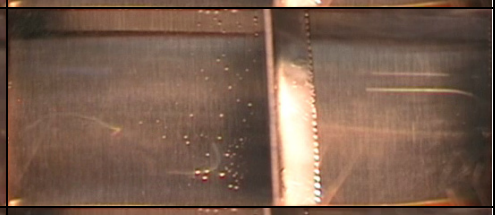
03:00		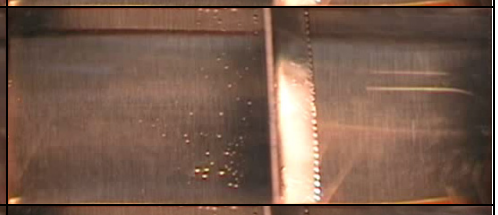
05:00		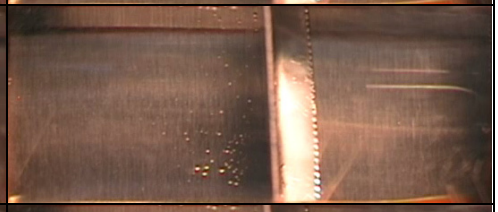
07:00		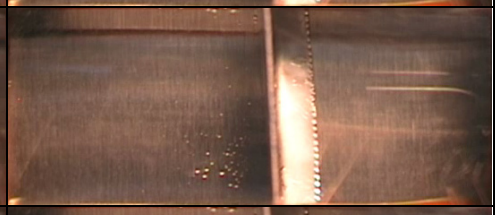
09:00		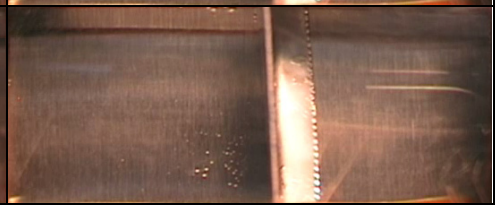

Figure 4.47 Video stills showing the effect of an obstruction on bubble behaviour on the MPHE heated surface processing water.

An immediate query in air bubble fouling is the relative contribution of the wake created behind the bubbles compared to the contribution made by proteins moving to the plate through spreading on the surface of the bubbles. To separate the hydrodynamic action of the bubble (wake effect) and the chemical action (air-liquid interface effect), a number of glue drops were placed on plates (5 in total) and installed in the modules of the MPHE. A run was performed with a WPC solution (0.1%) flowing at 46 l/h with a pressure of 131 kPa.g (R2.17) through the MPHE rig resulting in 5 replicates. At that pressure minimal bubbles formed on the surface as observed with the plate installed in the windowed module. The glue drops reproduced the geometry of the air bubbles without the interfacial properties. The wake regions behind the glue drops were quite small but one or two tiny air bubbles could be seen there and appeared to last for the whole 50 minutes of the run, which is to be expected from the WPC visualisation reported earlier in section 4.3.2.1.

Fouling on the plates (R2.17) was, however, too small to detect by the weighing method used previously. There was no tell-tale ring of fouling to be observed where the tiny bubbles were located (Figure 4.48). However, there was a slight blue discolouration that defined the wake region very clearly and while this may have been too light to detect gravimetrically, it has been reported as evidence of slight deposition at high pressures (e.g. Tissier & Lalande, 1986).

The above experiments suggest that disturbances to the main stream flow can create fouling by a change of flow pattern. But this effect is substantially smaller than the effect of air bubble fouling.

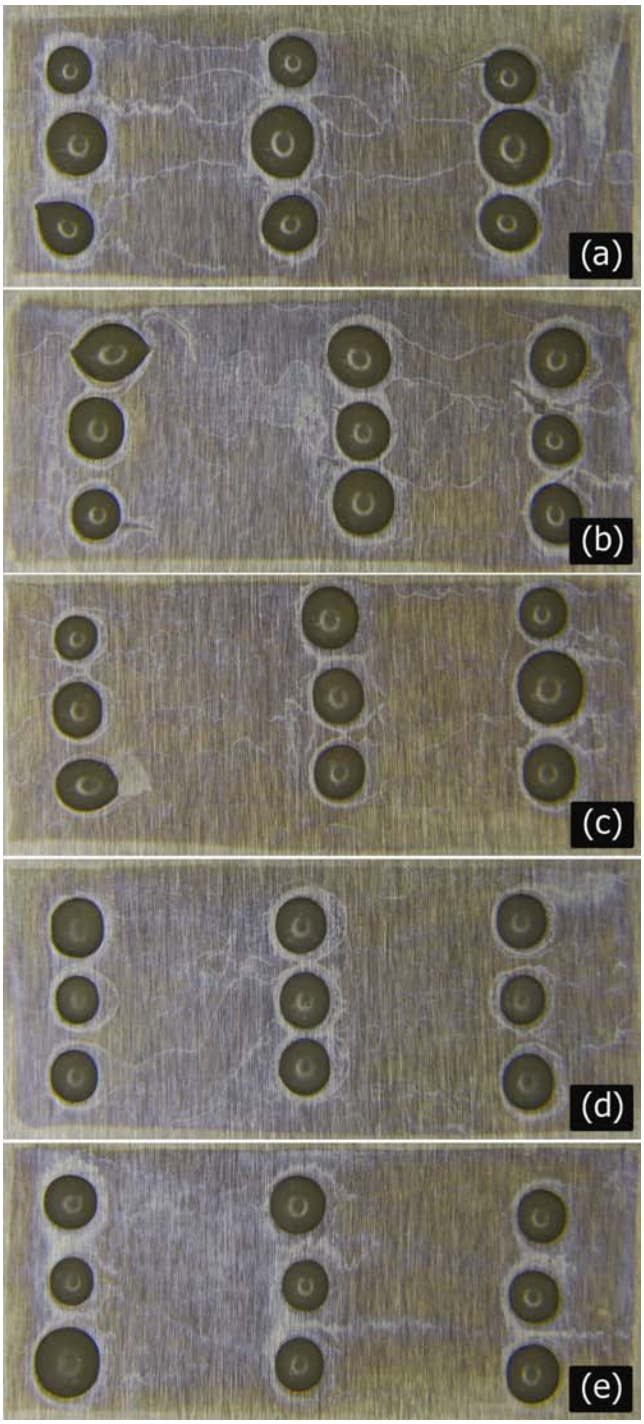

Figure 4.48 Topography of MPHE test plates with glue drops attached after processing WPC solution at 46 l/h and 131 kPa.g. (R2.17) (a) module 1 (b) module 2 (c) module 4 (d) module 5 (e) module 6 [(a) – (e) 5 replicates].

4.3.3 Influence of start up procedure on fouling

4.3.3.1 Dry start versus wet start

In previous work (Bennett, 2000) it was found that slight modifications in start up procedure had a major effect on the development of fouling by whole milk on heated surfaces. A start up protocol was developed that extended the induction period of the fouling curve by as much as 9 hours. This procedure was named Surface Conditioning by Operational Protocol (SCOP).

Due to its importance a series of experiments were conducted to check the validity and reproducibility of the SCOP and to identify its mechanism. The fundamental idea behind the SCOP is that a run should be started with water already flowing through the system and the hot side switched off. Then the milk is fed into the system and the hot fluid switched on a period of time later. The delay in heating had a dramatic effect on the induction period.

The development of air bubbles on the heated surface differed in dry and wet start runs. In dry start runs the MPHE modules were drained and the hot side turned on before the milk was fed in. In wet start runs, water was passed through the system, the hot side turned on and then the milk was fed in to displace the water. The amount of fouling was larger in dry start runs than wet start runs for the same flow rate and surface temperature (Bennett, 2000). Figure 4.49 shows the development of bubbles in water during a dry start (R2.10) and a wet start run (R2.18). Both runs were operated at a flow rate of 45 l/h under a pressure of 80 kPa.g. In the dry start run (R2.8) tiny bubbles started to form as soon as the product hit the surface and grew in size until about 30 minutes as reported previously. In the wet start the flow was throttled back from about 2 000 l/h of water with no bubbles on the heated surface to 45 l/h at time zero. Relatively large bubbles covered the entire surface instantaneously and grew in size until they started leaving approximately 20 minutes into the run as shown in Figure 4.49.

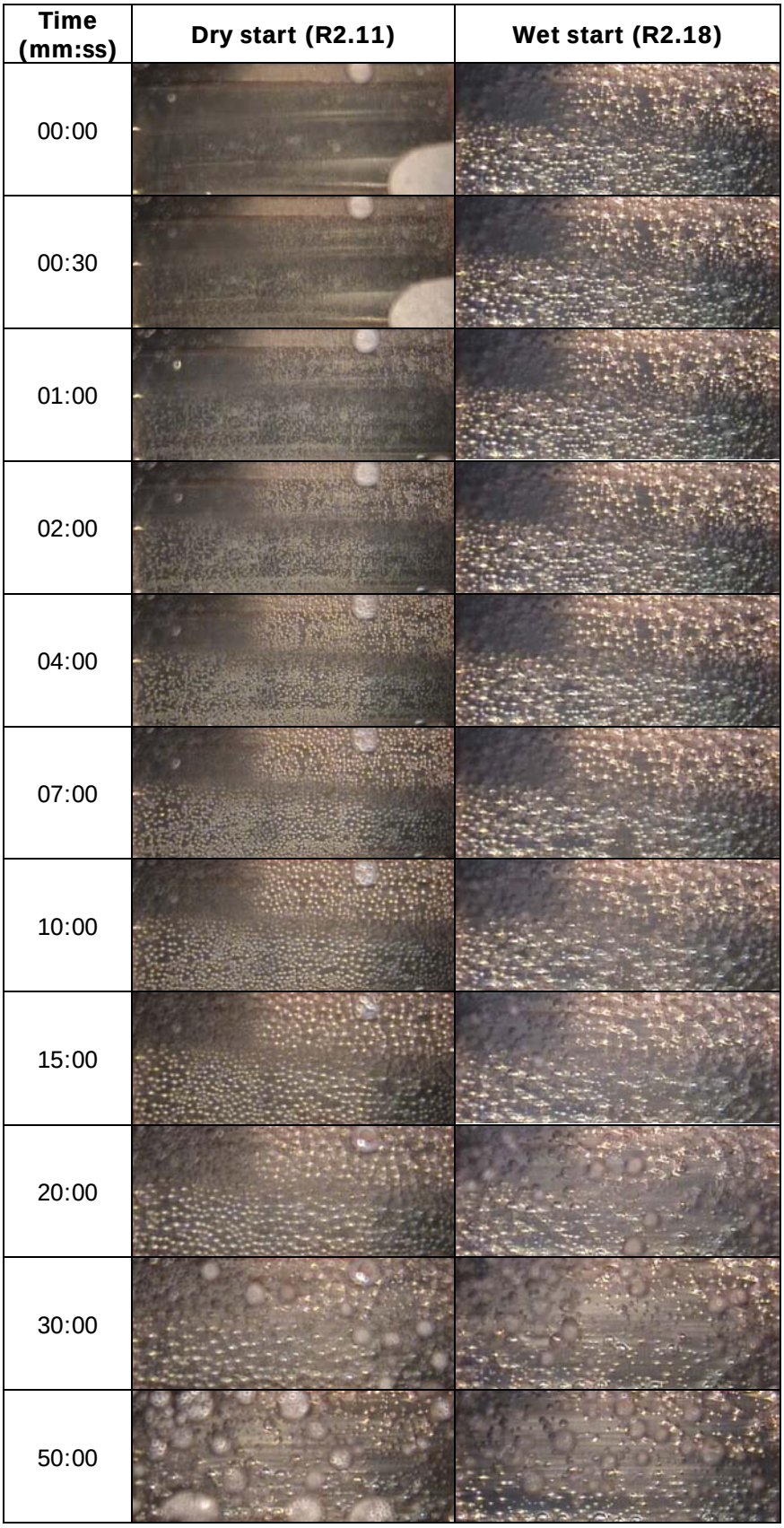

Figure 4.49 Video stills showing the effect of dry and wet starts on bubble behaviour on the MPHE heated surface processing water.

4.3.3.2 Delayed heating

Figure 4.50 compares a dry run at 30 kPa.g (R2.10) with a SCOP run at the same pressure and flow rate (45 l/h). This visualisation of the SCOP (R2.19) uses water to help the clarity of the video. The water was fed into the module with the hot side off and the heat was only turned on 5 minutes later. There is not only a delay in the formation of bubbles at the surface, the number of surface bubbles was reduced by the SCOP procedure. This is shown clearly by comparing stills of R2.10 and R2.19 at minutes 4, 10 and 20.

When the SCOP was conducted with WPC solutions the difference was even more pronounced. Figure 4.51 compares a dry start WPC run (R2.4) with a SCOP WPC run (R2.20) both conducted at 30 kPa.g and 45 l/h. The number of bubbles present in the SCOP does not cover the entire surface whereas it does in the dry run. Consequently, the fouling pattern on the plate at the end of 50 minutes (Figure 4.52) reflects clearly the pattern of bubbles during the run as observed in section 4.3.1. Table 4.13 summaries the results of these runs.

Table 4.13 Mass of dry foulant and foulant loading on plates installed in the MPHE rig after processing WPC solutions with different start up protocols (SCOP manipulation).

Run No.	SCOP	Mass of dry foulant (kg/m^2)	Area covered in fouling (%)	Foulant loading (kg/m^2)
R2.4	No	3.12×10^{-3}	74	4.32×10^{-3}
R2.20	Yes	0.82×10^{-3}	23	3.58×10^{-3}

Table 4.13 indicates that within experimental uncertainty the foulant loading is the same in the runs with and without SCOP and the difference in final fouling rate simply reflects the area of heat exchange surface covered by bubbles and fouling.

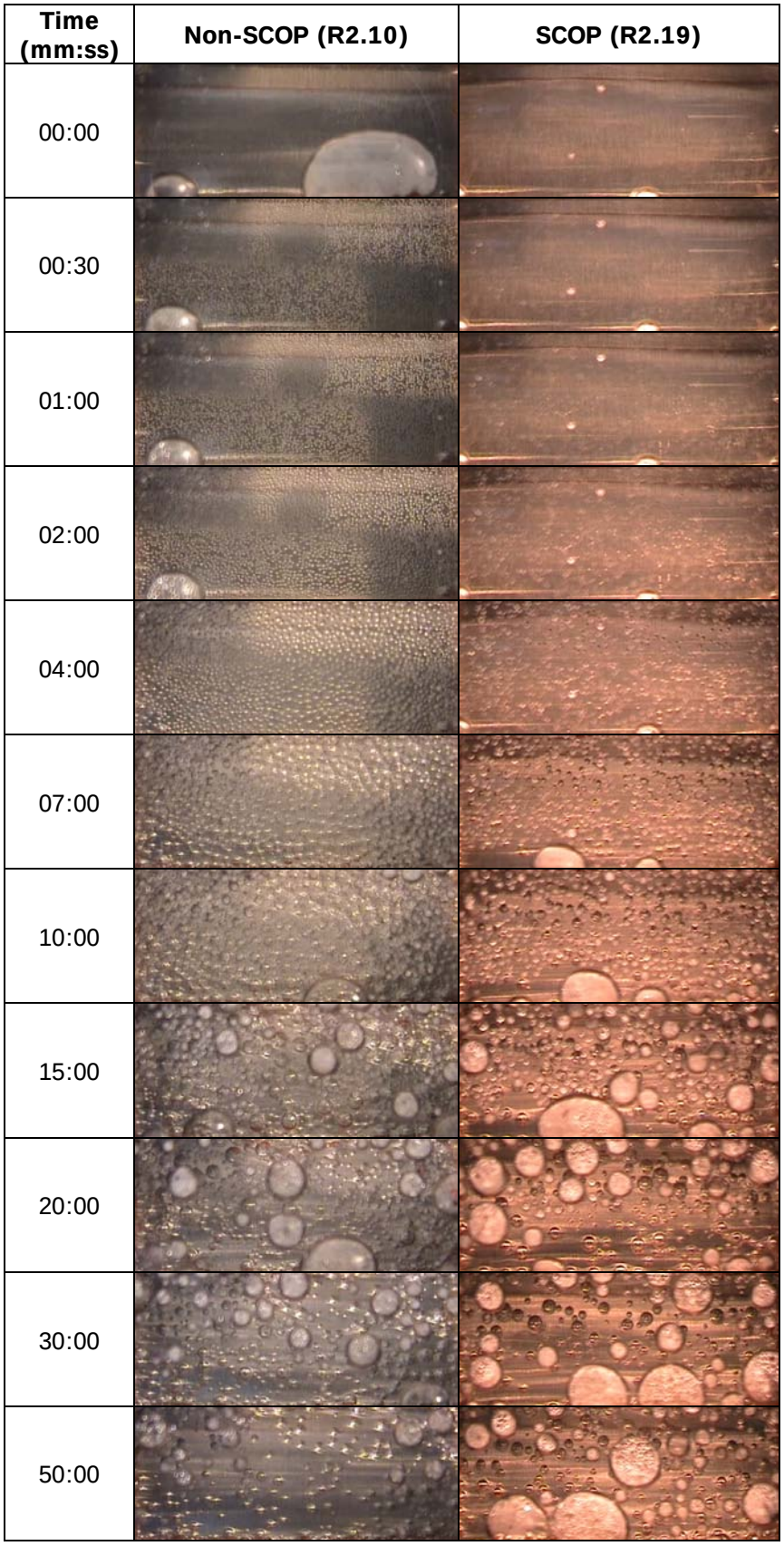

Figure 4.50 Video stills showing the effect of SCOP and non-SCOP starts on bubble behaviour on the MPHE heated surface processing water.

Time (mm:ss)	Non-SCOP (R2.4)	SCOP (R2.20)
00:00		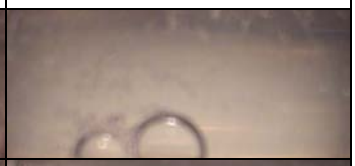
00:30	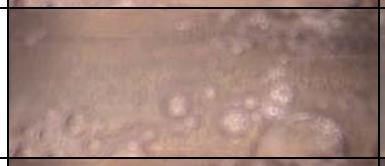	
01:00		
02:00	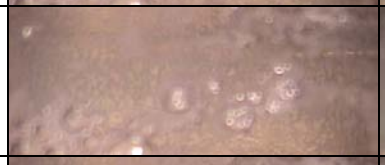	
04:00	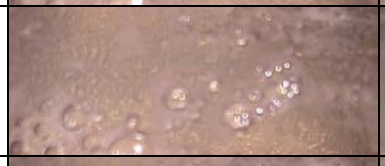	
07:00		
10:00	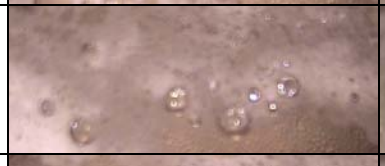	
15:00		
20:00	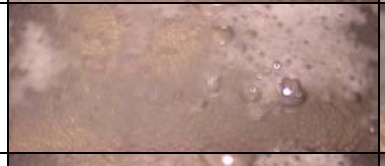	
30:00	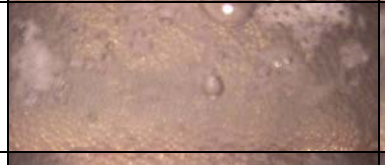	
50:00		

Figure 4.51 Video stills showing the effect of SCOP and non-SCOP starts on bubble behaviour on the MPHE heated surface processing WPC solutions.

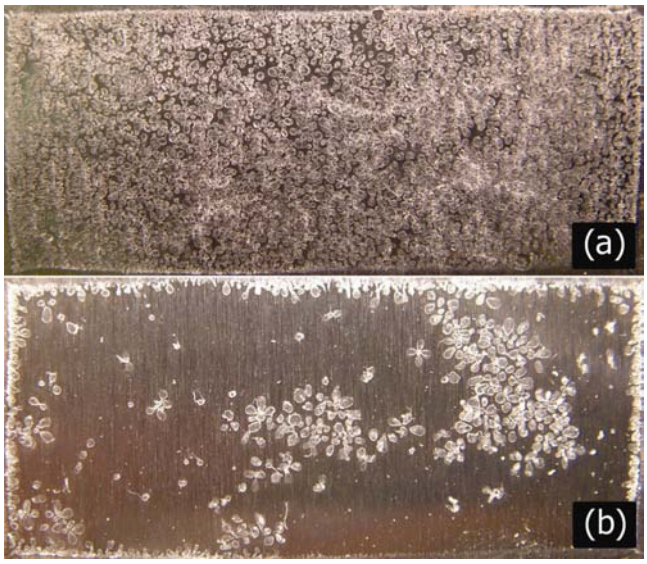

Figure 4.52 Topography of MPHE test plates after processing WPC solutions with different start up procedures (a) non-SCOP - R2.4 (b) SCOP - R2.20.

The change in N_f with time in a typical whole milk run (R2.21) is shown in Figure 4.53 with and without SCOP. Modules 2 & 4 were run under wet start conditions and modules 1 & 3 were run under SCOP start conditions. Since the milk flowed sequentially through all the modules there was no significant difference in milk composition between the modules and the comparison was fairly rigorous. The hot side temperature (89°C) dropped by less than 1°C between modules 1 and 4 and the product temperature differed by less than 1°C between successive modules. In hindsight, these heat losses could have even been further reduced if insulating layers had been added to the modules themselves in addition to the insulation foam on the piping. During the run, plates were taken out, weighed and photographed so that a comparison could be made with the N_f traces.

In module 3 (SCOP, 9.3 h) the N_f only started to drop after 9 hours indicating a very long induction period. By contrast the N_f in the wet start modules (2 & 4) dropped sharply and almost instantaneously from the start of the run. The impact on the fouling layer can be clearly seen in Figure 4.54. In this run one module from each type of start up was isolated after 20 minutes into the run (modules 1 & 2). The two remaining modules (3 & 4) were not isolated until a further 9 hours had passed (modules 3 & 4). Thus, the ability of the SCOP to change the nucleation pattern of air bubbles on the surface has a direct impact on the texture of the fouling layer and its rate of development.

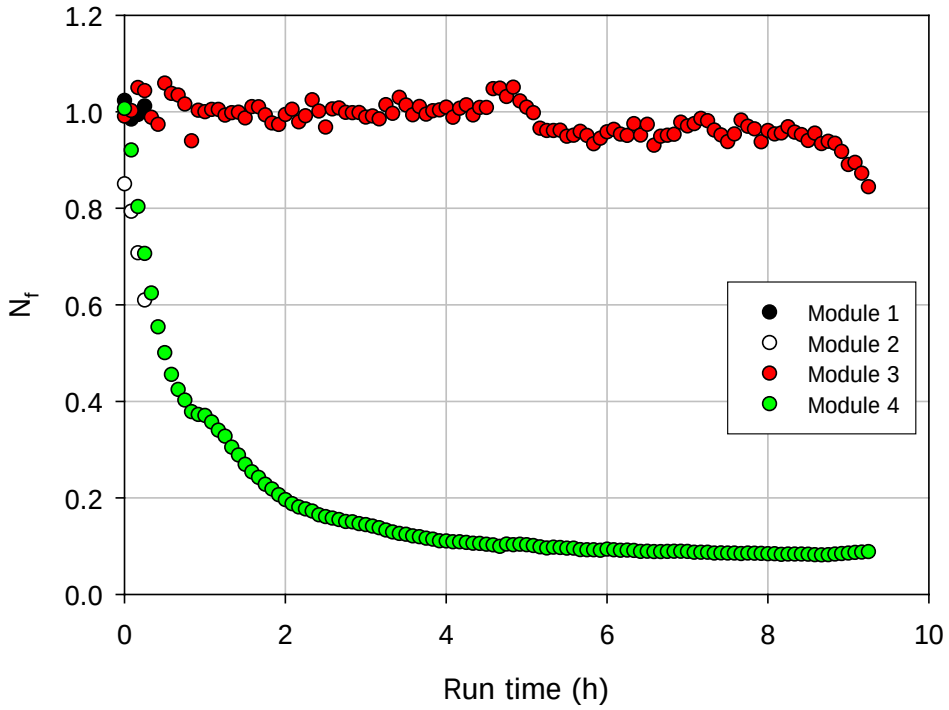

Figure 4.53 N_f versus time for different start up procedures used with the MPHE processing whole milk: modules 1 & 3 (SCOP), modules 2 &4 (non-SCOP).

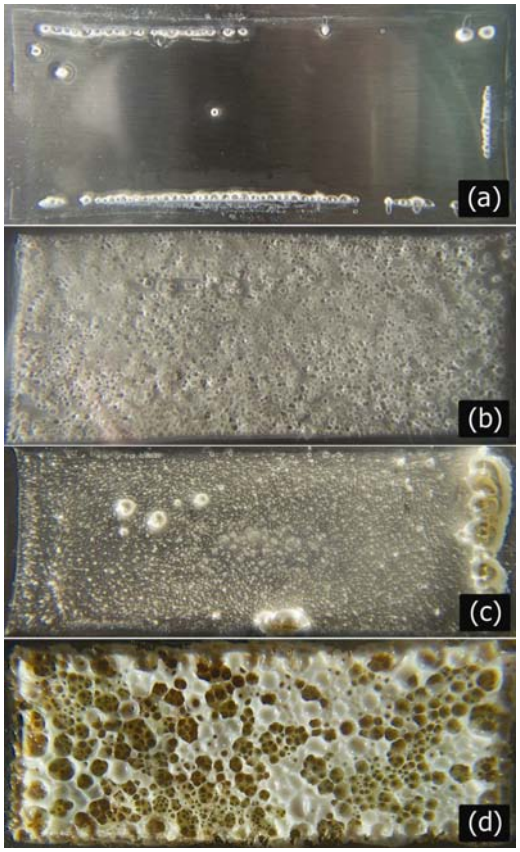

Figure 4.54 Topography of MPHE test plates after processing whole milk with different start up procedures R2.21 (a) module 1 SCOP 20 min (b) module 2 non-SCOP 20 min (c) module 3 SCOP 9.3 h (d) module 4 non-SCOP 9.3 h.

4.3.3.3 Validation

The time delay between the start of the run and the switching on of the hot side of the SCOP has an impact on its effectiveness for whole milk being processed in the MPHE rig as shown in Figure 4.55. The time delay ranged from zero seconds to 60 minutes in the six modules operated in R2.22. A delay of only a few seconds (module 2) was not effective. But significant reductions had occurred with a 10 minute delay (module 3) and showed continued improvement after 60 minutes delay (module 6). Of course, a 60 minute delay time means that the hot side was only switched on for 3 hours. However, the photos indicated that the amount of fouling reduction between module 1 and 6 was much more significant than the 4:3 ratio in heating times.

In all modules the bubbles seem to form much more easily at the rim of the plate where the gasket also made contact with the milk in all cases. This may be explained by two observations; (1) the local velocity at the rim surface is zero (2) the surface charge and surface tension is different from the stainless steel. Either or both of these abnormities would have contributed to bubbles forming more easily at the rim.

The SCOP procedure works with a variety of systems, not just pasteurised whole milk supplied by Fonterra or WPC solutions. Figure 4.56 shows the fouling on test plates after processing Neutrase treated and normal whole milk in the MPHE rig (R2.23). Untreated whole milk was run through modules 1 (non-SCOP) and 2 (SCOP) while Neutrase treated whole milk ran through modules 3 (non-SCOP) and 4 (SCOP). The effectiveness of the SCOP was clearly seen even in the case of the Neutrase treated whole milk which normally results in a significant increase in fouling (section 4.2.4). Note that the textures of the fouling from modules 1 & 3 are different. When the fouled plates were taken out of the modules normally bubbles can be seen on the surface and these collapse quickly to leave behind a crater type structure. When Neutrase treated milk was processed these bubbles would often take much longer to collapse. Since caseins are more active in Neutrase treated milk the emulsification properties of the caseins may have changed the surface tension of the bubbles leading to a much longer life of the bubbles after module isolation.

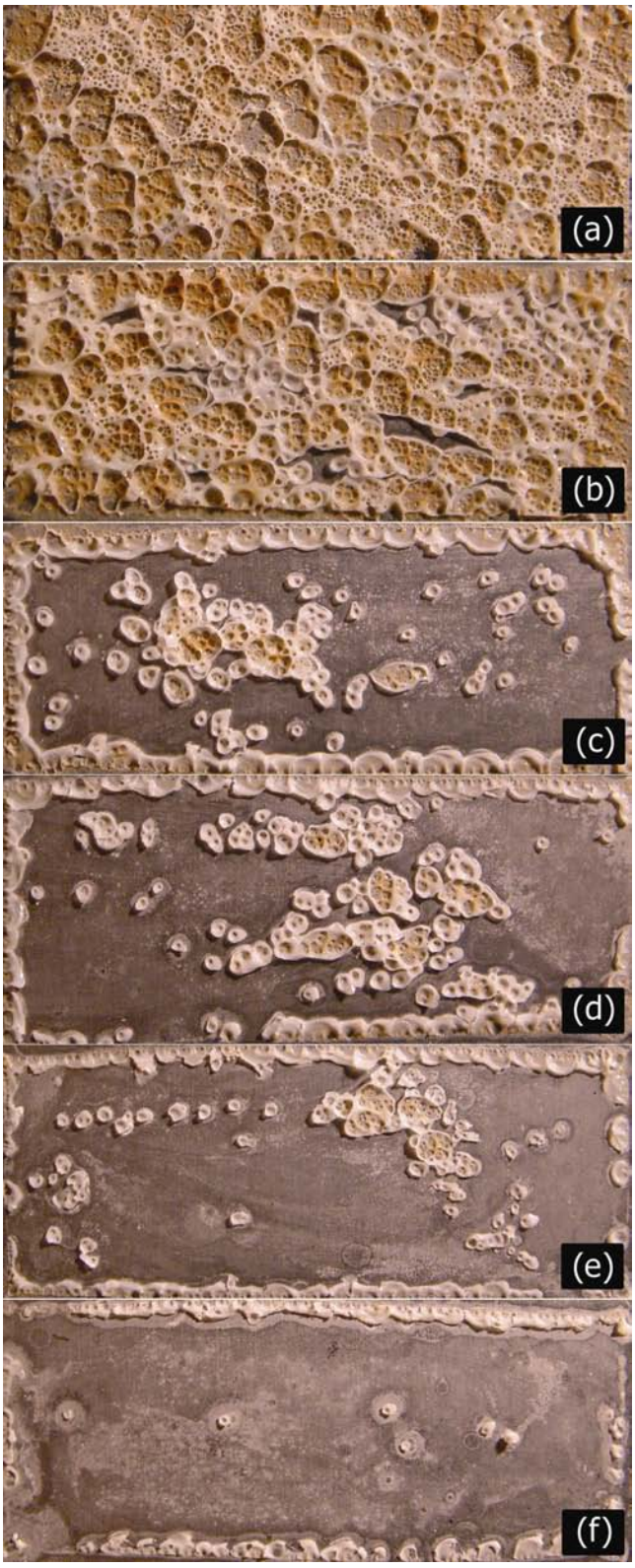

Figure 4.55 Topography of MPHE test plates after processing whole milk with different start up procedures R2.22 (a) module 1 non-SCOP (b) module 2 SCOP 5 seconds delay (c) module 3 SCOP 10 minutes delay (d) module 4 SCOP 20 minutes delay (e) module 5 SCOP 40 minutes delay (f) module 6 SCOP 60 minutes delay.

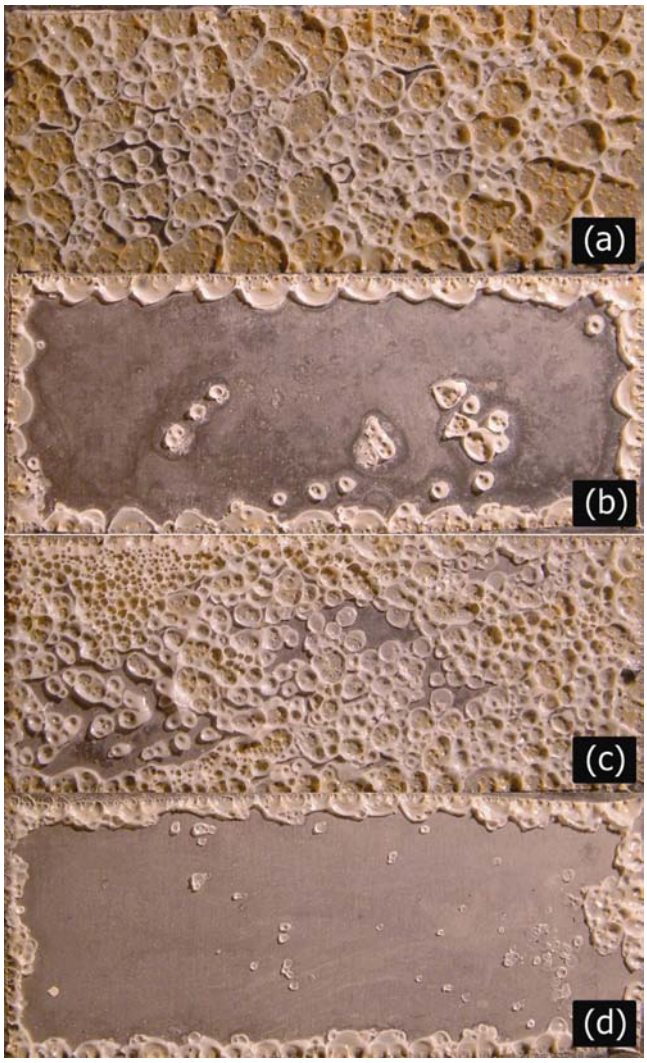

Figure 4.56 Topography of MPHE test plates after processing whole milk with and without Neutrase addition with different start up procedures R2.23 (a) module 1 whole milk non-SCOP (b) module 2 whole milk SCOP (c) module 3 Neutrase treated whole milk non-SCOP (d) module 4 Neutrase treated whole milk SCOP.

4.3.3.4 Surface coatings

It is evident that in bubble type fouling the SCOP works by preventing the attachment of bubbles and therefore prolonging the duration of the induction period significantly. Since the components of the milk were not changed by the SCOP it was of interest to investigate further the mechanism of the SCOP. A validation of the SCOP with the fouling in the absence of air bubbles (for example at higher pressures) was not attempted because each run would have to be much longer, presumably 20 hours, before significant fouling could be observed. Secondly, such tests would be prohibitably expensive in an already costly PhD and thirdly, the PhD project had a time constraint and a large amount of work was already completed. A preliminary attempt (R2.24) to identify the component/s in milk that generate the action of the SCOP was made by dipping clean plates for 30 minutes in solutions of β-Lg (module 2), α-La (module 3), casein (module 4), calcium phosphate (module 5) and lactose (module 6). A control test plate was installed in module 1 that had not been dipped in any solution. After the plates were installed in the MPHE rig a WPC solution (0.1 %) was processed at a hot side temperature of 90°C under an operating pressure of 30 kPa.g. The advantage of combining many coatings in a single run was that the WPC composition, temperature and operating pressure were very similar across the modules of the MPHE rig.

Figure 4.57 shows that a coating with β-Lg halves the amount of fouling whereas a calcium phosphate coating increases it significantly. The effect of the others does not seem to be significant. The photographs of the fouled plates after 50 minutes of processing are shown in Figure 4.58. The fouling structure of the control, α-La, casein and lactose dipped plates are similar. The two plates with a different fouling structure were dipped in β-Lg (fewer fouling craters) and calcium phosphate (considerably finer grains which are presumably calcium phosphate crystals and the total absence of craters). Thus, the physical appearance of the fouling patterns correlates well with the mass of fouling.

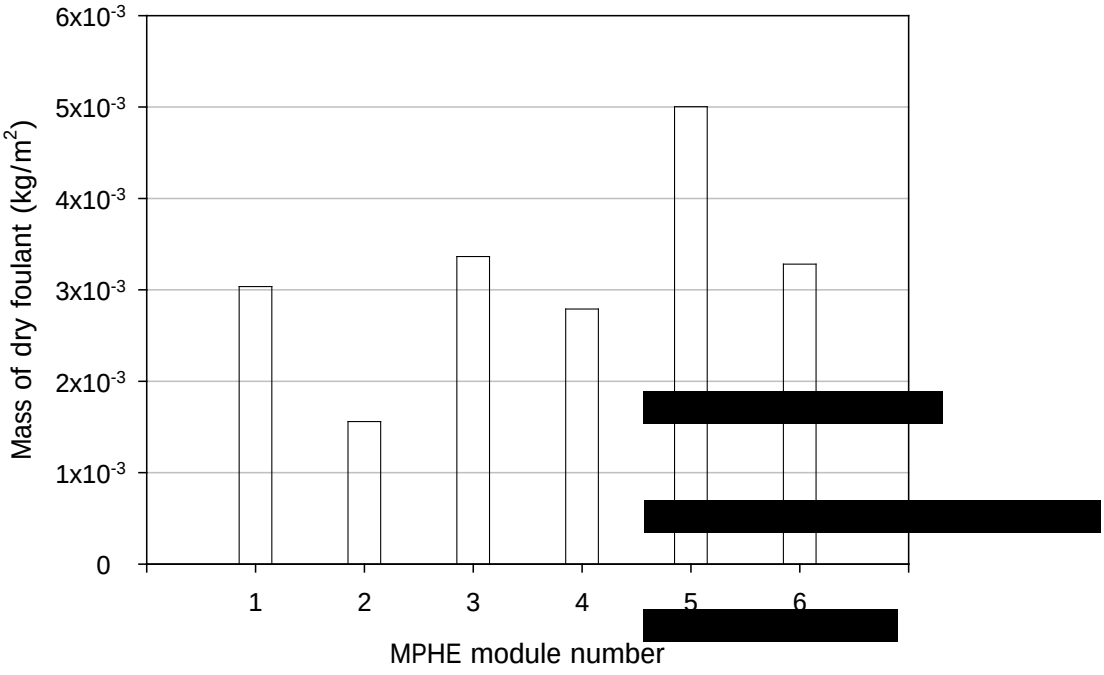

Figure 4.57 The effect of dipping the test plates [redacted] for 30 minutes on the mass of dry foulant produced in the MPHE rig when a solution of WPC was processed (R2.24). Dipping solutions: module 1 – none, module 2 - β-Lg, module 3 - α-La, module 4 – casein, module 5 - calcium phosphate, module 6 – lactose.

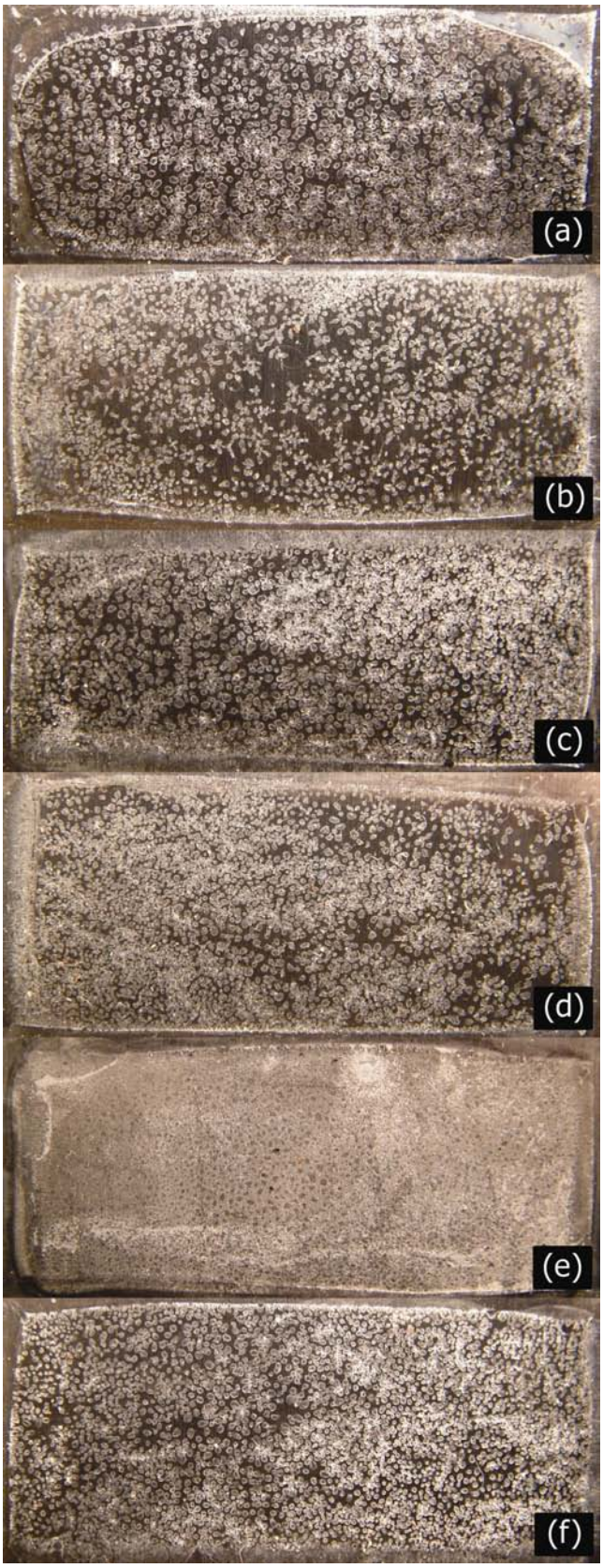

Figure 4.58 Topography of MPHE test plates dipped in solutions for 30 minutes before processing a WPC solution in the MPHE rig (a) module 1 none (b) module 2 β-Lg (c) module 3 α-La (d) module 4 casein (e) module 5 calcium phosphate (f) module 6 lactose.

DISCUSSION

The overall aim of the umbrella project under which this study was undertaken was to investigate the relationship between thermophiles and fouling deposits in milk powder processing plants. The investigation took the form of two subprojects, each taking a separate approach.

The first subproject (Hinton, 2003) focussed on colonisation by thermophilic bacteria of surfaces both clean and fouled and the subsequent contamination of the bulk stream from these surface colonies. The purpose of that project, which started three years before the current project, was to investigate interactions between thermophiles and fouling layers in preheating heat exchangers. Hinton (2003) found that the presence of fouling in the heat exchangers did not increase the release of thermophiles into the bulk milk compared to clean stainless steel surfaces. However, Hinton *et al*. (2002) found that fouling layers protected the thermophiles during the cleaning process and if cleaning was incomplete, recontamination at the beginning of the next run was substantial, up to 8 hours faster than a clean system. Therefore reduction or complete removal of fouling layers, particularly in difficult to clean areas of the plant, would help to alleviate the thermophilic contamination problem.

The second (current) subproject complemented Hinton's results of thermophilic contamination in a milk powder pilot plant by the investigation of contamination as the product passed through a pilot plant evaporator and auxiliary equipment (results reported and discussed elsewhere e.g. Bennett *et al.*, 2002). The focus then shifted to the study of fouling in heat transfer equipment, its structure, parameters and control. Thus, unlike Hinton's study this subproject did not focus on the bacteria themselves, but on the fouling layers that protect them. The results and experimental methodologies of the fouling investigation are discussed in this chapter.

5.1 PROTOCOL OF FOULING RUNS AND METHODS OF MEASUREMENT

Before any fouling investigations could take place it was important to develop accurate and reliable methods of measurement. This project used both direct and indirect types of measurement traditionally used by researchers of fouling. However,

extensive modifications, particularly to the indirect methods, were required before meaningful results were obtained in the current system. For example, it was important to ensure that the two temperature sensors of the local system were synchronised. If not, the resulting trace would possess much instability and would more than likely report erroneous values. Examples of instability in the reported heat transfer coefficient are found in the two theses (Bennett, 2000; Croy, 2000). Fine tuning of the sensor's response during the commissioning period resulted in traces that were less noisy as shown in the reproducibility section 4.2.2.

Once all methods of measurement were tested and deemed reliable, the indirect measurements were compared with relevant direct measurements of fouling deposition. Specifically, the final value of N_f from the global system was compared with the mass of fouling per unit area of the THE. The final value of N_f from the local system was compared with that of the height of the fouling layer at the position of the wall heat flux sensor. In the global system a good linear correlation was observed indicating that the indirect method worked well over the range of experimental conditions used in this study. The same was not observed for the local system where measurements made at very low heat flux values must be considered with care because of the sensitivity limits of the probe itself. Although, there appeared to be a limiting sensitivity associated with the local measurement, comparisons made between the local and global measurements for runs under identical conditions showed no contradictions. Despite its limitations in sensitivity, the local system had the ability to pick up variations in the local fouling thickness over the surface area of the heat exchanger. Design geometry and small disturbances in the fluid stream had a significant effect on the spatial pattern of heat flux on the heat exchanger surface which affects fouling.

There are few publications that have attempted to correlate the on-line measurements with weight or volume of fouling and the use of the heat transfer coefficient as a measure of fouling has been based more on theoretical arguments than proof, especially as far as the local heat flux sensor is concerned. Since the thermopile in this sensor is very small, accurate location of the physical measurement of fouling height is essential for validation rather than just random measurements over the whole fouled surface.

It was also important to design a system that allowed access to fouling surfaces both during and after a run. In this project, equipment was constructed that simulated conditions found in tube and plate type heat exchangers. Here surfaces from both apparatuses could be isolated at any point in the run and removed for physical inspection (although this feature was not used for fouling runs conducted with the THE of the current project). In the case of the plate type heat exchanger, direct observations could be made of the heated surface as the product flowed through the heat exchanger by way of a windowed module. This allowed specific observations and deductions to be made with regards to dairy fouling not usually reported in the literature.

Due to the biological nature of milk, the results of fouling experiments reported in the literature often vary greatly, particularly when a raw product is used as the process fluid. Efforts were made to reduce this variability among fouling runs by the development of an experimental protocol. During commissioning runs important factors affecting fouling were identified and ways of controlling them incorporated into the protocol. For example, it was found that air played an important role in the system in a number of ways. Firstly, residual air must be removed from the process lines during start up. If not, there was a risk that an air "slug" may travel through the plant disturbing process stability, sensor readings and ultimately the monitoring of fouling. Secondly, the air released, as a result of heating the product, periodically must be removed to avoid a similar situation to the one described above. Finally, the rate of air nucleation on the heated surfaces must be controlled. It was found that air bubble formation had a large effect on the onset and build up of fouling. Therefore, to investigate other factors that affect fouling it was important to control the rate of air bubble formation between runs. This was achieved by a precise and complex start up procedure and accurate control of the operating pressure of the system. The final mass results of experiments run using the final protocol varied by less than 10% compared with an average of 60% in the published literature. The ratio between maximum and minimum fouling rates in repeat runs in this work was 1.12.

The details of the N_f curves of repeat runs were however less reproducible even though the general trend was the same for all. For example, the length of the induction period for the 30 kPa.g replicate runs ranged from 30 to 60 minutes

(Figure 4.9). Replicate fouling curves have not been published in any work in the open literature and all claims of reproducibility have been made on the basis of final fouling mass. It is not known why these differences are observed in Figure 4.9 but one may speculate on a number of causes. Firstly, the pattern of flow is influenced by disturbances coming into the test section. Slight differences in alignments in the heat exchanger assembly between runs would be sufficient to alter the local pattern of fouling. Secondly, the milk obtained from the supplier may have slightly different levels of enzymes between collection days and this will cause differences in rates of fouling as discussed in section 4.2.4. Thirdly, the estimation of U_0 is subjective and it is possible that a more objective method of estimating this value may reduce the variation observed in induction periods among repeat runs.

The ratio between maximum and minimum fouling rates in repeat runs of 1.12 in this work is a clear indication that not all causes of variations between fouling runs have been mastered or even identified. Nonetheless, it indicates that much better control has been achieved compared to experiments published in the literature where this ratio ranges from 3 to 9. It is doubtful that perfect reproducibility of fouling runs can ever be achieved since the level of enzymes in the milk for example varies not only with microbial growth, which cannot be fully controlled, but also with seasonal and even day to day variation in milk composition.

5.2 DISCUSSION OF RESULTS OF FOULING RUNS

The results in this project confirm that the presence of a proteolytic enzyme extracted from a psychrotrophic culture (Neutrase) in whole milk increased fouling proportionally to enzyme activity, as shown previously by Jeurnink (1991) and Ma *et al*. (2001). However, enzymes produced by a strain of thermophilic bacteria (*B. stearothermophilus* B12 Cm) have no effect on fouling. An explanation of this difference in behaviour was suggested by the SDS-PAGE analysis. This analysis showed that while Neutrase hydrolyses κ-casein to para-κ-casein in the liquid milk, the thermophilic enzymes did not. The hydrolysis of κ-casein to para-κ-casein by psychrotrophic bacteria found here is consistent with results reported elsewhere (e.g. Adams *et al*., 1976; Law, 1979; Law *et al*., 1979; Jeurnink, 1991). This degradation leads to a reduced heat stability of the milk (Fox & Hearn, 1978). Although a similar SDS-PAGE analysis showed the presence of para-κ-casein in the fouling deposits produced from the Neutrase modified milk, one cannot take this as a proof that

para-κ-casein is an agent that promotes the deposition of more proteins, particularly caseins, onto the fouling deposit. It is well accepted however, that the presence of para-κ-casein in milk is clear evidence of destabilisation of casein micelles by modification of their surface charge. Jeurnink (1991) suggested that additional deposit obtained in the psychrotrophic enzyme modified run was due to decreased heat stability of the casein micelles. In the current work, further evidence has been presented to support this hypothesis because the protein to fat ratio in the deposit increased with addition of Neutrase. This relationship between heat stability and fouling is further illustrated by the SDS-PAGE analysis of milk exposed to the thermophilic enzyme solutions that showed no degradation of κ-casein and no increase in fouling. The important point illustrated by these results is that the growth of psychrotrophs in milk can lead to increases in fouling but the growth of thermophiles does not. The reader is cautioned that the lack of an effect of thermophilic enzymes on fouling by whole milk has been shown in this work with only one strain of *B. stearothermophilus* (B12 Cm) and it would be premature to argue that enzymes produced by other species of thermophiles would behave in the same manner.

The amount of fouling obtained by adding Neutrase to commercial milk supplied by Fonterra was greater, at all wall temperatures investigated, than the fouling of unmodified milk processed under identical conditions and on the same day. Since, Ma *et al*. (2001) had shown that the fouling rate increased with enzyme concentration this study focussed more on the effect of wall temperature at one enzyme concentration (1.25 ml of "0.8L Neutrase" (supplier's nomenclature) to 200 litres of milk). The percentage increase remained relatively stable between each temperature level investigated which suggests that the stability of the milk (and therefore, enzyme activity) is not affected by the wall temperature. In hindsight, these results appear logical because the time the product stream spends at elevated temperature levels is relatively short, about 2 minutes between the thermising PHE and the THE and 20 seconds in the THE itself, compared with the incubation time (minimum of 1 hour). It is more likely that the incubation temperature, which was kept constant throughout these runs, would be the key temperature affecting enzyme activity. Therefore the model of Ma *et al*. (2001) does not need a product temperature correction in the enzyme coefficient.

The fact that the increase in rate of fouling due to the enzyme addition remained constant at six different temperatures suggests either of two things. The change in wall temperature does not affect the concentration of destabilised casein micelles in the bulk milk because of its short residence time in the heat exchanger. Alternatively, it is also possible that the activity of the Neutrase is not affected by temperature variations within the range studied. It was not possible to determine which explanation is the right one because the enzyme activity was not measured in the heat exchanger.

The results presented here suggest the presence of two fouling mechanisms. Since the fouling deposits increase over the wall temperature range investigated here (68 – 93°C), as evidenced by the control runs, there is obviously a mechanism associated with wall temperature. A second mechanism is associated with the decreased heat stability of the casein micelles upon Neutrase addition. The author agrees with the argument of Jeurnink (1991) and Ma *et al*. (2001) that destabilised casein micelles are a new species found in certain types of milk fouling deposits in addition to the widely reported whey proteins. The effect of temperature on the deposition of this new species appears complex. As discussed previously, the rate and percentage increase of this new species is the same within the range of wall temperatures tested (68 - 93°C). However, since no deposits from Neutrase modified milk were observed at low temperatures (for example, in the storage vat) throughout the runs, one must assume that there is a minimum activation temperature for this new species. Unfortunately, this was not formally investigated in this experimental program even though, (with hindsight) it should have been.

In practical terms, the raw milk should be processed as fast as possible upon reception at the plant. If raw milk is not to be processed immediately it should be heated first to avoid the growth of psychrotrophic bacteria that produce enzymes similar to one studied here (Neutrase). Heating the milk may encourage the growth of thermophilic bacteria but if one accepts that thermophilic enzymes do not affect fouling rates (as was the case with *B. stearothermophilus* strain studied here) there will be no risk of enhanced deposits when the milk is finally processed. In addition, the mixing of new and old milk (that contains a high level of psychrotrophs) should be avoided because it may lead to additional protein deposit even though the overall bacteria population of the mixed milk is small.

A number of observations not mentioned before in the literature were made here linking air bubble generation at the wall with fouling. The unique ability to observe the behaviour of air bubbles during fouling runs proved to be particularly useful in explaining the mechanism of what is called air bubble fouling in this thesis. There was a strong visual correlation between the pattern of air nucleation observed during a run and the pattern of the deposit observed at the end of the run. It was found that the residence time of the bubble at the surface had a major effect on the area of fouling deposits. Bubbles that stayed for a short amount of time produced less fouling than bubbles that stayed on the surface a long time. More surprising it was determined that a bubble need only stay at the heated surface for approximately 12 seconds before fouling deposits could be observed around the bubble by the naked eye. While there is a large number of tiny bubbles in the first 30 seconds of a run (Figure 4.23) these do not contribute to the fouling pattern observed on the plate after 50 minutes (Figure 4.24). One possible explanation is that small bubbles act like solid spheres and only relatively large bubbles have surface mobility (e.g. Calderbank, 1967). This is discussed further in the presentation of a possible mechanism of air bubble fouling later in the chapter.

The ability to observe bubble behaviour during a fouling run and better analysis of bubble growth, residence time and movement together with microscopic observation of fouling patterns have given new observations of bubble type fouling. For example, Figure 4.26 shows that bubbles attached to the surface are not stationary but actually move with the local current. They also grow during this period of attachment to the surface. Each time the bubble occupies a new position, it creates a fouling ring, which is called a fouling footprint in this work, within a matter of seconds (12 seconds in a crude estimation from results reported here). Therefore, there is an increase in mass of fouling with residence time at the surface but it is not due to further deposits on existing fouling rings, although that may exist, but more to the fast creation of footprints. Even when the local currents are weak (low Reynolds number) there is clear evidence of multiple fouling footprints as the bubbles grow and coalesce in almost the same spot (Figure 4.27). The fast creation of fouling footprints cannot be explained by any of the present theories based on denaturation of proteins.

A number of process variables linked with air nucleation on the surface have been studied to assess their potential effect on fouling. The pressure of the system has a profound effect on the rate and structure of fouling. There is a major reduction in the fouling rate and number of bubbles generated at the surface as the pressure increases (Figures 4.29 & 4.31). The new observation here is made possible by the estimate of fouling coverage using digital image analysis (section 4.3.2.1) which indicates that the increase in rate of fouling with pressure reduction is linked to the number of bubbles generated. The rate of deposition around each bubble does not appear to be effectively altered by the change in pressure. This is a new observation not mentioned in any discussion on the effect of pressure on air bubble fouling. It was estimated in section 4.3.2.1 by extrapolation of experimental data that air bubble nucleation on a surface at 90°C would stop at 130 kPa.g and this was later corroborated with a run using WPC at 130 kPa.g where no bubbles formed (R2.5). This is in agreement with Grasshoff (1988) who suggested 125 kPa.g for essentially the same conditions of flow and heating.

Grasshoff (1988) also noted that a sponge like porous deposit ceased to form at 0.7 m/s which would correspond to a 1300 l/h run in the MPHE. This was consistent with results of the present study where a small number of bubbles were observed at 500 l/h and none at 2 000 l/h. High linear velocities in the heat exchangers were shown in the present work to decrease the residence time of the bubbles on the surface, which agrees with the argument by previous authors that strong local currents tend to sweep the bubbles away.

It is interesting to note that even at the flow rate when no bubbles are observed there is a hint of a very thin deposit that shows as a blue/green reflection on the surface (e.g. Figure 4.22 (d)). Others have reported similar deposits (e.g. Johnson & Roland, 1940a; Thom, 1975; Tissier & Lalande, 1986). Tissier & Lalande (1986) suggested that “the wavelength of this colour probably corresponded to the deposit thickness”. Even at a lower velocity this type of thin deposit can coexist with fouling created around bubbles.

The geometric design of the channels has a strong influence on the flow pattern as can be expected from fundamental fluid mechanics analysis and modern computer fluid dynamics packages. It has been experimentally demonstrated in this study that

when an obstruction is placed in a fluid stream that it generates bubbles in its wake, whereas none were observed in the unobstructed case for the same experimental velocity and pressure. Similarly, when glue drops were attached to the surface to simulate the hydrodynamic effect of attached air bubbles there was a slight blue/grey discolouration in their wake but the deposit was much thinner than the footprints of air bubbles. Unfortunately, this important variable affecting fouling deposits has been overlooked and insufficiently researched; in particular its interaction with pressure and flow rate has been ignored.

Many authors have argued that an efficient way of controlling fouling is to decrease the ability of milk solids to attach to the wall, especially during the induction phase. The traditional approach has been to modify the surface charge, for example, by bombarding it with heavy metals (e.g. Muller-Steinhagen & Zhao, 1997). The present work has introduced a new approach; passivation of the surface by precoating with a thin layer of undenatured milk protein/s (SCOP section 4.3.3). The SCOP manipulation reduces the ability of air bubbles to attach, most probably by a change in surface tension. It is possible that the SCOP manipulation will also decrease fouling in the absence of air bubbles.

Although the SCOP procedure offers the potential to improve the length of runs in dairy plants, further research is required. Obtaining a greater understanding of the underlying process fundamentals is paramount. Also, practical considerations need to be addressed before commercial application can take place. These include issues associated with the minimum protein concentration and the surface coating time of the passivating solution.

5.3 MECHANISMS OF FOULING WITH SPECIAL REFERENCE TO BUBBLES

It is actually quite difficult to get a clear idea of the present understanding of the role of air in fouling by dairy products. While many authors have argued that bubble nucleation increases fouling substantially (e.g. Johnson & Roland, 1940a; Burton, 1965; Burton, 1966; Burton, 1968; Gordon *et al.*, 1968; Thom, 1975; Hermans, 1981; Wennerberg, 1981; Tissier & Lalande, 1986; Grasshoff, 1988; Fryer & Belmar-Beiny, 1991; Calvo & Rafael, 1995; Jeurnink, 1995a; Jeurnink *et al.*, 1996c; Changani *et al.*, 1997; Tirumalesh *et al.*, 1997; Walstra *et al.*, 1999; Grijspeerdt *et al.*, 2003) most of these authors have cited only four main sources where there is actual

experimental work (Burton, 1965; Thom, 1975; Grasshoff, 1988; Jeurnink, 1995a). The most cited papers are by Jeurnink and Burton (25 citations in total). The problem is that some of the later authors tended to quote opinions by previous authors as fact. Some authors even quoted their own hypothesis in earlier papers as established fact. For example, Jeurnink (1995b) said protein deposits "probably took place via drying of the membrane of air/vapour bubbles containing caseins, as described by Jeurnink (8)". However, Jeurnink (8) (Jeurnink (1995a) in this thesis) only speculated that the interfacial membrane deposited when the air bubbles "dried out" but never described experimental observations of that fact. Again, Vissier & Jeurnink (1997), quoted the same Jeurnink paper (Jeurnink, 1995a) to argue that "the addition deposition of the stabilising casein micelles accumulated at the gas-liquid interface, onto the heated surface…from the collapse of the adhering bubbles…as Jeurnink has shown [73]". The problem here is that Jeurnink (1995a) only showed micrographs of fouling deposits in the form of craters and reasoned that they must have been created by bubbles which were later described in subsequent papers variously as having burst, collapsed (Jeurnink *et al.*, 1996c) or dried out but showed no experimental evidence of any of these three mechanisms. Yet an unsuspecting reader looking through the later papers may well believe that these three mechanisms were "shown" by actual physical observations. It must be noted that these descriptions are physically impossible for an air bubble surrounded by water and one must assume Jeurnink has confused the situation with that of a soap film bubble where words like "burst", "collapse" and "dried out" have meaning.

The writer does not wish to give the impression of being specifically critical of Jeurnink and his co-workers only. For example, Grijspeerdt *et al.* (2003) referred to Visser *et al.* (1997) as detailing the effect of plate geometry and to Tirumalesh *et al.* (1997) for the importance of the presence of air bubbles on fouling. However, there is no discussion to be found on the effect of plate geometry on fouling in the Visser *et al.* (1997) paper and Tirumalesh *et al.* (1997) simply cited Burton (1968) to argue that sufficient back pressure will prevent "separation of dissolved gases"…and thus minimise fouling. They presented absolutely no experimental work but mysteriously gave a quantitative guideline: "a back pressure of at least 1 bar above the corresponding highest product temperature in the heat exchanger is required".

The Burton (1968) paper that many authors quoted in fact does not present any data showing the relation between air content and fouling. It merely quoted, in two short paragraphs, three groups of authors (Gynning *et al.*, 1958, Buchwald, 1965; Ito & Nakanishi, 1967) who talk of the importance of air content. Ironically, there was no consensus between these three groups where Gynning *et al.* (1958) were quoted as saying "that deposits were reduced when air was removed" but Buchwald (1965) was not able to make the same claim. In fact, the experimental evidence on bubble fouling came in two other papers by Burton (Burton, 1965; Burton, 1966) that described the use of an electrically heated platinum wire immersed in milk to study fouling. It is therefore extremely important in reading fouling literature always to compare quotations (or misquotations) with the evidence presented in the original paper referenced. It is useful to compare statements by previous researchers with the observations made in this project.

Jeurnink (1995a) argued that air bubbles increase fouling deposits by leaving behind a portion of the stabilising proteins that coat the air/liquid interface. In the present work there is evidence of bubbles that persisted until the end of the run but already had fouling attached. In fact, the fouling footprints are formed very quickly and do not prevent the formation of additional footprints as the bubble moves along the surface. Jeurnink (1995a) never presented photographic evidence of this phenomenon taking place.

The hydrodynamic effect of the bubbles was discussed by Thom (1975) who noted that his photographs showed that bubbles that stayed a long time on the surface developed fouling in their wake. Originally, this candidate's photographic evidence showed oblong deposits on long lasting bubbles similar to Thom's (Thom, 1975 Figure 9). But with high resolution photographs it turned out that this pattern was created by a large number of footprints in the direction of local flow, not by deposits in the wake of a stationary bubble. In fact, the hydrodynamic effect of a bubble-shaped protrusion is very small and cannot be compared with fouling near an actual bubble (e.g. Figure 4.48). These observations indicate that the nature of the interactions at the bubble interface are far more important than the hydrodynamic effect of the shape of the bubble as originally postulated by Thom (1975). Thom also had observed that "throughout the further evolution of porous crust the number of round entities increased". Could these be compared to fouling footprints identified in

this thesis? They certainly are not indicative of more bubbles being formed which the visualisation presented in this work can clearly discount.

The bubble visualisation in this study gives rough guidelines to a limiting velocity and pressure for air bubble nucleation and consequent fouling that agree with existing work. They also are in agreement with arguments by Walstra *et al*. (1999) that the presence of proteins, that can deposit on the air/liquid interfaces, stabilises the bubble.

A large number of studies presented in the literature appear to have been conducted at linear velocities past the heated surfaces where bubbles should have been created according to the present results. But most authors neither discussed nor even mentioned the existence of air bubbles in their experiments. Apparently, the only authors that discuss an air/bubble fouling phenomenon in their work are those that see the evidence of rings or craters in their fouling deposits. Even these authors did not have the benefit of observing the presence or absence of bubbles during their runs. The evidence in this work shows that the craters can be slowly filled by deposits of milk solids onto already-formed fouling. This is clearly shown in Figure 4.20 where the original crater has been completely masked by a curd like deposit that occurred very quickly, in this case because of the destabilising effect of Neutrase on casein. Hinton (2003) also showed in his work that, given enough time, milk deposits can fill the craters created by air bubbles even with deposits from milk without enzyme treatment. Thom (1975) had already postulated that the craters that formed around air bubbles should eventually be filled in more slowly by direct deposits of milk proteins. Thus it is easy for authors who only observe the final deposit at the end of the run to miss completely the possibility of fouling around air bubbles in the early part of the run. One should suspect that the occurrence of air bubble fouling is much more widespread that has been reported in the literature.

Many authors compare the structure of their ‘Type A’ deposit to Burton’s description (Burton, 1968) as spongy and curd-like. Gordon *et al*. (1968) rightly pointed out that Burton attributed this structure “of deposit to dissolved gases separating as bubbles on heated surface”. Yet the number of authors who report a curd-like spongy deposit is so large and their experimental conditions so varied that it is possible that some of these experiments would involve air bubbles and some not. It is thus imperative to

reanalyse the experimental conditions reported by previous authors. Unfortunately, they are not always reported completely in the published papers. As shown by the SCOP experiments the occurrence of air bubble fouling is not only dependent on the temperature, pressure and flow rate of the fluid but also on very small changes to operation protocols. There is no way of assessing whether similar effects to the SCOP have affected the results of some of the published work in the literature. For exactly the same conditions and in fact in the same run, fouling deposits of skim milk on the underside of the THE are spongy and on the topside are leather-like (Appendix H). It is suspected that this is due to the ease of retention of the bubbles on the heated surface underneath the THE whereas the gases released on the top surface would be freer to move away from the surface. Unfortunately, there was no time to set up bubble visualisation in the THE to test this hypothesis. It can be said, however, that the orientation in the equipment (as well as pressure, flow rate and temperature) can affect both the amount and the structure of the fouling deposits.

Some authors speculate that surface denaturation of proteins occurs at the liquid/gas interface of the bubble (e.g. Burton, 1965). Surface denaturation alone cannot explain the increase in deposition observed in our experiments. For example, if we assume that the average film thickness of a bubble is 2 μm and that the entire plate is covered in bubbles with an average radius of 1 mm the total amount of material available to deposit is approximately 0.004 g. Experiments run with the same variables used in the above calculation result in an average fouling mass of approximately 0.25 g. Even if all the material encapsulated on the surface of the bubble were to deposit when the bubble leaves the surface, it is still a factor of 50 lower than the weight of deposits found in the current experiments. The only way of resolving this discrepancy is to postulate that the surface of the bubble renews itself continuously. This is only possible if the bubble surface is mobile and proteins are continuously moving from the top of the bubble to the periphery where they would attach to the ring-like footprints. This postulate would explain the fact that small bubbles in the first few seconds of the experiment did not contribute to fouling (e.g. Figures 4.23 & 4.24): because they act like rigid solids due to the very high surface tension in small bubbles. It must be emphasised that it cannot be argued that surface denaturation does not play a role in bubble fouling, but it is not the only factor behind the increase in fouling in the presence of air bubbles.

Another suggestion made in the literature is that the presence of air bubbles introduces a concentration effect which leads to increased deposition of proteins (Walstra *et al.*, 1999). Here it is proposed that bubbles act as insulators on the surface resulting in a temperature difference between the heated surface and the apex of the bubble in the milk stream. “A substantial driving force for water” exists between these two points resulting in the liquid near the bubble/metal rim becoming concentrated. Walstra *et al.* (1999) and Jeurnink (1995a) argue that this higher concentration leads to greatly enhanced deposition of protein. After intense scrutiny of the theories of Walstra and Jeurnink and discussions between the candidate and his supervisors, the candidate has to admit to being completely in the dark as to how this theory works. There were two major points of concern that none of the papers of this group (Jeurnink, 1995a; Jeurnink, 1995b; Jeurnink *et al.*, 1996c; Walstra *et al.*, 1999) address:

1. Even with a temperature differential between the heated surface and the apex of the bubble one finds it hard to visualise that the concentration of milk solids even locally would be so high as to create deposition. Even if skim milk is concentrated from the usual 9 to 40% total solids (a removal of 75% of the water) as often performed in evaporators, there is no evidence of deposition unless the milk literally dries out by maldistribution. This drying out cannot occur in a heater which would be completely flooded with milk. A 40% total solid solution of milk does not coagulate even after 1 hour of heating at 75°C (e.g. Trinh *et al.*, 2007).

2. Some authors have noted that fouling created around air bubbles has a higher content of casein than other fouling which is mainly made up of β-Lg and minerals. The results in this work confirm this observation but show even more strongly that all the solids present in the milk are found in the fouling layer formed around air bubbles. There is an argument that this phenomenon is encouraged by the denaturation of proteins when they spread on the bubble interface. This is used to explain how caseins that do not normally contribute to fouling by heating alone are found in air bubble fouling (Jeurnink, 1995a). However, Walstra *et al.* (1999) and Jeurnink (1995a) discuss only the concentration of casein in the liquid near the metal/bubble interface. The candidate fails to understand how these concentrated caseins can deposit since they have not been denatured by spreading on the bubble surface itself.

The argument that the denaturation of casein makes it more susceptible to fouling is attractive and well supported by this and other work at IFNHH (e.g. Ma *et al.*, 2001). However, two points need to be emphasised:

a) When enzymes are added not all destabilised caseins will necessarily contribute to fouling. Many of the destabilised casein micelles can aggregate among themselves or with other milk components before reaching the wall resulting in loss of their reactivity. This can clearly be shown from calculations of Neutrase enzyme activity and weight of fouling collected after 4 hours of run time.
b) The denatured casein on the surface of the bubble can attach to the footprints at the rim of the bubble but possibly the more important factor is the fact that caseins that spread out on the bubble surface move very quickly towards the rim. This would explain why the fouling footprints of bubbles can form in less than 12 seconds in any particular location.

This argument also suggests that all the caseins that have been spread at the surface end up in the fouling layer whether they have been modified by enzyme activity or not. But the caseins in the milk solution have a much lower probability of being deposited on the fouling layer. These arguments suggest that the biggest impact of bubbles resides in the transportation term rather than in the concentration term, at least as far as the caseins are concerned. Walstra *et al.*, 1999 argued that proteins from the milk deposit on the air/water interface stabilise it as soon as it is created. The surface convection current theory postulated here would bring these proteins to the rim of the bubble quickly too.

The components analysis conducted in this work suggests that all solids in the milk deposit in approximately the same ratio found in the liquid milk (on a dry basis), including the whey to casein ratio. The only component that does not deposit in approximately the same ratio is lactose, presumably due to its high water solubility. These results suggest that surface denaturation does not favour casein deposition into the fouling layer over other components like whey and fat. These observations do not compare well with the statements made by Jeurnink (1995a) who argued that caseins preferentially spread on the surface of bubbles compared to whey proteins. He quotes in his argument “in foams caseins tend to adsorb at the air/liquid in preference to serum proteins (Dickinson *et al.*, 1989).” This may be true for foams

but the implication that that would lead to more casein in the fouling layer than whey proteins when air bubbles are present has not been proved.

To recapitulate, the theory of air bubble induced fouling of heated surfaces by dairy products, proposed in this thesis, is as follows:

1. When bubbles nucleate at the surface a layer of proteins and fat adsorbs to the liquid/gas interface immediately.
2. If the bubble is large enough convection currents develop on its surface. This surface mobility brings the protein and fat, spread on the surface, to the periphery of the bubble where they attach to the metal surface.
3. The proteins and other milk solids attach rapidly to the metal surface at that periphery creating a fouling footprint (within 12 seconds in our experiments).
4. The creation of a footprint depletes the air/liquid interface of its stabilising solids and fresh solids immediately enter and spread out on this interface from the adjacent liquid milk.
5. If the milk local velocity is strong the bubble is unlikely to remain stationary and moves along the heated surface creating a series of footprints, thus greatly increasing the amount of fouling with time.
6. In low currents one may see the gradual coalescence of several bubbles and their foot prints can nestle within one another.
7. The bubble grows with time and eventually ceases to be spherical in shape and develops into a “hot-air balloon” shape.
8. If the bubble stays reasonably stationary the proteins, newly spread on the air/liquid interface, attach to the existing footprints which grow in height. For larger bubbles with a hot-air balloon shape the footprint left behind eventually looks like an inverted cone.
9. When an air bubble leaves the surface no new bubble is created at that position during the run. This is probably the result of a change in surface tension of the metal.
10. The proteins from the milk can attach to the wall or to existing fouling deposits if they are activated either by heat or by enzyme and able to aggregate. This mechanism has been thoroughly described for β-Lg denaturation in the literature but also applies to caseins that have been

treated with proteolytic enzymes. This mechanism is independent of and co-exists with the air-bubble fouling mechanism.

11. The activation, transport and attachment mechanism of fouling is considerably slower than the air bubble mechanism.
12. Eventually, the deposition of proteins and fat from the milk fill the craters originally created by air bubble fouling.
13. Higher linear velocities decrease the number of bubbles generated on heated surfaces but do not necessarily suppress them everywhere, especially in recirculation regions of equipment with complex geometries.
14. It is more effective to control air nucleation by increasing the pressure of the system than by using high linear velocities. Unfortunately, the maximum pressure used in industrial plants is dictated partly by cost. There is a relationship between the limiting pressure at which air bubbles cease to nucleate and the temperature of the milk. In this work the value is 130 kPa.g for a hot side temperature of 90°C.
15. A complicating factor but one which holds great promise in anti-fouling strategies is the ability to prevent air-bubble nucleation by conditioning the surface of the heat exchanger with undenatured proteins at the start of the run (SCOP manipulation).

CONCLUSIONS AND RECOMMENDATIONS

Two systems were developed that allowed the global and local fouling rates to be monitored on-line and in real time. The outputs of the systems agree well with direct measurements of the fouling deposits.

These improved monitoring systems were incorporated into specifically designed heat exchangers which allowed deductions to be made in terms of fouling processes occurring at the surface. The final operating protocol developed for the equipment gave final fouling mass results with reproducibility better than 10% for the same operating conditions.

The results of experiments conducted with this equipment showed that air nucleation on the heated surface had a major influence on the process of fouling. In the presence of surface air bubbles the fouling:

- induction period was reduced
- rate was increased
- structure was determined by the behaviour of bubbles at the surface
- consisted of all solid components found in the processed solution (except lactose in the case of milk)

In this work it was found that air bubble induced fouling could be:

- eliminated by a backpressure of 130 kPa.g at a surface temperature of 90°C
- reduced by increases in linear velocities until it was completely eliminated at a velocity of 1.0 m/s at a surface temperature of 90°C
- triggered by obstructions installed in the flow path, even at higher linear velocities
- reduced by conditioning the surface with a thin layer of inactive protein/s at the start of a run

These observations should be validated with work in commercial plants to assess the effect of scale on the extent of bubble induced fouling.

It was also shown that when casein micelles in the milk were destabilised by a proteolytic enzyme (Neutrase derived from *Bacillus amyloliquefaciens*) fouling increased. The same action was not observed with thermophilic enzymes generated by the growth of *Bacillus stearothermophilus* (B12 Cm) derived from commercial milk powder plants.

It is recommended that in commercial plants:

- The monitoring systems should be incorporated and tested to ascertain their ability to follow the progress of CIP and fouling in real-time.
- The level of proteolytic enzymes (or psychrotrophic bacteria) should be monitored in the raw milk and appropriate control procedures should be used if the level of enzymes is found to be significant.
- An audit should be carried out to identify plant locations where air bubble induced fouling is present, particularly in evaporators where the pressure is low and in recirculation regions and dead spots.
- If air bubble induced fouling is found to be significant investigations should be made to determine where and how the milk should be deaerated.
- Trials should be carried out to incorporate the SCOP procedure in plant operations.

Further research work is needed:

- To determine the components, processes and physical state of the protective layer formed under the SCOP.
- To determine the effect of incubation time and temperature of Neutrase modified milk on the rate of fouling.
- To investigate the mobility of the air bubble surface particularly with very small bubbles.
- To investigate the attachment reaction of air bubble induced fouling.

REFERENCES

Adams, D. M., Barach, J. T. & Speck, M. L. (1976). Effect of psychrotrophic bacteria from raw-milk on milk-proteins and stability of milk-proteins to ultrahigh temperature treatment. *Journal of Dairy Science,* 59 (5), 823-827.

Al-Roubaie, S. M. & Burton, H. (1979). Effect of free fatty acids on the amount of deposit formed from milk on heated surfaces. *Journal of Dairy Research,* 46 (3), 463-471.

Andritsos, N., Yiantsios, S. & Karabelas, A. J. (2002). Calcium phosphate scale formation from SMUF solutions. In *Fouling, Cleaning and Disinfection in Food Processing*. Cambridge, UK.

Anema, S. G. (2001). Kinetics of the irreversible thermal denaturation and disulfide aggregation of alpha-lactalbumin in milk samples of various concentrations. *Journal of Food Science,* 66 (1), 2-9.

Baier, R. E. (1981). Modification of surfaces to reduce fouling and/or improve cleaning. In *Fundamentals and Applications of Surface Phenomena Associated with Fouling and Cleaning in Food Processing*. Tylosand, Sweden.

Bell, K. J. & Sanders, C. F. (1944). Prevention of milkstone formation in a high-temperature-short-time heater by preheating milk, skim milk and whey. *Journal of Dairy Science,* 27, 499-504.

Belmar-Beiny, M. T. & Fryer, P. J. (1992). Bulk and surface effects on the initial stages of whey fouling. *Food and Bioproducts Processing,* 70 (Part C), 193-199.

Belmar-Beiny, M. T. & Fryer, P. J. (1993). Preliminary stages of fouling from whey-protein solutions. *Journal of Dairy Research,* 60 (4), 467-483.

Belmar-Beiny, M. T., Gotham, S. M., Paterson, W. R. & Fryer, P. J. (1993). The effect of Reynolds-number and fluid temperature in whey-protein fouling. *Journal of Food Engineering,* 19 (2), 119-139.

Bennett, H. A. E. (2000). *Whole milk fouling of heated surfaces*. Masters Thesis. Massey University, Palmerston North, New Zealand.

Bennett, H. A. E., Trinh, K. T. & Manderson, G. (2002). Thermophilic growth in the evaporator section of a milk powder pilot plant. In *9th APCChE Congress and CHEMECA 2002* . Christchurch, New Zealand.

Benning, R., Petermeier, H., Delgado, A., Hinrichs, J., Kulozik, U. & Becker, T. (2003). Process design for improved fouling behaviour in dairy heat exchangers using a hybrid modelling approach. *Food and Bioproducts Processing,* 81 (C3), 266-274.

Beuf, M., G. Rizzo, G., Leuliet, J. C., Müller-Steinhagen, H., Yiantsios, S., Karabelas, A. & Benezech, T. (2003). Fouling and cleaning of modified stainless steel plate heat exchangers processing milk products. In *Conference on Heat Exchanger Fouling and Cleaning: Fundamentals and Applications*. New Mexico, USA.

Bixby, D. G. (1974). Fouling of heat exchange surfaces by skim milk. *Dissertation Abstracts International,* 35 (3), 1287-1288.

Bott, T. R. (1989). Fouling of exchangers: a review. R. W. Field, & J. A. Howell (eds), *Process engineering in the food industry: developments and opportunities*. London, UK: Elsevier Applied Science.

Bott, T. R. (1990). *Fouling Notebook*. Rugby, England: Institution of Chemical Engineers.

Bradley, S. E. & Fryer, P. J. (1992). A comparison of two fouling-resistant heat exchangers. *Biofouling,* 5, 295-314.

Britten, M., Green, M. L., Boulet, M. & Paquin, P. (1988). Deposit formation on heated surfaces - effect of interface energetics. *Journal of Dairy Research,* 55 (4), 551-562.

Burdett, M. (1974). Effect of phosphates in lowering amount of deposit formation during heat-treatment of milk. *Journal of Dairy Research,* 41 (1), 123-129.

Burton, H. (1961). A laboratory method for the investigation of milk deposits on heat exchange surfaces. *Journal of Dairy Research,* 28, 255-263.

Burton, H. (1965). A method for studying the factors in milk which influence the deposition of milk solids on a heated surface. *Journal of Dairy Research,* 32, 65-78.

Burton, H. (1966). A comparison between a hot-wire laboratory apparatus and a plate heat exchanger for determining the sensitivity of milk to deposit formation. *Journal of Dairy Research,* 33, 317-324.

Burton, H. (1968). Reviews of the progress of dairy science. *Journal of Dairy Research,* 35, 317-330.

Burton, H. (1972). Changes throughout lactation in amount of deposit formation from milk of individual cows. *Journal of Dairy Research,* 39 (2), 183-187.

Burton, H. (1984). Reviews of the progress of dairy science - the bacteriological, chemical, biochemical and physical changes that occur in milk at temperatures of 100-150-degrees-C. *Journal of Dairy Research,* 51 (2), 341-363.

Burton, H. (1988). *Ultra-high-temperature processing of milk and milk products.* Glasgow, UK: Blackie Academic & Professional.

Calderbank, P. H. (1967). N. Blakebrough (Ed), *Biochemical and Biological Engineering Science* (Vol. 1), 102. London: Academic Press.

Calvo, M. M. & Rafael, D. d. (1995). Deposit formation in a heat exchanger during pasteurization of CO2-acidified milk. *Journal of Dairy Research,* 62 (4), 641-644.

Changani, S. D., Belmar-Beiny, M. T. & Fryer, P. J. (1997). Engineering and chemical factors associated with fouling and cleaning in milk processing. *Experimental Thermal and Fluid Science,* 14 (4), 392-406.

Christian, G. K., Changani, S. D. & Fryer, P. J. (2002). The effect of adding minerals on fouling from whey protein concentrate - development of a model fouling fluid for a plate heat exchanger. *Food and Bioproducts Processing,* 80 (C4), 231-239.

Corredig, M. & Dalgleish, D. G. (1996a). Effect of temperature and pH on the interactions of whey proteins with casein micelles in skim milk. *Food Research International,* 29 (1), 49-55.

Corredig, M. & Dalgleish, D. G. (1996b). Effect of different heat treatments on the strong binding interactions between whey proteins and milk fat globules in whole milk. *Journal of Dairy Research,* 63 (3), 441-449.

Corrieu, G., Lalande, M. & Ferret, R. (1986). On-line measurement of fouling and cleaning of industrial UHT heat exchanger. (Mesure en Ligne de l'Encrassement et du Nettoyage d'un Sterilisateur UHT Industriel). *Journal of Food Engineering,* 5, 231-248.

Creamer, L. K., Berry, G. P. & Matheson, A. R. (1978). Effect of pH on protein aggregation in heated skim milk. *New Zealand Journal of Dairy Science and Technology,* 13 (1), 9-15.

Croy, R. J. (2000). *Development of an in-line CIP sensor*. Masters Thesis. Massey University, Palmerston North, New Zealand.

Croy, R. J., Trinh, K. T., Smith, T. & Tredwell, S. (2002). Monitoring CIP using heat flux sensors. In *Fouling, Cleaning and Disinfection in Food Processing.* Cambridge, UK.

Davies, T. J., Henstridge, S. C., Gillham, C. R. & Wilson, D. I. (1997). Investigation of whey protein deposit properties using heat flux sensors. *Food and Bioproducts Processing,* 75 (C2), 106-110.

De Jong, P. (1997). Impact and control of fouling in milk processing. *Trends in Food Science & Technology,* 8 (12), 401-405.

De Jong, P., Bouman, S. & Linden, H. J. L. J. v. d. (1992). Fouling of heat-treatment equipment in relation to the denaturation of beta-lactoglobulin. *Journal of the Society of Dairy Technology,* 45 (1), 3-8.

Delplace, F. & Leuliet, J. C. (1995). Modeling fouling of a plate heat-exchanger with different flow arrangements by whey-protein solutions. *Food and Bioproducts Processing,* 73 (C3), 112-120.

Delplace, F., Leuliet, J. C. & Levieux, D. (1997). A reaction engineering approach to the analysis of fouling by whey proteins of a six-channels-per-pass plate heat exchanger. *Journal of Food Engineering,* 34 (1), 91-108.

Delplace, F., Leuliet, J. C. & Tissier, J. P. (1994). Fouling experiments of a plate heat exchanger by whey protein solutions. *Trans IChemE,* 72, 163-169.

Delsing, B. M. A. & Hiddink, J. (1983). Fouling of heat-transfer surfaces by dairy liquids. *Netherlands Milk and Dairy Journal,* 37 (3), 139-148.

Dickinson, E., Mauffret, A., Rolfe, S. E. & Woskett, C. M. (1989). Adsorption at interfaces in dairy systems. *Journal of the Society of Dairy Technology,* 42 (1), 18-22.

Flint, S. H., Brooks, J. D. & Bremer, P. J. (2000). Properties of the stainless steel substrate, influencing the adhesion of thermo-resistant streptococci. *Journal of Food Engineering,* 43 (4), 235-242.

Foster, C. L., Britten, M. & Green, M. L. (1989). A model heat-exchange apparatus for the investigation of fouling of stainless-steel surfaces by milk. 1. Deposit formation at 100-degrees-C. *Journal of Dairy Research,* 56 (2), 201-209.

Foster, C. L. & Green, M. L. (1990). A model heat-exchange apparatus for the investigation of fouling of stainless-steel surfaces by milk. 2. Deposition of fouling material at 140-degrees-C, its adhesion and depth profiling. *Journal of Dairy Research,* 57 (3), 339-348.

Fox, P. F. (1995). *Heat-induced changes in milk*. Belgium: International Dairy Federation.

Fox, P. F. & Hearn, C. M. (1978). Heat-stability of milk - influence of kappa-casein hydrolysis. *Journal of Dairy Research,* 45 (2), 173-181.

Fryer, P. J. (1989). The uses of fouling models in the design of food process plant. *Journal of the Society of Dairy Technology,* 42 (1), 23-29.

Fryer, P. J. & Belmar-Beiny, M. T. (1991). Fouling of heat exchangers in the food industry: a chemical engineering perspective. *Trends in Food Science & Technology,* 2 (2), 33-37.

Fryer, P. J., Belmar-Beiny, M. T. & Schreier, P. J. R. (1995). Fouling and cleaning in milk processing. P. F. Fox (eds.) *Heat-induced changes in milk* (2nd ed.), 364-395. Belgium: International Dairy Federation.

Fryer, P. J. & Bird, M. R. (1994). Factors which affect the kinetics of cleaning dairy soils. *Food Science & Technology Today,* 8 (1), 36-42.

Fryer, P. J. & Pritchard, A. M. (1989). A comparison of two possible fouling monitors for the food processing industry. R. W. Field, & J. A. Howell (eds.), *Process engineering in the food industry: developments and opportunities* (131-141). London, UK: Elsevier Applied Science.

Fryer, P. J., Pritchard, A. M., Slater, N. K. H. & Laws, J. F. (1985). A possible online fouling sensor for the food processing industry. In *Fouling and Cleaning in Food Processing.* Wisconsin, USA.

Fryer, P. J., Robbins, P. T., Green, C., Schreier, P. J. R., Pritchard, A. M., Hasting, A. P. M., Royston, D. G. & Richardon, J. F. (1996). A statistical model for fouling of a plate heat exchanger by whey protein solution at UHT conditions. *Food and Bioproducts Processing,* 74 (C4), 189-199.

Fryer, P. J. & Slater, N. K. H. (1994). Factors which affect the kinetics of cleaning dairy soils. *Food Science & Technology Today,* 8 (1), 36-42.

Fung, L. (1998). *The effect of fat globule membrane damage in the absence of air on fouling in heat exchangers.* Masters Thesis. Massey University, Palmerston North.

Gordon, K. P., Hankison, D. J. & Carver, C. E. (1968). Deposition of milk solids on heated surfaces. *Journal of Dairy Science,* 51 (4), 520-526.

Gotham, S. M., Fryer, P. J. & Pritchard, A. M. (1992). Beta-lactoglobulin denaturation and aggregation reactions and fouling deposit formation - a DSC study. *International Journal of Food Science and Technology,* 27 (3), 313-327.

Grandison, A. S. (1988). UHT processing of milk - seasonal-variation in deposit formation in heat-exchangers. *Journal of the Society of Dairy Technology,* 41 (2), 43-49.

Grandison, A. S. (1996). Foul Play. *Dairy Industries International,* 61 (4), 15-17.

Grasshoff, A. (1988). Studies on deposit formation on heat-exchanger surfaces during heating of milk in a laboratory-scale heat-exchanger equipment. *Milchwissenschaft-Milk Science International,* 43 (12), 780-783.

Grijspeerdt, K., Hazarika, B. & Vucinic, D. (2003). Application of computational fluid dynamics to model the hydrodynamics of plate heat exchangers for milk processing. *Journal of Food Engineering,* 57 (3), 237-242.

Gynning, K., Thome, K. E. & Samuelsson, E. G. (1958). The burning of milk in plate pasteurizers. *Milchwissenshaft,* 13, 62.

Hegg, P. O., Castberg, H. B. & Lundh, G. (1985). Fouling of whey proteins on stainless-steel at different temperatures. *Journal of Dairy Research,* 52 (1), 213-218.

Hegg, P. O. & Larsson, K. (1981). Ellipsometry studies of adsorbed lipids and milk proteins on metal surfaces. In *Fundamentals and Applications of Surface Phenomena Associated with Fouling and Cleaning in Food Processing.* Tylosand, Sweden.

Hermans, W. F. (1981). Fouling, cleaning and corrosion aspects in tubular heat exchangers for the dairy and food industry. In *Fundamentals and Applications of Surface Phenomena Associated with Fouling and Cleaning in Food Processing.* Tylosand, Sweden.

Hinton, A. R. (2003). *Thermophiles and fouling deposits in milk powder plants*. Doctoral Thesis. Massey University, Palmerston North, New Zealand.

Hinton, A. R., Trinh, K. T., Brooks, J. D. & Manderson, G. J. (2002). Thermophile survival in milk fouling and on stainless steel during cleaning. *Food and Bioproducts Processing,* 80 (C4), 299-304.

Houlihan, A. V., Goddard, P. A., Nottingham, S. M., Kitchen, B. J. & Masters, C. J. (1992). Interactions between the bovine-milk fat globule-membrane and skim milk components on heating whole milk. *Journal of Dairy Research,* 59 (2), 187-195.

Huppertz, T., Fox, P. F. & Kelly, A. L. (2004). High pressure treatment of bovine milk: effects on casein micelles and whey proteins. *Journal of Dairy Research,* 71 (1), 97-106.

Huppertz, T., Kelly, A. L. & Fox, P. F. (2002). Effects of high pressure on constituents and properties of milk. *International Dairy Journal,* 12, 561-572.

Ito, R. & Nakanishi, T. (1967). Formation of milk deposits on heat exchange surfaces in UHT pasteurizing plant. XI. Laboratory investigation of the factors influencing milk deposit formation. *Japan Journal of Dairy Science,* 16 (2).

Itoh, H., Nagata, A., Toyomasu, T., Sakiyama, T., Nagai, T., Saeki, T. & Nakanishi, K. (1995). Adsorption of beta-lactoglobulin onto the surface of stainless-steel particles. *Bioscience Biotechnology and Biochemistry,* 59 (9), 1648-1651.

Jeurnink, T. J. M. (1991). Effect of proteolysis in milk on fouling in heat-exchangers. *Netherlands Milk and Dairy Journal,* 45 (1), 23-32.

Jeurnink, T. J. M. (1992). Changes in milk on mild heating - turbidity measurements. *Netherlands Milk and Dairy Journal,* 46 (3-4), 183-196.

Jeurnink, T. J. M. (1995a). Fouling of heat-exchangers by fresh and reconstituted milk and the influence of air bubbles. *Milchwissenschaft-Milk Science International,* 50 (4), 189-193.

Jeurnink, T. J. M. (1995b). Fouling of heat-exchangers in relation to the serum-protein concentration in milk. *Milchwissenschaft-Milk Science International,* 50 (5), 257-260.

Jeurnink, T. J. M. & Brinkman, D. W. (1994). The cleaning of heat exchangers and evaporators after processing milk or whey. *International Dairy Journal,* 4 (4), 347-368.

Jeurnink, T. J. M., Brinkman, D. W. & Stemerdink, A. D. (1989). Distribution and composition of deposit in heat exchangers. In *Proceeding of the Third International Conference on Fouling and Cleaning in Food Processing* (25-35). University of Munich. Munich, Germany.

Jeurnink, T. J. M. & Kruif, K. G. d. (1995). Calcium-concentration in milk in relation to heat-stability and fouling. *Netherlands Milk and Dairy Journal,* 49 (2-3), 151-165.

Jeurnink, T. J. M., Verheul, M., Stuart, M. A. C. & Kruif, C. G. d. (1996a). Relation between the denaturation and fouling behaviour of beta-lactoglobulin. In *Proceeding of Heat Treatments & Alternative Methods.* (73-82). Brussels, Belgium: International Dairy Federation.

Jeurnink, T. J. M., Verheul, M., Stuart, M. A. C. & Kruif, C. G. d. (1996b). Deposition of heated whey proteins on a chromium oxide surface. *Colloids and Surfaces B-Biointerfaces,* 6 (4-5), 291-307.

Jeurnink, T. J. M., Walstra, P. & Kruif, C. G. d. (1996c). Mechanisms of fouling in dairy processing. *Netherlands Milk and Dairy Journal,* 50 (3), 407-426.

Johnson, J. J. & Roland, C. T. (1940a). Study of dairy cleaning problems. I. Films and deposits on hot milk equipment. *Journal of Dairy Science,* 23, 457-461.

Johnson, J. J. & Roland, C. T. (1940b). Study of dairy cleaning problems. II. Effectiveness of alkalies in removing heat-deposited milk solids and butterfat films. *Journal of Dairy Science,* 23, 463-469.

Jones, A. D., Ward, N. J. & Fryer, P. J. (1994). The use of a heat flux sensor to monitor milk fluid fouling. In *Fouling and Cleaning in Food Processing* (199-205). University of Cambridge. Cambridge, U.K.

Kessler, H. G. & Beyer, H. J. (1991). Thermal-denaturation of whey proteins and its effect in dairy-technology. *International Journal of Biological Macromolecules,* 13 (3), 165-173.

Kessler, H. G. & Schraml, J. E. (1996). Effects of concentration and product composition on fouling structure. In *Fouling and cleaning in food processing.* Brussels: European Commission.

Kim, J. C. & Lund, D. B. (1998). Milk protein stainless steel interaction relevant to the initial stage of fouling in thermal processing. *Journal of Food Process Engineering,* 21 (5), 369-386.

Lalande, M. & Corrieu, G. (1981). Fouling of a plate heat exchanger by milk. In *Fundamentals and Applications of Surface Phenomena Associated with Fouling and Cleaning in Food Processing.* Tylosand, Sweden.

Lalande, M., Tissier, J. P. & Corrieu, G. (1984). Fouling of a plate heat-exchanger used in ultra-high-temperature sterilization of milk. *Journal of Dairy Research,* 51 (4), 557-568.

Lalande, M., Tissier, J. P. & Corrieu, G. (1985). Fouling of heat-transfer surfaces related to beta-lactoglobulin denaturation during heat processing of milk. *Biotechnology Progress,* 1 (2), 131-139.

Law, B. A. (1979). Reviews of the progress of dairy science - enzymes of psychrotrophic bacteria and their effects on milk and milk-products. *Journal of Dairy Research,* 46 (3), 573-588.

Law, B. A., Andrews, A. T., Cliffe, A. J., Sharpe, M. E. & Chapman, H. R. (1979). Effect of proteolytic raw-milk psychrotrophs on cheddar cheese-making with stored milk. *Journal of Dairy Research,* 46 (3), 497-507.

Lund, D. B. & Bixby, D. (1975). Fouling of heat exchange surfaces by milk. *Process Biochemistry,* 10 (9), 52-55.

Lund, D. B. & Sandu, C. (1981). State-of-the-art of fouling: heat transfer surfaces. In *Fundamentals and Applications of Surface Phenomena Associated with Fouling and Cleaning in Food Processing.* Tylosand, Sweden.

Lyster, R. L. J. (1965). The composition of milk deposits in an ultra-high-temperature plant. *Journal of Dairy Research,* 32, 203-208.

Ma, C. H. C., Trinh, K. T., Brooks, J. D. & Kitson, K. E. (2001). Effect of commercial and microbial proteinases on fouling of whole milk. In *6th World Congress of Chemical Engineers.* Melbourne, Australia.

Ma, C. H. C., Trinh, K. T., Brooks, J. D. & Maddox, I. S. (1998). Effect of fat content on the rate of fouling on heated surfaces by milk. In *5th Annual New Zealand Engineering and Technology Postgraduate Conference.* Palmerston North, New Zealand.

McCabe, W. L., Smith, J. C. & Harriott, P. (2001). *Unit Operations of Chemical Engineering*. Boston, USA: McGraw Hill.

Morison, K. R. & Tie, S. H. (2002). The development and investigation of a model milk mineral fouling solution. *Food and Bioproducts Processing,* 80 (C4), 326-331.

Mottar, J. & Moermans, R. (1988). Optimization of the forewarming process with respect to deposit formation in indirect ultra high-temperature plants and the quality of milk. *Journal of Dairy Research,* 55 (4), 563-568.

Muller-Steinhagen, H. & Zhao, Q. (1997). Investigation of low fouling surface alloys made by ion implantation technology. *Chemical Engineering Science,* 52 (19), 3321-3332.

Mulvihill, D. M. & Donovan, M. (1987). Whey proteins and their thermal-denaturation - a review. *Irish Journal of Food Science and Technology,* 11 (1), 43-75.

Murray, B. S. & Deshaires, C. (2000). Monitoring protein fouling of metal surfaces via a quartz crystal microbalance. *Journal of Colloid and Interface Science,* 227 (1), 32-41.

Newstead, D. F., Groube, G. F., Smith, A. F. & Eiger, R. N. (1998). Fouling of UHT plants by recombined and fresh milk some effects of preheat treatment. In *Fouling and Cleaning in Food Processing '98.* Cambridge, UK.

Norton, T. & Sun, D. W. (2006). Computational fluid dynamics (CFD) - an effective and efficient design and analysis tool for the food industry: a review. *Trends in Food Science & Technology,* 17 (11), 600-620.

Oldfield, D. J., Singh, H. & Taylor, M. W. (1998a). Association of beta-lactoglobulin and alpha-lactalbumin with the casein micelles in skim milk heated in an ultra-high temperature plant. *International Dairy Journal,* 8 (9), 765-770.

Oldfield, D. J., Singh, H., Taylor, M. W. & Pearce, K. N. (1998b). Kinetics of denaturation and aggregation of whey proteins in skim milk heated in an ultra-high temperature (UHT) pilot plant. *International Dairy Journal,* 8 (4), 311-318.

Parnellclunies, E., Kakuda, Y., Irvine, D. & Mullen, K. (1988). Heat-induced protein-changes in milk processed by vat and continuous heating-systems. *Journal of Dairy Science,* 71 (6), 1472-1483.

Paterson, W. R. & Fryer, P. J. (1988). A reaction-engineering approach to the analysis of fouling. *Chemical Engineering Science,* 43 (7), 1714-1717.

Pelan, B. M. C., Watts, K. M., Campbell, I. J. & Lips, A. (1997). The stability of aerated milk protein emulsions in the presence of small molecule surfactants. *Journal of Dairy Science,* 80 (10), 2631-2638.

Petermeier, H., Benning, R., Delgado, A., Kulozik, U., Hinrichs, J. & Becker, T. (2002). Hybrid model of the fouling process in tubular heat exchangers for the dairy industry. *Journal of Food Engineering,* 55 (1), 9-17.

Refstrup, E. (1998). Heat treatment of milk prior to evaporation and drying. In *Proceedings of the 25th International Dairy Congress* (228-233).

Refstrup, E. (2000). Evaporation and drying technology developments. *International Journal of Dairy Technology,* 53 (4), 163-167.

Robbins, P. T., Elliott, B. L., Fryer, P. J., Belmar, M. T. & Hasting, A. P. (1999). A comparison of milk and whey fouling in a pilot scale plate heat exchanger: implications for modelling and mechanistic studies. *Food and Bioproducts Processing,* 77 (C2), 97-106.

Roefs, S. P. F. M. & Kruif, K. G. d. (1994). A model for the denaturation and aggregation of beta-lactoglobulin. *European Journal of Biochemistry,* 226 (3), 883-889.

Roscoe, S. G. & Fuller, K. L. (1994). Fouling of model surfaces: adsorption and removal of whole unpasteurized milk. *Food Research International,* 27 (4), 363-369.

Rosmaninho, R., Visser, H. & Melo, L. F. (2002). Effect of surface tension on the growth rate and density of calcium phosphate deposits formed on stainless steel. In *Fouling, Cleaning and Disinfection in Food Processing.* Cambridge, UK.

Sander, R. (1999) *Compilation of Henry's Law Constants for Inorganic and Organic Species of Potential Importance in Environmental Chemistry* [Web Page]. URL http://www.henrys-law.org [accessed 10/05/2006].

Sandu, C., Lund, D., O'Neal, B., Singh, R. & Almas, K. (1984). A plate heat exchanger designed to study fouling in food processing. *Engineering and Food. Vol. I. Engineering Sciences in the Food Industry,* 1, 199-207.

Santos, O., Nylander, T., Rosmaninho, R., Rizzo, G., Yiantsios, S., Andritsos, N., Karabelas, A., Muller-Steinhagen, H., Melo, L., Boulange- Petermann, L., Gabet, C., Braem, A., Tragardh, C. & Paulsson, M. (2004). Modified stainless steel surfaces targeted to reduce fouling - surface characterization. *Journal of Food Engineering,* 64 (1), 63-79.

Schraml, J. E. & Kessler, H. G. (1996). Effects of concentration on fouling at hot surfaces. In *Fouling and cleaning in food processing.* Brussels: European Commission.

Schreier, P. J., Green, R. C. H., Pritchard, A. M. & Fryer, P. J. (1996). Heat Exchanger fouling by whey protein solutions. In *Fouling and cleaning in food processing.* Brussels: European Commission.

Schreier, P. J. R. & Fryer, P. J. (1995). Heat-exchanger fouling - a model study of the scaleup of laboratory data. *Chemical Engineering Science,* 50 (8), 1311-1321.

Singh, H. & Creamer, L. K. (1991). Denaturation, aggregation and heat-stability of milk protein during the manufacture of skim milk powder. *Journal of Dairy Research,* 58 (3), 269-283.

Singh, H. & Fox, P. F. (1985). Heat-stability of milk - pH-dependent dissociation of micellar kappa-casein on heating milk at ultra high-temperatures. *Journal of Dairy Research,* 52 (4), 529-538.

Singh, H. & Fox, P. F. (1986). Heat-stability of milk - further-studies on the pH-dependent dissociation of micellar kappa-casein. *Journal of Dairy Research,* 53 (2), 237-248.

Skudder, P. J. (1981). The role of sulphydryl groups in the formation of proteinaceous deposit from milk on heated surfaces. In *Fundamentals and Applications of Surface Phenomena Associated with Fouling and Cleaning in Food Processing.* Tylosand, Sweden.

Skudder, P. J., Brooker, B. E., Bonsey, A. D. & Alvarezguerrero, N. R. (1986). Effect of pH on the formation of deposit from milk on heated surfaces during ultra high-temperature processing. *Journal of Dairy Research,* 53 (1), 75-87.

Skudder, P. J., Thomas, E. L., Pavey, J. A. & Perkin, A. G. (1981). Effects of adding potassium iodate to milk before UHT Treatment. 1. Reduction in the amount of deposit on the heated surfaces. *Journal of Dairy Research,* 48 (1), 99-113.

Swartzel, K. R. (1983). Tubular heat-exchanger fouling by milk during ultra high-temperature processing. *Journal of Food Science,* 48 (5), 1507-1511.

Thom, R. (1975). Formation of milk deposits in plate heaters. *Milchwissenschaft,* 30 (2), 84-89.

Thomson, W. J. (2000). *Introduction to transport phenomena*. Upper Saddle River, NJ.: Prentice Hall.

Tirumalesh, A., Ramachandra Rao, H. G. & Jayaprakash, H. M. (1997). Fouling of heat exchangers. *Indian Journal of Dairy and Biosciences,* 8, 41-44.

Tissier, J. P. & Lalande, M. (1986). Experimental device and methods for studying milk deposit formation on heat-exchange surfaces. *Biotechnology Progress,* 2 (4), 218-229.

Tissier, J. P., Lalande, M. & Corrieu, G. (1984). A study of milk deposit on heat exchange surface during UHT treatment. *Engineering and Food. Vol. I. Engineering Sciences in the Food Industry,* 1, 49-58.

Trinh, B., Trinh, K. T. & Haisman, D. (2007). Effect of total solids content and temperature on the rheological behaviour of reconstituted whole milk concentrates. *Journal of Dairy Research,* 74 (1), 116-123.

Truong, H. T. (2001). *Fouling of stainless steel surfaces by heated whole milk*. Doctoral Thesis. Massey University, Palmerston North, New Zealand.

Truong, H. T., Anema, S., Kirkpatrick, K. & Trinh, K. T. (1998). In-line measurements of fouling and CIP in milk powder plants. In *Fouling and cleaning in food processing.* Brussels: European Commission.

Truong, H. T., Trinh, K. T. & Mackereth, A. R. (1996). Structural change of fouling deposits from whole milk in heat treatment equipment. In *IPENZ Annual Conference 1996 "Engineering Providing the Foundations for Society"* .

Truong, T., Anema, S., Kirkpatrick, K. & Chen, H. (2002). The use of a heat flux sensor for in-line monitoring of fouling of non-heated surfaces. *Food and Bioproducts Processing,* 80 (C4), 260-269.

Visser, H., Jeurnink, T. J. M., Schraml, J. E., Fryer, P. & Delplace, F. (1997). Fouling of heat treatment equipment. *Bulletin of the International Dairy Federation,* 328, 7-31.

Visser, J. & Jeurnink, T. J. M. (1997). Fouling of heat exchangers in the dairy industry. *Experimental Thermal and Fluid Science,* 14 (4), 407-424.

Walstra, P., Geurts, T. J., Noomen, A., Jellema, A. & Boekel, M. A. J. S. v. (1999). *Dairy Technology: Principles of milk properties and processes*. Marcel Dekker, Inc.; New York; USA.

Walstra, P. & Jenness, R. (1984). *Dairy Chemistry & Physics.* John Wiley & Sons; New York; USA.

Wennerberg, J. (1981). Observations on the behaviour of fouling and cleaning in industrial processes. In *Fundamentals and Applications of Surface Phenomena Associated with Fouling and Cleaning in Food Processing.* Tylosand, Sweden.

Withers, P. M. (1994). Ultrasonic sensor for the detection of fouling in UHT processing Plants. *Food Control,* 5 (2), 67-72.

Withers, P. M. (1996). Ultrasonic, acoustic and optical techniques for the non-invasive detection of fouling in food processing equipment. *Trends in Food Science & Technology,* 7 (9), 293-298.

Wood, P. W. (1996). *Physical Properties of Dairy Products* (3rd ed.). New Zealand: MAF Quality Management, Ministry of Agriculture.

Yoon, J. & Lund, D. B. (1989). Effect of operating conditions, surface coatings and pretreatment on milk fouling in a plate heat exchanger. In *Proceeding of the Third International Conference on Fouling and Cleaning in Food Processing*. University of Munich. Munich, Germany.

Yoon, J. & Lund, D. B. (1994a). Comparison of two operating methods of a plate heat exchanger under constant heat flux condition and their effect on the temperature profile during milk fouling. *Journal of Food Process Engineering,* 17, 243-262.

Yoon, J. & Lund, D. B. (1994b). Magnetic treatment of milk and surface-treatment of plate heat-exchangers - effects on milk fouling. *Journal of Food Science,* 59 (5), 964-969.

APPENDICES

APPENDIX A OVERVIEW OF EQUIPMENT AND MATERIALS

Table A.1 lists all the components used in the construction of the pilot plant including the instrumentation devices and control equipment. Table A.2 lists the major analytical equipment and Table A.3 lists the major consumables used in this project.

Figures A.1 - A.3 are P & ID for various sections of the pilot plant. Dimension drawings of the major research equipment used in this project are given in Figures A.5 – A.6.

Table A.1 List of pilot plant components.

Item	Drawing abbrev.	Drawing no.	Description	Source
Tanks				
Storage vat	SV	A1	850 l, Model No. 1R1309L.	Berry Ltd., Palmerston North, N.Z.
Heating medium reservoir	HM	A1	50 l, Custom built - Commercial.	Berry Ltd., Palmerston North, N.Z.
CIP tank 1	CIP1	A1	500 l, Custom built - Commercial.	MacDonalds Machinery Ltd., Auckland, N.Z.
CIP tank 2	CIP2	A1	500 l, Custom built - Commercial.	MacDonalds Machinery Ltd., Auckland, N.Z.
CIP tank 3	CIP3	A1	350 l, Custom built - Commercial.	MacDonalds Machinery Ltd., Auckland, N.Z.
Heat transfer devices				
Refrigeration unit	HE1	A1	Storage vat refrigeration unit, Model No. ERJ 0200 TAD.	Ellis, Hardie and Syminton Ltd., Auckland, N.Z.
Plate heat exchanger	PHE	A1	Plate heat exchanger, Model No. U265R.	APV, Denmark.
Thermising steam injectors	DSI1	A1	Custom built - Massey postgraduate students.	Components sourced from various suppliers.
Preheating steam injectors	DSI2	A1	Custom built - Massey postgraduate students.	Components sourced from various suppliers.
Heating element	HE2	A1	Heating medium reservoir heating element, Eutro, 3kW.	Stewarts Electrical Supplies, Palmerston North, N.Z.
Miniature plate heat exchanger	MPHE	A2	Custom built - Commercial and Massey postgraduate students.	Components sourced from various suppliers.
Tubular heat exchanger	THE	A3	Custom built - Massey postgraduate students.	Components sourced from various suppliers.
Other				
Agitator	SVA	A1	Storage vat agitator, Leroy Somer, Model No. IEC44-1.	Fonterra Co-op Ltd., Longburn, N.Z.
Holding tubes	HT	A1	Custom built – Massey postgraduate students.	Components sourced from various suppliers

Table A.1 (continued)

Item	Drawing abbrev.	Drawing no.	Description	Source
Stainless steel components				
Test plates	-	-	MPHE test plates, 0.6 mm thick, T304.	NZF Stainless Ltd., Palmerston North, N.Z.
Test tubes	-	-	THE test tubes, 12.7 mm OD, T304.	NZF Stainless Ltd., Palmerston North, N.Z.
Ball valves BSP	-	-	Two-piece, variable sizes, T304.	NZF Stainless Ltd., Palmerston North, N.Z.
Kleanflow butterfly valves	-	-	25.4 mm, T304.	NZF Stainless Ltd., Palmerston North, N.Z.
Kleanflow fittings	-	-	Male, blank, slotted nut, clamps, variable sizes, T304.	NZF Stainless Ltd., Palmerston North, N.Z.
Bolts & wing nuts	-	-	Size M5.	NZF Stainless Ltd., Palmerston North, N.Z.
Unions	-	-	Variable sizes, T304.	NZF Stainless Ltd., Palmerston North, N.Z.
Hexagon nipples	-	-	Variable sizes, T304.	NZF Stainless Ltd., Palmerston North, N.Z.
Hexagon reducing nipples	-	-	Variable sizes, T304.	NZF Stainless Ltd., Palmerston North, N.Z.
Welding nipples	-	-	Variable sizes, T304.	NZF Stainless Ltd., Palmerston North, N.Z.
Tees	-	-	Variable sizes, T304.	NZF Stainless Ltd., Palmerston North, N.Z.
Concentric reducers	-	-	Variable sizes, T304.	NZF Stainless Ltd., Palmerston North, N.Z.
90° bends	-	-	Variable sizes, T304.	NZF Stainless Ltd., Palmerston North, N.Z.
Piping	-	-	Variable sizes, T304 & T316.	NZF Stainless Ltd., Palmerston North, N.Z.
Tube socket weld unions	-	-	Swagelok, Product No. SS-400-6-4W.	Swagelok Ltd., Auckland, N.Z.
Non-stainless steel components				
'O' - rings	-	-	Variable sizes.	Engineering Plastics Ltd., Palmerston North, N.Z.
Teflon column	-	-	40 mm OD.	Engineering Plastics Ltd., Palmerston North, N.Z.
Silicone sheets	-	-	MPHE gaskets, 2.36 mm thick, Product No. SRS2.36FDA.	Engineering Plastics Ltd., Palmerston North, N.Z.

Table A.1 (continued)

Item	Drawing abbrev.	Drawing no.	Description	Source
Perspex sheets	-	-	6 mm thick.	Engineering Plastics Ltd., Palmerston North, N.Z.
Topic ball valves	-	-	One-piece, 12.7 mm.	Harold Pierard Ltd., Palmerston North, N.Z.
Needle valves	-	-	One-piece, 12.7 mm.	Harold Pierard Ltd., Palmerston North, N.Z.
Globe valves	-	-	Variable sizes.	Harold Pierard Ltd., Palmerston North, N.Z.
Flexible hose	-	-	Hi-temperature Push-Lok flexible hose.	General Machinery Ltd., Palmerston North, N.Z
Pumps	-	-		
Preheating pump	PM1	A1	Centrifugal pump, Ebara, Model No. CDX70/05, 0.37kW.	Keith R.Norling Ltd., Palmerston North, N.Z.
Heating medium pump	PM2	A1	Centrifugal pump, Ebara, Model No. CDX70/05, 0.37kW.	Keith R.Norling Ltd., Palmerston North, N.Z.
CIP pump	PM3	A1	Centrifugal pump, Model No. FP712KF, 1.1kW.	Fristam, Auckland, N.Z.
Temperature sensors				
Preheat RTDs	T1-T8	A1	PT100 RTD, Custom built - Commercial and Massey postgraduate students.	Components sourced from various suppliers
MPHE thermocouples	T9-T20	A2	T type thermocouples, Custom built - Massey postgraduate students.	RS Components Ltd., Auckland, N.Z.
THE thermocouples	T21-T31	A3	T type thermocouples, Custom built - Massey postgraduate students.	RS Components Ltd., Auckland, N.Z.
Heat flux sensors				
MPHE	H1-H6	A2	Micro-foil heat flux sensors, Model No. 27036-3.	RdF Corporation, New Hampshire, U.S.A.
Pressure sensors				
Post PHE	P1	A1	Pressure transmitter, Data Instruments, Model XPRO 0-50PSIG.	EMC Industrial Instrumentation, Auckland, N.Z.
DSI1 steam	P2	A1	Pressure transmitter, Data Instruments, Model XPRO 0-50PSIG.	EMC Industrial Instrumentation, Auckland, N.Z.
Post MPHE & THE	P3	A1	Pressure transmitter, Data Instruments, Model XPRO 0-50PSIG.	EMC Industrial Instrumentation, Auckland, N.Z.

Table A.1(continued)

Item	Drawing abbrev.	Drawing no.	Description	Source
DSI2 steam	P4	A1	Pressure transmitter, Data Instruments, Model XPRO 0-50PSIG.	EMC Industrial Instrumentation, Auckland, N.Z.
Flow sensors				
Preheat low range	F1	A1	Electromagnetic flow meter, Endress-Hauser Picomag, Model No. 11 PM 165333.	EMC Industrial Instrumentation, Auckland, N.Z.
Preheat high range	F2	A1	Electromagnetic flow meter, Endress-Hauser Promag, Model No. 30FT25-AA1AA11A21B.	EMC Industrial Instrumentation, Auckland, N.Z.
Control valves				
DSI 1	CV1	A1	Steam control valve, WAF, Model No. V201 BUE.	W. Arthur Fisher Ltd., Auckland, N.Z.
DSI 2	CV2	A1	Steam control valve, WAF, Model No. V201 BUE.	W. Arthur Fisher Ltd., Auckland, N.Z.
Control equipment				
Control computer	-	-	Intel Celeron Pentium II-400, Model No. 128/6.4/CDSB.	Advantage Computers Ltd., Palmerston North, N.Z.
Programmable logic controller	-	-	PLC, Allen-Bradley SLC 500, 13-slot modular chassis X2.	Rockwell Automation Ltd., Palmerston North, N.Z.
I/P converters	-	-	Current to pressure transducers, Brandt, Model No. Pi-CPT-2141.	Bristol Babcock Controls Ltd., Auckland, N.Z.
Variable speed drives	VSD1-VSD2	A1	Variable speed drive, Allen-Bradley, Model No. 60-BA04NSF1.	Rockwell Automation Ltd., Palmerston North, N.Z.
Reception equipment				
Milk reception pump	-	-	Mono pump, Mono Pump Ltd., Model No. CP25.	Keith R.Norling Ltd., Palmerston North, N.Z.
Flexible tubing	-	-	Tubing 25mm, Rubicon, Product No. 9102.	General Machinery Ltd., Palmerston North, N.Z

Table A.2 List of measuring and optical equipment.

Item	Drawing abbrev.	Drawing no.	Description	Source
Measuring equipment				
Depth gauge	-	-	Digital dial depth gauge, Mitutoyo, Model No. 1DC-112E.	Mitutoyo Corporation, Aurora, U.S.A.
Multimeter	-	-	Brymen, Model No. BM727.	Dick Smith Electronics, Palmerston North, N.Z.
Balance	-	-	Mettler, Model No. AE240.	Biolab Ltd., Auckland, N.Z.
Balance	-	-	Mettler, Model No. PG503.	Biolab Ltd., Auckland, N.Z.
Visual equipment				
Digital camera	-	-	Fujifilm, Model No. FinePix S602.	Bruce Watt Photography, Palmerston North, N.Z.
Digital video camera	-	-	Sony, Model No. DCR- TRV140E.	Bruce Watt Photography, Palmerston North, N.Z.

Table A.3 List of consumables used in the current project

Item	Drawing Abbrev.	Drawing No.	Description	Source
Whole milk	-	-	3.2% protein, 3.3% cream, homogenised and pasteurised full cream milk.	Fonterra Co-op Ltd., Longburn, N.Z.
Skim milk	-	-	3.3% protein, 0.1% cream, pasteurised skim milk.	Fonterra Co-op Ltd., Longburn, N.Z.
Whey protein concentrate	-	-	ALACEN 322, 80.5% protein, 5.4% fat, whey protein concentrate 80% (sulphuric).	Fonterra Co-op Ltd., Edgecumbe, N.Z.
CIP solution - Caustic	-	-	Liquid caustic soda, 50% w/w solution, Product No. 000031006701.	Orica Chemnet Ltd., Tauranga, N.Z.
CIP solution - Nitric	-	-	Nitric acid, 68% w/w solution, Product No. 000034074301.	Orica Chemnet Ltd., Tauranga, N.Z.
Neutrase	-	-	Neutrase 0.8L.	Chemcolour Industries Ltd., Auckland, N.Z.
Aluminium tape	-	-	3M Scotch, Product No. 425.	General Machinery Ltd., Palmerston North, N.Z
Heat transfer paste	-	-	Electrolube, Product No. HTC103 & HTS35SL.	Spectron Electronics Ltd., Palmerston North, N.Z.
Heat transfer oil	-	-	Mobiltherm 603, Product No. 988688.	ExxonMobil Ltd., Wellington, N.Z.
Polymer adhesive	-	-	Super strength araldite epoxy resin.	Shelleys Chemical Company Pty. Ltd., Auckland, N.Z.
Syringes	-	-	Sterile 30 ml, Terumo.	Terumo Corporation, Tokyo, Japan.
Needles	-	-	20 gauge - 0.9 x 25 mm, Precision glide.	Becton Dickinson Medical Pte. Ltd., Singapore.
Rubber septa	-	-	Septa 77.	Chromatography Research Supplies Inc., U.S.A.

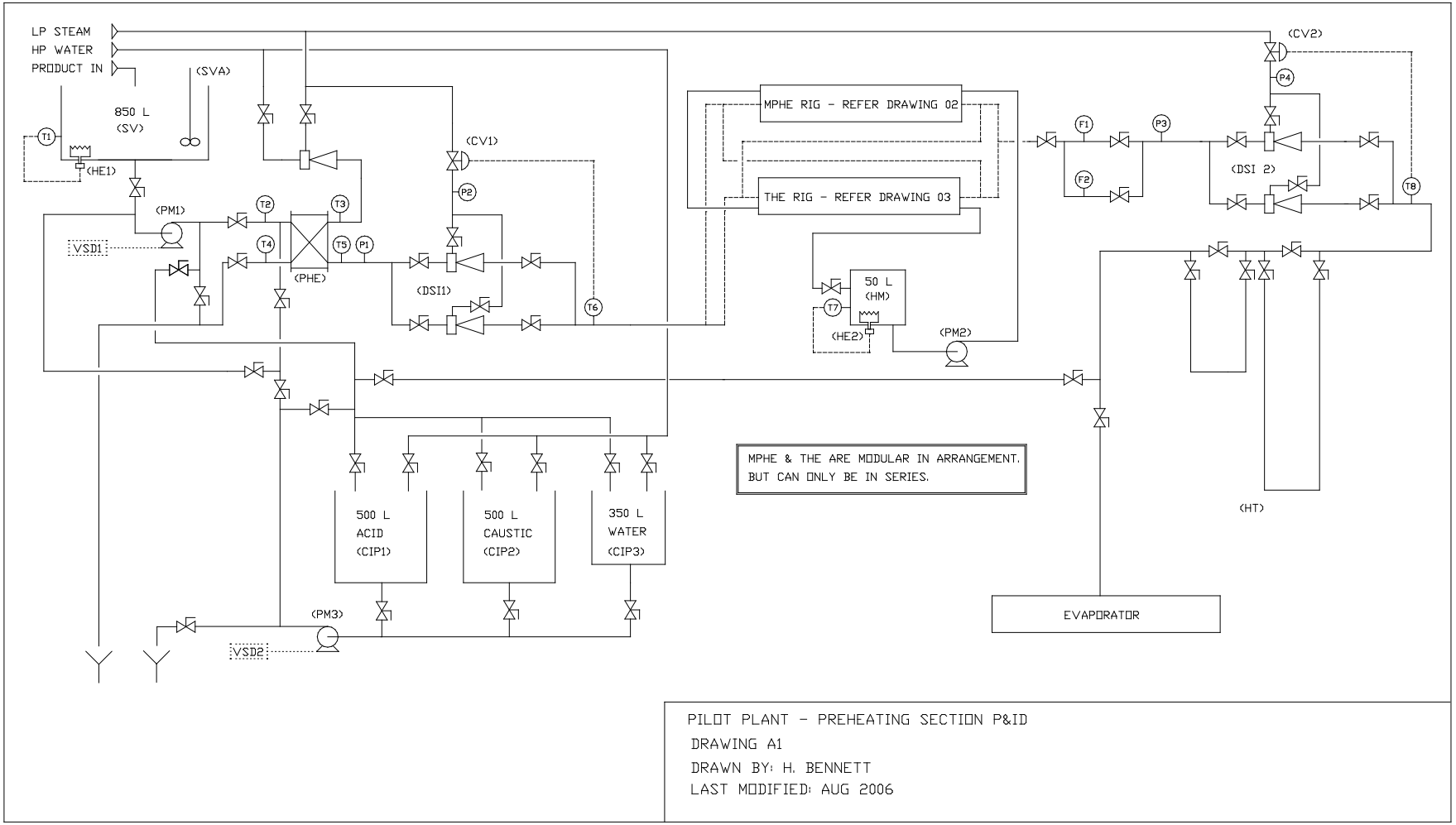

Figure A.1 Drawing A1 Preheating section P&ID

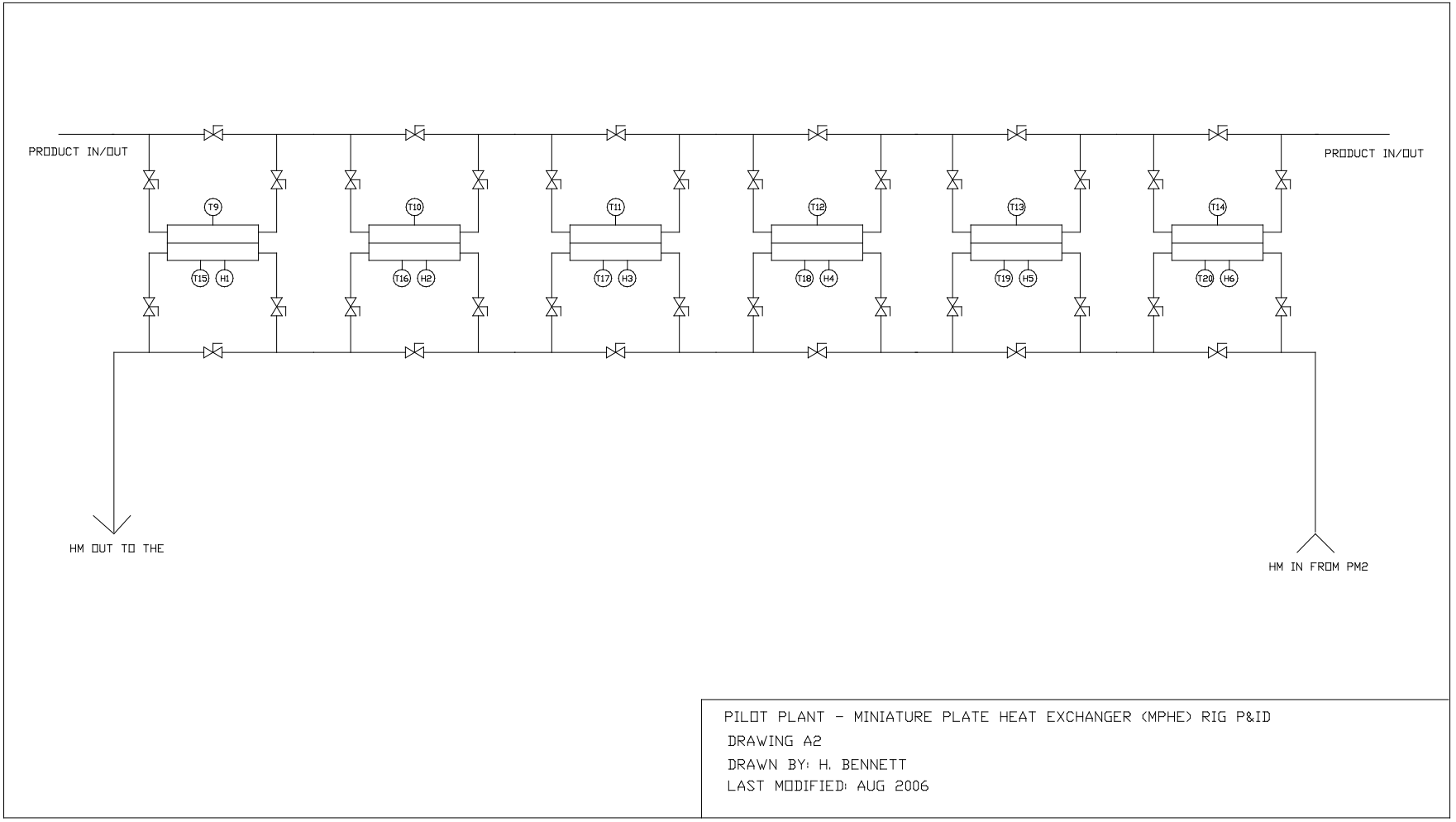

Figure A.2 Drawing A2 Miniature plate heat exchanger rig P&ID

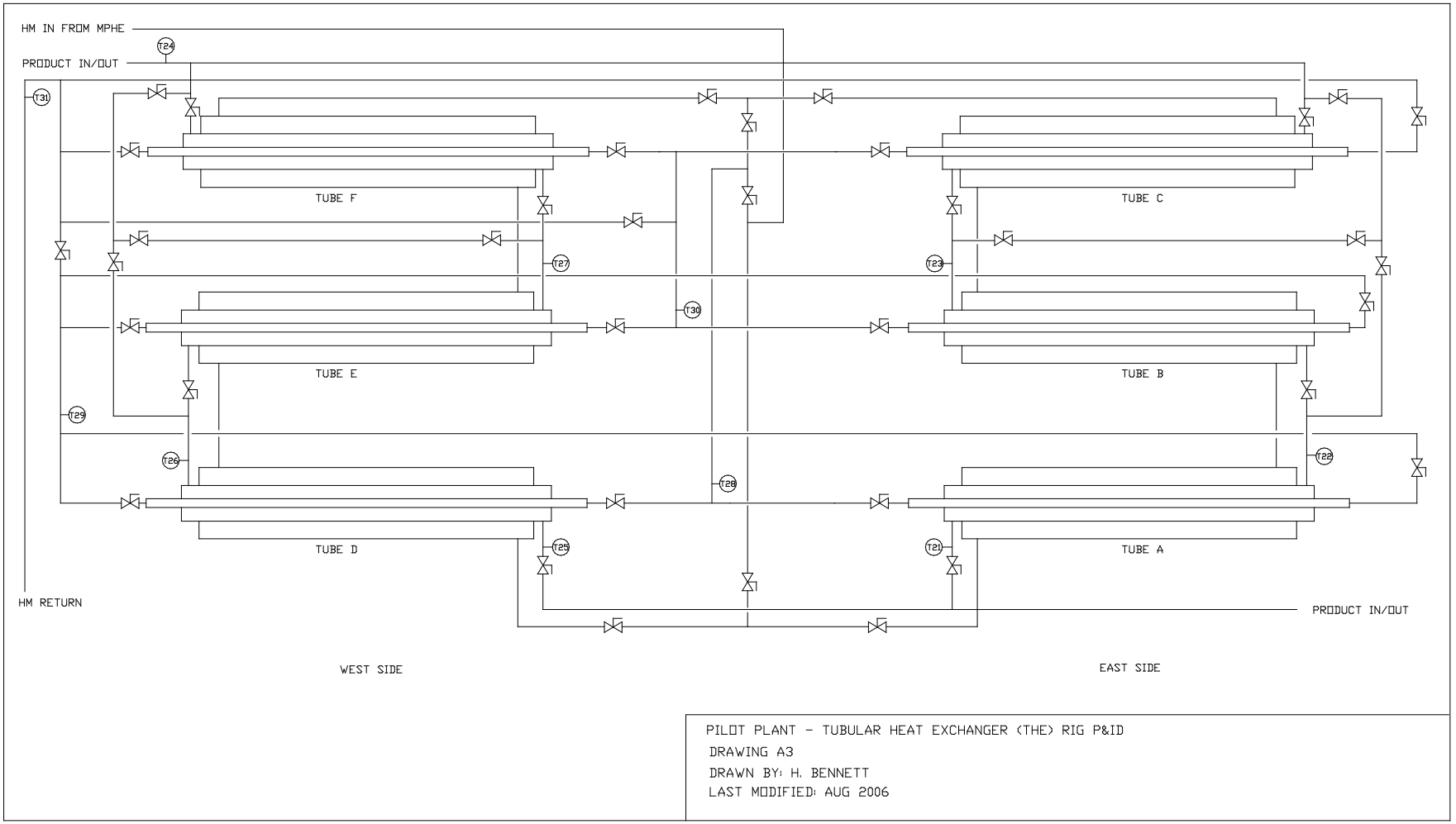

Figure A.3 Drawing A3 Tubular heat exchanger rig P&ID

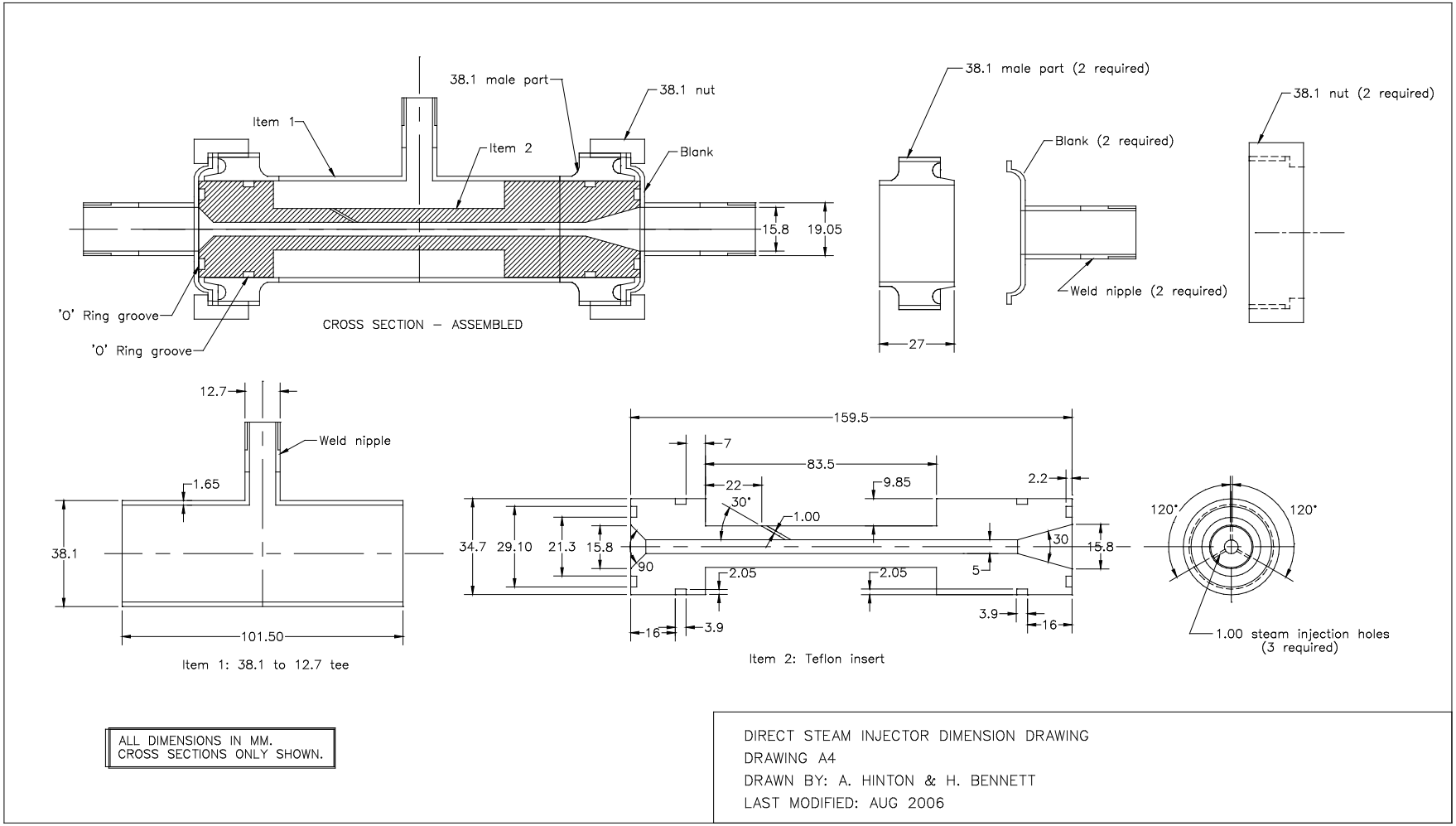

Figure A.4 Drawing A4 Direct steam injector dimension drawing

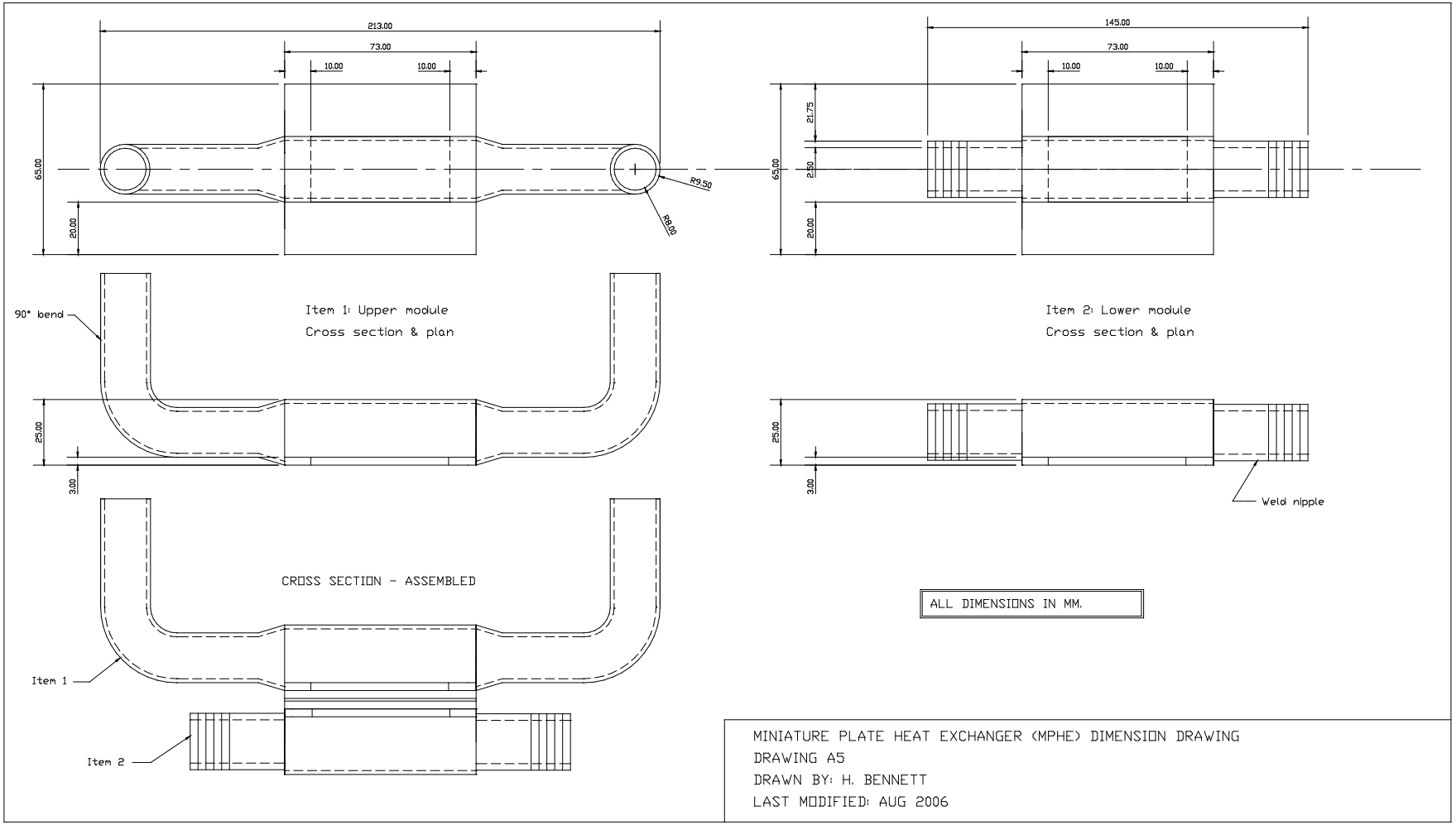

Figure A.5 Drawing A5 Miniature plate heat exchanger dimension drawing

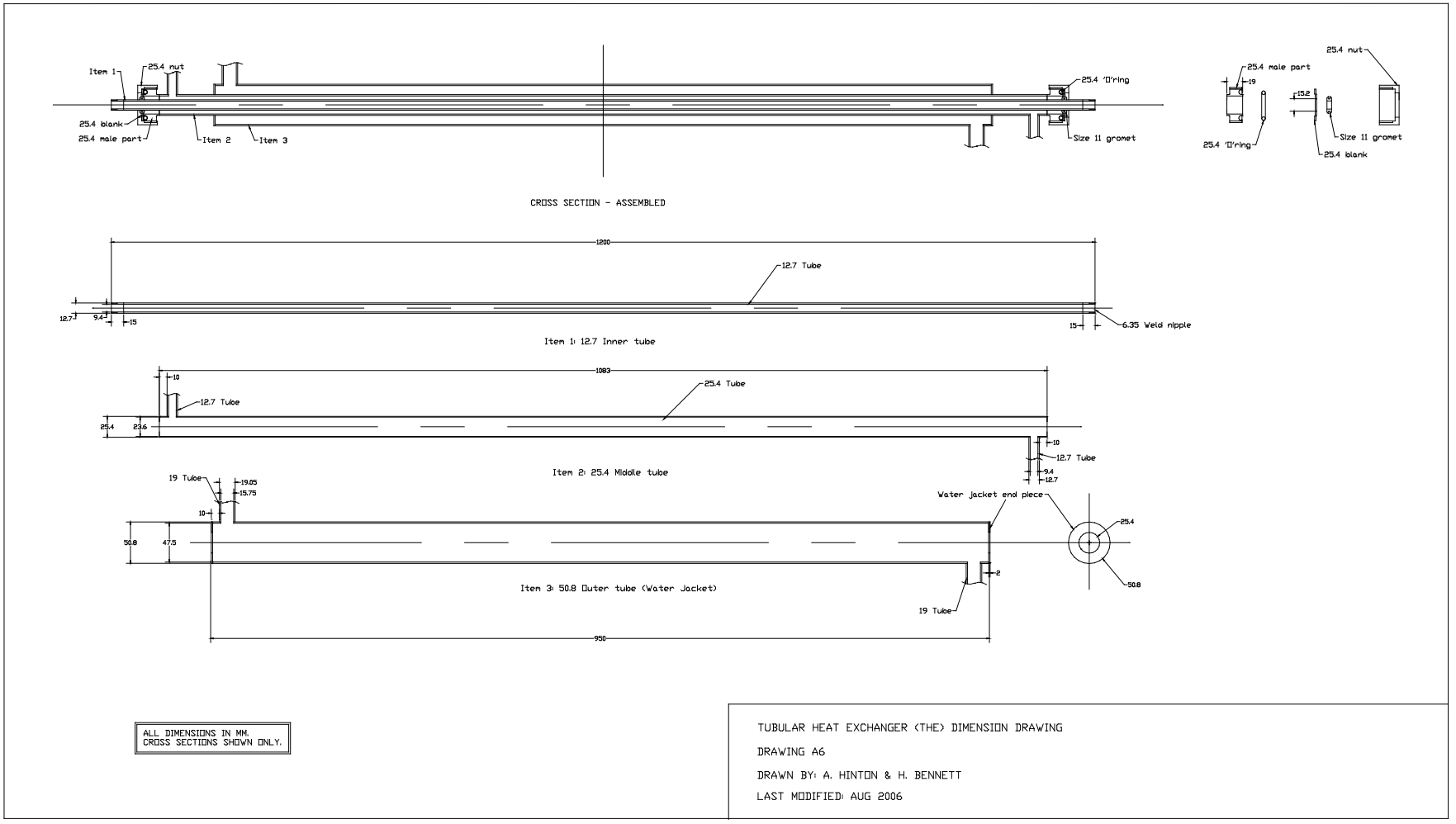

Figure A.6 Drawing A6 Tubular heat exchanger dimension drawing

APPENDIX A.1 Detailed information on selected equipment

Description of direct steam injection units

Figure A.7 shows a schematic diagram of a DSI unit. Each unit consists of a Teflon insert surrounded by a stainless steel outer tube. The shape of the insert allows steam to accumulate in an outer chamber while the product passes through a centre venturi. Steam passes through to the product stream via 1 mm holes drilled in the Teflon. The size and number of holes were calculated based on product flow rates and likely maximum temperature increases required as detailed by Hinton (2003). The DSI units were designed so that only one was required to heat the product stream, however two DSI units were installed in parallel to allow continuous running in the case one failed from fouling build up mid-run. In practice, each unit lasted for approximately 10 hours before fouling build up prevented the unit from heating the process fluid effectively.

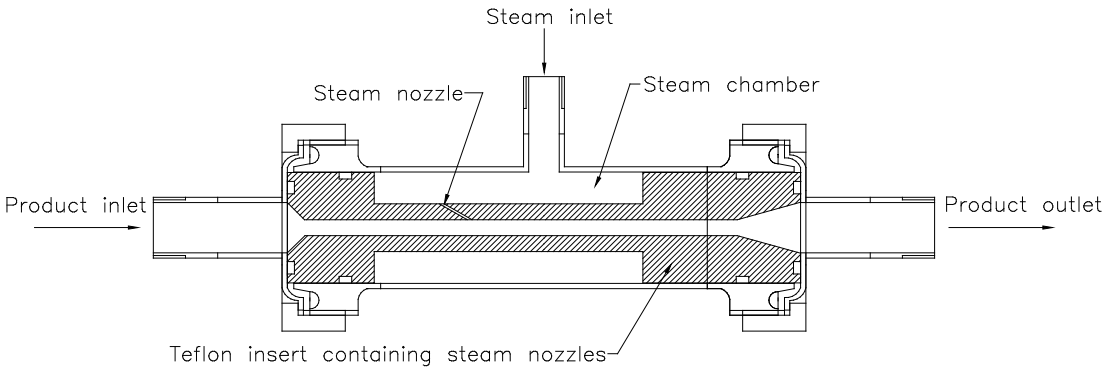

Figure A.7 Schematic diagram of a direct steam injection (DSI) unit.

Saturated steam (215 kPa.g) mixed with the process fluid in the throat of the venturi and immediately condensed in the downstream diverging outlet, giving up its latent heat of vaporisation thus heating the process fluid almost instantaneously. During runs investigating thermophile contamination of the bulk product stream the DSI units provided little opportunity for contamination due to the relatively small surface area available for colonisation (compared with the large surface area of the heat exchangers). This meant growth of thermophiles were targeted downstream of the DSI units.

Heat flux sensor technical properties

Selected information taken from product specifications sheet provided by RdF Corporation.

Configuration	6 x 18 mm with TC 4 x 2 mm HF sensor
Part number	27036-3
Nominal sensitivity	0.317 $\mu V/W.m^{-2}$
Maximum flux @ < 38°C	114 kW/m^2
Time constant including bond	0.40 s
Sensor resistance	10 Ω (max)
Max operating temperature	260°C
Nominal thickness	0.3 mm
Heat capacity	0.088 $W/K.m^{-2}$
Thermal resistance	0.002 $K/W.m^{-2}$

APPENDIX B OPERATING PROTOCOL

The following worksheet was filled out for a standard fouling run of the pilot plant used in the current research by inserting appropriate information in the boxes provided. Example data have been inserted in red for fictional runs.

Date: 21-02-2005
Expt: 30 (am) & 40 (pm) kPa pressure runs
Aim: Obtain the fouling rate of whole milk processed at 30 & 40 kPa.g pressures

Experiment preparation.	
Order milk at least two days before the required delivery date.	✓
Order the milk transporting truck from works and services.	✓
Order the steam to be turned off late the night of the run (~10:00pm).	✓

Milk handling and storage.	
Milk can be transported either by pallecon (P) or plastic bladders (B).	P
Prepare appropriate equipment depending on the mode of milk transport.	✓
To avoid differences in storage it is recommended that all the milk be placed in the refrigerated SV tank.	✓
When the milk is first transferred to the SV tank turn off the HE1 element when the milk temperature reaches 4°C.	✓

Plant configuration.	
Ensure all the sensors are operating correctly especially the temperature sensors on the THE rig.	✓
It is recommended that the THE & MPHE sensors be recalibrated before each run.	✓
Configure the plant so that the product flows through the MPHE rig and then the THE rig.	✓
The product should travel through one DSI only.	✓
Let the product go to drain immediately after the THE i.e. do not send to holding tubes.	✓
Ensure the plant is completely drained.	✓

Test surface preparation.		
Prepare gaskets, fittings etc. for the test surfaces.		✓
Clean all the test surfaces in following manner:	Tube	Plate
• 1% w/w caustic solution soak (1 hour). Start Time: 13:00	✓	✓
• Water rinse.	✓	✓
• Scrub with cloth.	✓	✓
• Water rinse.	✓	✓
• 1% w/w acid solution soak (1 hour). Start Time: 15:00	✓	✓
• Water rinse.	✓	✓
• Scrub with cloth.	✓	✓
• Water rinse.	✓	✓
• Allow to air dry.	✓	✓
Weigh the test plates and tubes.		✓
Install all the test surfaces in the appropriate fouling rigs.		✓

Layout of the fouling rigs:

MPHE rig

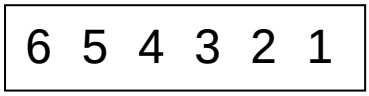

THE rig

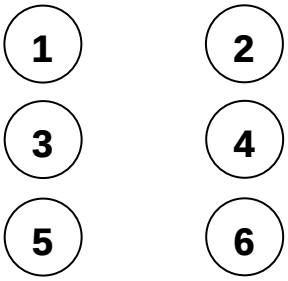

Test surface information.			Weight (g)	
Test surface	**Code**	**Description**	**Before**	**After**
Plate 1 am				
Plate 2 am				
Plate 3 am				
Plate 4 am	S	SCOP start 30 kPa.g	15.501	15.751
Plate 5 am	T	Dry start 30 kPa.g	16.039	16.689
Plate 6 am	U	Wet start 30 kPa.g	16.021	16.621
Tube 1 am				
Tube 2 am				
Tube 3 am				
Tube 4 am				
Tube 5 am				
Tube 6 am	D	Wet start 30 kPa.g	552.55	563.70
Plate 1 pm				
Plate 2 pm				
Plate 3 pm				
Plate 4 pm	V	SCOP start 40 kPa.g	16.012	16.232
Plate 5 pm	W	Dry start 40 kPa.g	15.848	16.398
Plate 6 pm	X	Wet start 40 kPa.g	15.538	16.038
Tube 1 pm				
Tube 2 pm				
Tube 3 pm				
Tube 4 pm				
Tube 5 pm				
Tube 6 pm	E	Wet start 40 kPa.g	535.83	544.24

Notes on the experimental protocol:
Experiment am: The SCOP start plate (4) will have a 5 minute delay on the heating side i.e. the valves on the hot side will be turned on 5 minutes after the milk enters the module. The product valves of the dry start plate (5) will be opened after the product stream has been switched to milk and the flow has stabilised. The valves of the wet start plate (6) will be opened before the start up procedure.
Experiment pm: The SCOP start plate (4) will have a 5 minute delay on the heating side i.e. the valves on the hot side will be turned on 5 minutes after the milk enters the module. The product valves of the dry start plate (5) will be opened after the product stream has been switched to milk and the flow has stabilised. The valves of the wet start plate (6) will be opened before the start up procedure.

Plant start-up.		
	Check the data logger is on.	✓
	Fill the HM tank with water and set the HE2 controller to the desired temperature.	✓
	Set the PHE DSI to the desired temperature.	✓
	Fill the CIP3 tank with cold water.	✓
	Ensure all valves on the MPHE plate 6 are open.	✓
	Once the heating medium has reached the required constant temperature start the PM2 pump and allow the temperature to stabilise.	✓
	Manipulate the plant valves so the water flows from the CIP3 tank through to the PM1 pump.	✓

Parameters	PHE DSI water		PHE DSI	MPHE	THE milk		Pressure	
	in	out	milk out	milk in	in	out	before	after
Initial value	71.3	68.7	72.2	66.6	65.5	76.1	77.4	30.0
Final value	71.8	69.5	72.7	66.0	65.0	75.4	78.5	30.4

Experiment (am)		**Start Time:** 09:17
00:00:00	Start the PM3 pump at 20 Hz. Increase VSD2 speed to 30Hz after the flow rate stabilises.	✓
00:02:00	Remove air through the ports before and after the PHE.	✓
00:06:00	Throttle the valve located at DSI1 until the desired flow rate is reached.	✓
	Allow the temperatures to stabilise.	✓
	Monitor the pressures before and after the throttling valve. VSD2 may need increasing during this period.	✓
00:26:00	Stop the PM3 pump.	✓
	Close the CIP line valve.	✓
00:28:00	Open the valve under the SV tank.	✓
Start	Start the PM1 pump at a speed of 20 Hz.	✓
Time:	Increase the VSD1 speed until the desired flow rate is reached.	✓
_09:45__	Note the time the PM1 pump was started.	✓
	Increase the VSD1 speed as required.	✓
00:30:00	Remove air through the ports.	✓
01:00:00	Remove air through the ports.	✓
01:30:00	Remove air through the ports.	✓
02:00:00	Remove air through the ports.	✓
02:30:00	Remove air through the ports.	✓
03:00:00	Remove air through the ports.	✓
	Start filling the CIP1 tank with water from the PHE DSI.	✓
03:30:00	Remove air through the ports.	✓
04:00:00	Remove air through the ports.	✓
	Start filling the CIP2 tank with water from the PHE DSI.	✓
04:30:00	Stop the PM1 and PM2 pumps.	✓
	Close the valve under the SV tank.	✓
	Close any opened valves on the MPHE rig.	✓
	Close the heating medium valves on the THE rig.	✓
	Remove any test surfaces used.	✓
	Take milk sample if required.	✓

Experiment notes (am):
The flow rate was stable throughout the run. No instabilities to report.

Cleaning.		
04:45:00	Install blanks where the test surfaces were removed.	✓
04:50:00	Open the CIP line valve.	✓
	Open the DSI1 throttling valve.	✓
	Open the MPHE rig valves.	✓
	Start the PM3 pump at 50 Hz.	✓
05:00:00	Stop the PM3 pump.	✓
	Add the required amount of caustic to the water in the CIP2 tank to make a 1% w/w solution.	✓
	Disconnect the pipe after the PHE.	✓
	Start the PM3 pump at 20 Hz.	✓
	Undo the bottom sample port at the inlet of the tubular heat exchanger used in experiment am.	✓
	Open all the MPHE rig valves on the product side.	✓
	Remove and drain the section of pipe between DSI1 and the MPHE rig.	✓
	Undo the two dairy unions on the tubular heat exchanger used in experiment am.	✓
	Unpack any MPHE modules used in experiment am and drain.	✓
05:15:00	Stop the PM3 pump.	✓
	Redirect the flow from the CIP2 tank to the CIP1 tank.	✓
	Start the PM3 pump at 20 Hz.	✓
	Repack any MPHE modules needed for experiment pm.	✓
	Stop the PM3 pump.	✓
05:25:00	Disconnect the union under the SV tank.	✓
	Turn off the DSI to the PHE.	✓
	Reinstall the PHE pipe.	✓
	Reinstall the pipe between DSI1 and the MPHE rig.	✓
	Reinstall the bottom sample port at inlet of the tubular heat exchanger used in experiment am.	✓
	Install any THE test tubes needed for experiment pm.	✓
	Check the water level of the HM tank. Refill if necessary.	✓
	Check all the pipes are connected and the valves are in the correct position for the start up of experiment pm.	✓
	Set the PHE DSI to the desired temperature.	✓
05:40:00	Start the PM2 pump.	✓
	Connect the union under the SV tank.	✓
	Open the MPHE heating medium valves.	✓
	Check the water level of the CIP3 tank. Refill if necessary.	✓

Parameters	PHE DSI water in	PHE DSI water out	PHE DSI milk out	MPHE milk in	THE milk in	THE milk out	Pressure before	Pressure after
Initial value	70.2	67.4	71.4	66.8	65.8	74.7	85.5	40.0
Final value	69.8	67.1	70.9	66.2	65.2	74.2	84.9	39.8

Experiment (pm)		**Start Time:** 14:55
06:00:00	Start the PM3 pump at 20 Hz. Increase VSD2 speed to 30Hz after the flow rate stabilises.	✓
06:02:00	Remove air through the ports before and after the PHE.	✓
06:06:00	Throttle the valve located at DSI1 until the desired flow rate is reached.	✓
	Allow the temperatures to stabilise.	✓
	Monitor the pressures before and after the throttling valve. VSD2 may need increasing during this period.	✓
06:26:00	Stop the PM3 pump.	✓
	Close the CIP line valve.	✓
06:28:00 **Start Time:** 15:23	Open the valve under the SV tank.	✓
	Start the PM1 pump at a speed of 20 Hz.	✓
	Increase the VSD1 speed until the desired flow rate is reached.	✓
	Note the time the PM1 pump was started.	✓
	Increase the VSD1 speed as required.	✓
	Take milk sample if required.	✓
06:30:00	Remove air through the ports.	✓
07:00:00	Remove air through the ports.	✓
07:30:00	Remove air through the ports.	✓
08:00:00	Remove air through the ports.	✓
08:30:00	Remove air through the ports.	✓
	Take milk sample if required.	✓
09:00:00	Remove air through the ports.	✓
	Start filling the CIP1 tank with water from the PHE DSI.	✓
09:30:00	Remove air through the ports.	✓
10:00:00	Remove air through the ports.	✓
	Start filling the CIP2 tank with water from the PHE DSI.	✓
10:30:00	Stop the PM1 and PM2 pumps.	✓
	Close the valve under the SV tank.	✓
	Close any opened valves on the MPHE rig.	✓
	Close the heating medium valves on the THE rig.	✓
	Remove any test surfaces used.	✓
	Take milk sample if required.	✓

Experiment notes (am):

The flow rate was stable throughout the run. No instabilities to report.

APPENDIX C SUMMARY OF EXPERIMENTAL RUNS

Table C.1 Conditions of formal runs conducted with the THE rig.

Section	Experiment nomenclature	Experiment title	Product	Flow rate (l/h)	Linear velocity (m/s)	Rig pressure (kPa.g)	Heating medium temperature (°C)	Product temperature (°C)	Run time (hh:mm)
THE	R1.1	Replicate (30kPa.g)/Pressure (30kPa.g)	Whole milk	45.21 (2.1)	0.047 (2.1)	30.08 (2.2)	83.89 (0.1)	64.65 (0.8)	04:00
THE	R1.2	Replicate (30kPa.g)	Whole milk	45.26 (2.3)	0.047 (2.3)	30.32 (1.2)	83.15 (0.3)	65.54 (0.7)	04:00
THE	R1.3	Replicate (30kPa.g)	Whole milk	45.19 (2.0)	0.047 (2.0)	29.88 (1.9)	82.53 (0.2)	65.41 (0.6)	04:00
THE	R1.4	Replicate (50kPa.g)	Whole milk	44.93 (1.9)	0.047 (1.9)	50.44 (1.0)	83.85 (0.1)	65.11 (0.5)	04:00
THE	R1.5	Replicate (50kPa.g)/R1.15 control (without Neutrase)	Whole milk	44.76 (1.9)	0.046 (1.9)	50.25 (0.9)	83.51 (0.1)	65.32 (0.6)	04:00
THE	R1.6	Pressure (40kPa.g)	Whole milk	45.31 (2.2)	0.047 (2.2)	40.27 (1.2)	83.85 (0.1)	64.78 (0.6)	04:00
THE	R1.7	Pressure (60kPa.g)	Whole milk	44.87 (2.2)	0.047 (2.2)	60.38 (1.0)	83.67 (0.1)	65.18 (0.7)	04:00
THE	R1.8	Pressure (70kPa.g)	Whole milk	45.51 (1.9)	0.047 (1.9)	70.27 (0.6)	83.91 (0.1)	65.77 (0.7)	04:00
THE	R1.9	Pressure (80kPa.g)	Whole milk	45.57 (2.0)	0.047 (2.0)	80.47 (0.5)	83.79 (0.1)	65.41 (0.6)	04:00
THE	R1.10	Thermophilic enzymes addition (88°C)	Whole milk	44.85 (1.8)	0.047 (1.8)	50.07 (1.1)	88.47 (0.1)	63.86 (0.5)	04:00
THE	R1.11	Neutrase addition (88°C)	Whole milk	44.64 (2.5)	0.046 (2.5)	50.25 (1.8)	88.30 (0.1)	63.57 (1.4)	04:00
THE	R1.12	Neutrase addition (68°C)	Whole milk	44.81 (2.0)	0.047 (2.0)	52.11 (1.5)	68.52 (0.3)	65.88 (2.0)	04:00
THE	R1.13	Neutrase addition (73°C)	Whole milk	44.79 (1.7)	0.047 (1.7)	50.26 (1.1)	73.61 (0.2)	64.73 (0.6)	04:00
THE	R1.14	Neutrase addition (78°C)	Whole milk	44.69 (1.6)	0.046 (1.6)	50.18 (0.7)	78.48 (0.1)	64.21 (1.0)	04:00
THE	R1.15	Neutrase addition (83°C)	Whole milk	44.75 (2.1)	0.047 (2.1)	50.30 (1.4)	83.68 (0.3)	65.44 (0.9)	04:00
THE	R1.16	Neutrase addition (93°C)	Whole milk	44.79 (2.8)	0.047 (2.8)	52.06 (2.5)	93.69 (0.2)	64.50 (0.5)	04:00
THE	R1.17	R1.10 control (without thermophilic enzymes)	Whole milk	44.75 (2.0)	0.046 (2.0)	50.00 (1.2)	88.44 (0.1)	63.50 (0.7)	04:00
THE	R1.18	R1.11 control (without Neutrase)	Whole milk	44.88 (3.0)	0.047 (3.0)	50.23 (1.7)	88.43 (0.1)	63.60 (1.2)	04:00
THE	R1.19	R1.12 control (without Neutrase)	Whole milk	44.89 (2.4)	0.047 (2.4)	51.96 (1.7)	68.71 (0.4)	65.99 (0.8)	04:00
THE	R1.20	R1.13 control (without Neutrase)	Whole milk	44.65 (1.5)	0.046 (1.5)	50.07 (0.9)	73.76 (0.3)	64.82 (0.7)	04:00

Table C.1 (continued)

Section	Experiment nomenclature	Experiment title	Product	Flow rate (l/h)	Linear velocity (m/s)	Rig pressure (kPa.g)	Heating medium temperature (°C)	Product temperature (°C)	Run time (hh:mm)
THE	R1.21	R1.14 control (without Neutrase)	Whole milk	44.65 (2.1)	0.046 (2.1)	49.98 (1.2)	78.40 (0.1)	63.98 (1.0)	04:00
THE	R1.22	R1.16 control (without Neutrase)	Whole milk	44.92 (2.2)	0.047 (2.2)	52.10 (1.3)	94.05 (0.2)	64.29 (1.0)	04:00
THE	R1.23	Skim milk (83°C)	Skim milk	44.90 (4.6)	0.047 (4.6)	29.98 (2.7)	83.41 (0.1)	63.00 (2.7)	04:00

Table C.2 Conditions of formal runs conducted with the MPHE rig.

Section	Experiment nomenclature	Experiment title	Product	Flow rate (l/h)	Linear velocity (m/s)	Rig pressure (kPa.g)	Heating medium temperature (°C)	Product temperature (°C)	Run time (hh:mm)
MPHE	R2.1	Example run (N_f calculation)	Whole milk	44.95 (2.7)	0.024 (2.7)	NM	86.42 (0.8)	63.72 (1.0)	03:11
MPHE	R2.2	Example run (induction period)	Whole milk	46.80 (2.3)	0.025 (2.3)	NM	87.17 (0.2)	66.68 (0.8)	04:00
MPHE	R2.3	Comparison of direct and indirect measurements of fouling	Whole milk	44.45 (2.3)	0.024 (2.3)	NM	88.58 (1.0)	65.76 (1.8)	Varied
MPHE	R2.4	Whey visualisation (standard run)	Whey (0.1%)	45.12 (2.1)	0.024 (2.1)	30.31 (0.6)	90.04 (0.3)	66.30 (0.4)	00:50
MPHE	R2.5	Whey visualisation (130 kPa.g)	Whey (0.1%)	44.86 (2.9)	0.024 (2.9)	130.02 (1.2)	90.06 (0.3)	67.25 (0.5)	00:50
MPHE	R2.6	Whey visualisation (500 l/h)	Whey (0.1%)	502.24 (1.0)	0.270 (1.0)	29.51 (0.6)	90.06 (0.3)	65.77 (0.4)	00:50
MPHE	R2.7	Whey visualisation (80 kPa.g)	Whey (0.1%)	45.27 (2.7)	0.024 (2.7)	80.76 (1.0)	90.04 (0.3)	68.11 (0.5)	00:50
MPHE	R2.8	Whey visualisation (2 000 l/h)	Whey (0.1%)	1940.46 (0.5)	1.043 (0.5)	59.12 (0.7)	90.86 (0.2)	68.89 (0.4)	00:50
MPHE	R2.9	Whey visualisation (standard run)	Whey (0.1%)	45.31 (2.0)	0.024 (2.0)	30.18 (0.9)	90.04 (0.3)	66.60 (1.6)	00:50
MPHE	R2.10	Water visualisation (standard run)	Water	44.45 (1.9)	0.024 (1.9)	29.89 (2.1)	90.60 (0.3)	64.90 (0.5)	00:50
MPHE	R2.11	Water visualisation (80 kPa.g)	Water	44.60 (1.5)	0.024 (1.5)	79.97 (0.7)	90.66 (0.2)	65.09 (1.2)	00:50
MPHE	R2.12	Water visualisation (130 kPa.g)	Water	44.65 (1.7)	0.024 (1.7)	129.82 (1.3)	90.06 (0.3)	66.58 (0.6)	00:50
MPHE	R2.13	Water visualisation (250 l/h)	Water	251.44 (1.3)	0.135 (1.3)	30.16 (1.9)	90.04 (0.2)	67.04 (0.9)	00:50
MPHE	R2.14	Water visualisation (2 000 l/h)	Water	1939.58 (0.5)	1.042 (0.5)	58.94 (0.8)	90.75 (0.2)	69.05 (0.3)	00:50
MPHE	R2.15	Water visualisation (obstruction control 1 000 l/h)	Water	998.53 (0.2)	0.536 (0.2)	35.11 (0.6)	90.78 (0.3)	66.26 (0.6)	00:10
MPHE	R2.16	Water visualisation (obstruction 1 000 l/h)	Water	1002.42 (0.3)	0.539 (0.3)	35.25 (0.7)	90.06 (0.2)	64.90 (0.9)	00:10

Table C.2 (continued)

Section	Experiment nomenclature	Experiment title	Product	Flow rate (l/h)	Linear velocity (m/s)	Rig pressure (kPa.g)	Heating medium temperature (°C)	Product temperature (°C)	Run time (hh:mm)
MPHE	R2.17	Whey visualisation (hydrodynamic - glue drops)	Whey (0.1%)	45.91 (3.0)	0.025 (3.0)	130.57 (0.8)	90.03 (0.3)	64.92 (0.5)	00:50
MPHE	R2.18	Water visualisation (wet start)	Water	44.71 (1.7)	0.024 (1.7)	79.99 (0.6)	90.60 (0.2)	64.97 (0.9)	00:50
MPHE	R2.19	Water visualisation (SCOP)	Water	44.37 (3.1)	0.024 (3.1)	29.64 (1.9)	90.05 (0.2)	66.27 (0.5)	00:50
MPHE	R2.20	Whey visualisation (SCOP)	Whey (0.1%)	44.56 (2.9)	0.024 (2.9)	29.64 (2.1)	90.06 (0.3)	66.79 (0.5)	00:50
MPHE	R2.21	SCOP	Whole milk	44.96 (3.5)	0.024 (3.5)	NM	89.46 (0.4)	67.80 (1.0)	Varied
MPHE	R2.22	SCOP (delay time)	Whole milk	43.59 (5.3)	0.023 (5.3)	NM	92.77 (0.5)	73.49 (0.5)	03:50
MPHE	R2.23	SCOP (Neutrase)	Whole milk	44.08 (1.7)	0.024 (1.7)	NM	87.90 (0.2)	70.19 (0.4)	04:00
MPHE	R2.24	SCOP (surface coatings)	Whey (0.1%)	45.22 (2.3)	0.024 (2.3)	30.30 (1.7)	90.02 (0.3)	64.32 (0.5)	00:50

Table C.3 Summary of commissioning and prerun trials conducted with the THE rig.

Section	Experiment nomenclature	Product	Experiment description and solutions to problems identified
THE	C1.1	Whole milk	Testing of different procedures to prepare heat exchange surfaces. Testing the effect of nitric and acid solutions on fouling deposits.
THE	C1.2	Whole milk	
THE	C1.3	Whole milk	
THE	C1.4	Whole milk	Developing the operating protocol used for fouling runs.
THE	C1.5	Whole milk	
THE	C1.6	Whole milk	
THE	C1.7	Whole milk	
THE	C1.8	Whole milk	
THE	C1.9	Whole milk	Testing the operating protocol used for fouling runs.
THE	C1.10	Whole milk	
THE	C1.11	Whole milk	
THE	C1.12	Whole milk	
THE	C1.13	Whole milk	
THE	C1.14	Whole milk	
THE	C1.15	Whole milk	Pressure prerun trials.
THE	C1.16	Whole milk	
THE	C1.17	Whole milk	
THE	C1.18	Whole milk	
THE	C1.19	Whole milk	
THE	C1.20	Whole milk	
THE	C1.21	Whole milk	Enzyme addition prerun trials.
THE	C1.22	Whole milk	
THE	C1.23	Whole milk	
THE	C1.24	Whole milk	
THE	C1.25	Whole milk	
THE	C1.26	Whole milk	

Table C.4 Summary of commissioning and prerun trials conducted with the MPHE rig.

Section	Experiment nomenclature	Product	Experiment description and solutions to problems identified
MPHE	C2.1	Whole milk	SCOP prerun trials.
MPHE	C2.2	Whole milk	
MPHE	C2.3	Whole milk	
MPHE	C2.4	Whole milk	
MPHE	C2.5	Whole milk	Developing of operating protocol for visualisation runs.
MPHE	C2.6	Whole milk	
MPHE	C2.7	Whole milk	
MPHE	C2.8	Whole milk	Whey visualisation prerun trials.
MPHE	C2.9	Whole milk	
MPHE	C2.10	Whole milk	
MPHE	C2.11	Whole milk	
MPHE	C2.12	Whole milk	Water visualisation prerun trials.
MPHE	C2.13	Whole milk	
MPHE	C2.14	Whole milk	
MPHE	C2.15	Whole milk	
MPHE	C2.16	Whole milk	
MPHE	C2.17	Whole milk	

APPENDIX D SAMPLE CALCULATIONS

APPENDIX D.1 Calibration constants for temperature sensors

Table D.1 Recorded calibration temperatures and calculated regression coefficients for selected temperature sensors installed in the pilot plant.

Sensor abbrev.	Recorded temperature for ice/water slurry, θ_0 (°C)	Recorded temperature for boiling water, θ_{100} (°C)*	Regression coefficients	
			a	b
T1	-0.04	99.8	1.002	0.0432
T2	0.2	100.3	1.000	-0.2323
T3	1.1	100.7	1.004	-1.133
T4	0.06	99.8	1.002	-0.06
T5	0.1	100.4	0.997	-0.1333
T6	1.4	100.7	1.006	-1.362
T7	-0.111	99.6	1.002	0.112
T8	-0.3	99.9	0.997	0.3275
T9	1.1	100.8	1.004	-1.139
T10	0.02	99.9	1.001	-0.024
T11	-0.3	99.9	0.998	0.3004
T12	1.0	100.6	1.003	-0.963
T13	-0.09	99.8	1.002	0.091
T14	-0.1	99.7	1.001	0.145

*Errors associated with the apparent boiling point of the barometric pressure or superheating were insignificant in comparison with other experimental errors.

Sample calculations:

For sensor T1 the regression coefficients are:

$$a = \frac{100}{\theta_{100} - \theta_0} = \frac{100}{99.8 - (-0.04)} = 1.002$$

$$b = -a\,\theta_0 = -1.002\left(-0.04\right) = 0.0432$$

If a read temperature from sensor T1 was 75°C then the calibrated value would be:

$$\theta_c = a\ \theta_r + b = 1.002\,(75) + 0.0432 = 75.2°C$$

APPENDIX D.2 Calibration of heat flux sensors

The heat flux sensors were connected to Allen Bradley "thermocouple/mV" modules which are 16 bit analog to digital convertors that transform a maximum ± 50mV signal to a binary number in the range ± 32 767 (2^{16}). These binary outputs were converted to heat flux values in SI units using FIX DMACS software installed on the pilot plant's control computer.

Table D.2 Manufacturer's calibrated outputs for a selection of heat flux sensors installed in the pilot plant

Heat flux sensor label	H1	H2	H3	H4	H5	H6
Output at 21°C ($\mu VW/m^2$)	4.1641	4.0694	4.1325	4.0694	4.1325	4.0694

Using the calibrated output supplied by the manufacturer the heat flux corresponding to the maximum voltage of 50mV was calculated for each sensor. For sensor H1:

$$q_{50mV} = 50000 \text{ x output } (\mu VW / m^2) = 50000 \text{ x } 4.1641 = 208203 \text{ W} / m^2$$

A factor (F) was calculated to convert a binary unit to heat flux in SI units. For sensor H1:

$$F = \frac{q_{50mV}}{32767} = \frac{208203}{32767} = 6.354 \text{ W.m}^{-2} / \text{binary unit}$$

Table D.3 lists the q_{50mV} and F values for a selection of heat flux sensors.

Table D.3 Heat flux corresponding to the maximum voltage of 50mV and the factors used to convert the heat fluxes to SI units for a selection of heat flux sensors installed in the pilot plant

Heat flux sensor label	H1	H2	H3	H4	H5	H6
q_{50mV} (W/m^2)	208203	203471	206626	203471	206626	203471
F ($W.m^{-2}$/binary unit)	6.354	6.2096	6.3059	6.2096	6.3059	6.2096

The calculated F values were inputted into the FIX DMACS software to display and record heat fluxes in real-time rather than the binary numbers logged by the "thermocouple/mV" modules.

APPENDIX D.3 Fouling monitoring systems

Sample calculations for the system monitoring fouling locally (using a heat flux sensor)

Variables relating to the MSExcel spreadsheet listed in Table D.4 for R2.1:

Measured variables (logged by control computer during a run):

Q	flow rate of process fluid (l/h)	= Column H
q	heat transfer flux (W/m^2)	= Column I, J, K
θ_p	temperature of process fluid (°C)	= Column L, M, N
θ_{hf}	outer temperature of heat flux sensor (°C)	= Column O, P, Q

Calculated variables (calculated in real time during a run via FIX DMACS software):

U_i	internal heat transfer coefficient (equation (3.4)) ($W/m^2.K$)	= Column R, S, T

Estimated constants (estimated after a run and inputted into an MSExcel spreadsheet):

U_{i0}	initial heat transfer coefficient* ($W/m^2.K$)	= B2, B3, B4

*Methodology outlined in sections 3.3.2.1 & 4.2.1

Calculated variables (calculated after a run via MSExcel software):

N_f	normalised heat transfer coefficient (equation (3.7)) (no units)	= Column U, V, W

Table D.4 Sample of the MSExcel spreadsheet listing measured, estimated and calculated variables for R2.1

	A	B	C	D	E	F	G	H	I	J	K
1	Constants:				Time	Time (s)	Time (h)	Q	q_1	q_2	q_3
2	U_{i01}	344			13:30:20	0	0	45.6	4635.4	5806.65	5063.15
3	U_{i02}	285			13:30:24	4	0.001111	45	4872.46	5601.4	5823.72
4	U_{i03}	322			13:30:28	8	0.002222	45.6	5488.81	5974.58	5919.25
5					13:30:32	12	0.003333	45	4941.75	5698.43	5191.75
6					13:30:36	16	0.004444	44.4	5018.34	5411.08	4956.59
7					13:30:40	20	0.005556	45.6	5175.16	5926.07	5441.6
8					13:30:44	24	0.006667	45.6	5594.57	5403.62	5915.58
9					13:30:48	28	0.007778	45.6	5244.46	5620.06	5125.61
10					13:30:52	32	0.008889	45	4675.52	6090.27	4974.97
11					13:30:56	36	0.01	45	4927.16	5780.53	4978.64
12					13:31:00	40	0.011111	45	4949.05	5500.65	5037.43
13					13:31:04	44	0.012222	45.6	5244.46	5213.3	4956.59

Table D.4 (continued)

	L	M	N	O	P	Q	R	S	T	U	V	W
1	θ_{p1}	θ_{p2}	θ_{p3}	θ_{hf1}	θ_{hf2}	θ_{hf3}	U_{i1}	U_{i2}	U_{i3}	N_{f1}	N_{f2}	N_{f3}
2	66.07629	64.63231	66.5474	82.31	84.06	85.94	285.5416	298.8852	261.0867	0.831266	1.04872	0.810828
3	65.13656	64.52267	66.61731	81.91	84.26	85.84	290.4866	283.7973	302.9608	0.845661	0.99578	0.940872
4	64.88663	64.75191	66.43753	82.11	84.06	85.64	318.6838	309.434	308.2546	0.927749	1.085733	0.957312
5	64.85664	64.40307	66.02801	82.11	84.46	86.14	286.4224	284.1128	258.1421	0.83383	0.996887	0.801683
6	64.88663	64.45291	66.09793	82.21	84.26	86.24	289.6861	273.189	246.0814	0.843331	0.958558	0.764228
7	64.90662	64.54261	66.73717	82.11	84.36	85.84	300.8223	299.0338	284.8584	0.875751	1.049241	0.884653

Calculations for system 1 at time = 0 s (shaded cells):

Calculated variables (calculated in real time during a run via FIX DMACS software):

Internal heat transfer coefficient was calculated as:

$$U_{i1} = \frac{q_1}{\theta_{hf1} - \theta_{p1}} = \frac{I2}{L2 - O2} = \frac{4635.40}{66.08 - 82.31} = 285.54\,W/m^2.K = R2$$

Estimated constants (estimated after a run and inputted into an MSExcel spreadsheet):

In this example (R2.1) U_{i01} was estimated from the average of the first 315 readings:

$$U_{i01} = \frac{(U_1 + ... + U_{315})}{315} = \frac{(T2 + ... + T316)}{315} = \frac{(285.54 + ... + 308.24)}{315} = 344\,W/m^2.K = B2$$

Calculated variables (calculated after a run via MSExcel software):

Normalised heat transfer coefficient was calculated as:

$$N_{f1} = \frac{U_{i1}}{U_{i01}} = \frac{R2}{B2} = \frac{285.54}{344} = 0.831 = U2$$

Sample calculations for the system monitoring fouling globally (using temperature and flow sensors)

Variables relating to the MSExcel spreadsheet listed in Table D.5 for R1.18:

Process fluid constants (process fluid was milk in this example. Source: (Wood, 1996):

$c_{p,p}$	heat capacity of process fluid (kJ/kg.K)	3.852	= B2
μ_p	viscosity of process fluid (Pa.s)	1.60×10^{-3}	= B3
ρ_p	density of process fluid (kg/m^3)	1035	= B4

Dimensions of an individual THE tube stack:

D_i	inner diameter of outside tube (m)	0.0224	= B5
D_o	outer diameter of outside tube (m)	0.0254	= B6
d_i	inner diameter of inside tube (m)	0.0097	= B7
d_o	outer diameter of inside tube (m)	0.0127	= B8
L	length of inner tube fouling region (m)	1.15	= B9

Calculated dimensions of an individual tube stack:

A	heat exchange surface area (m^2)	0.0459	= B10
S	cross sectional area of process fluid (m^2)	2.67×10^{-4}	= B11
d_e	equal diameter of process fluid cross section (m)	9.7×10^{-3}	= B12

Measured variables (logged by control computer during a run):

Q	flow rate of process fluid (l/h)	= Column H
θ_p	inlet temperature of process fluid (°C)	= Column I
θ_{hm}	inlet temperature of heating medium (°C)	= Column J
Θ_p	outlet temperature of process fluid (°C)	= Column K
Θ_{hm}	outlet temperature of heating medium (°C)	= Column L

Calculated variables (calculated in real time during a run via FIX DMACS software):

V	milk velocity (m/s)	= Column M
Re	Reynolds number (no dimensions)	= Column N
$\Delta\theta_1$	temperature difference of side 1 (°C)	= Column O
$\Delta\theta_2$	temperature difference of side 2 (°C)	= Column P
$\Delta\theta_{LMTD}$	logarithmic temperature difference (equation (3.10)) (°C)	= Column Q
$\dot{m}$	mass flow rate of process fluid (kg/s)	= Column R
ϕ_p	rate of heat gained by process fluid (equation (3.11)) (W)	= Column S
U	overall heat transfer coefficient (equation (3.9)) ($W/m^2.K$)	= Column T

Estimated constants (estimated after a run and inputted into an MSExcel spreadsheet):

U_0	initial heat transfer coefficient* ($W/m^2.K$)	= B13

*Methodology outlined in sections 3.3.2.1 & 4.2.1

Calculated variables (calculated after a run via MSExcel software):

N_f normalised heat transfer coefficient (equation (3.7)) (no units) = Column U

Table D.5 Sample of the MSExcel spreadsheet listing process fluid constants and measured, estimated and calculated variables for R1.18

	A	B	C	D	E	F	G	H	I	J	K	L
1	Constants:				Time	Time (s)	Time (h)	Q	θ_p	θ_{hm}	Θ_p	Θ_{hm}
2	$c_{p,p}$	3.852			09:47:00	0	0	46.7	63.67	88.56	75.55	87.92
3	μ_p	0.0016			09:47:05	5	0.001389	45.3	63.78	88.56	75.25	87.92
4	ρ_p	1035			09:47:10	10	0.002778	44.2	63.78	88.46	75.35	87.92
5	D_i	0.0224			09:47:15	15	0.004167	44.1	63.78	88.46	74.94	87.82
6	D_o	0.0254			09:47:20	20	0.005556	42.9	63.78	88.36	74.94	87.71
7	d_i	0.0097			09:47:25	25	0.006944	46.6	63.88	88.36	75.15	87.82
8	d_o	0.0127			09:47:30	30	0.008333	45.6	63.88	88.36	74.84	87.71
9	L	1.15			09:47:35	35	0.009722	44.8	63.88	88.36	74.74	87.71
10	A	0.0459			09:47:40	40	0.011111	45.8	63.78	88.46	74.94	87.82
11	S	2.67E-04			09:47:45	45	0.0125	44.1	63.78	88.46	74.54	87.82
12	d_e	9.70E-03			09:47:50	50	0.013889	44.1	63.78	88.46	74.74	87.92
13	U_o	600			09:47:55	55	0.015278	44.4	63.78	88.46	74.54	87.92

Table D.5 (continued)

	M	N	O	P	Q	R	S	T	U
1	V	Re	$\Delta\theta_1$	$\Delta\theta_2$	$\Delta\theta_{LMTD}$	m	ϕ_p	U	N_f
2	0.048512	304.3952	13.01	24.25	18.05047	0.013426	614.4088	741.8522	1.23642
3	0.047057	295.2698	13.31	24.14	18.19084	0.013024	575.4211	689.4163	1.149027
4	0.045915	288.0999	13.11	24.14	18.06731	0.012708	566.3433	683.1796	1.138633
5	0.045811	287.4481	13.52	24.04	18.2782	0.012679	545.0382	649.8933	1.083156
6	0.044564	279.6264	13.42	23.93	18.17123	0.012334	530.2072	635.9307	1.059885
7	0.048408	303.7434	13.21	23.94	18.04646	0.013398	581.6128	702.4099	1.170683

Calculations at time = 0 s (shaded cells):

Calculated dimensions (calculated before a run and inputted as constants in FIX DMACS software for variable calculations):

Heat exchange surface area was calculated as:

$$A = \pi d_0 L = \pi \text{ x B8 x B9} = \pi \text{ x } 0.0127 \text{ x } 1.15 = 0.0459 \text{ m}^2 = \text{B10}$$

Cross-sectional area of the process fluid was calculated as:

$$S = \frac{\pi}{4}(D_i^2 - d_0^2) = \frac{\pi}{4}(\text{B5}^2 - \text{B8}^2) = \frac{\pi}{4}(0.0224^2 - 0.0127^2) = 2.67 \text{ x } 10^{-4} \text{ m}^2 = \text{B11}$$

Equal diameter of the process fluid cross section was calculated as:

$$d_e = D_i - d_0 = \text{B5} - \text{B8} = 0.0224 - 0.0127 = 9.70 \text{ x } 10^{-3} \text{ m} = \text{B12}$$

Calculated variables (calculated in real time during a run via FIX DMACS software):

Milk velocity was calculated as:

$$V = \frac{Q}{(3600000 \text{ x S})} = \frac{\text{H2}}{3600000 \text{ x B11}} = \frac{46.7}{3600000 \text{ x } 2.67 \text{ x } 10^{-4}} = 0.0485 \text{ m / s} = \text{M2}$$

Reynolds number was calculated as:

$$\text{Re} = \frac{\rho_p V d_e}{\mu_p} = \frac{\text{B4 x M2 x B12}}{\text{B3}} = \frac{1035 \text{ x } 0.0485 \text{ x } 9.70 \text{ x } 10^{-3}}{1.60 \text{ x } 10^{-3}} = 304 = \text{N2}$$

Temperature difference of side 1 was calculated as:

$$\Delta\theta_1 = \theta_{hm} - \Theta_p = J2 - K2 = 88.56 - 75.55 = 13.01\,°C = O2$$

Temperature difference of side 2 was calculated as:

$$\Delta\theta_2 = \Theta_{hm} - \theta_p = L2 - I2 = 87.92 - 63.67 = 24.25\,°C = P2$$

Logarithmic temperature difference was calculated as:

$$\Delta\theta_{LMTD} = \frac{\Delta\theta_1 - \Delta\theta_2}{\ln\left(\frac{\Delta\theta_1}{\Delta\theta_2}\right)} = \frac{O2 - P2}{\ln\left(\frac{O2}{P2}\right)} = \frac{13.01 - 24.25}{\ln\left(\frac{13.01}{24.25}\right)} = 18.05\,°C = Q2$$

Mass flow rate was calculated as:

$$\dot{m} = \frac{Q\,\rho_p}{3600000} = \frac{H2\,x\,B4}{3600000} = \frac{46.7\,x\,1035}{3600000} = 0.0134\,kg/s = R2$$

Rate of heat gained by the process fluid was calculated as:

$$\phi_p = c_{p,p}\,m\,(\Theta_p - \theta_p) \times 1000 = B2\,x\,R2\,x\,(K2 - I2)\,x\,1000 = 3.852\,x\,0.0134\,x\,(75.55 - 63.67)\,x\,1000 = 614\,W = S2$$

Overall heat transfer coefficient was calculated as:

$$U = \frac{\phi_p}{A\Delta\theta_{LMTD}} = \frac{S2}{B10\,x\,Q2} = \frac{614}{0.0459\,x\,18.05} = 741.8522\,W/m^2.K = T2$$

Estimated constants (estimated after a run and inputted into an MSExcel spreadsheet):

In this example (R1.18) U_0 was estimated from the average of the first 350 readings:

$$U_0 = \frac{(U_1 + ... + U_{350})}{350} = \frac{(T2 + ... + T351)}{350} = \frac{(741.85 + ... + 547.70)}{350} = 600\,W/m^2.K = B13$$

Calculated variables (calculated after a run via MSExcel software):

Normalised heat transfer coefficient was calculated as:

$$N_f = \frac{U}{U_0} = \frac{T2}{B13} = \frac{741.8522}{600} = 1.23642 = U2$$

APPENDIX D.4 Fouling curves

Calculating the fouling rate from an N_f versus time plot

A trace line was first drawn on the plot that best describes the linear proportion of the fouling period. Two points that intersect the trace line were selected and their corresponding x and y co-ordinates were determined from the N_f - time data (Table D.6). In the following example (R1.9) the two points selected corresponded to N_f values at times 1.27 (point 1) and 3.80 (point 2) hours into the run as shown in Figure D.1.

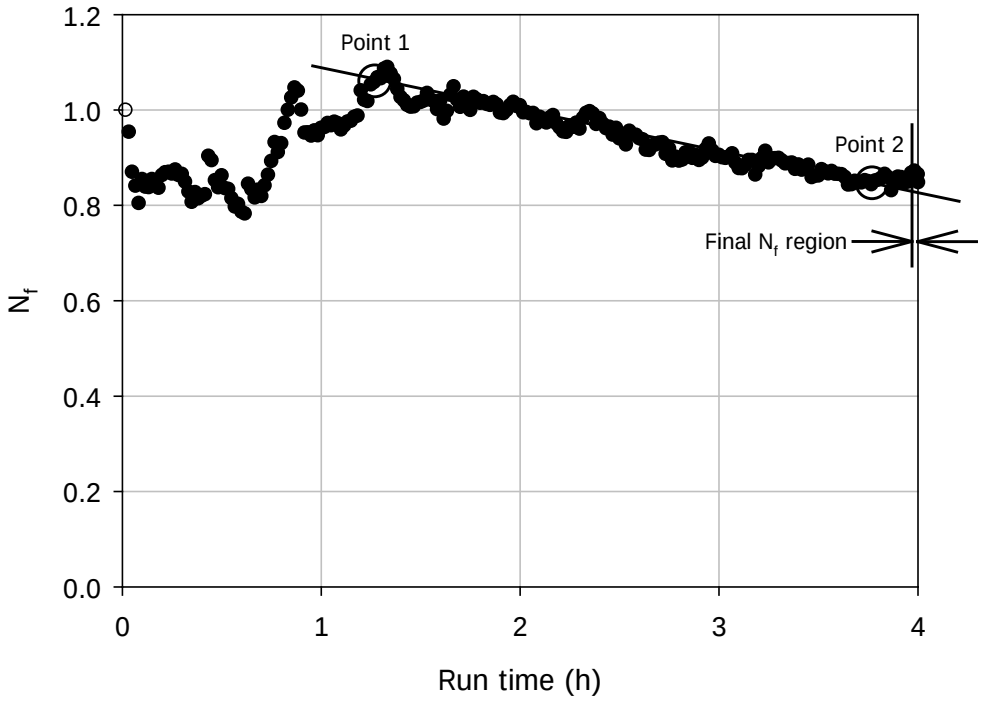

Figure D.1 N_f versus run time for R1.9.

The slope of the line between these two points was calculated using linear regression analysis via the MSExcel formula:

=INDEX(LINEST(E2:E3,D2:D3),1)=-0.081=F2

The absolute value of the slope was used to calculate the fouling rate:

$$\frac{dN_f}{dt} = \frac{|m|}{3600} = \frac{|F2|}{3600} = \frac{|-0.081|}{3600} = 2.25 \times 10^{-5}\ s^{-1} = H2$$

The MSExcel spreadsheet corresponding to these calculations is given in Table D.6.

Table D.6 Sample of the MSExcel spreadsheet showing the fouling rate calculation for R1.9.

	A	B	C	D	E	F	G	H
1	Time (h)	N_f	Point	X-Co-Or	Y-Co-Or	m	c	N_f/dt
2	0.015278	1.0002	1	1.26528	1.0586	-0.08094	1.16101	2.25E-05
3	0.031944	0.9543	2	3.79861	0.85355			
4	0.048611	0.8701						
5	0.065278	0.8411						
6	0.081944	0.8049						
7	0.098611	0.855						

Estimating the final N_f value

The region of the N_f curve that was used to estimate the final N_f value is shown in Figure D.1. This region corresponds to the N_f values from the last two minutes of the run. These data were averaged to give an estimate of the final N_f value:

$$\text{Final } N_f = \frac{(N_{f1} + \ldots + N_{f4})}{4} = \frac{(J2 + \ldots + J5)}{4} = \frac{(0.8683 + \ldots + 0.8487)}{4} = 0.8638 = K2$$

The MSExcel spreadsheet corresponding to this calculation is given in Table D.7.

Table D.7 Sample of the MSExcel spreadsheet showing the final N_f value estimation for R1.9.

	I	J	K
1	Time (h)	N_f	Final N_f
2	3.965278	0.8683	0.86377
3	3.981944	0.8726	
4	3.998611	0.8655	
5	4	0.8487	
6			
7			

APPENDIX D.5 Product linear velocity of an industrial heat exchanger

Description of the heat exchanger

The following information was taken from the data print supplied by the manufacturer:

Supplier	Alfa-Laval Thermal
Model	PHE-Type CLIP 10-RM
Mass flow rate ($\dot{m}$)	52 370 kg/h
No. of plates	116
No. of passages	58 milk side, 57 condensate side
No. of passes	2
Distance between plates (z)	3.87×10^{-3} m
Plate width (y)	0.426 m

Calculations

The mass flow rate was converted to volumetric flow rate (Q) as follows:

$$Q = \frac{\dot{m}}{\rho_p} = \frac{52370}{1035} = 50.6\,m^3/h$$

Assuming the flow was distributed evenly through each channel the milk flow rate through an individual channel was calculated as:

$$Q = \frac{50.6}{29} = 1.74\ m^3/h = 4.85 \times 10^{-4}\ m^3/s$$

The cross-sectional area of a channel (S) was calculated as:

$$S = zy = 3.87 \times 10^{-3} \times 0.426 = 1.65 \times 10^{-3} m^2$$

The linear velocity of the milk (V) was calculated as:

$$V = \frac{Q}{S} = \frac{4.85 \times 10^{-4}}{1.65 \times 10^{-3}} = 0.29\,m/s$$

APPENDIX E SIGMASCAN METHODOLOGIES

The following are examples of methodologies used with the Sigmascan Pro Image Analysis Version 5.0 software package.

Area of heat exchange surface covered in fouling:

Figure E.1 shows screen shots of the Sigmascan software using the following technique. In this example, the area of heat exchange surface covered by fouling was approximately 23%.

1. Import the image of the heat exchange surface into Sigmascan and crop areas not required for analysis (usually areas outside of the test surface).
2. Configure Sigmascan to measure desired characteristics of the image (in this case, number of pixels).
3. Increase the contrast between the fouled and non-fouled regions using the historical stretch function.
4. Apply an overlay to the fouled area (usually achieved by assigning a pixel intensity threshold). This overlay is represented by the blue regions in Figure E.1 (b).
5. Apply an overlay to any area outside of the heat exchange surface. This overlay is represented by the green regions in Figure E.2 (b).
6. Activate the count.
7. Calculate the percentage of heat exchange area covered by fouling from the resulting data.

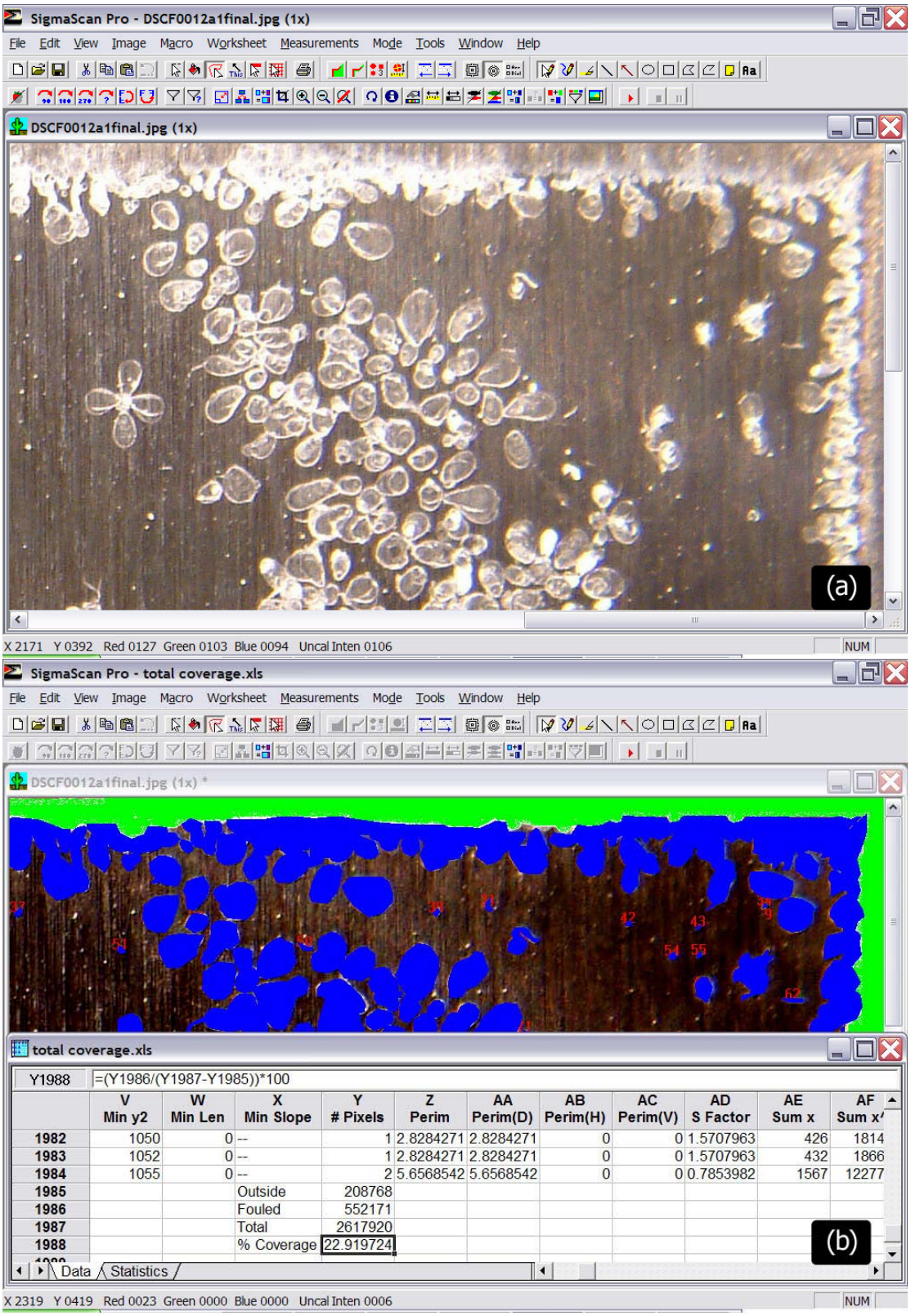

	V Min y2	W Min Len	X Min Slope	Y # Pixels	Z Perim	AA Perim(D)	AB Perim(H)	AC Perim(V)	AD S Factor	AE Sum x	AF Sum x'
1982	1050	0	--	1	2.8284271	2.8284271	0	0	1.5707963	426	1814
1983	1052	0	--	1	2.8284271	2.8284271	0	0	1.5707963	432	1866
1984	1055	0	--	2	5.6568542	5.6568542	0	0	0.7853982	1567	12277
1985			Outside	208768							
1986			Fouled	552171							
1987			Total	2617920							
1988			% Coverage	22.919724							

Figure E.1 Screen shots of Sigmascan when used to calculate the heat exchange surface area covered in fouling: (a) raw non-manipulated image (b) manipulated image with overlays applied and results worksheet showing a sample of raw and calculated data.

Size and number of bubbles on the heat exchange surface during a run:

Figure E.2 shows screen shots of the Sigmascan software using the following technique. In this example there were 117 objects of an average area of 0.08 mm^2 counted in the 25 mm^2 sector.

1. Import the image of the video still taken during the run showing the pattern of bubble nucleation on the heat exchange surface.
2. Configure Sigmascan to measure desired characteristics of the image (in this case, number and area of objects).
3. Input calibration factor based on measured dimensions of heat exchange surface.
4. Apply a grid overlay that divides the heat exchanger area into 25 mm^2 sectors. This overlay is represented by the red grid in Figure E.2 (b).
5. Select a sector that has a bubble nucleation pattern representative of the entire surface.
6. Trace around the circumference of all the bubbles located in the selected 25 mm^2 sector. This overlay is represented by the green regions in Figure E.2 (b).
7. Activate the count.
8. Calculate the average area and number of the bubbles located in the 25 mm^2 sector from the resulting data.

Figure E.2 Screen shots of Sigmascan when used to estimate the average size and number of bubbles in a 25 mm^2 sector: (a) raw non-manipulated image (b) image with grid overlay and bubble shape traced and counted.

Quantification of electrophoresis gels.

Figure E.3 shows a screen shot of the Sigmascan software using the following technique.

1. Import an image of a gel into Sigmascan.
2. Configure Sigmascan to measure desired characteristics of the image (in this case, distance along y-axis).
3. Input calibration factor based on densitometry outputs.
4. Apply a line overlay along the y-axis of each column of the gel. This overlay is represented by the red line in Figure E.3.
5. Mark along the line overlay of each column of the gel the start and finish point of each band.
6. Activate the count.
7. Use the results from Sigmascan to estimate more accurately the protein composition measured by the gels from the densitometry outputs.

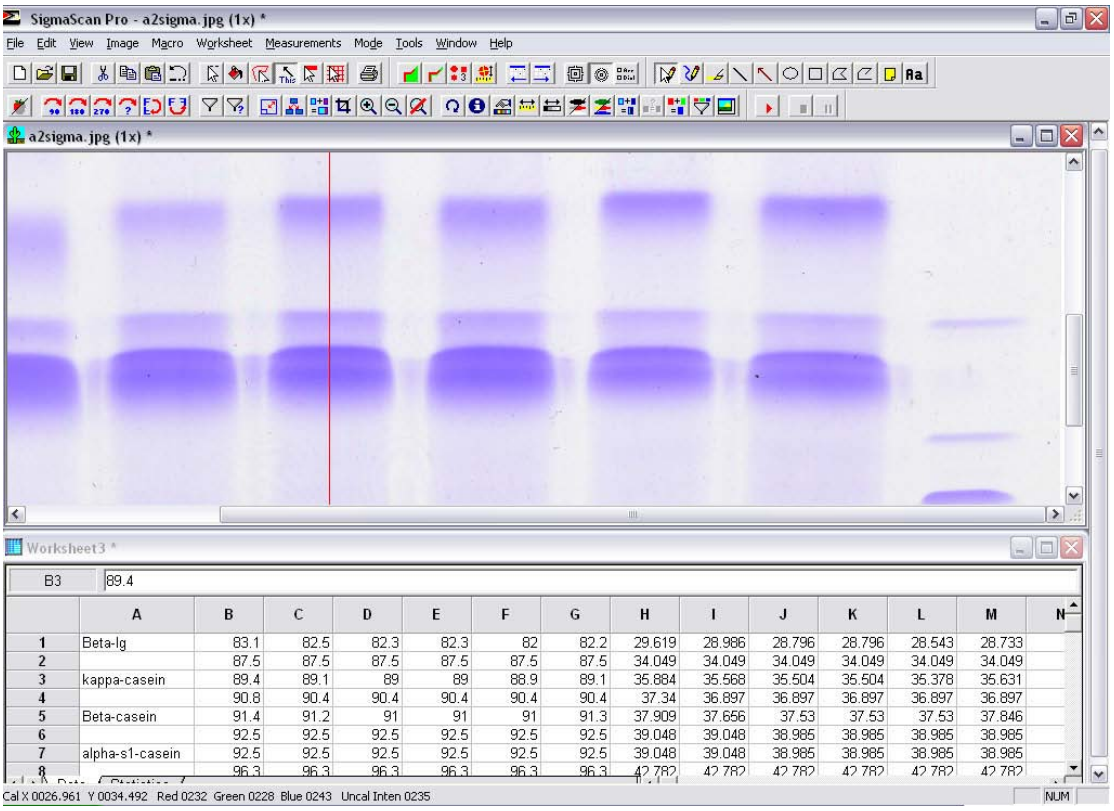

	A	B	C	D	E	F	G	H	I	J	K	L	M	N
1	Beta-lg	83.1	82.5	82.3	82.3	82	82.2	29.619	28.986	28.796	28.796	28.543	28.733	
2		87.5	87.5	87.5	87.5	87.5	87.5	34.049	34.049	34.049	34.049	34.049	34.049	
3	kappa-casein	89.4	89.1	89	89	88.9	89.1	35.884	35.568	35.504	35.504	35.378	35.631	
4		90.8	90.4	90.4	90.4	90.4	90.4	37.34	36.897	36.897	36.897	36.897	36.897	
5	Beta-casein	91.4	91.2	91	91	91	91.3	37.909	37.656	37.53	37.53	37.53	37.846	
6		92.5	92.5	92.5	92.5	92.5	92.5	39.048	39.048	38.985	38.985	38.985	38.985	
7	alpha-s1-casein	92.5	92.5	92.5	92.5	92.5	92.5	39.048	39.048	38.985	38.985	38.985	38.985	
8		96.3	96.3	96.3	96.3	96.3	96.3	42.782	42.782	42.782	42.782	42.782	42.782	

Figure E.3 Screen shot of Sigmascan when used to assist in the quantification of proteins from electrophoresis gels.

Macros used in Sigmascan.

Due to the large amounts of images produced in any single run macros based on the Visual Basic language were written. These automated the complex image analysis tasks that would otherwise be carried out manually. Figure E.4 shows an example of a macro used to calculate the surface area of fouling for runs operating under different pressures.

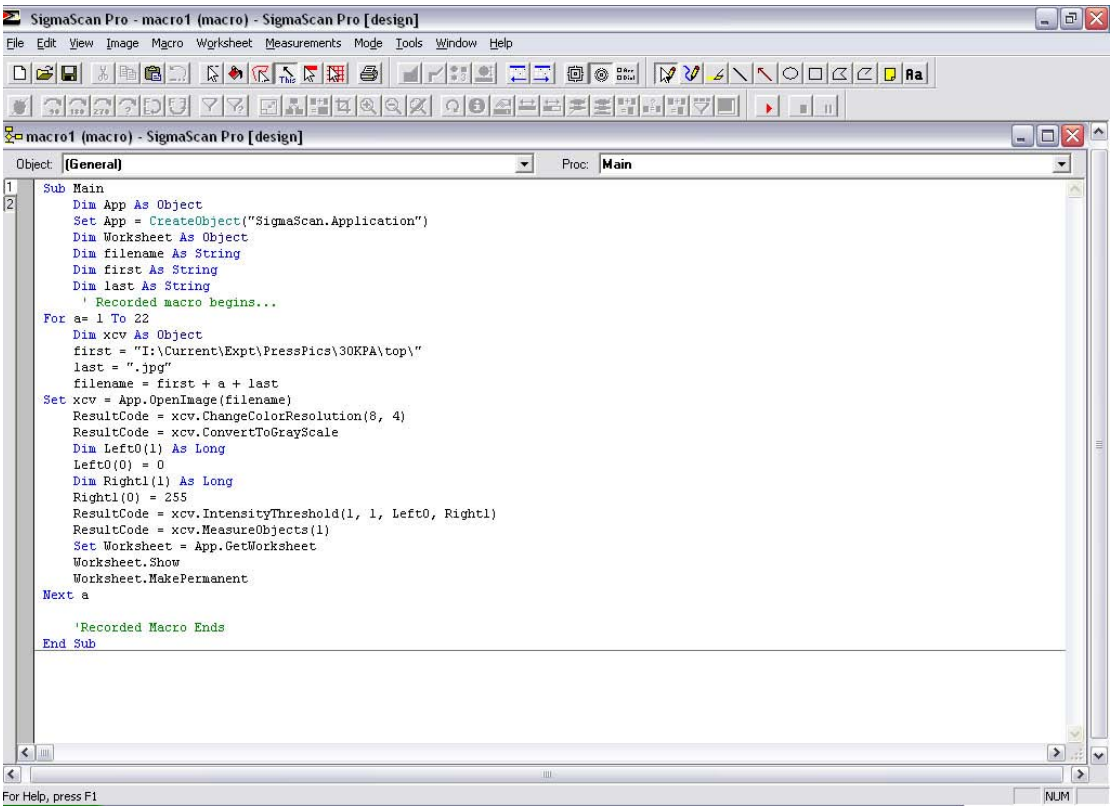

Figure E.4 Screen shot of Sigmascan showing a macro used in automating the image analysis process.

APPENDIX F MATERIAL PROPERTIES

APPENDIX F.1 Neutrase

Selected information taken from product data sheet provided by Novozymes A/S Ltd.

Description

Neutrase is a bacterial protease produced by submerged fermentation of a selected strain of *Bacillus amyloliquefaciens.* The enzyme protein is separated and purified from the production organism.

Neutrase is an endoprotease which can be used in most cases where proteins have to be broken down either moderately or more extensively to peptides.

Neutrase contains only the neutral part of *Bacillus amyloliquefaciens* proteases, whereas most other commercial preparations also contain the alkaline proteinase.

Neutrase contains a non-standardised amount of beta-glucanase.

Product Characteristics

Commercial product name	Neutrase 0.8L
Supplier	Novozymes A/S, Denmark
Description	Aqueous protease enzyme preparation
Enzyme class	Protease (neutral)
Declared activity	0.8 AU-NH/g
Appearance	Brown liquid
Stabiliser	Sodium chloride
	Sorbitol
Production organism	Bacillus amyloliquefaciens

Product Specification

	Lower Limit	Upper Limit	Unit
Proteolytic Units AU-NH	0.8		/g
Total Viable Count	-	50 000	/g
Coliform Bacteria	-	30	/g
Enteropathogenic E. Coli		None Detected	/25g
Salmonella		None Detected	/25g

The product complies with the recommended purity specifications for food-grade enzymes given by the Joint FAO/WHO Expert Committee on Food Additives (JECFA) and the Food Chemical Codex (FCC).

APPENDIX F.2 Whey Protein Concentrate

Selected information taken from product data sheet provided by Fonterra Co-op Ltd.

Product Characteristics

Commercial product name	ALACEN 322
Supplier name	Fonterra Ingredients, NZ
Product type	Whey
Product group	WPC 80% (Sulphuric)

Composition

		Unit
Ash	3.8 %	m/m
Fat	5.4 %	m/m
Lactose	5.8 %	m/m
Moisture	4.4 %	m/m
Protein	80.5 %	m/m

Compliance Statements

The product is HALAL and KOSHER and in compliance with European food law.

APPENDIX F.3 Milk

Selected information taken from product data sheet provided by Fonterra Co-op Ltd.

Product Characteristics

Commercial product name	Export homo 3.3% milk
Supplier name	Mainland Beverages Limited, NZ
Product type	Homogenised milk
Product group	3.3% fat homogenised milk

Chemistry (example)

		Unit
Fat	3.2 %	m/m
SNF	8.25 %	m/m
Acidity	0.131%	
Sensory	Finest	

Microbiology (example)

		Unit
Coliform	< 1	CFU/ml
APC @ 30°C	620	CFU/ml

Compliance Statements

All pastuerisers comply with standards: MRD-Stan3, MRD-Stan 4.

APPENDIX G CHEMICAL METHODOLOGIES

APPENDIX G.1 Moisture analysis

Moisture is normally considered to be the material lost by foodstuff on heating at a temperature around that of boiling water or by allowing the sample to stand over a dehydrating agent or by some similar form of measurement. It is generally considered to be water but is actually the total volatile matter lost or drained off under these particular conditions. The residue remaining is termed the total solids.

Apparatus

1. Aluminium moisture dishes, diameter 55 mm, height 40 mm, provided with well fitting slipover covers. Previously dry at 108 ± 5^{o}C and keep in a desiccator at room temperature.
2. Desiccator, air-tight, containing dry silica gel or phosphorus pentoxide.
3. Air oven capable of being accurately maintained at 108 ± 5^{o}C and provided with openings for ventilation. Thermometer should pass into the oven in such a way that the tip of the bulb is level with the top of moisture dishes and is not directly exposed in currents of escaping water vapour.
4. Note: Always use metal tongs when handling metal dishes and lids. Never use hands, as moisture and oils from hands can cause a significant error in the measurements.

Procedure

1. Accurately weigh a dry, cooled aluminium moisture dish and lid. Add approximately 2g of sample to the dish, replace the lid and quickly reweigh.
2. Place the dish, lid, and contents in the air oven at the prescribed temperature for 3 hours. Remove the lid from the dish and place the dish inside the lid to avoid confusion later. Before removing from the oven, cover the dish with the lid and transfer rapidly to the desiccator.
3. Once cool, weigh accurately.
4. Return to oven and repeat steps 2 and 3. Repeat until the weight in step 3 is constant.

Calculation

$$\%\ \text{total moisture and volatile matter} = \frac{100(A - B)}{A}$$

where A = original weight of sample (g)
B = final dry weight of sample (g)

APPENDIX G.2 Ash analysis

The ash of a food is the inorganic residue remaining after the organic matter has been burnt away. The ash obtained is not necessarily of exactly the same composition as the mineral matter present in the original food as there may be losses due to volatilisation or some interaction between constituents. The ash can be regarded as a general measure of quality and often is a useful criterion in identifying the food or as an index of the presence of an adulterant.

Procedure

1. Heat a silica or platinum dish (or crucible) for 60 minutes in the muffle furnace at 525-550^{o}C. Cool in a desiccator for at least 60 minutes.
2. Using forceps remove a cooled crucible and accurately weigh.
3. Accurately weigh about 1-2 g of sample into the crucible spreading the sample uniformly in the crucible before weighing.
4. Char over a Bunsen burner, taking care that sample does not ignite.
5. Place the dish in muffle furnace at 525-550^{o}C and ash for 5 hours.
6. Remove the dish from the muffle furnace, cool thoroughly and weigh.

Calculation

Ash content is the final weigh of residue remaining in the crucible.

APPENDIX G.3 Protein analysis

The quantitative determination of total organic nitrogen in foods is often desired for estimating the total protein content but the method will include other nitrogenous compounds present usually in minor proportions. The crude protein is calculated by multiplying the total nitrogen by an empirical factor (for dairy product, 6.38). This figure for protein often includes some non-protein nitrogenous compounds and also that nitrogen in certain forms (e.g. nitrates, nitrites and nitroso compounds) is not estimated in the Kjeldahl process. Hence, a second test for non-protein nitrogen was performed and this value was subtracted from the total protein estimated by the Kjeldahl process.

Apparatus

1. Kjeldahl 1026 system (Tecator Sweden)

Reagents

1. Concentrated H_2SO_4
2. Kjeltabs
3. 4% boric acid solution
4. 250 ml conical flask
5. 0.1 M HCl

Digestion

1. Accurately weigh about 0.5 g sample into the digestion tube.
2. Add two kjeltabs (each containing 3.5 g K_2SO_4 and 0.0035g Se) and then 15 ml concentrated H_2SO_4.

3. Carry on a blank digestion at the same time (no sample, but all other reagents). Set up block digestor unit and digest sample at 420°C for 40 minutes or until clear.
4. Remove the tubes carefully from the heating unit, leaving the exhaust manifold in place and water aspirator about half on. Allow to cool until the tops of the tubes are cool to touch.
5. Add approximately 70 ml hot distilled water to each tube and shake gently to mix. Ensure all solids have been dissolved.

Distillation and titration

1. Add 25 ml 4% boric acid solution to 250 ml conical flask.
2. The distilling unit has been prepared for distillation and is set on “automatic”
3. Connect the digestion tube with the first sample to be distilled in position.
4. Place the receiver flask and boric acid solution on the platform and raise it to its upper position. To avoid contamination don’t touch the glass outlet tube with your fingers. Hold it by its plastic tubing.
5. Close the safety door. The distillation automatically starts.
6. When the distillation is complete, the machine will “beep” several times. Remove the digestion tube and the receiver flask.
7. Titrate the sample with 0.1M HCl to grey-mauve end point.

Calculation

$$\%N = \frac{1400(A \times B)}{1000C}$$

$$\%\,\text{Protein} = \%N \times 6.38$$

where A = ml HCl used
B = exact molarity (normality) of HCl
C = weight of original sample taken (g)

APPENDIX G.4 Fat analysis

Apparatus

1. Water bath
2. Beaker, 50ml
3. Mojonnier for extraction apparatus
4. Steam bath
5. Drying oven
6. Centrifuge, Mojonnier type

Reagents

1. Ethyl alcohol (95%)
2. Diethyl ether, free from residue on evaporation
3. Petroleum ether, boiling point below 60°C
4. 35% w/w ammonium hydroxide
5. 2% phenolphthalein

Procedure

1. Weigh accurately sufficient sample to give between 0.3 and 0.7g of extracted fat into a dry Mojonnier tube (e.g. 10ml milk; 1-2 g milk powder). Make up to 10 ml if necessary with water, and shake to dissolve or blend.
2. Add 2 ml ammonium hydroxide and mix well in the lower bulb. Place in 60^{o}C water bath for about 5 minutes and swirl occasionally. Cool. Add 2-4 drops phenolphthalein.
3. Add 10 ml of ethyl alcohol and mix by allowing the liquid to flow backwards and forwards between the two bulbs; avoid bringing the liquid too near the neck of the tube. The complete extraction of the fat dependent on satisfactory mixing at each stage.
4. Add 25 ml of diethyl ether, close the tube with the stopper and shake gently for about one minute.
5. Remove the stopper and add 25 ml petroleum ether, using the first few ml to rinse the stopper and the neck of the tube, allowing the rinsing to run into the tube.
6. Replace the stopper, again wetted with water, and rock carefully for 30 seconds.
7. Centrifuge Mojonnier flask for 2 minutes at 60 RMP.
8. Examine the tube to see if the interface of the liquid is in line with the upper junction of the neck of the tube. If it is below this, it should be raise by the addition of a little water run down the side of the tube.
9. Remove the cork and carefully decant as much as possible of the organic solvent layer into a preweighed short-necked flask by gradually bringing the cylindrical bulb of the tube into horizontal position.
10. Add 5 ml ethyl alcohol and mix. This helps prevent emulsions forming and is in accord with the AOAC method.
11. Repeat the extraction using 15 ml of diethyl ether and 15 ml petroleum ether (step 4 to 9). Add second extract into the same flask as used in step 9.
12. Distil carefully the solvents from the flask using rotary evaporator and dry the flask in the oven at 100^{o}C for 90 minutes, taking precautions to remove all traces of solvent vapour, prior to placing in the oven.
13. Allow the flask to cool to room temperature. Do not use a desiccator.
14. Weigh the flask, and record the fat content of the sample.
15. At the same time as the above procedure is carried out, make a blank determination with 10 ml of water in place of the sample. Use a similar extraction apparatus, the same reagents and the same technique throughout. Correct the apparatus weight of fat for the change, if any, in the weight if the flask used for the blank determination.

Calculation

Crude fat content is the final weight of residue remaining in the flask, expressed as a percentage of the weight of the original sample.

APPENDIX G.5 Reducing SDS-PAGE analysis procedure

Reagents preparation

1. Acrylamide 30%T
(%T refers to %(W/V) of total concentration of monomer (Acrylamide + Bis) in solution)

Stock solution made up from 30 g Bis/Acrylamide mixture 37.1:1 (2.6% C) to 100 ml with purified water.

Acrylamide	29.2 g
Bis	0.8 g

Dissolve acrylamide/bis mixture with ~60 ml milliQ water, then make up to 100 ml with milliQ water in volumetric flask. Filter and store at 4°C in DARK bottle.

NB. This solution should be polymerised and discarded if older than 1 month.

2. 0.1(W/V) Bromophenol blue
Stock solution available.

3. Brilliant Blue Staining Solution

Brilliant Blue	3 g
Acetic Acid (glacial)	200 ml
Propan-2-ol	500 ml

Make up to 2 litre with milliQ water in volumetric flask.

4. Destaining Solution

Volume to make up:	1l	10l	5l
Propan-2-ol	100ml	1l	500ml
Acetic acid (glacial)	100ml	1l	500ml
MilliQ water	800ml	8l	4l

Buffer solution preparation

1. 1.5M Tris-HCl Buffer
To a 100 ml beaker add 18.15 g Tris base, add about 60 ml distilled water. Mix and adjust pH to 8.8 with 6M HCl. Using a measuring cylinder bring to 100 ml volume. Store at 4°C.

2. 0.5M Tris-HCl Buffer
To a 100 ml beaker add 6.0 g Tris base. Add about 60 ml distilled water, mix and adjust pH to 6.8. Using a measuring cylinder bring to 100 ml volume. Store at 4°C.

3. 10% SDS
Dissolve 10 g SDS in water with gentle stirring and bring to 100 ml volume with distilled water.

4. Sample buffer

Distilled Water	3.3 ml	50 ml	500 ml
0.5M Tris-HCl pH 6.8	1.0 ml	12.5 ml	125.0 ml
Glycerol	0.8 ml	10.0 ml	100.0 ml
10% (W/V) SDS	1.6 ml	20.0 ml	200.0 ml
0.05% (W/V) Bromophenol Blue	0.4 ml	2.5 ml	25.0 ml
Total volume	8.0 ml	100 ml	1 L

Keep sample buffer at room temperature.

Dilute sample with sample buffer so that it contains approximately 0.1% of protein. Add 2β-mercaptoethanol (5% of sample volume) just before sample is heated. Vortex. Heat sample at 95^{o}C for 4 minutes. Vortex. Let it cool down before used.

Note: The β-mercaptoethanol should be added fresh each time as it will oxidize on storage.

5. Electrode Buffer

Total volume to make up:	600 ml	900 ml
Tris Base	9.0 g	13.5 g
Glycine	43.2 g	64.8 g
SDS	3.0 g	4.5g

Bring to the required volume with distilled water. Check pH. Should be 8.3 – 8.5. Store at 4^{o}C. Dilute 5X stock (60 ml buffer with 240 ml distilled water for one electrophoresis run).

Gel preparation

1. Resolving gel

	2 gels	4 gels
Milli-Q water	2.02 ml	4.04 ml
1.5 M Tris-HCl buffer	2.5 ml	5 ml
10% SDS	100 μl	200 μl
Acrylamide (30%)	5.3 ml	10.6 ml

Degas for 15 mins

Temed	5 μl	10 μl
Ammonium persulphate	50 μl	100 μl

Ammonium persulphate must be freshly made to 10% (W/V) e.g. 0.2 g in 2 ml milli-Q water.

Pour resolving gel gently into electrophoresis brace ensuring no bubbles form. Top up with milli-Q water and leave to set for approximately 40 minutes until a distinct line is seen.

2. Stacking gel

	2 gels	4 gels
Distilled water	3.05 ml	6.1 ml
1.5 M Tris-HCl buffer	1.25 ml	2.5 ml
10% SDS	50 μl	100 μl
Acrylamide (30%)	0.65 ml	1.3 ml
	Degas for 15 mins	
Temed	5 μl	10 μl
Ammonium persulphate	25 μl	50 μl

Pour stacking gel gently into electrophoresis brace ensuring no bubbles form. Place the comb in the brace and leave to set.

After the gel has set remove the comb and add sample into the wells of the stacking gel. Run the gel at x for 50 minutes.

Stain gel for 1 hour with staining solution. Destain gel for 24 hours with destaining gel.

APPENDIX H DATA DISK

The data disk contains various files associated with the experiments conducted in this work (e.g. photos of fouling layers, example video clips and plant processing data). Please see the disk's 'Readme' file for a detailed description of its contents.